CORROSION INHIBITION IN SELF-COMPACTING CONCRETE

Marva Angela Blankson

Thesis submitted to the University of Nottingham
For the degree of Doctor of Philosophy

November, 2013

ABSTRACT

This research was undertaken to investigate the effectiveness of carboxylic corrosion inhibitor in fly ash and silica fume (respectively FM and SM) samples and nitrite-based corrosion inhibitors in fly ash (FGC) sample. The findings from this research show that the addition of the carboxylic inhibitor altered the hydration of fly ash and silica fume self-compaction concretes (SCCs) by delaying the formation of ettrngite and the production of portlandite in the FM and SM samples and ultimately causing the calcium aluminate hydrates to surround the fly ash and cement particles. It was shown that this resulted in slight setting retardation in the silica fume particles but significant delay in the hydration of the fly ash SCC. Further, this development brought about by the use of the carboxylic inhibitor contributed bleeding of different levels in the fly ash and silica fume samples and this condition was shown to increase the heterogeneity of the FM and SM SCCs. Although addition of the nitrite-based inhibitor retarded the setting of paste of the fly ash SCC, no noticeable delay in the hardening of the concrete was manifested. When the nitrite-based inhibitor was included in the fly ash SCC, the physical structure of the interfacial transition zone and the bulk of the mortar were found to be less porous and hence the concrete displayed a higher level of homogeneity.

The incorporation of the carboxylic inhibitor increased the corrosion resistance of the silica fume concrete to chloride –induced corrosion but the corrosion resistance of the fly ash SCC was only improved when exposed to low concentration of chloride ions. The reduction in the inhibiting capacity of the FM SCC to high chloride load was the result of the elevated degree of porosity and higher propensity to chloride migration resulting from the use of the

carboxylic compound. On the other hand, when the nitrite compound was used in the fly ash SCC, the current density was reduced which is ascribed to the effectiveness of the inhibitor and the reduction in the porosity and chloride migration that resulted from the incorporation of the inorganic compound. However, as the concentration of the corrosion inhibitors increased, the corrosion resistance of the inhibited SCCs reduced. The study also shows that the nitrite fly ash SCC showed the ability to undergo self-healing of corroded reinforced concrete but the carboxylic inhibited types of SCCs (FM and SM) could only prevent further corrosion after the corrosive environment is removed. Comparative testing showed that, in all three types of inhibited SCCs, there is a high probability that the inhibiting capacity will become depleted under certain conditions of chloride exposure.

Using the nitrite inhibitor in the fly ash SCC also imparted moderate to significant improvement to the 7 - 60-day compressive strengths but the long term strength of the concrete was slightly lower than that of the traditional fly ash SCC. When the carboxylic compound was used in the fly ash SCC, the 7 - 28-day compressive strengths were marginally lowered and the 60 - 90-day compressive strengths were profoundly reduced. The addition of the carboxylic inhibitor to the silica fume SCC also significantly reduced the 28 - 90-day compressive strengths of the concrete.

ACKNOWLEDGEMENT

I would like to convey my deepest gratitude to Associate Professor Andrew Dawson and Dr. Nicholas Thom for the guidance and encouragement offered to me throughout out my tenure at UoN. To my main supervisor, Associate Prof. Dawson, I appreciate the methods that you used to get the work done. A successful supervisor knows all the strategies of getting the researcher to work in an effective and timely manner. A great supervisor has those skills but he is also sensitive and caring and these are the qualities that the researcher will remember most as he/she moves on in life. Thanks Sir Dawson, you are a great supervisor.

Thanks to the staff members of NTEC, Structures and Wolfson laboratories that assisted in the testing programme herein. I would also like to convey my gratitude to Associate Professor Matthew Hall for his kind assistance in the review process. I also appreciate the kind assistance of my examiners - Dr. Dionysios Bournas, and Professor Peter Claisse, in a vital phase of the research project.

Thanks also to my colleagues in NTEC who helped to make this academic journey pleasant and fruitful. Special thanks to Dr. Erdem for the different forms of support that were provided in difficult situations. I would also like to express my appreciation to Dr. Young, Dr. Brown and my Church family for the encouragement to make it to each milestone of this journey. Thanks also to Dr. Buchanan for the kind assistance provided when requests were made.

To my husband, Robert and my sons Jason and Ashton, words are not sufficient to express my gratitude for the unconditional love, understanding and overall support that was shown to me throughout the research programme. Thanks also to my mother and my siblings for helping to maintain my confidence in challenging times.

Most of all, I give thanks to the Almighty God who has shown once again that He is the great provider and keeper.

This thesis is dedicated to Robert, Jason and Ashton

DECLARATION

The work described in this thesis was conducted at the Department of the Civil Engineering, University of Nottingham between October 2008 and October 2011. I declare that the work is my own and has not been submitted to any other university for a degree.

Marva A. Blankson

Nottingham

November, 2013

TABLE OF CONTENTS

LIST OF FIGURES

LIST OF TABLES

LIST OF ABBREVIATIONS AND NOTATIONS

A	Cross-sectional area of specimen
A_{cs}	Surface area of corroded steel
Afm	Monosulphoaluminate
Aft	Ettringite
Al_2O_3	Aluminum oxide
B	Linear polarization resistance constant
B_j	Blocking step
BSE	Back scattered electron
c/p	Cement/powder
C_2S	Dicalcium silicate
C_3A	Tricalcium aluminate
C_3S	Tricalcium silicate
C_4AF	Tetra-calcium aluminate ferrite
$Ca(OH)_2$	Calcium hydroxide
CAH	Calcium aluminate hydrate
CaO	Calcium oxide
CEM	British cement
CI	Chloride ions
CSE	Copper-copper sulphate electrode

C-S-H	Calcium silicate hydrate
D	Diameter
DC	Direct current
D_f	Diffusion coefficient
d_{jx}	Diameter of slump spread in the x-direction
d_{jy}	Diameter of slump spread in the y-direction
D_{max}	Maximum diameter of particle
d_{mc}	Average metal corrosion
D_{min}	Minimum diameter of particle
D_{nssm}	Electromigration coefficient
dp/dl	Pressure gradient
d_r	Distance between lattice planes in crystal
D_s	Diameter of steel
DTG	Differential thermogravimetric analysis
d_p	Diameter of pores intruded with mercury
E_{corr}	Corrosion potential
E_d	Dynamic modulus of elasticity
EDX	Energy dispersion x-ray analysis
ESEM	Environment scanning electron microscopy
F	Faraday constant
Fe	Iron
Fe^{2+}	Ferrous iron

Fe^{3+}	Ferric iron
g_c	Yield stress related parameter
G_f	Fracture energy
GGBS	Ground granulated blastfurnace slag
h_0	Height of concrete at centre position in J-ring test
H_2O	Water
h_c	Viscosity related parameter
h_o	Form factor
HRWRA	High range water reducing admixture
h_{x1}	Height of concrete at x1 position in J-ring test
h_{x2}	Height of concrete at x2 position in J-ring test
h_{y1}	Height of concrete at y1 position in J-ring test
h_{y2}	Height of concrete at y2 position in J-ring test
i_{corr}	Corrosion current density
I_{corr}	Corrosion current
ITZ	Interfacial transition Zone
J	Mass transport rate (flux)
k	Coefficient of permeability
K_2O	Potassium oxide
L	Length of specimen
LPR	Linear polarization resistance method

m	Mass of metal lost
m_c	Mass of concrete
MCI	Migratory corrosion inhibitor
m_d	Oven-dry mass
MgO	Magnesium oxide
MIP	Mercury intrusion porosity
m_p	Mass of receiver
m_{ps}	Mass of concrete and receiver
M_{ssd}	Saturated-surface dry mass
n	Number of electrons transferred
Na_2O	Sodium oxide
$NaCl$	Sodium chloride
$NaOH$	Sodium hydroxide
n_i	Integer in Bragg's equation
n_p	Percentage of water absorbed
OM	Optical Microscope
OPC	Ordinary Portland cement
P_{hg}	Pressure of mercury
P_s	Deepest pit penetration
$PUNDIT$	Portable ultrasonic non-destructive digital indicating tester
q	Heat of hydration rate

Q	Heat of hydration
r	Degree of reaction
R	Coefficient of correlation
$\dot{R}$	Gas constant
R_a	Surface roughness
r_c	Median radius
RCM	Rapid chloride migration
Re	Electrical resistance
R_p	Linear polarization resistance measurement
rpm	Revolutions per minute
r_t	Mass loss per area per unit time
SCC	Self-compacting concrete
SCE	Saturated calomel electrode
SE	Secondary electron
SEM	Scanning electron microscope
SF_j	J-ring slump flow
S_{ft}	Final setting time
SI	Segregation index
SiO_2	Silicon dioxide
SO_3	Sulphuric anhydride
S_{vp}	Specific surface
T	Temperature

t	Time
t_{500}	Slump flow time
TC	Traditional concrete
TGA	Thermogravimetric analysis
TiO_2	Titanium dioxide
t_{j500}	J-ring slump flow time
U	Absolute value of applied voltage
V	Ultrasonic wave velocity
v	Poisson's ratio
v_l	Velocity
V_t	Total specific volume
w	Constant
w/p	Water/powder ratio
x_n	Time elapsed after mixing concrete
x_p	Potential reading
XRD	X-ray diffraction
y_p	Work for plastic deformation
y_s	Surface energy
y_t	Predicted slump flow at specified time
Z	Atomic weight of metal
$\bar{z}$	Strain rate
Γ	Electricity resistivity

γ_s	Surface tension of mercury
η	Viscosity
θ_s	Contact angle of mercury
θ_x	Incident angle
I'	Initial setting time
λ_1	Wavelength of scattered wave in Bragg's equation
μ_o	Viscosity
ρ	Density of concrete
ρ_{st}	Density of steel
σ_e	Normal stress
τ	Shear stress
τ_0	Yield stress
φ	Tortuosity
Ψ	Porosity

INTRODUCTION

1.0. GENERAL

Chloride-induced corrosion is one of the major deteriorating agents leading to the degradation of reinforced concrete structures. The chloride from marine environments, de-icing agents, admixtures and even concrete constituents, can attack the steel in reinforced concrete and contributes not only to early deterioration but also to increased maintenance activities. At this point it should be pointed out that the protection strategy of many corrosion-inhibiting compounds seems satisfactory as far as staving off the initiation of corrosion in the first fifty years of reinforced concrete members. However, there is a plethora of important buildings that are established as monumental edifices (such as the Burj Al Arab, Dubai) and others that may form part of essential services (such as the Øresund Bridge, Sweden and the Sydney Harbour Bridge, Australia) that will require longevity. Moreover, with the present international emphasis on sustainability and low carbon emission, more consideration is given to reinforced concrete design that will not just span decades but centuries. However, there are other issues that are pertinent to the use of corrosion-inhibited SSC. With rising sea levels and the greater incidence of storm surges leading to inundation of the built environment, the issue of the reduction/depletion of the inhibiting capacity of the concrete and the matter of self-healing of corroded reinforced concrete will be of greater concern. This research will reveal whether corrosion-inhibited self-compacting concrete can offer greater resistance to chloride induced corrosion and provide a higher level of healing than the conventional self-compacting concrete and hence could help to further extend the service life of some reinforced concrete facilities.

For over 50 years corrosion inhibitor has been used in traditional reinforced concrete to protect the steel from corrosion. In more recent years SCC was developed and it is reported as having the potential to produce a durable material (Zhu and Bartos, 2003) mainly by nature of the refinement (Kanellopoulos et al, 2012) and relatively low level of porosity in the interfacial zone in its microstructure (Leemann et al, 2006). Currently, research is advancing the design of SCC admixed with corrosion inhibitor with a view to combine the attributes of the individual materials in one product. It is believed that this new product – inhibited SCC, will be the solution to aggressive chloride attack, which in many instances is responsible for the reduction in the durability of reinforced concrete.

However, SCC is formulated with appreciable levels of chemical and mineral admixtures and the addition of another reactive admixture may affect the performance of the concrete. Besides, there are reports of set alteration associated with the use of corrosion inhibitors in traditional concrete and there has always been concern about the sustainability of the inhibiting capacity of concrete incorporated with corrosion inhibitor.

1.1. AIM AND OBJECTIVES OF THE STUDY

The aim of this research is to investigate the implications of the interaction of corrosion inhibitors with the constituents of SCC and the resulting effects on the corrosion inhibiting capacity. The specific objectives are outlined below.

1. To investigate the impact of corrosion inhibitor on the setting and on the rheological behaviour of SCC.

2. To conduct a comparative study on the mechanical properties of traditional and corrosion-inhibited SCCs with a view to identify the effects that contribute to similarities or dissimilarities in the strength-related properties.
3. To analyse the pore structure of samples of inhibited SCC in order to detect any change in the penetrability and to identify the mechanism that supports the transport property.
4. To evaluate the effectiveness of the inhibiting capacity of corrosion-inhibited SCC under different conditions of chloride exposure and levels of concentrations.
5. To determine the relative potential for self-healing and for the depletion of the corrosion inhibitor from inhibited SCC.

1.2. RESEARCH PLAN

The following research plan is designed to meet the objectives of the research.

i. Carboxylic and nitrite-based corrosion inhibitors will be incorporated in fly ash SCCs to produce carboxylic fly ash SCC and nitrite fly ash SCC respectively. The carboxylic inhibitor will also be added to silica fume SCC to produce carboxylic silica fume SCC. The traditional fly ash SCC (that is, without inhibitor) will be used as a control sample for the fly ash SCCs that are admixed with nitrite and carboxylic inhibitors. The traditional silica fume SCC (that is, without inhibitor) will be used as a control for silica fume SCC that is admixed with carboxylic inhibitor. The following test will be carried out on these samples.

ii. The setting time test will be used to determine the effect of the corrosion inhibitor on the setting times of SCC pastes. Additionally, the slump flow, V-funnel, J-ring and

sieve segregation tests will be used to examine the effect of the corrosion inhibitor on the rheological behaviour of the inhibited SCC samples.

iii. The compression, tensile, and ultrasonic pulse tests will be used to undertake a comparative study on the mechanical properties of SCC with and without corrosion inhibitor.

iv. The porosity, absorption, rapid electrical migration, electrical resistivity and mercury intrusion porosimetry tests will be used to evaluate the penetrability and investigate the pore structure of the inhibited SCCs relative to the traditional SCCs.

v. The process of wetting and drying the inhibited SCC samples will be used to promote corrosion in chloride contaminated samples. Half cell potential test and current density test will be performed at regular intervals to determine the effectiveness of the corrosion inhibitor SCC. The linear polarization resistance test via a potentiostat/galvanostat instrument will be used for the determination of the (corrosion) current density.

vi. Further, some reinforced SCC samples with and without corrosion inhibitor will be placed in an electrochemical cell and subjected to an impressed voltage to advance corrosion. After two days the samples will be removed from the cell for 24 hours to determine the potential for self-healing via current density testing. The samples will be returned to the cell after the 24-hour period and corrosion density readings will be taken until the samples show signs of cracking on the surfaces.

vii. Another series of corrosion tests using impressed voltage will be conducted on inhibited-reinforced SCC samples to determine whether the inhibitor will become depleted after prolonged exposure to sea water. The samples will be soaked in saline water for 28 days before the corrosion test and their inhibiting capacity at 28 days will

be compared with SCC replicates that are kept in a moist environment that is free of chlorides.

viii. Some analytical tests and image processing tests will also be conducted to examine the micro-features of the SCC samples before and after corrosion with a view to determine the porosity of the ITZ and the mortar, the level of hydration products at different stages of the hydration process. These tests will give a greater understanding of the effect of the interaction of the corrosion inhibitors and constituents of the SCC and will help to construct the mechanism that governs the behaviour of any phenomenon that is observed. For these tests, thermogravimetric, mercury intrusion porosimetry, scanning electron microscopy, x ray diffraction and image analysis will be used. Assessment of the corroded steel bar will be done with the use of a stylus profilometer.

1.3. RESEARCH DESCRIPTION

Chapter 1 provides the background and problem definition of this research. The aim and objectives that will achieve the general aim of the research are also stated

Chapter 2 presents the review on the fundamental properties of concrete from literature and presents the existing knowledge on aspects of SCC that are pertinent to this study

Chapter 3 reviews literature on transport processes and properties and provides a short discourse on the electrochemical process that is involved in the corrosion of reinforced steel in concrete. The function, categories, and use of corrosion inhibitors are also covered in this chapter.

Chapter 4 presents the properties of materials, mix proportions, sample types; and preparations and production of samples. The test methods, and equipment are also provided in this chapter.

Chapter 5 gives the findings of the tests on the setting and rheology of the mixes, evaluates the findings and gives a conclusion on the performance of the plastic material.

Chapter 6 presents the test results on the mechanical properties of the SCC samples and discusses the significance of the test parameters; shows relationship between mechanical properties, and based on the relationships established, explains the behaviour of the SCC samples.

Chapter 7 shows the results of tests on the transport properties of the SCC samples and determines the relative quality of the pore system in inhibited SCC samples based on the capacity of the specimens to transport fluids and ions.

Chapter 8 shows the resistance of concrete under different conditions, identifies factors that control the corrosion process at the macro and micro levels, and develops relationships between relevant properties. A statistical model that predicts the time of corrosion in the SCC samples is shown in this chapter.

Chapter 9 summarizes the major findings on the inhibited SCC samples and gives recommendations for future research.

1.4. PUBLISHED WORK

The following two papers were produced during the research period.

Blankson, M., Erdem, S., Dawson, A. R. and Thom, N. H. (2011) *Comparative study on the rheological and durability characteristics of conventional and glass-enriched self-compacting concrete.* In: Cheung. S. O., Yazdani, F., Ghafoori, N. And Singh, A. (eds),

proceedings of Modern Methods and Advances in Structural Engineering and Construction, Switzerland, pp. 1291-1296.

Erdem, S. and Blankson, M. (2013) *Fractal-fracture analysis and characterization of impact-fractured surfaces in different types of concrete using digital image analysis and 3D nanomap laser profilometery.* Construction and Building Materials, 40, 70 – 76.

1.5. CONCLUSION

This research will be carried out to determine if inhibited SCC will deliver a higher level of corrosion resistance to chloride-induced corrosion and to conduct an investigation on the effects of interaction between the corrosion inhibitor and the ingredients of SCC. It is felt the design of the experimental program is adequate to fulfil the objectives of the research.

SELF-COMPACTING CONCRETE

2.1. INTRODUCTION

Self-compacting concrete (SCC) was formulated to address specific issues relating to durability of concrete. In 1980, Professor Okamura mentioned that the main factor contributing to poor durability of some of the concrete structures in Japan was insufficient compaction of the concrete at the construction stage (Vachon, 2002). The availability of skilled construction workers at the time was identified as the source of the problem. In order to prevent recurrence of such problem, a concrete that did not rely on the state of the workforce but which could be compacted without external energy was proposed (Okamura and Ouchi, 1999). With the traditional concrete mix this was virtually impossible as it is established knowledge that the maximization of durability within a given concrete is attained though effective compaction and this requires adequate skilled manpower. In 1988 self-compacting concrete was developed; the concrete that flows into even confined spaces, fills areas, and self-compacts with no manual input.

The principle of self-compacting concrete was not all new to the concrete industry. There are special highly fluid types of concrete that were introduced long before the 1980s but SCC is a significant breakthrough in an improved material and construction process that can be employed on many challenging construction projects as well as on less demanding jobs. It is reported that some of the significant benefits that demonstrate the superiority of well designed SCC are low permeability and surface absorption, improved resistance to freezing

and thawing and greater bond between reinforcement and concrete (Holton, 2004). These ameliorations along with the reported improvement in the interfacial transition zone (Leemann et al, 2006) and refined microstructure (Kanellopoulos et al, 2012) may result in an improved durability in this type of concrete. There is also improvement in the physical appearance of the concrete as there are fewer occurrences of surface defects such as blowholes and honeycombing. Although the strength of SCC can be lower than that of traditional concrete, it is also shown that at the same (and even higher) water/cement ratio, the strength in SCC can be higher than traditional concrete (Kanellopoulos et al, 2012; and Gibbs and Zhu, 1999). The benefits that are achieved in the utilization of SCC on construction projects however extend beyond the improvement in the quality of concrete to the improvement in production processes according to Skarendahl (2003). Some of these benefits are:

i. Reduced manpower for casting: SCC eliminates the need for some of the activities normally associated with compaction and hence fewer workers are needed for casting operations (Byfors, 1999).

ii. Increased speed of construction: The consistency of SCC not only eliminates the need for compaction but also facilitates easy delivery processes through pipelines (Okamura and Ouchi, 1999).

iii. Improved working conditions (Zhu and Bartos, 2003): Eliminating vibrators from construction projects reduces noise pollution, hand-arm vibration syndrome and strains from the lifting of heavy equipment (Holton, 2004).

iv. New design options: Whereas the practicality of constructing concrete structures that were complex in shape and size restricted architectural and structural designs, the

introduction of SCC has removed many of these limitations as demonstrated in Figure 2.1.

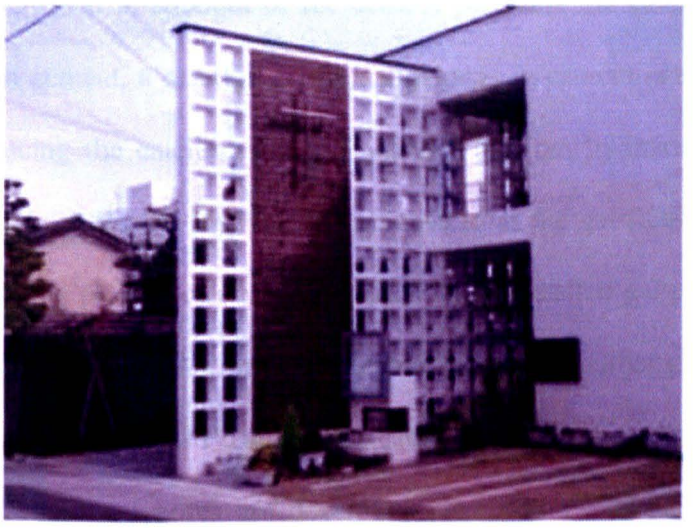

Figure 2.1 This lattice wall was cast with SCC from only one point at each floor
Source: Okamura and Ouchi, 2003a

However, SCC is quite sensitive to factors such as variation in proportions of materials and changes in the conditions of the ingredients (Skarendahl and Billberg, 2006). Since the sensitivity of the concrete can affect its performance, high level of quality control may be required for the production of SCC. Additionally, as a result of the chemical and mineral admixtures used in this concrete, the production of SCC is likely to be less economical than the traditional concrete. It is therefore imperative to assess the cost associated with the use SCC and the benefits to be derived when considering its use.

2.2. CHARACTERISTICS OF SELF-COMPACTING CONCRETE

2.2.1. Microstructure of concrete

The four principal compounds of cement are dicalcium silicate (C_2S), tricalcium silicate (C_3S), tricalcium aluminate (C_3A), and tetracalcium aluminoferrite (C_4AF). The main contributors to the growth in strength of the cement paste are the calcium silicates. When water is mixed with cement, a reaction of the compounds in cement is triggered (Equations 2.1 and 2.3), producing the calcium silicate hydrates, calcium hydroxide and other minor compounds. The calcium silicate hydrates are referred to as the gel (Kosmatka et al., 2008). This gel consists of the gel particles and interstitial cavities called gel pores. The pores are interconnected and their size is estimated to be less than 3 nm, although some reports give slightly larger values (Kumar and Bhattacharjee, 2003). As hydration progresses more gel is formed, and hence more gel pores are developed. The volume of these pores represents approximately 28% of the volume of all the gel (Mehta and Monteiro, 2006).

Complete hydration of C_3S:

$$2(3CaO.SiO_2) + 6H_2O \rightarrow 3CaO.2SiO_2.3H_2O + 3Ca(OH)_2 \quad (2.1)$$

This is expressed in cement nomenclature as:

$$2C_3S + 6H \rightarrow C_3S_2H_3 + 3CH \quad (2.2)$$

Complete hydration of C_2S:

$$2(2CaO.SiO_2) + 4H_2O \rightarrow 3CaO.2SiO_2.3H_2O + Ca(OH)_2 \quad (2.3)$$

This is expressed in cement nomenclature as:

$$2C_2S + 4H \rightarrow C_3S_2H_3 + CH \quad (2.4)$$

There is another type of cavity in the concrete that is germane to this topic. Water occupies space in the plastic paste of the concrete. As the reaction progresses some of the space that was originally occupied by the water is replaced by the product of the hydration. The residual space is called capillary pore (Neville, 2005). The hydrated product occupies more volume than the cement particles and therefore as hydration advances it will continue to expand into the capillary. Entrapped air and entrained air also occupy spaces in the concrete. The latter only exist when air is deliberately incorporated in concrete to improve for example, the concrete's resistance to freeze thaw effects. Entrapped air is the result of incomplete compaction of the cementitious material. These cavities contribute to the overall porosity of the cement and hence of the concrete of which it constitutes a part. The ranges of dimensions of the phases in the hardened cement paste are shown in Figure 2.2.

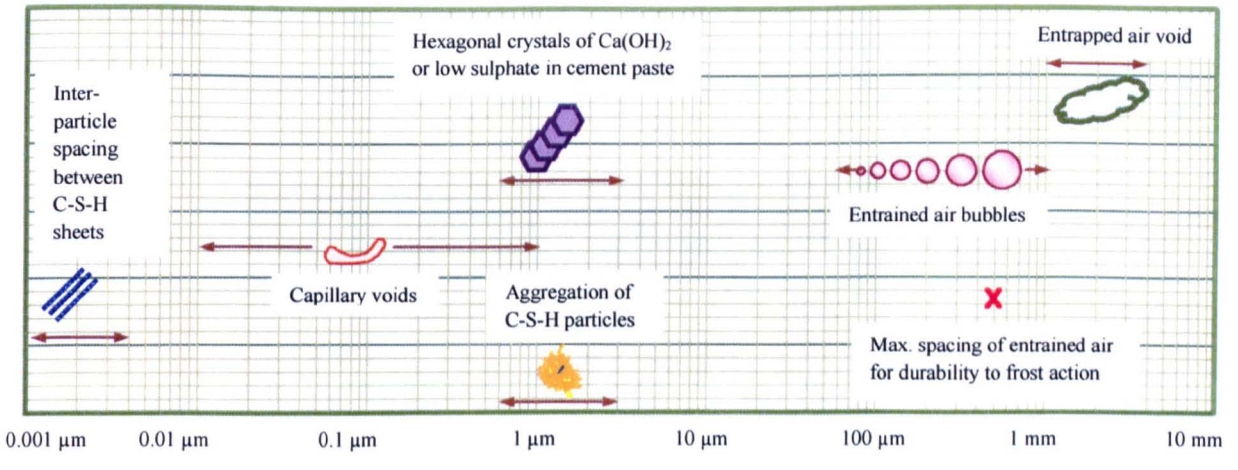

Figure 2.2 Typical dimensions of the different phases in the hardened cement paste
Source: Mehta and Monteiro, 2006

The aggregate-mortar interface warrants examination to determine its role in the porosity of concrete. The aggregates normally do not participate in the hydration process and therefore the growth of C-S-H in this zone is one-sided. Additionally, the packing density of the finer particles is low in this region. Both of these effects contribute to high level of porosity that is evident in the interfacial transition zone (ITZ). Some authors report that the width of this zone is up to 35 μm (Taylor, 1997) while others give measurements up to 50 μm (De Schutter et al, 2008).

The influence of compaction on the interfacial transition zone and the permeability of the concrete were studied by Leemann et al. (2006). Two types of traditional concrete (TC) and one self-compacting concrete were studied using optical microscope and environmental scanning electron microscope (ESEM). An image produced by the optical microscope (OM) is shown in Figure 2.3.

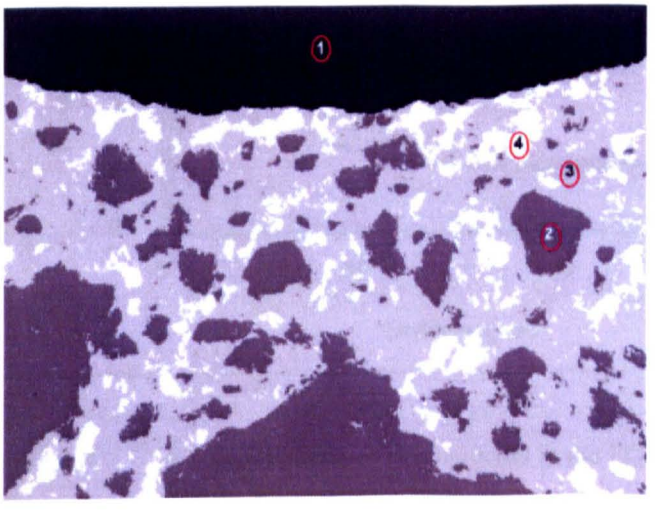

Figure 2.3 Paste below aggregate particle: black: aggregate (1), dark grey: aggregates and anhydrous cement (2), grey: unspecified areas (3), and light grey: porous paste (4)
Source: Leemann et al, 2006

The relative volume share of each different class in the two tests was analysed in relation to its distance to the aggregate. The ITZ in the study is defined as the area having pores and porous paste over 20% more than that of the bulk paste. The results of the study showed that the porosity in the interfacial zone is greater than that of the bulk paste in all three concrete mixes. However, the width of the ITZ in the SCC was 50 μm, which is 20 μm less than that of the TC samples. Figures 2.4 and 2.5 respectively, show that the volume of porous paste and the volume of pores were lowest in SCC. This is important as the reduction in porosity (if there is reduced connectivity between pores) can decrease the penetrability of the concrete and increase the durability. This would support statements made on the improvement in durability resulting from SCC.

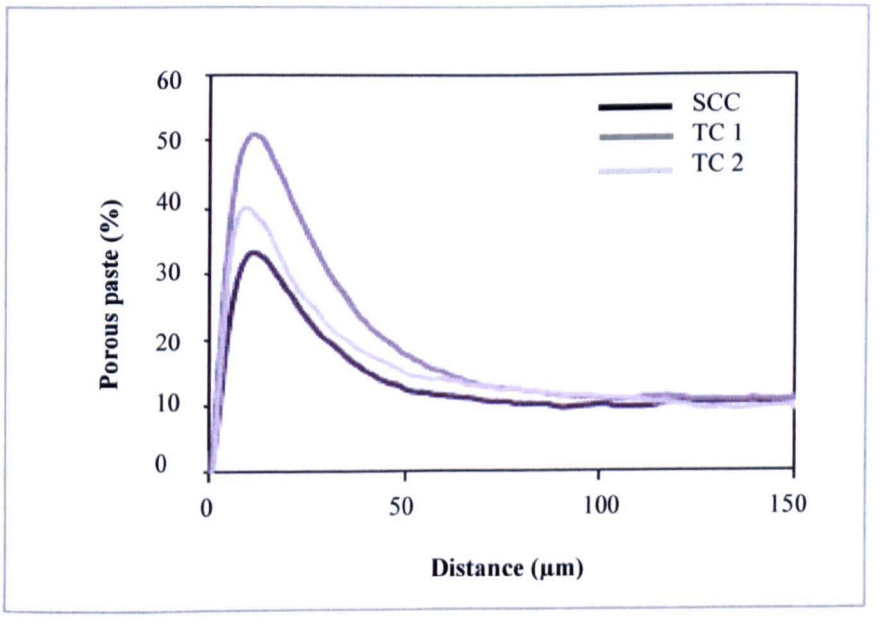

Figure 2.4 Average volume of porous paste in the ITZ (OM)
Source: Leemann et al, 2006

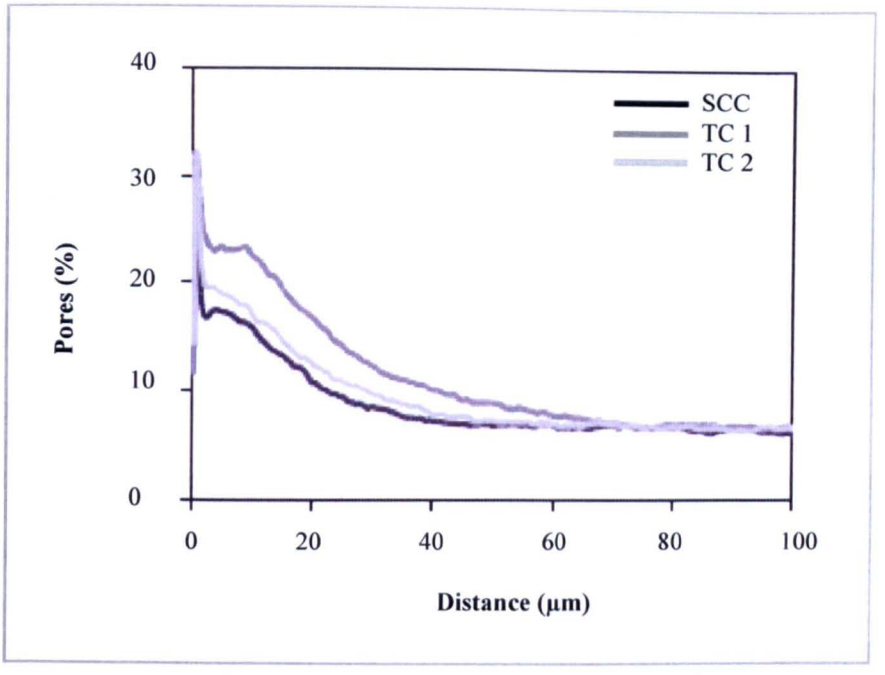

Figure 2.5 Average volume of pore in the ITZ (ESEM).
Source: Leemann et al, 2006

2.2.2. Hydration Process

Hardened concrete is a conglomerate of aggregates in a hydrated cement paste. The hydration of the cement is considered mainly an exothermic reaction which commences on the exposure of ordinary Portland cement particles to water. There are several periods in the hydration of cement paste (Hewlett, 1998).

Pre-induction period: This describes the very early stage in the hydration process after the rapid release of the ions from the C_3S, C_2S, C_3A, C_4AF and other minor phases from the cement into the mixing water. The cement reaction occurring in this period produces a high rate of heat evolution just a few minutes after the introduction of water. The development of calcium silicate can be seen in this stage.

Induction period: This stage, sometimes referred to as the dormant period, describes the stage of slow rate of hydration following the pre-induction period. At this time the

cement paste displays good workability for 1 to 2 hours (Neville, 2005). It is postulated that the reduction in hydration rate is a result of the early products formation at the surface of the cement particles, suggesting that this formation hinders the hydration of the non-reacted cement particles.

Acceleration period: This slow acceleration period occurs at about 3 to 12 hours after exposure to water and brings about setting of the cement. There is hydration of more grains as the surface covering is removed. Hydration of C_3S increases while the reaction of C_2S commences.

Post-acceleration period: There is a marked deceleration in the hydration rate as the quantity of non-reacted cement is reduced and this chemical reaction is controlled by the diffusion in the newly formed structure.

In SCC the microstructure of the concrete is modified by the addition of appreciable fine particles (Skarendahl, 2003) such as fly ash, pulverised limestone, silica fume and ground granulated blastfurnace slag. This modification may be the result of several mechanisms and the changes may be evident in the setting. Poppe and De Schutter (2005) studied the effect of high filler content cementitious materials on the heat of hydration. The samples were made with limestone and granite fillers and with different types of cements. One sample (1) made without filler was used for reference. Powder mixes were used for the isothermal hydration tests. From results of the test, the relationship between heat of hydration rate q (expressed in J/gh) and time was determined for each type of paste (Figure 2.6).

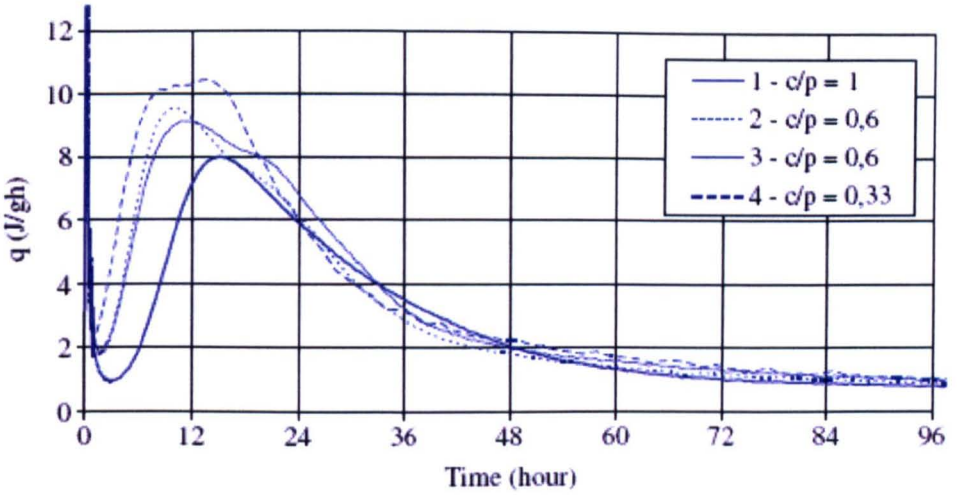

N.B. c/p = cement/powder ratio

Figure 2.6 Heat production rate for mixtures with CEM I 42.5 and limestone filler at 20°C
Source: Poppe and De Schutter, 2005.

Comparison of the curves shows that whereas the ordinary Portland cement paste has one peak in the acceleration period, the pastes made with limestone filler each had two peaks. Additionally, the graph reveals that the limestone filler pastes have shorter induction periods and higher heat production rates. The degree of reaction (r), defined as the fraction of heat that is produced at any point in the hydration process, was also determined using Equation 2.5.

$$r(t) = \frac{Q(t)}{Q_{max}} = \frac{1}{Q_{max}} \int_0^t q(t)dt. \qquad 2.5$$

The total heat of hydration Q_{max} (J/g) was found in the isothermal hydration test. Figure 2.7 shows the temperature of SCC and traditional concrete samples as time elapsed in the adiabatic test. The samples of SCC were made with the same type of filler used in the isothermal tests. The reference traditional concrete (TC) sample for each type of SCC is provided. For each type of test this paradigm is shown – the hydration reactions of SCC and powder pastes with limestone filler are modified as shown in Figure 2.8.

One of the hypotheses that Poppe and De Schutter (2005) used to account for the apparent increase in reaction activity is the generation of nucleating sites in the filler rich cement paste. This would concur with statement given by Neville (2005) as to the improvement imparted by the incorporation of limestone in cement. It is believed that limestone is inert and therefore does not contribute any direct cementitious value to the cement, but the fine particles serve as nucleating sites which promotes the hydration of cement grains.

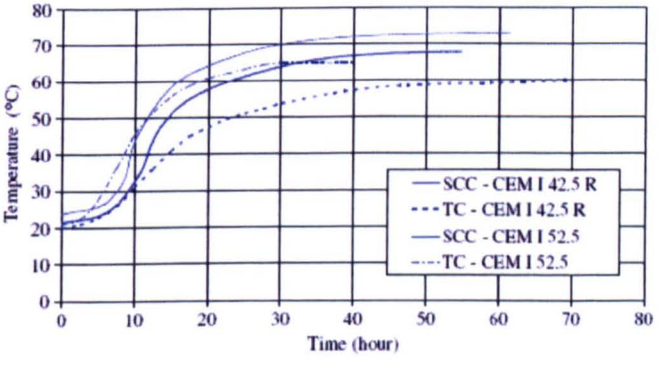

Figure 2.7 Results of adiabatic hydration tests
Source: Poppe and De Schutter, 2005

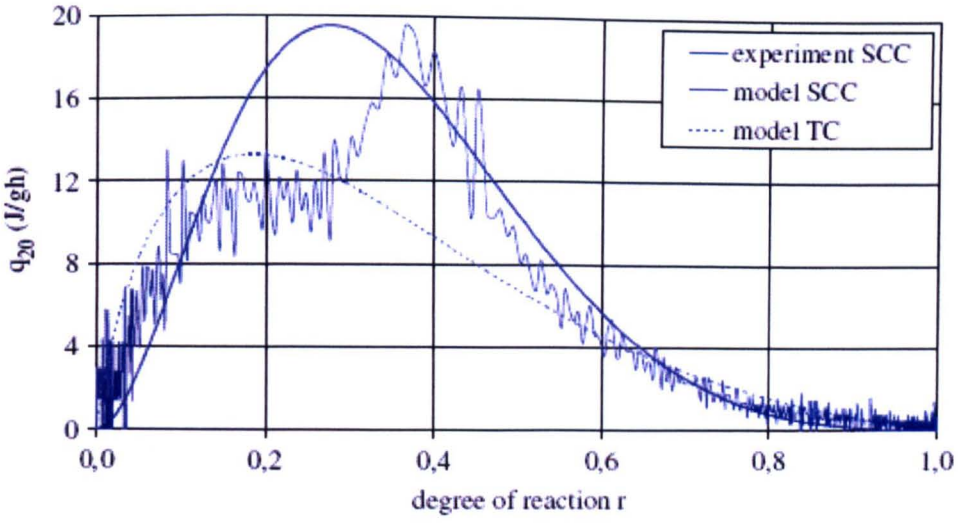

Figure 2.8 Adiabatic test CEM 1 42.5 R
Source: Poppe and De Schutter, 2005

2.2.3. Shrinkage

Shrinkage is an important concrete property as, depending on the magnitude, it can result in problems relating to dimension stability of concrete structures. There are three main classifications of concrete shrinkage. Plastic shrinkage takes place when the concrete is in its plastic state. As the hydration process advances, the volume of the plastic cement paste becomes less than the volume of the original mixing water and the dry cement. This results in shrinkage. Other factors such as evaporation can have an effect on plastic shrinkage. Autogenous shrinkage occurs after the concrete has set. The continued hydration process consumes more water and if water from external sources is not allowed to enter the system, water is extracted from the capillary pores to advance hydration – a process that is referred to as self-desiccation (Neville, 2005). At the end of a curing period the hardened concrete will begin to lose moisture. Moisture will be lost from the pores and eventually from the crystallized hydrates. This is the drying shrinkage that is associated with concrete. As the drying progresses the shrinkage in concrete is increased.

Studies carried out by Gram and Piiparinen (1999) show that plastic shrinkage is higher in SCC than normal concrete (Figure 2.9). This was later confirmed by Turcry and Loukili (2003). Nevertheless it is stated that plastic shrinkage is shown to be both higher and lower than those in vibrated concrete (De Schutter et al, 2008). Reports also suggest that the autogenous shrinkage displayed in SCC is the same or higher than that for vibrated concrete. Drying shrinkage too has values that fluctuate between the same as or a bit lower than the normal concrete. In explaining the discrepancy, De Schutter et al (2008) state that the increase in water/cement ratio normally enlarges the shrinkage as the porosity is increased. However, this effect is less pronounced in SCC as the surface area of fine particles requiring 'wetting' is higher in SCC.

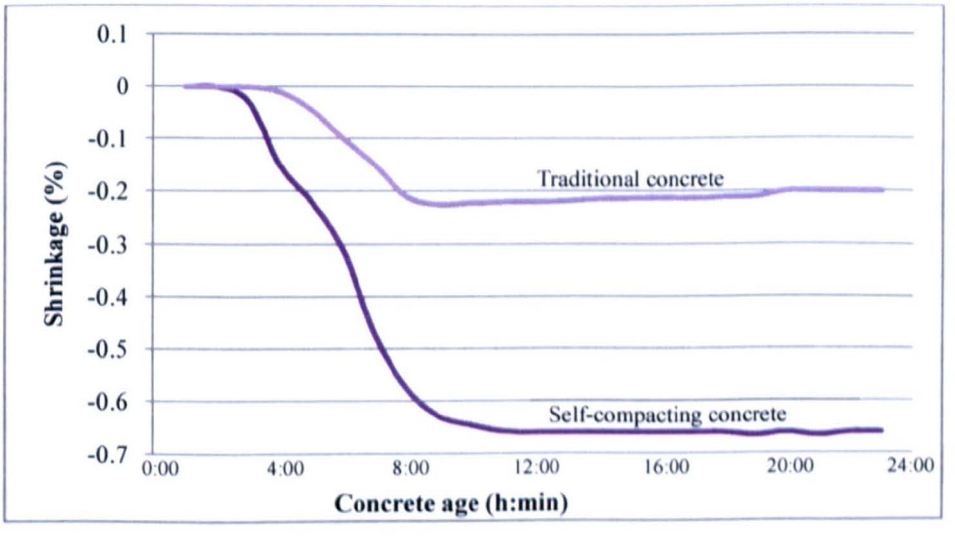

Figure 2.9 Plastic shrinkages of SCC and traditional concrete used in housing construction
Source: Gram and Piiparinen, 1999

What is evident, however, is that self-compacting concrete has little or no bleed water (Holton, 2004). This should be advantageous in that it militates against plastic settlement. Significant reduction in bleeding on the other hand increases the potential of high plastic

shrinkage cracking and therefore curing measures should be implemented immediately after casting (Holton, 2004) to minimize this injurious effect. This need is greater for concrete with large exposed surfaces.

2.2.4. Compressive Strength

The compressive strength of self-compacting concrete was of concern mainly because the concrete defies the established 'unspoken' maxim that highly fluid concrete has a great proclivity to segregation – a thought alluded to by Gibbs and Zhu (1999). It may be less of a concern currently as there are numerous reports that SCC can achieve higher than or at least the same strength as normal concrete. EFNARC (2005) for example describes SCC as a homogeneous material with very little voids that has the potential to produce high strength at early age.

Gibbs and Zhu (1999) conducted tests on SCC to determine the strength characteristics of hardened concrete. SCC and traditional concrete (reference concrete) with characteristic cube strength of 35 MPa were examined. The SCC was made with very fine limestone powder. The 28-day compressive strengths for the SCC and conventional concrete were 47.2 MPa and 37.1 MPa respectively. The development of strength for each type of concrete is shown in Figure 2.10. The rates of development of strength with respect to the 28-day strength are graphed in Figure 2.11. The compressive strength tests were also carried out on columns made with SCC and with traditional concrete. The results confirmed that the 28-day strength of SCC was higher than traditional concrete for each corresponding elevation where samples were taken from the column.

EFNARC (2005) confirms that at the same water/ powder ratio the strength of SCC is higher than that of traditional concrete. Skarendahl (2005) too states that, based on experiential work, the strength of SCC is higher than traditional concrete at the same water/cement ratio.

The higher strength is ascribed to the modification in the morphology of concrete. It is explained that the constitution of SCC as well as the absence of vibration result in an improved microstructure (Skarendahl, 2005). More specifically, it is stated that tightness especially in the interfacial transition zone contributes to a higher strength in SCC.

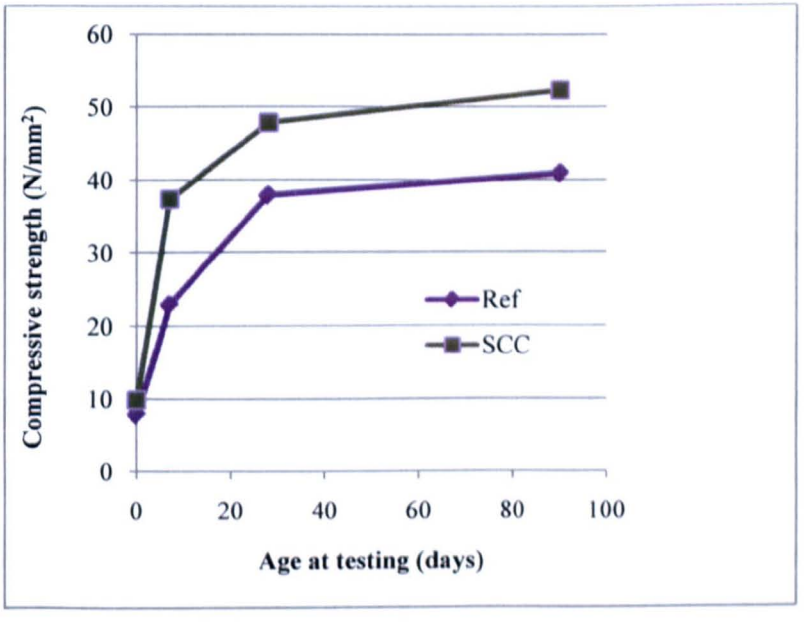

Figure 2.10 Pattern of strength development of SCC and reference concrete samples
Source: Gibbs and Zhu, 1999

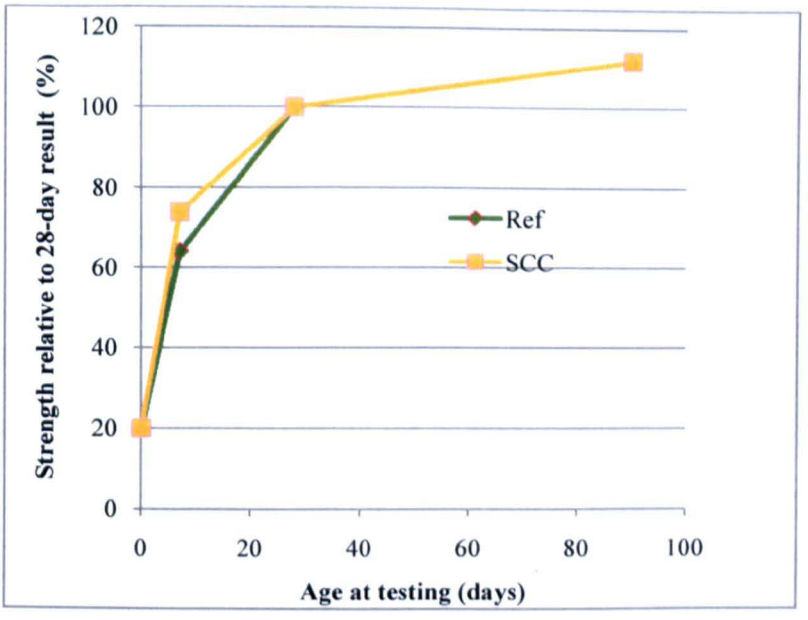

Figure 2.11 Compressive strengths (%) at different ages relative to 28-day strength, Source: Gibbs and Zhu, 1999.

2.3. CONSTITUENTS OF SELF-COMPACTING CONCRETE

The materials that are used in self-compacting concrete are described in this section.

2.3.1. Powder

The term powder refers collectively to all particles less than 150 μm in size (the actual value varies with the location) that are used in the concrete mix. This includes cement, mineral admixtures and the fine particles of fine and coarse aggregates. A high proportion of powder is used to produce the rheological behaviour that optimizes the functions of self-compacting concrete. In regard to hydraulic cement, its content has to be limited to prevent high heat generation. Early studies on SCC were based on the use of low heat, high belite content Portland cement but ordinary Portland cement with mineral admixtures is now used extensively. The mineral particles may be found as additions in the cement or as admixtures in the concrete. The main mineral particles used are pulverised limestone powder, fly ash,

microsilica and ground granulated blast furnace slag. The cement-substitutes import properties which help in the improvement of rheology, stability, and resistance to cracking (De Schutter et al, 2008).

2.3.2. Aggregates

Both fine and coarse aggregates are used in the production of self-compacting concrete. For coarse aggregates, it is recommended that the maximum size used is 20mm to reduce the risk of blocking in the vicinity of steel bars during the flow of SCC (The Concrete Society, 2005). Although larger particles increase the likelihood of segregation and should be avoided, aggregates as large as 40 mm were used in the SCC for the construction of the Akashi-Kaikyo Bridge in Japan (Okamura and Ouchi, 1999). Smooth, rounded aggregate particles are advantageous to the workability of SCC but crushed aggregates are commonly used, primarily because of availability as explained by De Schutter et al (2008). Researchers found that of 63 cases studied between 1993 and 2003, seventy-five percent used crushed rock as coarse aggregate in SCC mixes (De Schutter et al, 2008). As in conventional concrete, the ordinary fine aggregate complying with recognised standards is also used in SCC but the very fine particles are classified as powder. Fine aggregates with spherically shaped particles contribute to higher flow characteristics and hence are preferred. Compared to crushed sands, natural silica sands not only have rounded particles but contain fewer grains finer than 125 μm (if properly washed) and hence are more attractive for use in SCC.

For a given volume of SCC, the total aggregate content is usually less than traditional concrete (TC) that is vibrated. This reduction minimizes the packing density of the larger particles (especially in the case of coarse aggregates) and hence reduces the propensity for

blockages. Figure 2.12 shows graphically typical percentages of materials in the traditional concrete and SCC mixes from the US perspective. With regards to grading of the total aggregates, particles size distribution complying with a well graded curve is preferred for SCC. Researchers studied some SCC mixes and found that the particle size distribution of all particles (inclusive of powders) satisfy the Funk and Dinger's equation (Equation 2.6) when w is equal to 0.25 (De Schutter et al, 2008) whereas with the traditional concrete a value of 0.5 produces a better fit for the grain size distribution (Figure 2.13).

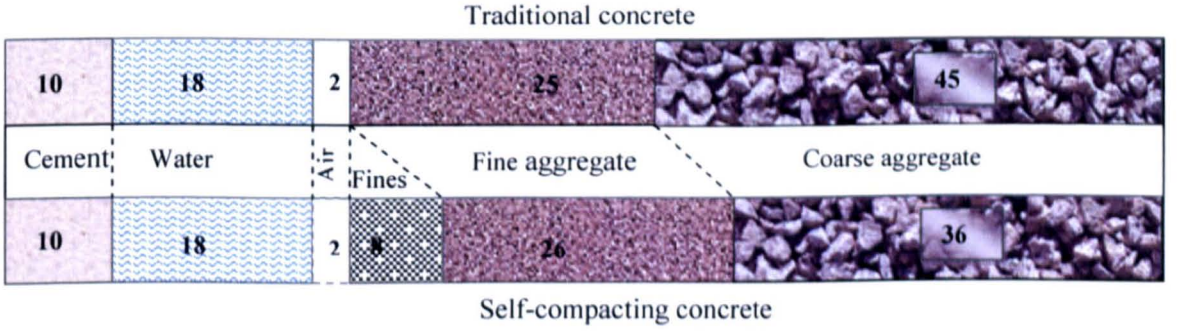

Figure 2.12 Comparison of proportions of ingredients in traditional self-compacting concrete
Source: Kosmatka et al, 2008

$$P(D) = \frac{(D^w - D^w_{min})}{(D^w_{max} - D^w_{min})} \qquad 2.6$$

Where $P(D)$ is the amount passing sieve size D (expressed in fraction),
D_{min} is the minimum particle size,
D_{max} is the maximum particle and
w is a constant.

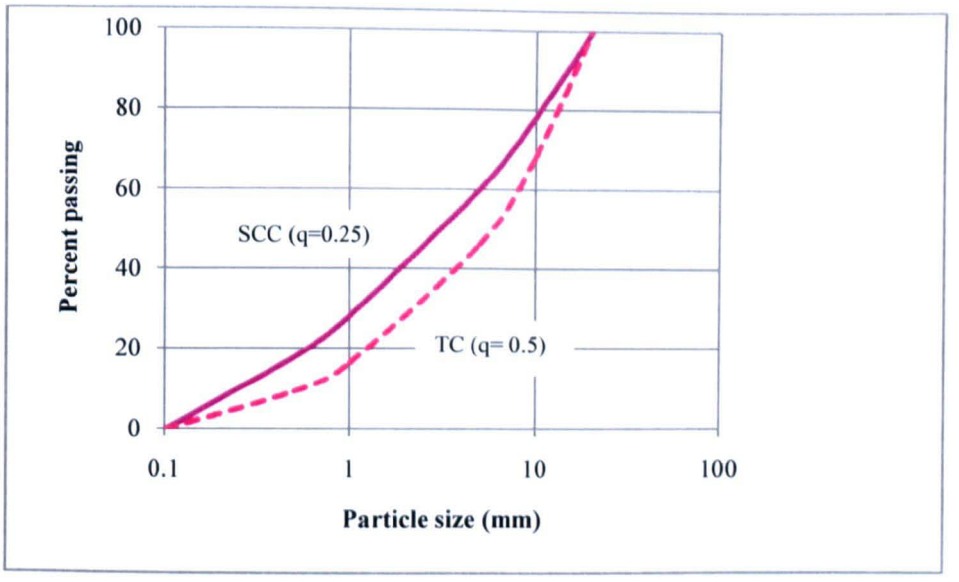

Figure 2.13 Preferred aggregate grading curves for SCC and TC
Source: De Schutter et al, 2008

2.3.3. Chemical Admixtures

Chemical admixtures play an important role in imparting properties that enhance the rheological behaviour of self-compacting concrete. The chemical substances utilized in SCC to improve on viscosity and yield stress are viscosity modifying agent and superplasticiser, respectively.

2.3.3.1. Superplasticiser

Superplasticisers, otherwise known as high range water reducing admixtures (HRWRA) are used effectively in SCC to impart qualities that produce flowing concrete. The newest formulation in superplasticiser is of polycarboxylic ether-base. Whereas the precursors, sulphonated melamine and naphthalene formaldehyde-based superplasticisers essentially served their purpose but showed some limitations in compatibility with some cement

properties, the polycarboxylate-based brands display a greater capacity to achieve the desired characteristics of high performance concrete. Compared to its counterparts, the use of polycarboxylate based superplasticisers results in lower water requirement and slower slump loss (McGovern, 2002).

High fluidity is essential for achieving the characteristics of SCC but the water requirement has to be kept at a minimum to ensure adequate viscosity. Superplasticiser is therefore introduced to provide the required fluidity while maintaining a low water/powder ratio in the mix. A certain minimum shear stress, referred to as yield stress is required for deformation to take place in the ordinary concrete. The addition of superplasticiser to SCC reduces the yield stress in the concrete to a low value. When the value is very low, a flowing concrete is achieved. The effectiveness of superplasticiser at increasing the consistency of concrete is achieved mainly through two mechanisms.

Typically, the superplasticisers are designed with charged side chains attached to a main molecular backbone (Figure 2.14). In a superplasticised concrete mixture, the admixture is adsorbed on the hydrating product (Rixom and Mailvaganam, 1999) resulting in negative charges on the surface of the cement particles. The result is an electrostatic system with particles repelling each other, causing dispersion in the system. The principle of stearic hindrance is also employed whereby the side chains are strategically designed to physically maintain separation (as shown in Figure 2.15) between particles (Winnefeld et al, 2007). This deflocculated system is now able to release any water that was trapped in the cement floccules and increase workability.

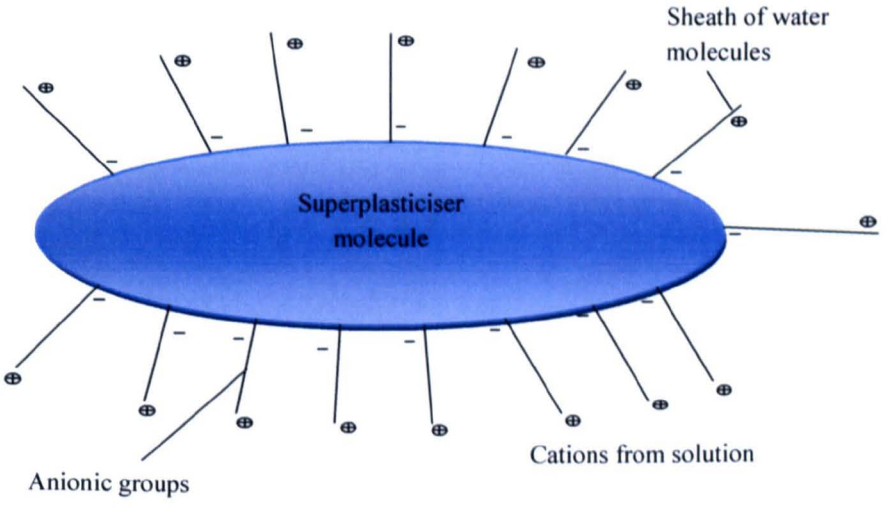

Figure 2.14 Representation of a superplasticiser molecule
Source: Hewlett, 1998

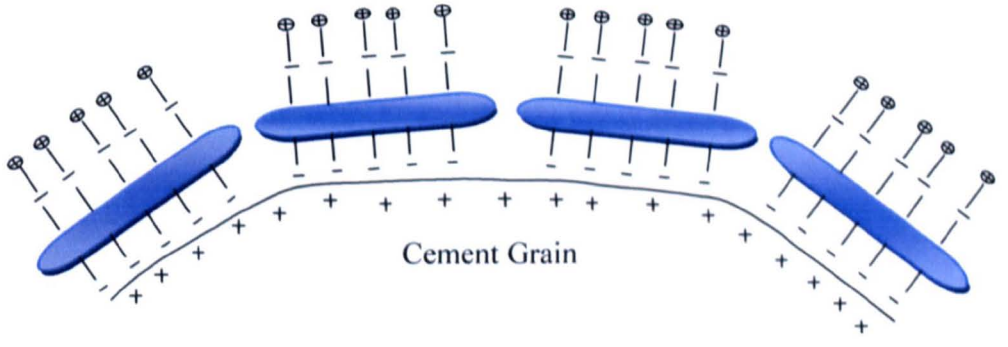

Figure 2.15 The mode of adsorption of superplasticiser on cement particle
Source: Hewlett, 1998

2.4. RHEOLOGY

Rheology is defined as the study of the flow of substances. The flow of most liquids is analysed as a Newtonian fluid in which the shear stress τ is proportional to the strain rate, $\bar{z}$, (Equation 2.7) and the constant for proportionality is the viscosity, η, (Tattersall and Bandfill,

1983). The relationship of shear stress, strain rate and viscosity is presented in Figure 2.16 where it is shown that the shear rate depends on the shear stress imposed on the fluid.

$$\tau = \eta.\bar{z} \qquad 2.7$$

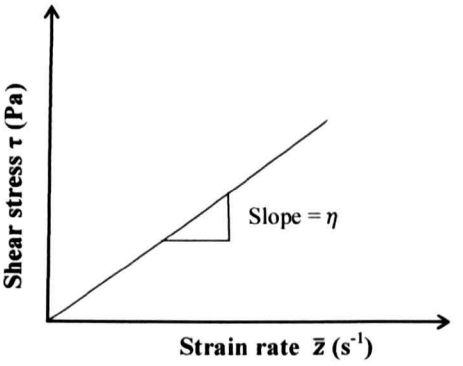

Figure 2.16 Typical shear stress/strain rate relationships of Newtonian fluids
Source: De Schutter et al, 2008

There are other types of fluids that will not deform until a certain amount of shear stress is applied. The shear stress that is required to initiate the flow is called yield stress τ_0. For example, line (b) in Figure 2.17 shows a liquid that commences flow at a given yield value and from there on has a linear relationship between shear stress and shear rate. This is typical of a certain type of non-Newtonian flow that fits the Bingham model (Tattersall and Bandfill, 1983) and the line is defined mathematically as:

$$\tau = \tau_0 + \eta\bar{z} \qquad 2.8$$

Figure 2.17 also shows two curves representing the behaviour of materials that have a yield point and experience viscoplastic shear. Curve (a) represents materials that have a reduction in viscosity (shear thinning) when the strain rate is increased and curve (c) is typical of materials that show an increase in viscosity (shear thickening) when the strain rate is increased (De Schutter et al, 2008).

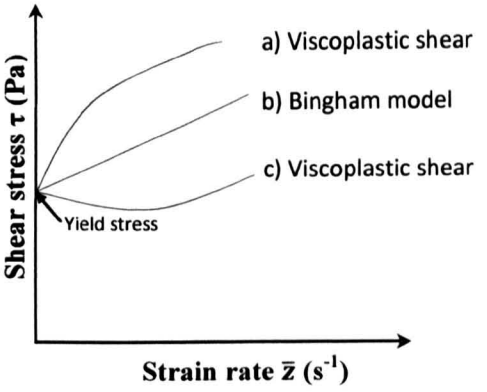

Figure 2.17 Models of non- Newtonian Fluids

2.4.1. Viscosity and Yield Value in SCC

While Ferraris (2005) states that there is evidence to support that at wide range in shear rates, the flow of the traditional concrete can also experience pseudoelastic shear thinning behaviour; there appears to be greater acceptance that the rheological behaviour of traditional concrete can generally categorised as non-Newtonian fluid conforming to the Bingham model. The equation for the Bingham model shows that, the yield stress τ_o has to be attained in the concrete for flow to be effected. In concrete with very high consistency such as that which is achieved in flowing concrete, the yield value is very low. It is believed that for these types of concrete mixes, the Newtonian model better describes the flow characteristics. There

are no established limits on the yield value and plastic viscosity for SCC but Wallevik (2003) showed that in Japan and many western countries, the SCCs used have yield values ranging from 0 - 60 N/mm^2 and values for plastic viscosity between 10 and 120 Pa.s. The rheological behaviour of self-compacting concrete is therefore believed to be better characterised by a Newtonian than a non-Newtonian fluid (De Schutter et al, 2008).

The yield value in SCC has to be very low for flow to be initiated. This means that there should be adequate fluidity or consistency in the concrete. In the traditional concrete, water is often used to help control the consistency. In SCC, the water content is kept low to ensure a low water/powder ratio. Consequently, high range water reducing admixture also known as superplasticiser is invariably utilised in SCC. The superplasticiser is efficacious in reducing the yield value and imparting mobility to the concrete.

Viscosity can be defined as that property that provides resistance to shear. To obtain an adequately viscous paste in SCC, a low water/powder ratio is needed. Additionally, high powder content is required to provide the requisite volume of paste. Powders such as fly ash, ground granulated blastfurnace slag, silica fume and limestone are used to augment the cement volume. Using mineral admixtures not only helps to achieve the desired powder volume and viscosity but also increases the economy of the product and helps to militate against an otherwise adverse effect that would be brought on by the high heat of hydration from a high cement content.

The characteristics and proportions of the constituents of SCC are integral to the attainment of self-compactibility. Emborg (1999) investigated the influence of a) aggregates, b) filler, c)

cement content, d) water content, e) superplasticiser and d) viscosity agent on the rheological parameters of SCC. Although some of the samples in the study could not be categorised as good examples of SCC, Figure 2.18 summarises the results of the study. The relationships of some of the variations in ingredients with rheological parameters h_c and g_c are close to that of viscosity and yield stress shown by Wallevik, (2003). It is interesting to see that the substitution of one type of natural fine aggregate, 0-8 mm (type A), to another natural fine aggregate of the same nominal size (type B) can result in noticeable changes in plastic viscosity and yield value and probably is indicative of the sensitivity of SCC.

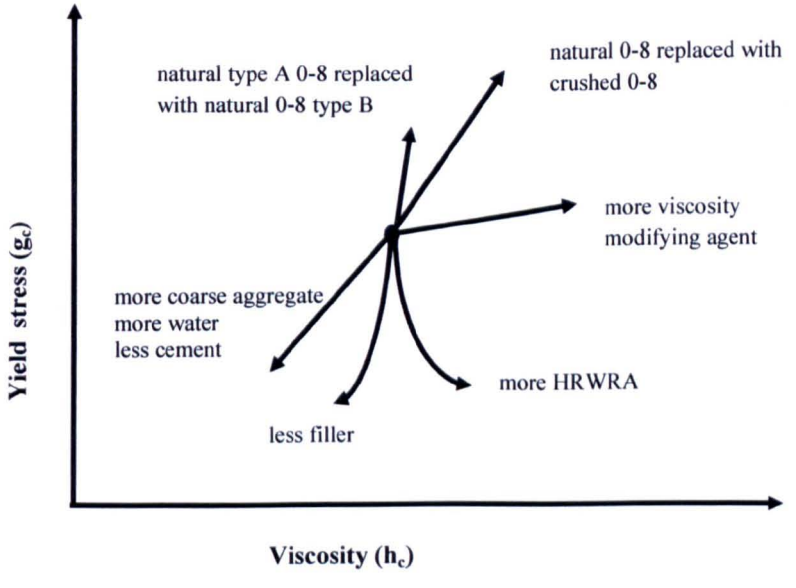

Figure 2.18 Possible influences on an original concrete mix when changing the composition Source: Emborg, 1999

2.5. COMPACTION IN SCC

In order to achieve self compactibility there has to be high deformability as well as segregation resistance (Okamura and Ouchi, 2003b). Although the main ingredients used in

self-compacting concrete are basically the same as those used in conventional concrete, there are significant differences in the proportioning of the ingredients in SCC mainly with the objective of achieving these two properties. Okamura and Ouchi (2003b), who pioneered the development of SCC, show in Figure 2.19 the method of achieving self-compactibility in mixes that use high powder content to achieve the desired viscosity.

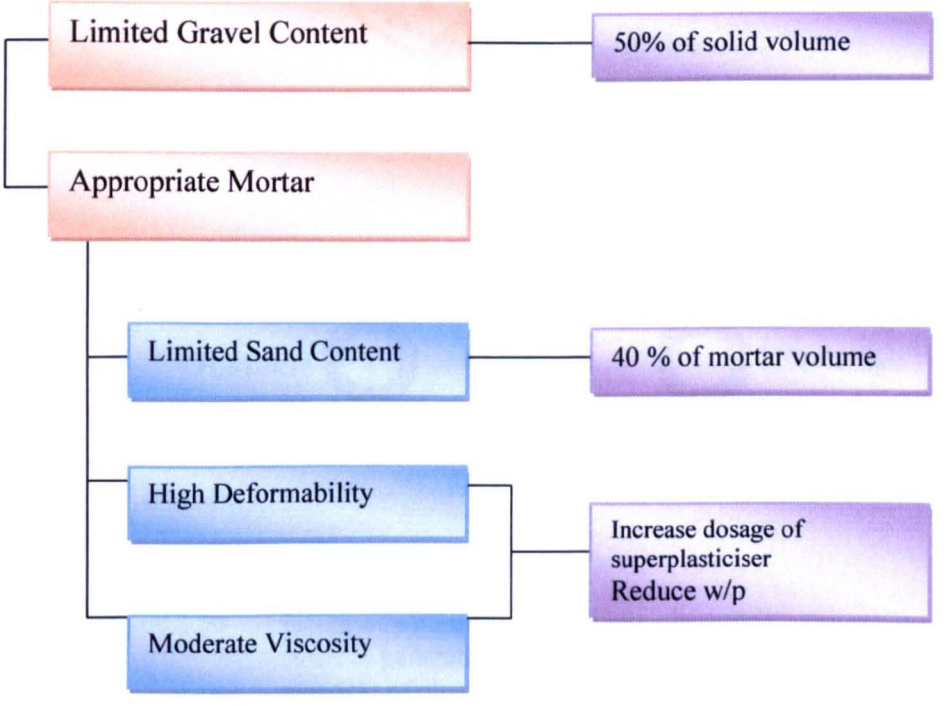

Figure 2.19 Method of achieving self-compactibility in SCC
Source: Okamura and Ouchi, 2003b

The viscosity of the binder is very influential in the performance of the aqueous and solid phases in the plastic SCC. The viscosity has to be sufficiently high to ensure that the heavy particles are kept afloat (Kosmatka et al, 2008). The viscosity of the paste is also instrumental in the prevention of blockage in the vicinity of obstacles. As flow takes place in the presence of obstacles, the mortar deforms while the packing of the particles is increased (Ouchi and

Edamatsu, 1999) (Figure 2.20). This sequence of events causes an increase in the normal stress σ_e and an increase in the shear stress τ due to deformability resistance (Ouchi and Edamatsu, 1999). SCC with a viscous paste is able to prevent or reduce the build-up of localised internal stress when deformation takes place (Ouchi, 2005).

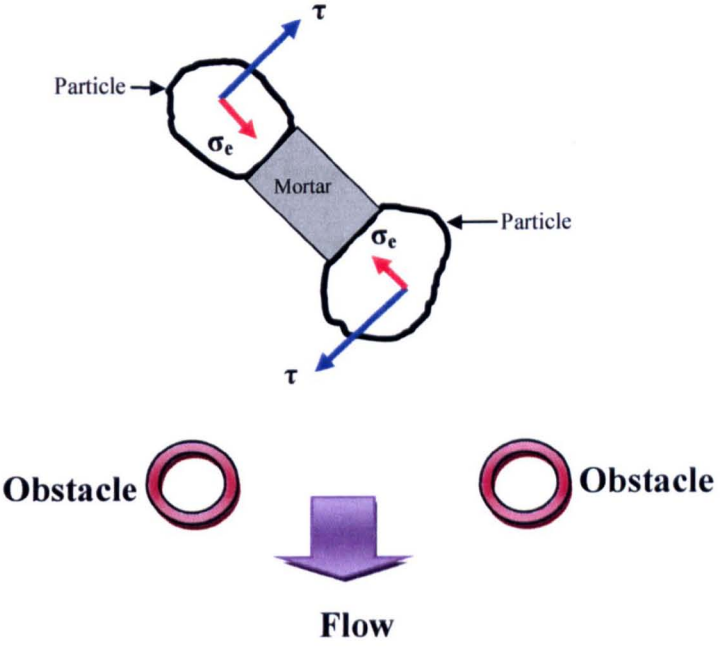

Figure 2.20 Increase in mortar's shear stress τ due to the normal stress σ_e generated when concrete deforms in the presence of obstacles
Source: Okamura and Ouchi, 2003b

2.5.1. Stability

Stability is a property that describes the ability of the concrete to keep solid particles uniformly in suspension during handling. It is the same property as segregation resistance. Concrete with higher viscosity is better able to resist segregation of the granular constituent. This is because the more viscous (and dense) mixture is capable of maintaining buoyancy of the heavy particles (Neville, 2005). Bleeding is a phenomenon that is associated with

segregation. The evidence of bleeding can be seen in the layer of water that rises to the surface of fresh concrete. A lack of cohesion can result in the aqueous phase separating from the solid phase, an anomaly referred to as pressure segregation. Pressure segregation can also occur when concrete is conveyed through pumping.

All forms of instability are potentially harmful as they not only contribute to low workability but they cause variability in the properties of hardened concrete. Significant segregation can produce weaker and less durable sections in concrete elements. It is reported however that in general, SCC does not show a propensity to bleeding (Holton, 2004). Zhu and Bartos (2003) mentioned that the high powder content and the viscosity enhancing agents help to stem bleeding. Three characteristics that can reduce and in some cases prevent segregation in self-compacting concrete are a) high plasticity, b) the presence of thixotropy and c) slow migration of liquid to the shearing zone (Wallevik, 2003).

2.6. PROPERTIES OF SCC

The ability of this concrete to self-compact is demonstrated by:

- the filling ability,
- the passing ability and
- the segregation resistance.

2.6.1. Filling Ability

As the name implies, this property of concrete refers to the ability of the concrete to flow horizontally and vertically under its own weight, and to fill the form in which it is placed (Petersson et al, 2003). Some of the tests that are used to determine filling ability are the slump flow with the Abram's cone and the J-ring. The slump range for SCC is 550 – 850 mm.

2.6.2. Passing Ability

This property refers to the ability of the concrete to negotiate any obstacles (that is reinforcing bar, constricted spaces, corners etc.) in its path as it flows. This function should be performed without segregation in the concrete or blocking at the juncture where the obstacle appears. The property is influenced by the ability of concrete to flow and fill the spaces and therefore is not totally independent of the filling ability of the concrete. Two tests that are used to determine passing ability are the L-Box and the J-ring.

2.6.3. Segregation Resistance

This characterises the property of the concrete to remain homogeneous during the production processes. Concrete that bleeds and shows sign of settlement is undergoing segregation. Another term that is used to describe this property is stability. The sieve segregation and penetration tests are used to determine segregation resistance in SCC.

2.7. CONCLUSION

The intrinsic properties of SCC presented herein should provide an understanding of SCC and an appreciation of the design of the SCC and the required characteristics of the materials needed for the fresh and hardened properties. Careful attention will have to be paid to the minimum requirements of the materials in order to optimise the attributes of self-compacting concrete.

DURABILITY CONSIDERATIONS

3.1. INTRODUCTION

The durability of concrete can be defined as the ability the material to perform in a manner expected under the defined conditions of use for the time expected. It was once believed that concrete was indeed a durable material that was able to perform in the designed conditions without any maintenance (Al-Amoudi et al, 2003). This is confirmed by Neville (2005) who stated that, for a period of time, strong reinforced concrete was synonymous with durable concrete. However, the deterioration of concrete bridge decks in the USA and Europe, concrete structures in Arabian Gulf (Al-Amoudi et al, 2003) and even in Japan (Okamura and Ouchi, 2003b) has brought greater awareness to the importance of durability characteristics in the design of concrete (Alonso and Andrade, 2002).

There are several deteriorating agents that can prevent concrete from achieving sustainable durability within the designed life but the more damaging agents are those that contribute to the corrosion of the bars in reinforced concrete. It is reported by Al-Mehthel et al (2009) and supported by Al-Amoudi et al (2003) that the corrosion of reinforced concrete is the predominant mode of deterioration in reinforced concrete structures worldwide. In Norway for example, researchers show that corrosion of reinforcement is the most devastating type of deterioration (Maage et al, 1994). In order to place the problem of durability in the right perspective, it should be mentioned that in the majority of cases, reinforced concrete is durable (Broomfield, 2007); however, exposure to aggressive environments such as coastal areas (Vedalakshmi et al, 2009) can contribute to severe corrosion in the reinforcing bars.

Two elements that can produce the deleterious effects of corrosion to steel in concrete are chloride ions and carbon dioxide (Al-Amoudi et al, 2003) but the primary deteriorating agent is chloride ions.

3.2. MECHANISMS OF TRANSPORT

The mechanisms that are associated with the transfer of fluids and ions into concrete are capillary suction, permeability and diffusion (fib, 2002). Capillary suction is the process by which fluids are taken in the pores of the concrete by wicking under the force of surface tension. Sorptivity is the constant of proportionality describing the linear relationship between the degree of uptake of water and the square root of the time for the uptake (The Concrete Society, 2008). The factors that dictate the level of sorptivity are the moisture gradient from the exterior to the interior of the concrete, the size of the pores and the extent of connectivity between pores (Jackson and Dhir, 1996). Absorption test is usually used to measure the volume of pores in the concrete. Technically, permeability refers to the property that describes the ease with which flow of fluids takes place under a pressure differential in the concrete (The Concrete Society, 2008). This too is influenced by the size and connectivity of capillary pores. Diffusion deals with the transmission of gas, vapour or ions through the capillary pores under a concentration gradient. Again, the size and degree of the connection between the capillary pores play an important role in the mechanism. Fick's law (Equation 3.1) shows the relationship between the mass transport rate and the concentration gradient.

$$J = -D_f \frac{\delta c}{\delta l} \qquad 3.1$$

Where:

J = the flux (mass transport rate)
$\frac{\delta c}{\delta l}$ = concentration gradient
D_f = diffusion coefficient

Generally, gases, liquid and ions in the aqueous phase can penetrate the concrete through pores in the binder, the interfacial transition zone and through micro cracks (Zhu and Bartos, 2003) and attack the concrete. Additionally, Pomeroy (1994) explains that the concrete's constituents can also contribute to contamination of the concrete.

In the case of chloride, all three transport mechanisms may occur concurrently (Audenaert and De Schutter, 2003). The chloride ions may be introduced into the concrete by the constituents; usually aggregates, admixtures or the mix water (Saricimen et al, 2002) but if there is adherence to standards such as BS EN 206-1, which gives the maximum chloride limits of concrete for various conditions there should not be any glaring deleterious effect arising from chloride. The external sources of chloride ions are seawater and de-icing salts (Söylev and Richardson, 2008) and the chloride may interface with the concrete through the soil, ground water, atmosphere (Saricimen et al, 2002) or directly. As the ingress of ions on concrete impinges on the durability of concrete, it is paramount that the penetrating capacity of the concrete to chloride be determined.

3.3. CHLORIDE KINETICS

Diffusion is important as it is reported to be the main transport mechanism through which the chloride ingresses reinforced concrete (Page et al, 1981) and triggers corrosion. The penetrability of the concrete dictates the rate at which deleterious substances such as chloride enter the concrete (Güneyisi et al, 2009), and the pore structure governs the penetrability of

the concrete. The development of the pore structure is already covered in Chapter 2 and hence will only be mentioned in brevity here. The paste in the concrete consists of a solid phase with hydrated and un-hydrated cement and an aqueous phase (Yuan et al, 2009). The level of chloride penetration in the interstices in the solid phase is inconsequential (Yuan et al, 2009) hence, the diffusion of chloride takes place in the pore solution of the concrete. The chloride then moves to the surface of the steel. Hence for the technical prediction of corrosion-related durability of reinforced concrete in chloride environment, the rate of the diffusion of has to be determined.

Page et al (1981) studied the coefficient of diffusion of chloride in ordinary Portland cement (OPC) paste with water/cement ratio of 0.4, 0.5 and 0.6 at various temperatures. The average coefficient of diffusion in cement paste with a water/powder ratio of 0.4 at 14.5°C is reported as 12.7×10^{-9} cm^2/s. The other results are shown in Figure 3.1. The tests were conducted in a diffusion cell as shown in Figure 3.2. It was revealed that the coefficients increased with the increase in the water/cement ratio and also with increase in temperature. The results of this work show that the water/cement ratio has a significant effect on the coefficient of diffusion of chloride in cementitious materials.

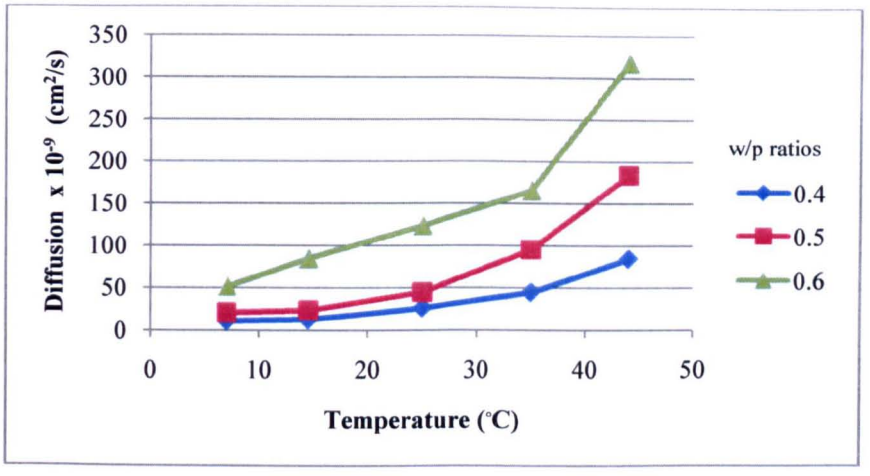

Figure 3.1 Diffusion coefficients of chloride ions in OPC pastes at different temperatures and w/p ratios
Source: Page, Short and Tarras, 1981

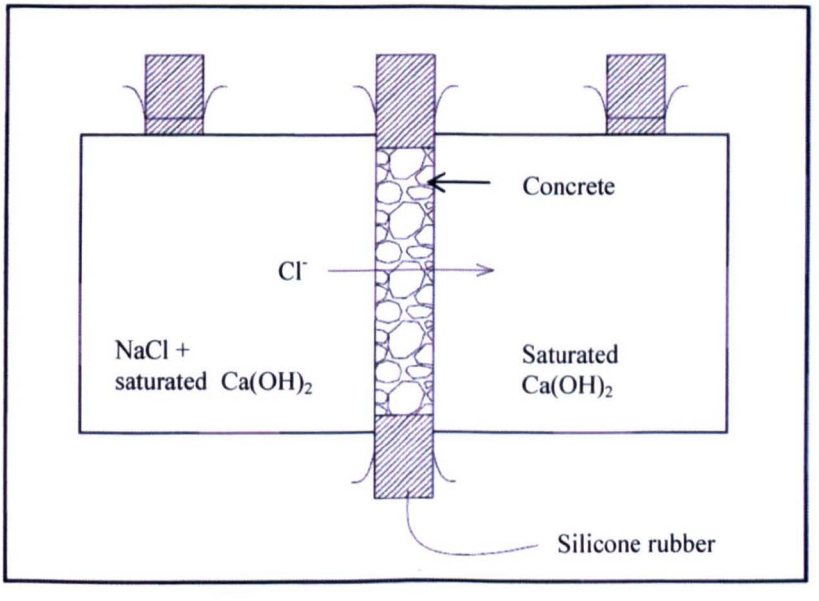

Figure 3.2 Diagram of chloride diffusion cell
Source: The Concrete Society, 2008

Tang and Nilsson (2009) also studied the non-steady state migration of chloride in concrete. A rapid chloride migration (RCM) test with a potential of 30 - 40 V (Figure 3.3) was used. The electromigration of OPC concrete at 28 days was 14.5×10^{-12} m^2/s. As the name implies, this test accelerates the migration of the chloride ions through the concrete and hence gives a quick result. The other commonly used accelerated test ASTM C1202, also reduces the time of testing but it is mentioned that the current conducted in the test is not associated to the chloride ions only but with all the ions in the solution. Besides, the test requires the application of 60 volts across the concrete which is shown to increase the temperature of the pore solution. There are no known issues associated with the RCM test, and it is mentioned that the level of variability is lower with this test than with the ASTM C1202 test.

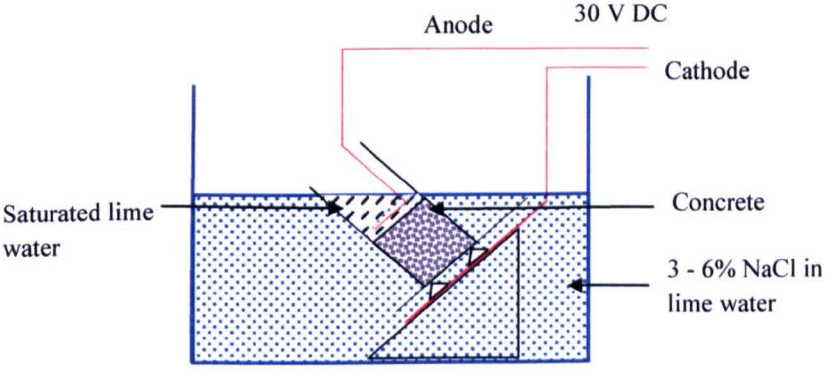

Figure 3.3 Experimental setup of rapid chloride electromigration test

3.4. EXPRESSIONS OF CHLORIDE

The chlorides in concrete can be broken down into free and bound chlorides (Mohammed and Hamada, 2003). Bound chlorides are adsorbed or chemically bonded to the hydrating products. With adsorption, the chloride ions are physically bonded to the walls of the C-S-H. In chemical binding, the chloride reacts with C_3A to form Friedel's salt in accordance with Equations 3.2 and 3.3. However, it is mentioned by Yuan et al, (2009) that C_4F, C_2S and C_3S also contribute to the binding of chloride.

$$Ca(OH)_2 + 2NaCl \rightarrow CaCl_2 + 2Na^+ + 2OH^- \quad 3.2$$

$$C_3A + CaCl_2 + 10H_2O \rightarrow C_3A \cdot CaCl_2 \cdot 10H_2O \quad 3.3$$

With the physical and chemical binding of some of the chloride, it was generally believed that only the residue, referred to as the free chloride contributes to corrosion in reinforcement (Mohammed and Hamada, 2003; Yuan et al, 2009) but under certain condition the bound chloride can become free and move towards the reinforcing bar (Yuan et al, 2009).

3.5. CHLORIDE ATTACK

Cement, when mixed with water in the concrete, produces hydration products with a pH ranging from 12.5 to 13.5. This environment helps in the development of a thin passivity oxide layer on the surface of steel embedded in the concrete. The steel reinforcement in the concrete is protected by this passivation layer (Ngala et al, 2002) and the oxide layer is maintained by the high alkalinity in the concrete. The dependence of the state of the steel on the corrosion potential and the pH in the concrete is demonstrated in Pourbaix diagram (Figure.3.4). This diagram shows that under normal conditions, the pH of the concrete supports passivity of the steel. Therefore, when the concentration of chloride in reinforced

concrete is low, it is ineffective in denuding the protection layer as the hydroxyl ions formed in the pore solution replenish the oxide film (Broomfield, 2007). However, when a sufficiently high chloride concentration is developed in the vicinity of the rebar, the oxide layer can be destroyed (Yuan et al, 2009). This critical concentration that triggers the onset of corrosion is referred to as the threshold value and is expressed as a concentration ratio between the chloride and hydroxyl ions, Cl^-/OH^-. Reports have the threshold value ranging from 0.35 to 1% of the mass of the cement (Alonso et al, 2000; Söylev and Richardson, 2008) but it is generally accepted that the value is 0.6 (Gonzalez et al, 1998).

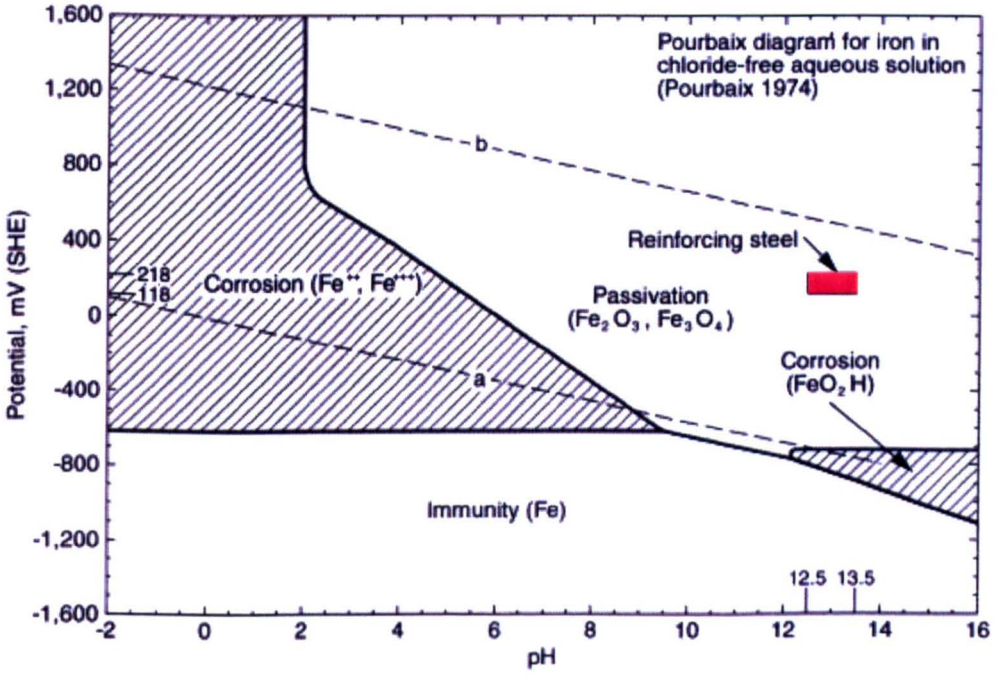

Figure 3.4 Pourbaix diagram for iron with the coloured area showing the ranges of pH and potential values of the steel in the concrete
Source: Shah and Hookham, 1998

There are several factors delineated below, that impinge on the chloride-induced corrosion.

i. The pH of the pore solution has effect on the initiation of corrosion (Alonso et al, 2000). Carbonation of the concrete can reduce the pH from 12.5 to about 11 (Müller and Rubner, 1994) and initiates pitting corrosion on the surface of the steel (Berke and Hicks, 2004).

ii. The characteristics of concrete cover. The composition of the concrete cover can impact on the time to depassivate reinforcing bars in concrete. The type of cement used, for example, can affect the degree of chloride binding. Cements low in C_3A (sulphate resisting cement) show a reduced capacity for chloride binding and hence the Cl^- penetration will be faster in concrete made from this type of cement (Maage et al, 1994). Some pozzolanas and cement replacements, chiefly fly ash, silica fume and ground granulated blastfurnace slag, are shown to increase the resistance of the concrete to chloride, therefore their incorporation in cementitious materials will help to reduce the initiation time for corrosion (Güneyisi et al, 2009).

iii. The availability of oxygen is important in the corrosion process. The oxygen is involved in the cathodic reaction (Vennesland et al, 2007) and when the concrete is submerged in water for example, unless under shallow immersion, the limited availability of oxygen suppresses the corrosion process even at high chloride content.

iv. The relative humidity in concrete also plays a key role in the electrochemical process. The concrete may be in a fairly dry environment and hence water is not available for the corrosion reaction.

3.6. ELECTROCHEMICAL ACTION OF CORROSION

As mentioned before, the passivation layer on the steel safeguards it against corrosion. At the critical chloride concentration at the steel interface, the layer can be penetrated and pitting corrosion is initiated in the presence of moisture and oxygen. Corrosion is an electrochemical phenomenon and the locations of the anode and cathode in the reinforced concrete are on the surface of the steel bar (Söylev and Richardson, 2008). The electrochemical process of corrosion of steel in concrete comprises four distinct parts (Vennesland et al, 2007; Bertolini et al, 2004) as explained below with Equations 3.4 – 3.5.

i. Oxidation of iron. Electrons are freed when iron is oxidized. The ferrous ions formed enter into the pore solution (electrolyte). The reaction promotes acidity.

$$Fe \rightarrow Fe^{2+} + 2e^{-} \qquad \text{Anodic reaction} \qquad 3.4$$

ii. Conveyance of electrons through the metal. The electrons move from the anodic site to the cathodic site. This produces a small electric current flowing in the opposite direction.

iii. Reduction of oxygen. The freed electrons are consumed in this reaction at the electrolyte. This reaction promotes alkalinity.

$$O_2 + 2H_2O + 4e^{-} \rightarrow 4OH^{-} \qquad \text{Cathodic reaction} \qquad 3.5$$

iv. The flow of current in the concrete pore solution. Transported by ions from the anodic region to cathodic region.

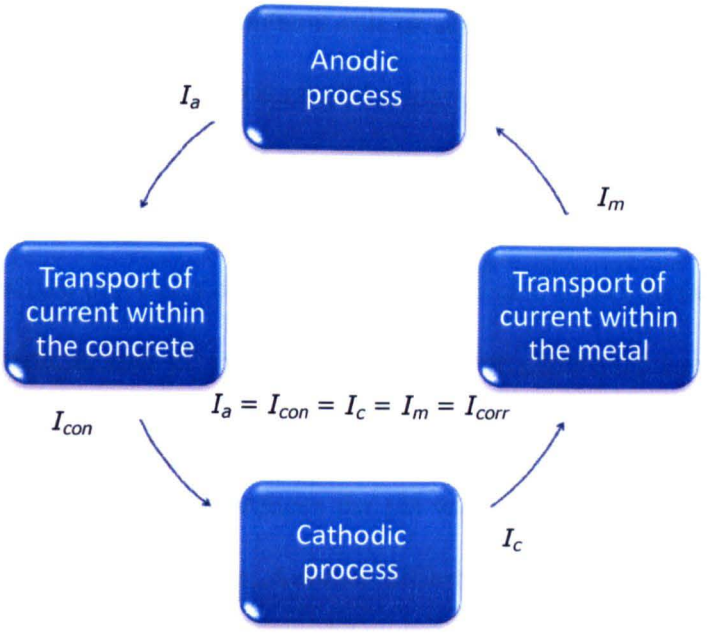

Anodic process

Iron + water → corrosion products of iron + acidity + electrons (within the metal phase)

Cathodic process

Oxygen + water + electrons (from the metal phase) → alkalinity

Transport of current within the concrete

Ion movement in the presence of water; enhanced by increase in pH and presence of chloride

Transport of current in the metal

Electrons move from the anode, where they are produced, towards the cathode, where they are consumed

Figure 3.5 Electrochemical mechanism of corrosion of steel in concrete
Source: Bertolini et al, 2004

Where:

I_{con} = current in concrete

I_a = current in the anode

I_m = current in the steel

I_c = current in the cathode

The four parts together form a galvanic cell as seen in Figure 3.5 (Vennesland et al, 2007) and the current that flows between each of the four parts is equal.

Pitting is a localised corrosion process (Berke and Hicks, 2004). In many ways the principle of pitting is same as that of general corrosion. One difference however is that with the establishment of pit, the chloride ions and ferrous ions form compounds as shown in Figure 3.6 (Gonzalez et al, 1998), that reduces the pH within the pit (Berke and Hicks, 2004) and exacerbates the corrosion process. Another difference is that the pore water system is the electrolyte, accounting for the high electrical resistivity of the concrete (Vennesland et al, 2007). The progress of corrosion, which is measured by the current density, is determined by the slowest of the four parts in the process, (Bertolini et al, 2004) which is considered to be in the concrete ($I_{con,}$) because of the high resistivity, (Vennesland et al, 2007) and the current in each part of the process is equal to $I_{corr.}$ (Equation 3.6).

$$I_a = I_c = I_m = I_{con} = I_{corr} \qquad 3.6$$

As electrochemical process progresses, the amount of steel loss increases and the steel lost can be calculated by using Faraday's law (Jones, 1996), as shown in Equation 3.7. From this equation, the relationship between the current density (i_{corr}) and the mass loss per area per unit time (r_l) is established (Equation 3.8). The current density is the current (I_{corr}) per unit area.

$$m = \frac{Ztl_{corr}}{nF} \quad 3.7$$

and

$$r_t = \frac{Zi_{corr}}{nF} \quad 3.8$$

where

m = weight of metal dissolving

Z = atomic weight of metal

t = time

n = number of electrons transferred

F = Faraday's constant

The understanding of the electrochemical process of corrosion in concrete is very important as the principles provide the fundamentals for the techniques used in electrochemical corrosion monitoring. An example is with the linear polarization resistance measurement where a relationship is established with the corrosion current density (i_{corr}). The determination of the corrosion rate in the steel can then be used for the assessment of the annual decay of the steel bar in reinforced concrete.

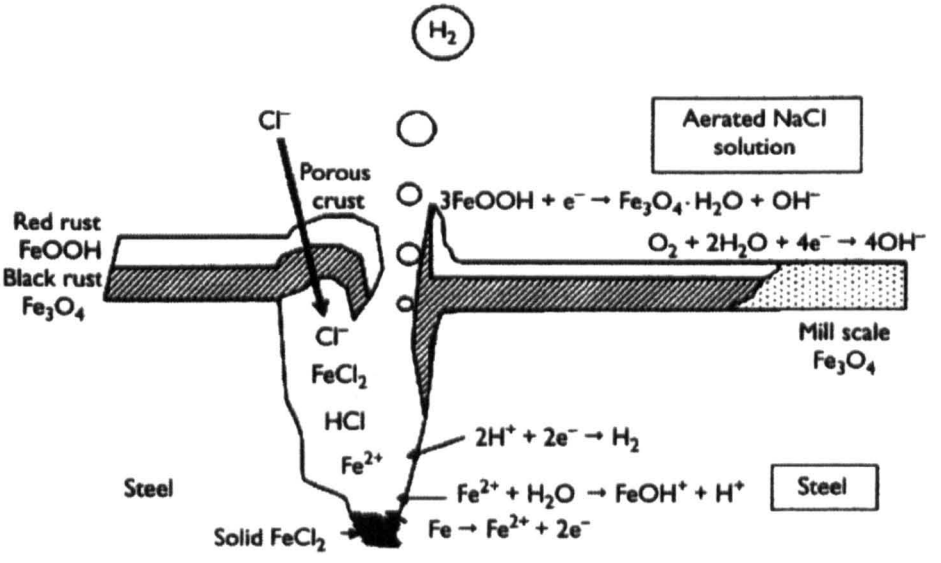

Figure 3.6 Corrosion model of pitting attack
Source: Broomfield, 2007

Half cell potential monitoring and linear polarization resistance method (LPR) can be used to detect the level of electrochemical activity of steel embedded in concrete. With half cell measurement, the corrosion potential of the steel (the working electrode) can be made after the installation of a suitable reference electrode and a voltmeter in a circuit as shown in Figure 4.13. A similar arrangement is used in the LPR test but an auxiliary electrode and a power supply are needed to apply a small current to polarize the steel. Upon polarization, a shift occurs in the potential of the steel. Within a small range on the potential versus current graph, the potential (mV) is proportional to the current (mA) and the linear polarization resistance (*Rp*) can be computed according to Equation 3.9. The Stern and Geary equation (Equation 3.10) was developed from this principle and shows the relationship between current density (mA/cm^2) and *Rp* ($ohm.cm^2$). The term 'B' is a constant with units in mV.

$$R_p = \frac{Change\ in\ potential}{applied\ current} \quad 3.9$$

$$i_{corr} = \frac{B}{R_p} \quad 3.10$$

3.7. INITIATION AND PROPAGATION OF CORROSION

Under chloride attack, corrosion is initiated when the chloride ions that migrate to the surface of the steel reinforcement reaches the threshold limit. At this point, the pH in the concrete is reduced and the potential of the steel becomes more negative. The corrosion products at this point accumulate in the space between the steel and the concrete but cracking is not initiated until the space is exhausted (Maaddawy and Soudki, 2007). Additional corrosion flakes begin to exert stress in the concrete, producing cracks when the tensile strength of the concrete is exceeded. The crack further extends in the concrete until it reaches the surface (Figure 3.7).

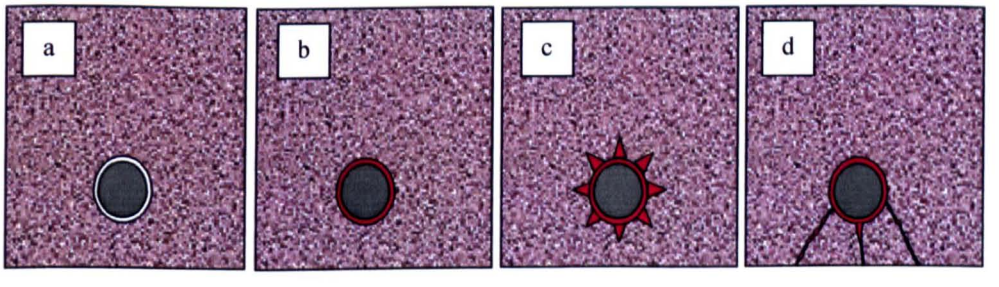

Figure 3.7 The progression of corrosion in reinforced concrete; a) initiation of corrosion; b) corrosion product in the space between the concrete and the steel; c) the corroded product exerts pressure in the concrete; and d) cracks develop in the concrete
Source: Maaddawy and Soudki, 2007

3.8. CORROSION PROTECTION FROM CONCRETE

Standards and codes provide guidelines to reduce the risk and severity of chloride attack. When reinforced concrete is situated in a chloride-containing environment, chloride ions enter through the cover, diffuse and accumulate at the surface of the steel and initiate corrosion. In order to improve the resistance of concrete to the degradation processes associated with chloride attack, it is recommended that the concrete should be made with low water/powder ratio, adequate concrete cover and suitable curing methods should be employed. Additional measures to extend the sustainability of concrete in chloride-laden environments are presented below.

3.8.1. Concrete with Mineral Admixture

The three main mineral admixtures that are known to improve the resistance of steel reinforced concrete to chloride attack and by extension its resistance to corrosion are (a) ground granulated blastfurnace slag, (b) fly ash and (c) silica fume. Concrete with a blend of one or more of these admixtures develops a refined microstructure that reduces permeability (Bassuoni and Nehdi, 2009). This diminishes the ingress and concomitant diffusion of chloride in concrete. In the case of fly ash, additional protection maybe gained from the binding of the chloride ions if other mechanisms to release the bonds ions are not triggered in the concrete. Fly ash, like silica fume, however, is a pozzolan and therefore it reacts with the $Ca(OH)_2$ to produce cementitious material (Zhang et al, 2000). As the $Ca(OH)_2$ is consumed in the process, the alkalinity of the concrete is reduced and hence the question may be asked, whether the capacity of one of the mechanisms that guard the reinforced concrete against corrosion is reduced.

Work was conducted by Alonso and Andrade (2002) to study the corrosion rate of concrete made with different binders, namely fly ash, ground granulated blastfurnace slag, ordinary Portland cement and a pozzolanic cement. The size of each specimen was 15 x 20 x 10 cm and each was proportioned with 400 kg/m^3 of binder and a water/binder ratio of 0.6. Reinforcing bars were placed at different positions in each sample to simulate different depth of cover. After 60 days of curing at 100% relative humidity, the specimens were kept in sea water at temperatures between 14°C and 24°C for over ten years.

An electrochemical testing technique via the standard Calomel electrode was used to determine the corrosion potential, E_{corr}, of the steel. Readings less than -250 mV were interpreted as the commencement of the corrosion reaction. It was revealed that the concrete samples made with fly ash and with ground granulated blastfurnace slag were able to better delay the onset of corrosion in steel. Linear polarization resistance was used to determine the corrosion current density, i_{corr}. It was interpreted that corrosion began when the corrosion density of the steel was greater than 0.1 μA/cm^2. The i_{corr} results indicated that the rate of the corrosion was lowest in concrete samples that were made from fly ash.

3.8.2. Concrete with Corrosion Inhibitors

Corrosion inhibitor is a chemical compound that, when present in the corrosion system in an appropriate dosage, mitigates the rate of corrosion without any alteration to the concentration of the other corrosion agents (ISO 8044). Corrosion inhibitors can be used for preventive and curative measures. For preventive work, the inhibitor can be admixed in the concrete or surface applied to existing concrete structures. This type of application results in an increase of initiation time and a reduction in corrosion rate when activation occurs. These effects will

serve to prolong the durability of reinforced concrete structures. The mechanistic actions of corrosion inhibitors in stemming pitting corrosion in reinforced concrete are (Elsener et al, 1998) by:

i. competing with chloride ions in the surface adsorption process,
ii. competing migration of inhibitor and chloride into the pit and/ or by
iii. increasing the pH in the pit

One way of classifying corrosion inhibitors is by their modes of action and is as follows.

i. Anodic inhibitors – are formulated to suppress corrosion at the anode by increasing the potential of the steel (Hansson et al, 1998).
ii. Cathodic inhibitors – are made to reduce corrosion at the cathode by acting on the oxygen reaction and decrease the corrosion potential.
iii. Ambiodic inhibitors – are designed to suppress electrochemical activities at the anode and cathode without any appreciable alteration in the corrosion potential (Söylev and Richardson, 2008).

Research work was carried out by Gonzalez et al (1998) on a nitrite based corrosion inhibitor, $NaNO_2$, to determine its ability to suppress the corrosion of reinforcement embedded in chloride-contaminated mortar specimens that were placed in different exposure conditions; that is, immersion in artificial sea water and open to the atmosphere. The chloride contamination in concrete took the form of artificial sea water which was added in a ratio of 0.4 or 0.6 (occasionally higher) to cement. Portland-450 cement was used and the ratios of cement/sand for the various mixes are 1:1, 1:3, 1:6 and 1:8. Samples were made with no

inhibitor, with 2 and 4% nitrite inhibitor and with two reinforcing steel rods in each mortar block. Effects of nitrite were determined with 80% and 100% relative humidity by immersion in distilled water and in artificial sea water.

A counter electrode in the form of a stainless wire was also placed in the concrete specimen. The i_{corr} results showed that the inhibitor lowered corrosion current density by about one order of magnitude at some points and successfully preserved the passivation of the steel embedded in chloride-contaminated concrete (Figure 3.8). Additional test however showed that the inhibitor can be leached from the concrete, the extent of which depended on the quality of the concrete. This resulted in a rapid activation of corrosion before 100 days while the samples that were not leached showed no sign of corrosion even after this period.

Nitrite-based inhibitors deserve special mention. It is well documented that calcium and sodium nitrites are anodic inhibitors that improve the corrosion resistance of the steel by competing with the chloride ions (Söylev and Richardson, 2008) for dissolved metal ions in the pit. The reactions between the ferrous ions and the nitrites (Equations 3.11 and 3.12) produce a stable passivating film on the surface of the steel (Gonzalez et al., 1998). The rates of the actions are fast and hence the ferrous ions are consumed before the iron chloride complexes are formed (Söylev and Richardson, 2008). The minimum concentration of nitrite inhibitors that effectively abates corrosion is expressed as $[NO_2^-]/[Cl^-]$ ratio and is often reported to be 0.6 but it is not unusual to see higher values quoted. This ratio is based on the inhibiting capacity of nitrite in chloride environments up to approximately 4% chloride (Elsener, 2001).

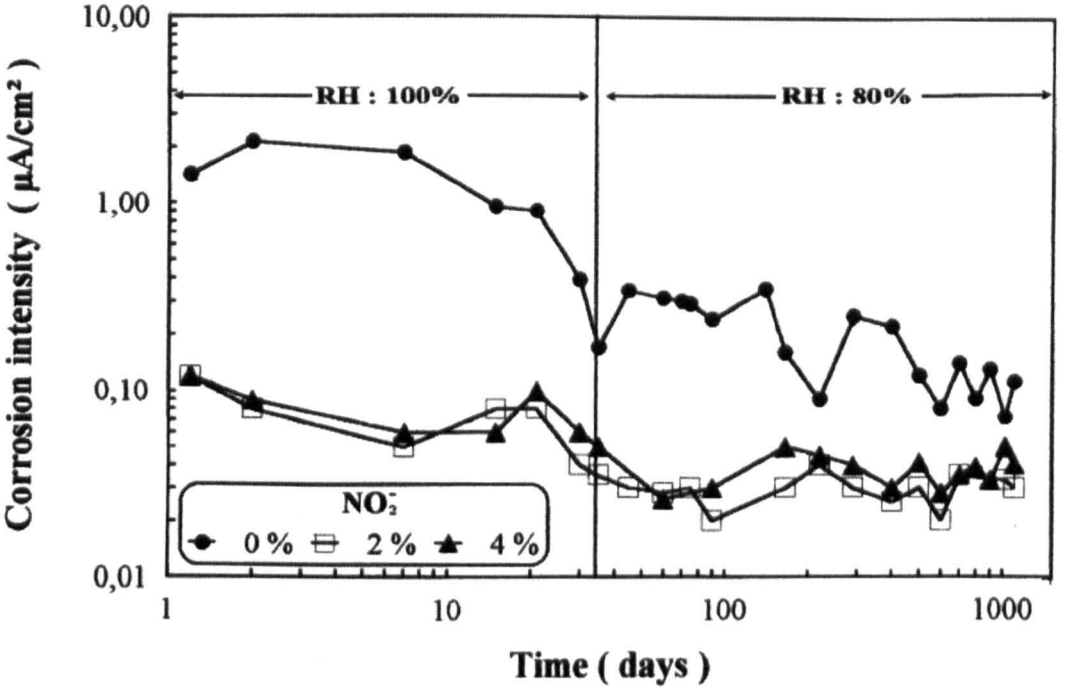

Figure 3.8 Current density over time of mortar with 1:3:0.4, cement /sand/ water proportions
Source: Gonzales et al, 1998

$$2Fe^{2+} + 2OH^- + 2NO_2^- \rightarrow 2NO + Fe_2O_3 + H_2O \quad 3.11$$

$$Fe^{2+} + OH^- + NO_2^- \rightarrow NO\uparrow + \gamma - FeOOH \quad 3.12$$

Corrosion inhibitors for applications to existing reinforced concrete structures are also available. Migratory inhibitors that can be applied to the surface or in drilled-holes of existing concrete usually have two phases; one phase which consists of the main compound is volatile; the other phase is non-volatile (Söylev and Richardson, 2008). This type of inhibitor can be used both for preventative and curative measures. The ability of migrating corrosion inhibitors to assuage corrosion is questionable as their effectiveness may be affected by the

thickness and density of the concrete cover. An insufficient number of applications of the inhibitor on the surface will also affect its performance (Bertolini et al, 2004).

3.8.3. Concrete with Corrosion Inhibitor and Mineral Admixture

Further enhancement of the corrosion resistance of concrete admixed with mineral admixture may be obtained by the incorporation the of corrosion inhibitors in the material. Al-Mehthel et al (2009) examined the performance of corrosion inhibitors in chloride contaminated silica fume concrete. In order to determine the effectiveness of inhibitor in delaying corrosion in silica fume concrete, chloride-contaminated cylindrical concrete samples were made and the inhibitors were added to some of the samples in dosages based on the manufacturers' instructions. One rebar was placed in the centre of each specimen. Four different types of corrosion inhibitors were used, of which one was calcium nitrite and another was calcium nitrate based. One set of concrete samples was subjected to wet and dry cycles, and a corrosion potential test was done monthly for twenty months to determine the initiation of corrosion.

Al-Mehthel et al (2009) determined the corrosion current density with i_{corr} measurement on steel in the chloride-contaminated concrete with and without inhibitor after 20 months. When comparisons were made between concrete samples with 0 percent Cl^- and with 0.04, 1.0 and 2.0 percent Cl^-, it was shown that the corrosion current density decreased with the use of inhibitors in the silica fume concrete (Figure 3.9).

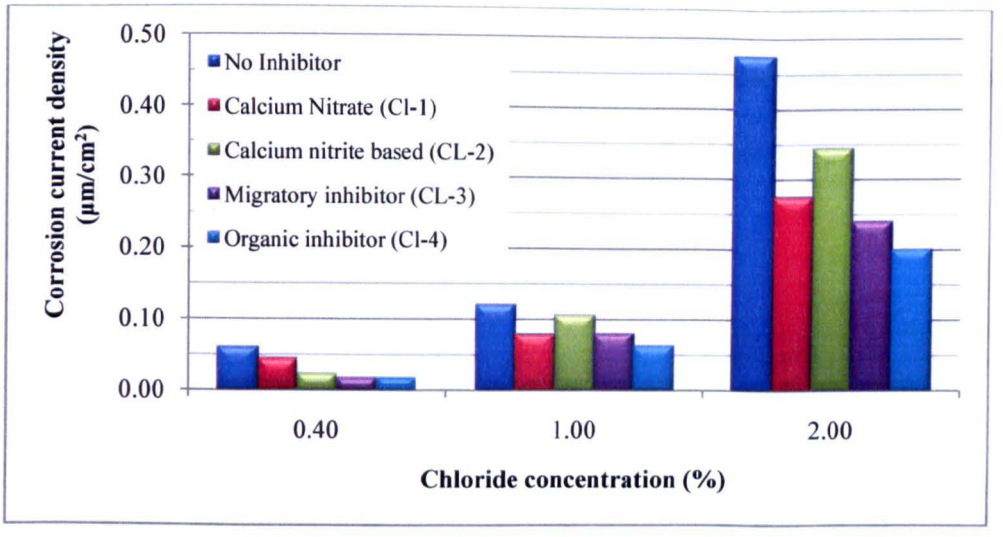

Figure 3.9 Corrosion current density on steel in concrete specimens with varying chloride concentrations and types of inhibitors
Source: Al-Mehthel et al, 2009

3.9. SELF-COMPACTING CONCRETE

The search to improve the performance of reinforced concrete will continue as researchers try to preserve some very important concrete facilities in chloride-laden environments. Self-compacting concrete was originally formulated to address durability deficiencies in concrete structures. Skarendahl (2005) postulates that the improvement in the microstructure of self-compacting concrete should result in a decrease in the penetration of fluids and this decrease should be accompanied by a reduction in the degradation process. Although this type of concrete has the potential to produce concrete with low chloride coefficient, tests on different types of mix show that the diffusivity of self-compacting concrete can be less, more than or equal to that of traditional concrete (TC) that is vibrated. Audenaert and team workers, (2005) studied the penetration of chloride in SCC by cyclic immersion. All samples of SCC were made with limestone filler except SCC 9 which had fly ash. The results of the tests showed the variation in penetration coefficient of chloride over square root of time, H, in SCC as

displayed in Figure 3.10. The values indicate that depending on the composition and the water/cement ratio, SCC can have penetrability less than, equal to or more than traditional concrete. However, when comparison is made with concrete at the same water/powder it is seen that the fly ash SCC reduced the ingress of chloride in the SCC.

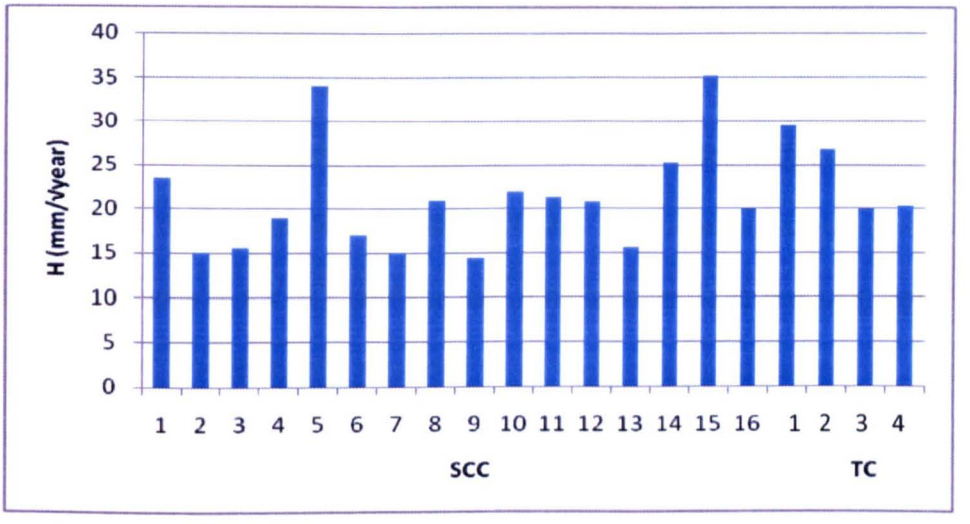

Legend

CEMENT TYPE	WATER /POWDER RATIO
SCC 2: CEM1 52.5; SCC 1, 5-16: CEM1 42.5R; TC 1 and TC 3: CEM1 42.5R; SCC 3 and TC 2: CEM111A 42.5LA; SCC 4 and TC 4: CEM1 52.5HSR	SCC 1-4, 8-10, 16 and TC 1, 2, and 4: 0.46; SCC 5 and 14: 0.55; SCC 6 and TC 3: 0.41; SCC7: 0.37; SCC 11: 0.48; SCC 12: 0.49; SCC 13: 0.40; SCC 15: 0.6.

Figure 3.10 Chloride penetration coefficient (H) for various types of SCC and traditional concrete
Audenaert et al, 2005

It was also shown in work carried out by Kanellopoulos et al (2012) that at a water/binder ratio of 0.5, the indications were that the durability of SCC is higher than traditional concrete. The assessment of durability was carried out through absorption, porosity and rapid chloride

permeability tests on SCC and traditional concrete made with CEM11 42.5R and with the SCC admixed with limestone filler. Further it was shown that the sorptivity, porosity and the chloride permeability values of the SCC samples increased as the water/powder ratio increased and decreased as the silica fume replacement level for cement increased up to 20%.

Corrosion test conducted by Hassan et al (2009) showed that, with the exception of small peculiarities, SCC reinforced concrete beam attained higher current values than the traditional reinforced concrete beam. Both types of beams were made from ordinary Portland and slag cements and the main differences between the SCC and traditional concrete mixes were a lower content of aggregate in the SCC and the use of high range water reducing agent in the SCC only. A 12 V DC power supply was used in an electrochemical process to accelerate corrosion in the beams. Corrosion in the beam was monitored by a computer-controlled data acquisition system which supplied information on the flow of current. All the beams used 25 M bars at the bottom and the maximum cover to the reinforcement was 40 mm. This is an example of the potential of the superior durability of SCC.

3.10. CONCLUSION

As seen, concrete made with cement replacements, in particular GGBS, fly ash and silica produces attributes that help to reduce the ingress of chloride in the concrete. The use of corrosion inhibitors has also increased the resistance of concrete to chloride-induced corrosion. SCC has the potential to deliver a highly durable concrete. At the commencement of this research, literature on the incorporation of SCC with corrosion inhibitor could not be found. This present study will examine the properties of SCCs made with corrosion inhibitors

and with mineral admixtures. The concerns are whether the interactions of the materials will interfere with the properties and performance of self-compacting concrete.

Fly ash and silica fume will be used to make the SCC samples and a carboxylic and a nitrite-based corrosion inhibitor will be added to the SCC mixtures. The carboxylic inhibitor is specially designed for making SCC. Tests will be conducted to determine the transport properties of this concrete and to determine the effectiveness of the inhibited SCC at delaying corrosion. The probability of leaching and/or consumption of the inhibitor and the self-healing capacity of reinforced SCC will be investigated in order to determine the overall performance of corrosion-inhibited SCC. The side effects of these inhibitors on the plastic and mechanical properties will be assessed and micro-structural analyses will be performed to study the mechanism behind any noticeable feature that results in differences between the traditional and inhibited SCCs.

EXPERIMENTAL PROGRAMME, MATERIALS AND METHODOLOGY

4.1. INTRODUCTION

In the previous chapter, the desired properties of materials were outlined. This chapter commences by selecting those that meet these desiderata while also maximising the likelihood of meeting the objectives of the research. This chapter provides the descriptions and specifications of the materials used and the justification for their inclusion in the experimental programme. Additionally, the procedures, requirements and limitations of the various tests conducted are outlined to give a comprehensive understanding of the experimental programme and provide the context in which analyses are made.

4.2. MATERIALS

Most of the materials that are used for the making of the concrete specimens are traditional materials. The other materials are included to achieve special effects in the concrete or in the environments in which the concrete will be placed or tested. A succinct and informative discourse is now provided on each.

4.2.1. Cement

Rapid-hardening Portland cement conforming to CEM1 52.5R in the BS EN 197-1 standard was used in this testing programme. The selection was primarily based on the fact that some of the objectives of the research are predicated on the study of SCC with known quantities of ordinary Portland cement whereas more commonly available cements are sold with unknown

quantities of inert powder (e.g. limestone dust) and pozzolanic extenders (e.g. fly ash). CEM1 52.5R was the only available pure ordinary Portland cement and hence it was used. It should also be mentioned that at the start of this project CEM 52.5R was marketed as CEM 42.5R. The physical properties of the cement are shown in Table 4.1 and the chemical properties are shown in Table 4.2. The grading of the cement, acquired from the manufacturer's quality control record for this batch of cement, is shown in Figure 4.1. Information on the properties is provided primarily to help in the interpretation of the results of tests, especially when cross reference is made with similar works in other literatures.

Table 4.1 Physical properties of cement

Cement	Specific Surface Area (m^2/kg)	Relative Density
CEM1 52.5R	515	3.15

Source: Castle Cement Ltd.

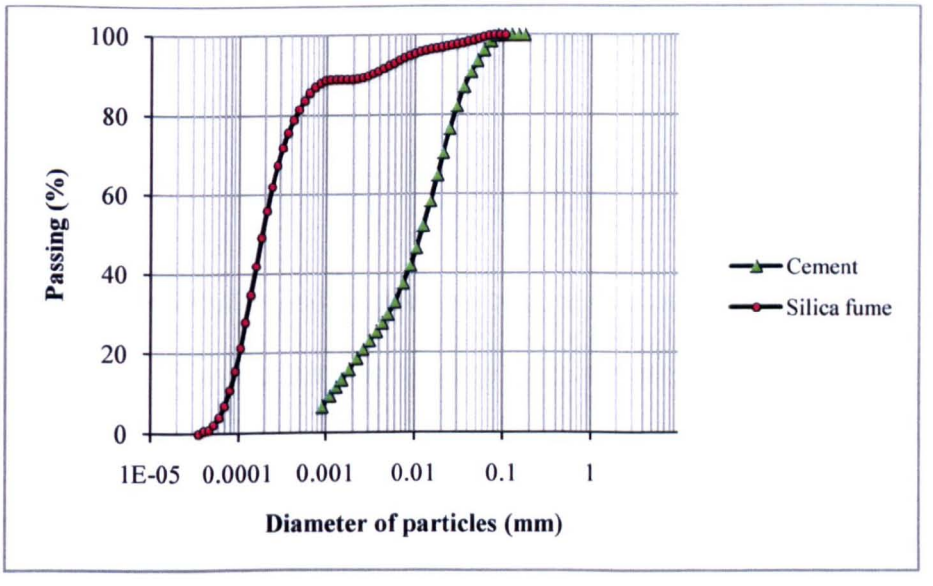

Figure 4.1 Particle size distribution of cement and silica fume

Table 4.2 Chemical composition of powders

Component	CEM1 52.5R (%)	Fly Ash (%)	Silica Fume (%)
SiO_2	21.5	48	>90
Al_2O_3	4.86	27	2*
Fe_2O_3	2.67	9.0	<1*
CaO	63.35	3.3	<1*
MgO	1.15	2.0	<1*
K_2O	0.64	3.3	<1*
Na_2O	0.24	1.2	<1*
SO_3	3.19	0.6	<1*
Cl	0.05	0.06	
TiO_2		0.9	
Loss on ignition	2.25		3.0
Unburnt carbon		4 – 8	

* Denotes typical values (Day, 1999)

4.2.2. Fly Ash

Fly ash enhances workability and suppresses corrosion in reinforced concrete. However, another advantage of fly ash is that it is likely to be more easily available in many countries because it is a by-product of many power plant companies. More study about the use of this material in concrete will promote further utilization of this by-product. The fly ash used in this research was obtained from a power-plant station that is situated near Nottingham, UK. The chemical composition is displayed in Table 4.2 and Figure 4.2 provides micrographs of

the particles with indication of the distribution of sizes. The micrographs were obtained from scanning electron microscope as set out in Section 4.5.2.6.

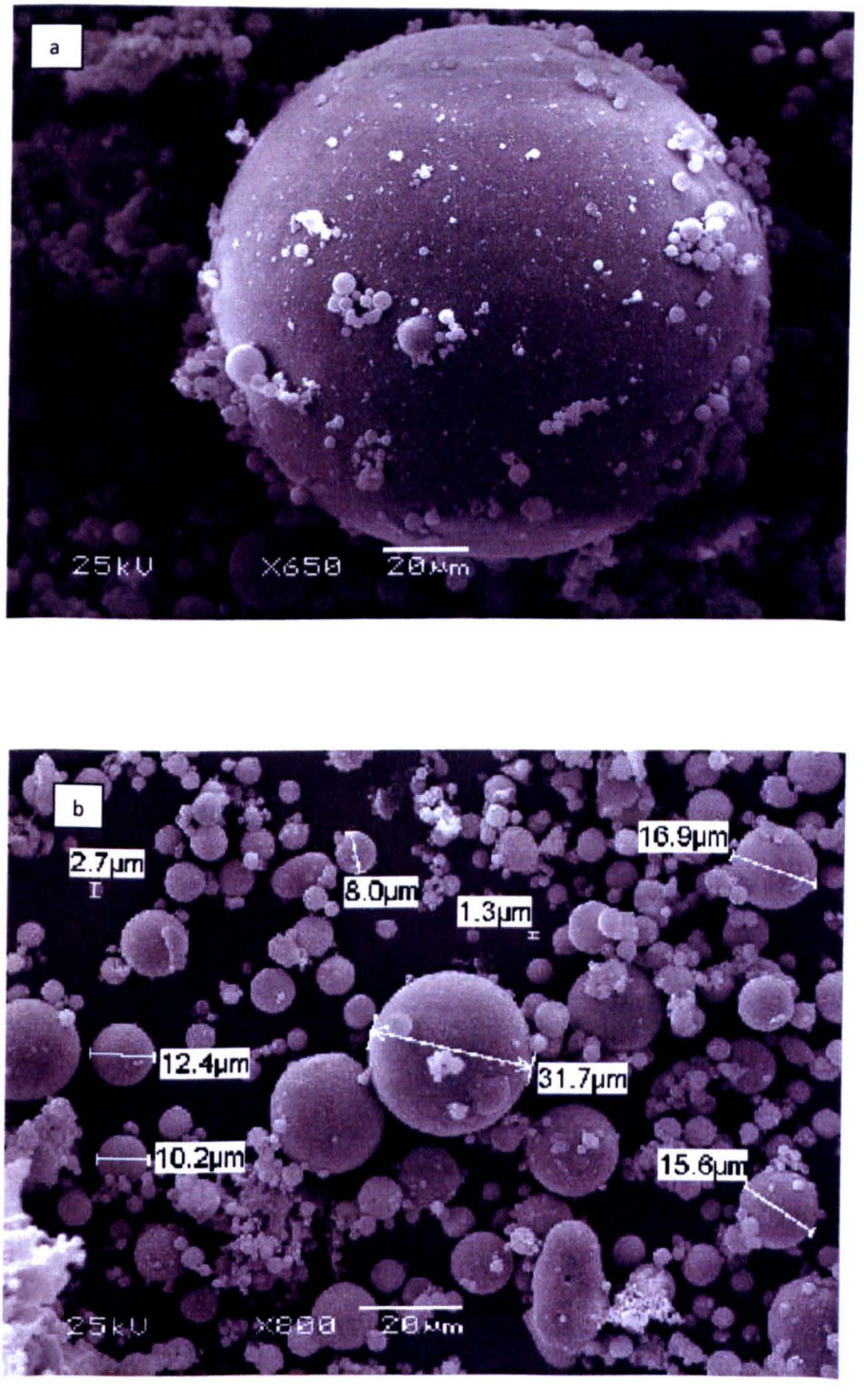

Figure 4.2 SEM images of fly ash particles showing; a) geometry and surface characteristics and b) particle size distribution

4.2.3. Silica Fume

Silica fume, as described earlier, promotes a low penetrability and hence can reduce the ingress of fluids (Berke and Hicks, 2004) through the different modes of transport mechanisms in concrete. Its inclusion in this research will enable the concrete to approach the lower limit of its penetrability. The silica fume was provided by Elkem ASA, Norway, in the densified form. The grading is provided in Figure 4.1 and the chemical constituents in Table 4.2.

4.2.4. Aggregates

A well distributed grading of the particles in all the aggregates is desired to ensure self-compatibility of SCC. The particle distribution of the granular material is defined by the mathematical model expressed in Equation 2.6. It is reported that the optimum particle distribution for SCC is obtained when w is equal to 0.25 (Brouwers and Radix, 2005). This was difficult to achieve with the available aggregates and so a curve satisfying the equation when $w = 0.4$ was used. In order to achieve this, two types of coarse aggregates and two types of fine aggregates were blended to obtain a combined aggregate that closely mirrors the ideal grading curve (Figure 4.3). The four types of granular materials originated from alluvial sources along the River Trent near Nottingham, UK.

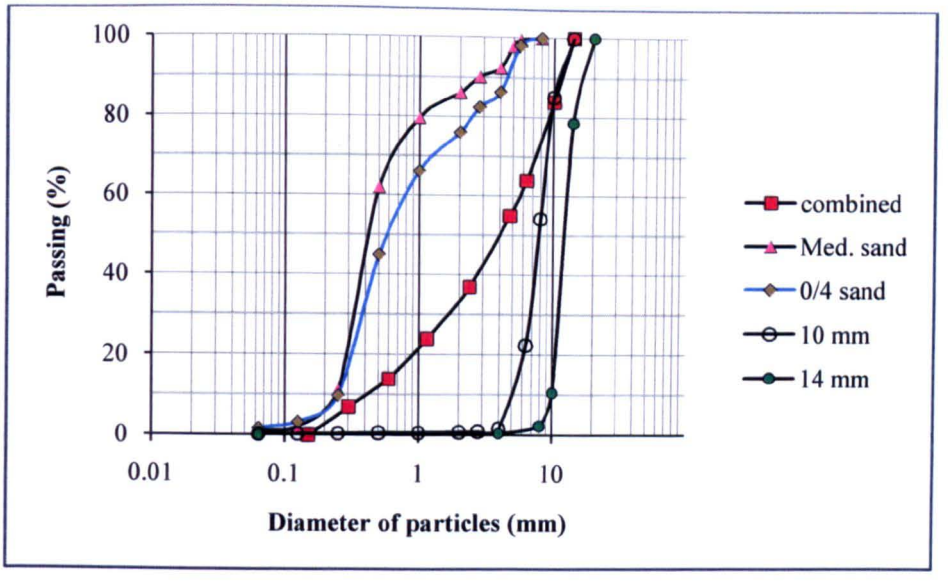

Figure 4.3 Particle size distribution of aggregates

Table 4.3 Properties of aggregates

Type of aggregate	Specific density	Absorption (%)	Fineness modulus
0/4 sand	2.68	0.7	2.6
Medium sand	2.67	1.1	2.1
10 mm coarse	2.69	1.75	2.0
14 mm coarse	2.68	0.66	1.9

Graphical depictions of the gradings of all four aggregates and the combined aggregate are exhibited in Figure 4.3. The coarse aggregates that were used are 14 mm and 10 mm gravels which had relative densities and absorption rates as shown in Table 4.3 as determined in accordance with BS EN 812-2. Included in this table is the fineness modulus which established the relative fineness of the aggregate. The aggregate is either coarse or fine depending whether the value is closer to 3 or 2 respectively. Similar properties for the sands are also provided in Table 4.3. Preference was given to gravel as the coarse aggregate because the smooth surface texture and rounded shape of the particles would help to promote better rheological performance (Graves, 2006).

4.2.5. Chemical Admixtures for Concrete

Three admixtures were used, two as corrosion inhibitors and one as a superplasticiser. One of the corrosion inhibitors is manufactured with a type of superplasticising compound. Each is now described.

4.2.5.1. CORROSION INHIBITORS

Carboxylic acid compound

This is an organic corrosion inhibitor with high range water reducing (HRWRA) and viscosity modifying phases. It is of a hue that is between dark yellow and amber and the pH is between 7.0 and 8.0. This compound has a migrating corrosion inhibiting (MCI) phase but it is suitable for admixing in new concrete works and hence should be effective where avoidance or attenuation of corrosion in concrete composites needs to be addressed. It was used without any other superplasticiser, as recommended for producing corrosion inhibited SCC.

Calcium nitrite compound

This type of inorganic inhibiting admixture is marketed by Grace. Its formulation is based on calcium nitrate and calcium nitrite, with the latter comprising a minimum of 30% of its contents. It is void of chloride and is available in the liquid state in a light brown colour. The specific gravity is 1.25 and the pH is 8.5 on average according to manufacturer's literature. The pure superplasticiser was used with this inhibitor to produce nitrite-inhibited SCC.

4.2.5.2. SUPERPLASTICISER

The superplasticiser was not only needed to reduce the yield value in order to promote deformability but also to achieve this at a low water/powder ratio. Glenium, a superplasticiser of polycarboxylate formulation was opted for as its superplasticising phase is similar to that of the carboxylic superplasticising corrosion inhibitor (Section 4.2.5.1). This reduced the variability in the constituents of the concrete samples and is expected to help in the analysis of the results. Additionally, this particular product, which is marketed by BASF Construction Chemical, is compatible with all types of cements, air entraining agents, curing agents and other concrete admixtures and hence was found suitable for this research work considering that several types of ingredients were used. The colour is off-white and the specific gravity is 1.095 ± 0.02 g/cm^3. The pH is 6.5 ± 1 and the chloride content is less than 0.10%.

4.2.6. Chemical Agents

Several chemical agents that are not normally incorporated intentionally in concrete were used to test and/or produce special effects. Each is described in this section.

4.2.6.1. SODIUM CHLORIDE

Two different dosages of sodium chloride (0.1 and 1.0% NaCl)) were introduced in some concrete samples (Sections 4.4.1) to simulate chloride-contaminated concrete with the respective lowest and highest maximum permissible chloride contents (BS EN 206-1). This was done with a view to study the response mechanism of the corrosion inhibitors used in the different types of concrete. Sodium chloride was also used in the solution of impressed voltage test and in the saline solution used for soaking specimens (Section 4.4.2.5). The rapid migration test in accordance with the Nordic standard, NT Build 492, also required the use of chemical grade NaCl. In this test, the chloride migrated from the area of high chloride concentration (upstream) towards an area of low concentration in order to provide data on the level of penetrability of the concrete and hence sodium chloride was needed.

4.2.6.2. SODIUM HYDROXIDE

The rapid chloride migration test also required the use of sodium hydroxide to produce a 'downstream' solution that is low (or void) of chloride. A chemical grade NaOH compound was used and prepared according to the Nordic NT Build 492 specification.

4.2.6.3. CALCIUM HYDROXIDE

A saturated calcium hydroxide ($Ca(OH)_2$) solution was used for the preconditioning of the concrete specimens before the rapid chloride diffusion test. Technical grade calcium hydroxide in the form of hydrated lime was used for this purpose.

4.2.6.4. SILVER NITRATE

A 0.1M concentration silver nitrate was sprayed on the broken concrete samples that were removed from the rapid migration test. The depth of penetration of chloride ions was detected by the presence of silver chloride which was white in colour.

4.2.7. Steel

Reinforcing mild steel bars were embedded in some of the concrete samples. The dimensions of the rib-less rods were 6 mm diameter x 150 mm long. In the potentiostat/galvanostat analysis (Section 4.5.5.3), a small current is applied to the working area of the steel. As the corrosion rate is proportional to the current density (current/unit area), ideally it is better to have a small area to obtain a significant corrosion rate in the limited time. Additionally, for the purpose of microstructural analysis, the scanning electron microscope can only accommodate small reinforced concrete specimens, and therefore 6 mm diameter size steel rod is suitable being large enough to show corrosion but small enough to be able to make reinforced specimens that will fit in the SEM chamber (Section 4.5.2.3). The metal was composed mainly of iron (Fe), approximately 98%, and traces of other elements all of which are shown in Figure 4.4. The chemical composition was determined with the use of an optical emission spectrometer (Section 4.5.2.5). The tensile strength of the steel was 680 MPa and the modulus of elasticity was 203 GPa.

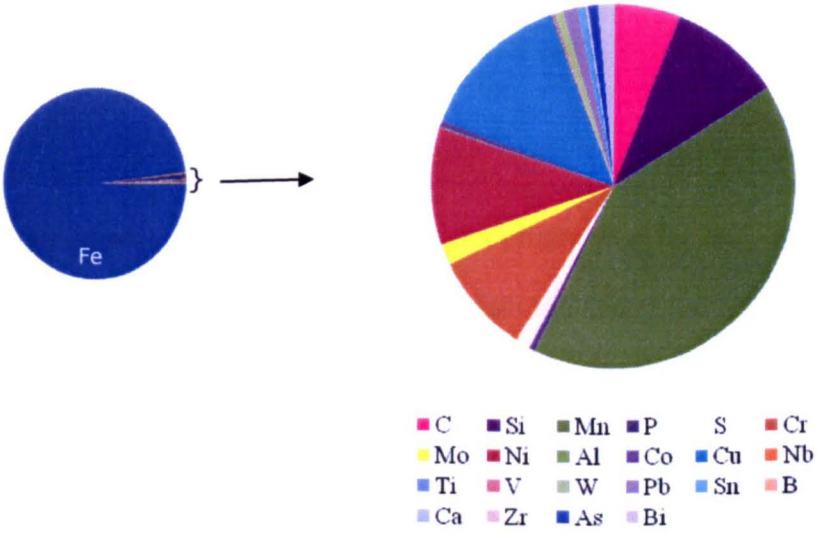

Figure 4.4 The major and minor chemical elements in mild steel specimen

4.3. PRODUCTION OF CEMENTITIOUS MIXTURES

4.3.1. Powder Pastes

It is reported that corrosion inhibitor can affect the setting time of cement in traditional concrete (Elsener, 2001). For this reason, the setting time test was used to determine if the cement will experience any further alteration and if so, the extent of the alteration in the setting of cement with corrosion inhibitor and appreciable addition of other admixtures that are commonly used in SCC.

Although the objective of using this test was to determine the effect of the corrosion inhibitor on the setting of concrete, the test was performed on the paste only as it comprises the materials that influence the chemical reaction in the concrete (Alarcon-Ruiz et al, 2005; Wombacher, 2007). The procedure for the setting time test was essentially an adaptation of

BS EN 196-3. Unlike the BS EN 196-3, the powder paste did not always constitute cement and water only but combinations of cement, water, mineral admixture and chemical admixtures in some cases.

Furthermore, pure cement paste was included in the programme for the setting time tests to establish the reference point for the setting times of all the other types of pastes. The setting of the blends of cement and superplasticiser and/or mineral admixture was also studied to isolate the impact of each material on the cement before the corrosion inhibitor was incorporated in the paste. The main mixes under study however, were the pastes with cement, superplasticiser and corrosion inhibitor.

4.3.1.1. PROPORTIONS OF POWDER PASTES

The range of powders used in this testing programme are CEM1 52.5R (1), fly ash (F), and silica fume (S). The calcium nitrite and the carboxylate types of corrosion inhibitors were used in some of the pastes. The pure superplasticiser compound was also used in some of the powder mixtures. The pastes with the proportions of the constituents are shown in Table 4.4. Paste mix 1 was made of cement only while paste mixes F and S were produced with cement and fly ash, and cement with silica fume respectively. Powder paste mix G incorporated the pure superplasticiser with cement but FG is a mixture of cement, fly ash and the same superplasticiser. Mix M on the other hand had cement and the migrating superplasticising corrosion inhibitor while FM had an extra ingredient – fly ash. The calcium nitrite based inhibitor, the superplasticiser and fly ash were mixed with cement to produce the FGC mixture and silica fume was mixed with cement to obtain the S mix. All the mixes defined above used CEM1 52.5R cement.

Table 4.4 Proportions of ingredients of cementitious pastes

Ingredients	Mass (g)										
	1	F	S	G	C	M	FM	FG	FG C	SM	SG
CEM1 52.5R (g)	500	300	475	500	500	500	300	300	300	475	475
Fly ash (g)		200					200	200	200		
Silica Fume (g)			25							25	25
HRWRA (%)				1				1	1		1
Calcium nitrite type inhibitor (%)					0.4				0.4		
Carboxylic Inhibitor (%)						0.3	0.3			0.3	
w/c ratio	0.26	0.43	0.27	0.26	0.26	0.26	0.43	0.43	0.43	0.27	0.27

4.3.1.2. TYPES OF SETTING TESTS

In order to carry out an in-depth study on the effect of corrosion inhibitor on the paste of SCC a testing programme that evaluated the setting times of normal, highly concentrated and high-temperature powder pastes was embarked on. It is common to carry out setting time test on cement paste at standard temperature but the evaluation of the setting characteristics of the powder at a higher temperature, a situation that the plastic concrete may have to endure in practice, allows assessment for summer periods when atmospheric temperature may rise up to 40°C. It was also deemed necessary to ascertain the performance of the paste in cases when higher dosages of corrosion inhibitor are used in concrete to provide greater protection to embedded steel.

Normal Paste

In preparing the samples, 500 g of cementitious powder was mixed with water. This mass is stipulated in BS EN 196-3. However, instead of using the normal consistency test to determine the quantity of water needed, a fixed quantity of 128 g of water was used in the mixing of the cement paste to provide a common basis for comparative evaluation. This quantity of water is in the range of that which would produce a paste of standard consistency. When an appreciable amount of superplasticiser or corrosion inhibitor in the aqueous form was used, the amount of water was reduced by the mass of the chemical admixture(s). The water/powder ratio for the normal pastes in all cases was therefore 0.26. The replacement levels of cement for silica fume and fly ash were 5 % and 40 % respectively. This reflects the cement replacement level of mineral admixtures in the concrete mixes. The basic dosages of corrosion inhibitors incorporated in the designated pastes are 0.3 % and 0.4 % respectively for the carboxylic type and the nitrite type based on gravimetric measurements. In this part of the setting time testing programme, the quantity of inhibitor used in the pastes adheres to the minimum recommendation in the manufacturers' literature.

Highly Concentrated Mixes

The concentration of the inhibitor was increased in the range of 2 to 3 times the dosages in this set of tests. The water that was used remained at 128 g. The temperature was also maintained at 20 ± 1°C and all the other ingredients remained the same. The test was according to the procedure used for the normal paste.

High Temperature Paste

For tests that were conducted at 30°C and 40°C, the mixing water and the mixing apparatus were acclimatized to the respective temperature. The temperature of the water bath was also

raised to satisfy the test requirements. The procedure for the testing of the normal paste was followed.

4.3.1.3. MIXING OF PASTES

A 3-litre Dito mixer was utilized in the mixing of the pastes. The Vicat apparatus was used for the setting time test. The Vicat needles were made of brass and were all in vertical alignment with the base of the mould. A temperature-controlled water bath, manufactured by Grant, was used to cure the specimens under test. The temperature range is 0 to 100°C and the stability is ± 0.02°C.

All the materials were proportioned according to Table 4.4. Where fly ash or silica fume was incorporated in the paste, it was intimately blended with the cement in the dry state before placing in the mixer. Some of the water was also mixed with any liquid ingredient used before introduction in the mixer. The powder was first placed in the moistened mixer, immediately followed by the water with any other aqueous admixture. The mixing commenced shortly thereafter and lasted for 90 seconds and then stopped. At this point a spatula was used to remove material adhering to the sides of the mixer and to mix this fraction with the rest of the material. The mixer was re-started and mixing continued for another 90 seconds. The test, described in Section 4.5.1.1, proceeded immediately thereafter.

For the viscosity test, the same proportions of the powder ingredients for FG, FM and FGC were used but the total mass used was 105 grams and the water/powder cement ratio was 0.45 (for reason explained in Section 4.5.1.2). The cementitious powder was placed in a container followed by the superplasticiser diluted with the water. When the calcium nitrite corrosion

inhibitor was used, it was mixed with some of the water and added before the introduction of the diluted superplasticiser. This mixture was stirred for approximately 30 seconds manually and then mixed with a mixer at 150 rpm. Total mixing of the paste lasted 2.5 minutes.

4.3.2. Concrete Mixtures

The principal aim of the project is to determine the performance of SCC with corrosion inhibitors. Two types of corrosion inhibitors were therefore used in different types of SCCs. Traditional self-compacting concrete mixes without corrosion inhibitor were also made for reference. The formulation for the SCC mixes consisted of high powder content, designed to ensure self-compactibility of all mixes. Fly ash and silica fume blend concretes have demonstrated a high capacity to reduce corroding tendencies of steel reinforcement in concrete (Section 3.8.1) and hence were incorporated in this research. High volume of these pozzolans is used in research to appreciably reduced corrosion (Montemor et al, 2000; and Dotto et al, 2004) and hence 40% cement replacement level was used for fly ash. Preliminary trial mix showed that a high volume of silica fume suppressed workability and therefore 5% cement replacement level was used for silica fume.

The pure superplasticiser product utilized in the concrete is quite popular with researchers (Pop et al, 2013; and Persson, 2003) and seems to have established a good track record. It is used herein as it has been shown to be effective in producing high fluidity concrete. The calcium nitrite corrosion inhibitor is selected because its formulation is nitrite based; a compound that is effective in abating corrosion in reinforced concrete. The carboxylate based corrosion inhibitor is used because its formulation is new and its performance in producing corrosion-inhibited SCC will be ascertained. More importantly however, is that calcium nitrite corrosion inhibitor is an inorganic material while the carboxylic compound is organic.

The study will be able to characterise the morphology of the two different types of corrosion inhibiting types of SCC and to identify and possibly differentiate between the kinetics involved in the mechanism that mitigate corrosion at the micro-scale.

4.3.2.1. PROPORTION OF CONCRETE MIXES

The basic design of the concrete was guided by the EFNARC (2005) specification and was checked against the ACI guidelines as shown in Table 4.5. The composition of each mix is detailed in Table 4.6. The three corrosion inhibited SCC mixes are FGC, FM and SM. The latter mix was produced with cement, silica fume (S) and the carboxylate type inhibitor (M). Mixes FGC and FM are both mixes blended with cement and fly ash (F), but the latter was made with migrating carboxylate corrosion inhibitor while the former was produced with superplasticiser and calcium nitrite formulated corrosion inhibitor (C). The other two types of SCC mixes are SG and FG. Both were composed of cement and superplasticiser; however the first is admixed with silica fume and the other with fly ash. CEM1 52.5R cement was used in all mixes. The corrosion inhibited SCCs were mixed with concentrations of corrosion inhibitor ranging from 1 – 2 times the minimum recommended dosages.

Table 4.5 Comparison of SCC mix proportions with standard specifications

Ingredients	Units	Research SCC	ACI	EFNARC
Powder	kg/m^3	570	385 - 475	380 - 600
Coarse aggregate	% (vol.)	32	28 - 32	27 - 36
Fine agg./total agg.	% (wt.)	47		48 - 55
Paste	% (vol.)	39	34 - 40	30 - 38
Mortar	% (vol.)	68	65 - 72	
Water/powder ratio	(wt./wt.)	0.32	0.32 – 0.45	
Water/powder ratio	(vol./vol.)	0.85		0.85 – 1.10

Table 4.6 Mix proportions of SCC mixes

Materials	SCC Mixes					
	Unit	FG	SG	FM	FGC	SM
Cement	kg/m^3	340	542	340	340	542
Fly ash	kg/m^3	230		230	230	
Silica fume	kg/m^3		28			28
Coarse aggregate	kg/m^3	830	868	830	830	868
Sand	kg/m^3	745	778	745	745	778
Water	kg/m^3	180	180	180	180	180
W/P ratio (wt.)		0.32	0.32	0.32	0.32	0.32
Corrosion inhibitor				carboxylic acid	calcium nitrite based	carboxylic acid
HRWRA		poly-carboxylate	poly-carboxylate		poly-carboxylate	

4.3.2.2. MIXING OF CONCRETE

A pan mixer was used for the mixing of the concrete. The batching was done in accordance with Table 4.6. The schematic diagram in Figure 4.5 shows the sequence of the mixing process. Three minutes after the water was added to the aggregate and mixed, the powder was introduced; mineral admixture first and then the cement. The superplasticiser was added at the end to optimise the efficiency of the admixture in fluidizing the concrete (Liu, 2010). After the addition of the superplasticiser in Stage 3, the concrete was mixed for approximately 2 minutes. When the nitrite-based inhibitor was used, it was combined with the portion of water that was added in Stage 1. This was done to minimise the probability of the emission of toxic fumes from the reaction of this inhibitor and the other ingredients. The mixing process after the addition of cement lasted for 5 minutes approximately. Testing and sampling of concrete followed immediately after mixing.

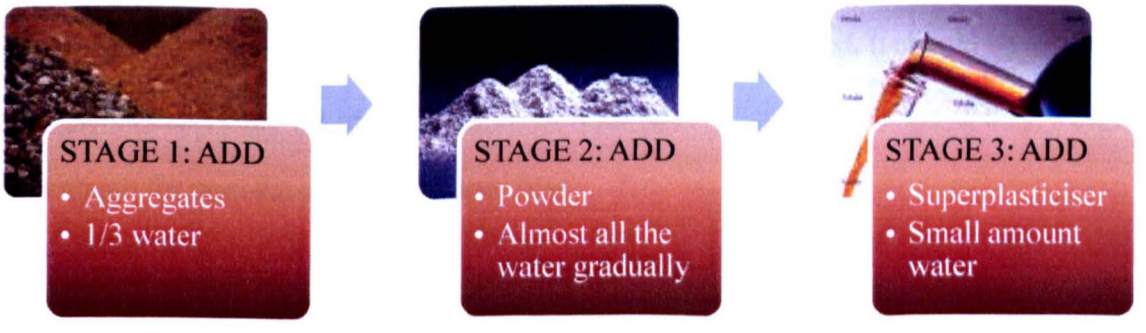

Figure 4.5 Sequence of the mixing process

Simulated reinforced concrete specimens called 'lollipops' were made with and without sodium chloride for corrosion testing and this was based on the mass cement (Section 4.4.1). The dosages of sodium chloride were 0.1, 0.6 and 1% for the respective sample. The mixing of concrete for these samples was done using a Hobart mixer following the same sequence of operations (Section 4.3.2.2) used for the rest of the concrete. However, when sodium chloride was used, it was incorporated in the aggregates. As the volume of concrete required for the making of these samples is quite small the mixing time was shorter, lasting about three minutes.

4.4 CASTING AND CURING REGIMES

4.4.1. Casting

Concrete samples made with 100 mm cubes and 100 x 100 x 500 mm long prisms were required for strength tests. Additionally, 100 mm diameter x150 mm high concrete cylinders were also needed for the rapid chloride migration tests as set out in the Nordic standard NT Built 492. The respective metal moulds were filled with concrete and covered with polyethylene material to prevent evaporation of moisture. The concrete samples were not vibrated. Approximately 24 hours after the samples were de-moulded. It should be mentioned that in some cases concrete remained in the moulds up to 48 and more hours as they were not firm enough for removal at the designated time.

In the case of test samples for the corrosion test, special provision was made for casting the steel-reinforced samples. Smooth steel bars of dimensions 6 mm x 150 mm long were cut for the making of the lollipop specimens. Each bar was prepared by polishing the surface with three grades of silicon carbide paper (P60, P120 and P240) and then washed, first with

acetone and then with water. The polishing removes imperfections such as mill scales which can alter the corrosion process (Pillai and Trejo, 2005) and the acetone removes grease (Gunasekaran et al, 2013). Subsequently, the steel bars were taped with 3M Scotch electrical tape to expose only 30 mm in some and 60 mm bare steel in the others (Figure 4.6). The smaller working surface is used for samples in the cyclic wetting and drying corrosion test (Section 4.4.2.3) while the larger exposed surface is used to promote cracking of samples in the impressed voltage corrosion test (Section 4.5.5.2). Experimental work done by Mietz et al (2000) showed that, of all the methods commonly used, 3M Electrical Scotch tape is the most effective at preventing corrosion of steel on the non-working area of the steel within the concrete.

Small cylindrical moulds were not available and therefore a special apparatus was designed and fabricated for the making of the lollipop samples (Figure 4.7). Plastic tubes 65 mm x 120 mm high were made for the casting of the concrete lollipops. These tubes were fitted in the base of a jig that had a circular indentation to accommodate 12 tubes as shown in Figure 4.7. A matching lid was made for the jig. After the assembly of the jig, the concrete was poured in the tubes and covered with the lid to help with the alignment of the steel and support of the tubes. The steel were immediately inserted in opening to a depth of 30 mm from the base of the concrete. Markers were placed at the top of the steel rods to ensure a 30 mm cover to the end of the rod. The entire assembly was left in place for 24 - 48 hours for the hardening of concrete after which the samples were extruded from the tubes. The samples were then moved to the curing containers (Section 4.2.2). Three specimens were made for each SCC samples but to ensure that substitute specimens were available in the event corrosion was initiated on areas outside of the working area of the steel, extra specimens of each SCC

sample was made. A total of approximately 160 specimens were made for testing and for contingency measure.

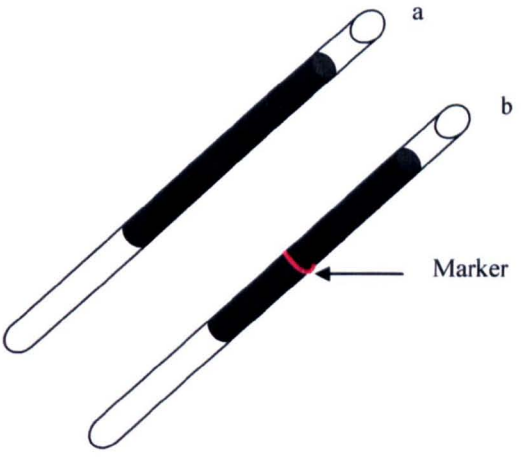

Figure 4.6 a) Steel bar wrapped with electrical tape to permit corrosion on the working surface only and b) marker on taped area to identify length for insertion in concrete

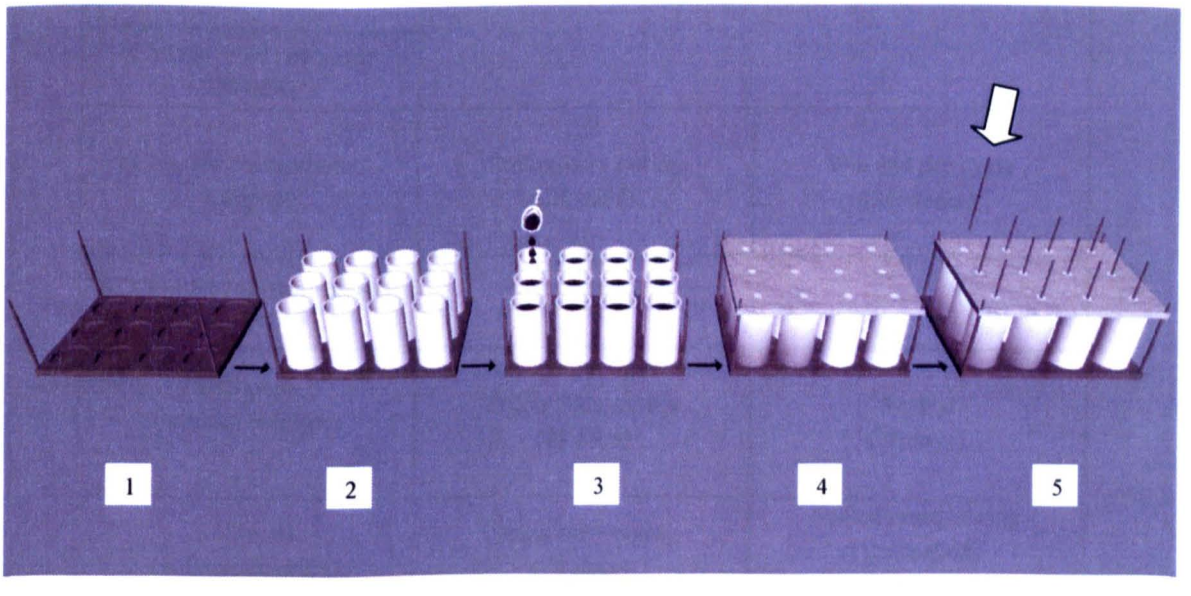

Figure 4.7 Process of casting reinforced concrete specimens; 1) base of jig that supports the moulds, 2) base with moulds in place, 3) placing of concrete, 4) fitting of lid to secure assembly, and 5) insertion of steel rods to pre-determined depth

4.4.2. Curing Conditions

4.4.2.1. WATER BATH

The concrete cubes and prisms were immersed in water at 21°C and approximately 70% relative humidity after demoulding. Most specimens were removed 24 hours after casting but some remained in the moulds for period up to 48 and more hours mainly because they were not firm enough for removal. The samples were kept in the curing tank until the time for testing. The curing regimes for the lollipop samples are shown in Table 4.7 and described immediately below.

Table 4.7 Curing regimes for lollipop samples

Type of corrosion test	**Curing conditions**	
CYCLIC WETTING AND DRYING		
Chloride contaminated lollipops	Preliminary curing (28 days)	Wet and dry cycle (36 weeks)
ACCELERATED (IMPRESSED VOLTAGE)		
Lollipops (without chloride)	Preliminary curing (28 days)	Soaked (28 days)
Lollipops (without chloride)	Preliminary curing (28 days)	Sealed moist-curing (Un-soaked) (28 days)

4.4.2.2. PRELIMINARY CURING

After the concrete lollipops were extruded they were all wrapped in moist fabric and placed in plastic bags. The plastic covering helped to maintain a relatively high relative humidity. The plastic-covered specimens were also stored in an area with high relative humidity.

4.4.2.3. WET AND DRY CYCLE

After the preliminary curing, some lollipop samples were exposed to wet and dry cycles to promote corrosion of the embedded steel as done by Al-Mehthel et al (2009). This was carried out by placing the samples in a water bath for 4 days while the other 3 days of the week the samples were placed in a conditioning cabinet at 35°C. This curing regime was repeated for 36 weeks. The wet cycle is required to provide a low resistivity in the concrete, promoting the migration of ions, in particular chloride ions, in the pore solution. The dry condition is more favourable to the diffusion of oxygen. The complete cycle is designed to provide an environment that enhances corrosion of the steel. Current density testing, using a potentiostat/galvanostat instrument (Section 4.5.5.3) and half cell potential test (Section 4.5.5.3), was carried out periodically on these samples.

4.4.2.4. SOAKING

It was desired to determine the likelihood of depletion of the inhibitor in the concrete. There are reports that corrosion inhibitor is more susceptible to leaching in seawater (Gonzalez et al, 1998 & Broomfield, 2007) than river water. Hence containers with artificial seawater made with 3.5% NaCl were provided to accommodate some of the lollipop samples in order to promote leaching (Figure 4.8). The samples were placed in the containers after preliminary

curing and remained in this condition for 28 days. The samples were later placed in the electrochemical cell (Section 4.5.5.2) with a high concentration of NaCl, to determine if, with these conditions, the corrosion inhibiting capacity would be lowered. Half cell potential test (Section 4.5.5.1) was also performed at the end of the soaking period.

Figure 4.8 Samples placed in aqueous solution (1g concrete to 10 g water) and covered to prevent evaporation

4.4.2.5. SEALED MOIST-CURING

The other set of uncontaminated samples were kept in double-layered plastic bags for 28 days after the preliminary period of curing. The outer bag contained water to maintain a high relative humidity while the inner bag protected the samples from direct contact with water. This condition was created to prevent leaching of the corrosion inhibitor from the specimens while providing an environment that would facilitate possible development in the microstructure as that which may have occurred in the other set of un-contaminated samples in the saline solution. Some of these specimens were also used to detect self-healing in corroded lollipop samples. All specimens were transferred to an electrochemical cell for accelerated corrosion (Section 4.5.5.2) after this extended period of curing.

4.5. TEST METHODS

4.5.1. Tests on Plastic Pastes and Concretes

4.5.1.1. SETTING TIME

Immediately after mixing each of the pastes as described in Section 4.3.1.3, in accordance with the proportions given in Table 4.4, they were placed in a lightly oiled Vicat mould and levelled with the rim of the mould. The filled mould was placed in a Pyrex dish and then placed in the temperature-controlled water bath. The water level was kept at approximately 8 mm above the base of the dish. In contrast to the procedure used in BS EN 196-3, the Vicat mould was not in direct contact with water at any time as this could result in a leak of the paste. For the normal pastes, the bath water was maintained at 20°C. Tests were also done at 30 and 40°C for the high temperature pastes as mentioned in Section 4.3.1.2.

To determine the initial set, the mould was removed from the bath and placed on the platform of the Vicat apparatus. The initial set needle, after positioning, was brought to the surface of the specimen and released. The penetration of the needle is then noted. The initial set is attained when the needle is 3-9 mm above the base of the specimen. The final set needle was fitted to the Vicat apparatus to establish the final set. Again, the needle was lowered until it was just in contact with the surface of the specimen and then released. The final set was achieved when the needle penetrated the sample by 0.5 mm. Readings for the initial set were taken at different time intervals; generally the interval got narrower (approaching 10 minutes) as the initial or final set drew nearer.

The advantage of the setting time test is that the Vicat apparatus that is utilised is a very simple device that does not by itself present any difficulty in operating. However, one of the limitations is that the Vicat apparatus used herein required manual operation and hence can be laborious if the setting time is, for example, 8 hours long. The flexibility in the consistency of the paste is constrained by the geometry of the mould which is made of a truncated cone with two open ends and this can allow leaking if the test is not set up carefully.

4.5.1.2. VISCOSITY TEST

The Brookfield rheometer was used to determine the effect of the corrosion inhibitor on the viscosity of the fly ash SCC paste. In order to keep within the operation range of the rheometer, the water/cement ratio had to be changed from 0.32 (which is used in the concrete) to 0.45. Even then, the viscosity of the control silica fume paste exceeded the measuring capacity of the equipment and hence the silica fume SCC pastes were eliminated from this test. To prevent slippage of the paste from the surface of the spindle, a vane was used (Saak et al, 2001). As the Brookfield LVD rheometer was not initially assembled with a vane spindle, it had to be calibrated against one of the cylindrical spindles in the kit that was similar in size. The calibration was done in glycerine at a temperature 21 ± 1°C at different speed (0.3 - 5 rpm), following the same procedure that was used for the actual test. This facilitated the determination of the viscosities of the pastes. After mixing (Section 4.3.1.3), the paste was immediately introduced into the glass cylinder (Lachemi et al, 2004) and then assembled as shown in Figure 4.9 with the bath water set at 21 ± 1 °C. Subsequently, the spindle was set to rotate at rate of 0.3 rpm and the measurement of viscosity taken.

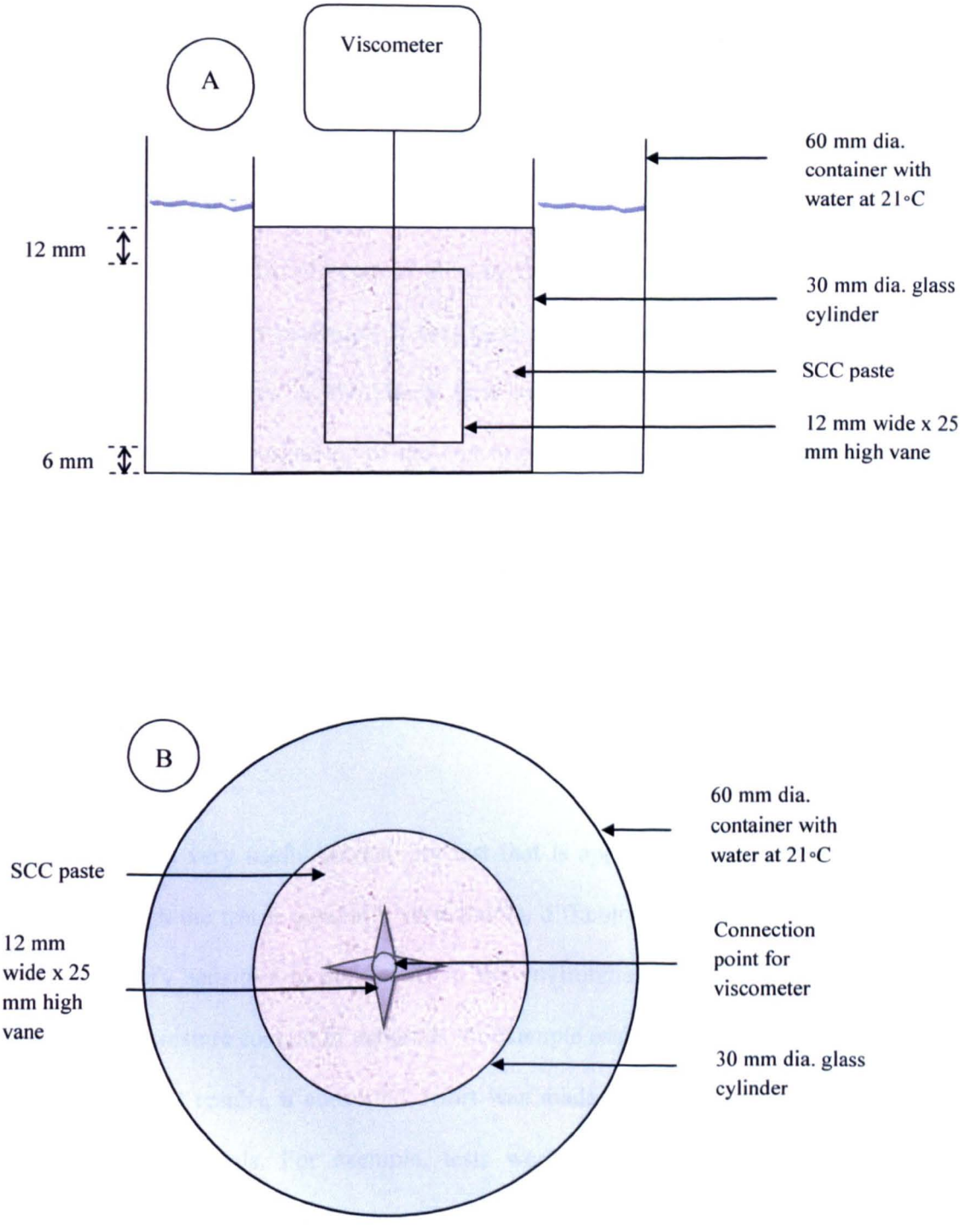

Figure 4.9 Elevation (A) and plan (B) of setup of viscometer with temperature-controlled bath for determination of viscosity of SCC paste

4.5.1.3. SLUMP TEST

A slump flow test was conducted with a standard Abram's cone that is typically used for the slump test of traditional concrete. The base plate had two concentric circles; the inner one was centrally placed and had a diameter of 200 mm. The outer circle had a diameter of 500 mm. After the cone was placed on the inner circle, it was filled with concrete. Upon removal of the cone the time for the concrete to flow to the 500 mm mark (t_{500}) was noted. The diameter of the spread was measured at two locations perpendicular to each other (Figure 4.10) and the average taken as the slump flow measurement. Any bleeding, marked by noticeable difference in consistency of the concrete around the edge, was also noted. This procedure conforms to that of EFNARC (2005) which apparently was the main body that provided guidelines on SCC in Europe up to 2009. However, checks have shown that the procedure conforms to the requirements of BS EN 12350-8 which was published in August 2010.

The slump test is a very useful workability test that is appropriate for laboratory and site purposes. Although the test is generally very simple, difficulty was experienced as this type of concrete is very sensitive to conditions in the environment and materials. Changes in temperature and moisture content in materials for example easily result in variation in results. To obtain consistent results, a concerted effort was made to control the conditions in the environment and materials. For example, tests were conducted with room temperature between 19 and 23°C. Further, the sequence of mixing was fixed and the same type of mixer was used throughout.

Figure 4.10 Measurement of ordinary slump flow of SCC

4.5.1.4. J-RING TEST

Procedurally, the set up of the J-ring test is the same as the slump flow test except that a J-ring is placed centrally around the cone. After the removal of the cone (Figure 4.11), the time for concrete to flow through the ring to the 500 mm mark (t_{j500}) and the two diameters, d_{jx} and d_{jy} of the spread were noted. The average of the two measurements of diameter represents the J-ring slump flow SF_J. The height of the concrete around the perimeter of the J-ring was also noted at four locations (h_{x1}, h_{x2}, h_{y1} *and* h_{y2}) positioned at 90° apart from each other. The height of the concrete in the centre of the ring (h_0) was also obtained. These heights were used in the computation of the blocking step (B_j) which provides a measure of the risk to blocking (Equation 4.1).

$$B_j = \frac{(h_{x1}+h_{x2}+h_{y1}+h_{y2})-h_o}{4} \qquad 4.1$$

Figure 4.11 The measurement of J-Ring flow and blocking step of SCC

4.5.1.5. V-FUNNEL TEST

The V-funnel test estimates the filling ability of the concrete. The apparatus consists of a metal 'V' shaped container, open at the top and with a sliding door at the base. The apparatus was filled with approximately 10.5 l of concrete. The door was then released and the timer started simultaneously. The V-funnel time is the period for the concrete to be emptied from the funnel.

4.5.1.6. SIEVE SEGREGATION

The segregation test is recognised as one of the tests that are frequently used in European countries to determine static segregation resistance in plastic SCC mixtures (The Concrete Society, 2005). The equipment needs for the test consisted of a balance, a 5mm testing sieve

with matching receiver and a container. A platform-type balance with a precision of 0.1g is also used.

At the beginning of the test, the mass of a receiver m_p was obtained and a container was filled with concrete and left to stand for 15 minutes. After this time has elapsed, approximately 5 kg of the concrete was poured from a height of about 500 mm onto a 4 mm sieve that had the receiver attached. The exact mass of this concrete m_c, was measured. After 2 minutes, the sieve with retained material was carefully removed and the mass of concrete plus the receiver was determined m_{ps} (De Schutter et al, 2008). The formula in Equation 4.2 was used to give the degree of segregation expressed as the Segregation Index (SI).

$$SI = \frac{m_{ps} - m_p}{m_c} x\ 100\% \qquad 4.2$$

4.5.2. Analytical Tests

4.5.2.1. MERCURY INTRUSION POROSIMETRY

The mercury intrusion porosity is a measurement of the mercury penetrated pores expressed as a fraction of the total volume of the sample (Galle, 2001). The principle of computing the porosity is based on the Washburn relationship that the intrusion mercury pressure (P_{Hg}) is inversely proportional to the diameter of the opening of the pore under injection (d_ρ) as shown in Equation 4.3. In this equation is seen that the surface tension of the mercury (γ_s) and the contact angle between the mercury and the pore surface (θ_s) have a bearing on the diameter of the pore.

$$d_\rho = \frac{(-4\gamma_s \cos\theta_s)}{P_{Hg}} \qquad 4.3$$

The shortcoming of using this method to quantify the porosity is due primarily to the ink bottle effect that is not taken into account in the general principle (Diamond, 2000). However, it is useful in measuring the total porosity down to 3 nm (Galle, 2001). This method of porosity evaluation was used to characterize the porosity of the different types of concrete to determine if there is any detectable modification of the pore structure when corrosion inhibitors are used. A value of 0.485 N/m was used for the surface tension and 130° was used for the contact angle. Approximately 4 to 6 representative fractions were taken from the mortar of the inner parts of the concrete samples to perform the test. The specimens were soaked in acetone for 20 minutes and the dried in the oven at 50°C for 24 hours.

4.5.2.2. SURFACE ROUGHNESS

The surface characteristic of the corroded steel rods from the un-soaked tests were determined by Stylus profilometer. The steel rods were polished with silicon carbide paper (P60 and P120) to remove the rust. After polishing, the steel rods were placed beneath the probe attached to the instrument. As the probe moved along the surface of the rod the roughness of the rod (R_a) was registered and a longitudinal profile produced. Aggregate particles that were tested were positioned similarly beneath the probe to obtain measurements.

4.5.2.3. THERMOGRAVIMETRIC ANALYSIS

Thermogravimetric analysis (TGA) was conducted on self-compacting concrete samples to determine the development in the cementitious mixtures. In order to conduct the test at predetermined time frames, fragments of the hardened pastes were removed from the samples prepared for the normal setting time test. For the concrete samples, the specimens were

removed from the lollipop samples after three days of accelerated corrosion. The fragments were then placed in a vacuum desiccator over silica gel for 24 minutes to dry the specimens and halt the hydration process. The fragments were then pulverised and passed through the 250 micron sieve. Approximately 10 mg of the fraction passing the 250 micron sieve was used for chemical analysis. A Perkin Elmer thermogravimetric analyser with ceramic pans was used in the execution of this test. The samples were individually placed in the ceramic crucibles and the precise weights of the samples were obtained. The analyser was programmed to heat the sample up to 600°C at a rate of 3°C per minute up to 220°C and 10°C per minute thereafter (Lothenbach and Winnefeld, 2006). Nitrogen gas was used to maintain an inert environment around the sample. For this research, the outputs of the experiment were the TGA curves showing the loss in weight per degree Celsius and the differential thermogravimetric (DTG) curves.

This test helps in the identification of some of the principal reaction products of hydrated cement. It is particularly useful in the quantification of the calcium hydroxide and the evaporable water (both free water and water incorporated into the mineral phases) (Loukili et al, 1999) and hence is used to explain a number of phenomenon relating to the hydration process.

4.5.2.4. X-RAY DIFFRACTION ANALYSIS

Approximately 100g of pulverised cement paste (prepared as in Section 4.5.2.3) was used for the X-ray diffraction (XRD) analysis. X-ray diffraction analysis is best suited for materials with crystalline phases in which the atoms are aligned in a regular patterns. This structure

enables each atom to produce a characteristic diffracted pattern when subjected to an incident ray. The pattern is produced in accordance with Bragg's equation (Equation 4.4).

$$2d_r Sin\theta_x = n_i \lambda_1 \qquad 4.4$$

where the characters in the equation are defined as:

d_r – the distance between lattice planes in the crystal

θ_x – is the incident/diffracted angle

n_i – is an integer

λ_1 – is the wavelength of the scattered wave

The samples were placed and levelled in the sample holder and then positioned in the chamber of a Bruker-AXS D8 Advance in which is installed a Cu-anode x-ray tube, a Göbel mirror, a diffracted beam collimator with a 0.12° Soller slit and a Sol-X energy-discriminating x-ray detector set for CuKα radiation. The scanning was conducted between 5 and 70° at a speed of 2° per minute.

This test also helps in the identification of the reaction products in the hydrated cement pastes and gives an indication on the relative proportion of the compounds. One of the limitations of the XRD test is that identification on the compound is carried out by software that is pre-programmed with the signature response of the commonly used compounds. Therefore the computer is unable to identify compounds that are not pre-programmed.

4.5.2.5. OPTICAL EMISSION SPECTROSCOPY

Optical emission spectroscopy was used to determine the chemical composition of the mild steel bars. A Foundry Master brand instrument was employed for the determination of the constituents of the metal which was carried out through an analysis of the radiation from exited atoms (Saghafifar, 2011). A stand is provided for the positioning of the sample and a spark is set off between the sample and an electrode. This causes the electrons of the atoms that comprise each element to emit light. The detectors in the polychromator of the analyzer measure the peak intensities in the spectral patterns that are obtained to produce an output on the quantitative and qualitative description of spectrum.

4.5.2.6. SCANNING ELECTRON MICROSCOPY

Scanning electron microscopy (SEM) analysis was carried out on the corroded and un-corroded SCC samples. Some lollipop samples were cored centrally around the steel bar. These cores were then sliced into 20 mm thick sections to obtain concrete disks for SEM examinations. Each disk was ground with No. 250 and 500 SiC grit and polished with diamond fabric. Fragments of concrete were also analysed. The specimens were placed in vacuum desiccators over silica gel for 24 hours and subsequently the surfaces of the samples were coated with aluminium. The scanning electron microscope was used to obtain micrographs from secondary electron, backscattered electron and energy dispersive x-ray modes as shown in Figure 4.12. An accelerating beam voltage of 20.0 kV with different magnifications was used in the test.

The SEM chamber can only accommodate small specimens and hence it is imperative that a representative specimen is obtained to ensure integrity in test results. Additionally, materials

like concrete are poor conductors and therefore an electrically conductive coating is essential to help in the transmission of the electrons from the surface of material.

Scanning electron microscopy was also used for the measurement of the fly particles. Samples of fly ash were placed onto 12 mm studs covered with sticky carbon discs. They were coated with gold on a sputter coater for 4 minutes to obtain a film of gold of approximately 24 nm thick. The samples were imaged at various magnifications on a Jeol 6060LV scanning electron microscope with an accelerating beam voltage of 25.0 kV.

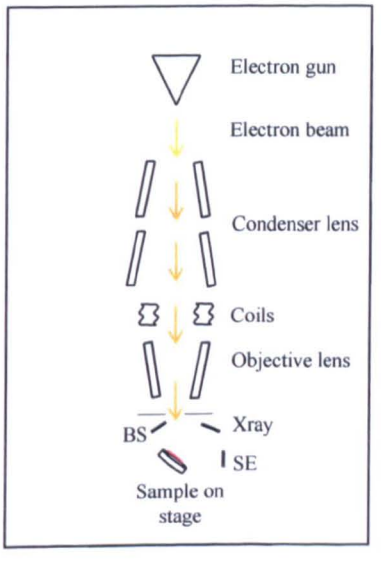

Figure 4.12 Diagram showing the SEM electron beam
Source: Dystra and Reuss, 1992; and Goodhew et al, 2000

Note
The SEM electron beam that is produced by tungsten filament is emitted by an electron gun. The beam travels down the electron column where it is focused to a minute spot by the condenser lens and with the aid of the coils and the objective lens is used to scan the surface of the sample. The backscatter (BS), secondary electron (SE) and X-ray detectors collect signals generated by the electron beam as it interacts with the specimen.

4.5.2.7. IMAGE ANALYSIS

Digitized images captured by SEM and photography can create 2-dimensional pixel arrays of objects and make it possible to carry out computerised analyses on images. A pixel is a representation, by shade of colour or shade of grey, of the density of back-scattered electrons in SEM images, or of the brightness of a photographic image, associated with a small but finite area. For example, an 8-bit image is composed of up to 256 levels of greys which define the different intensity of electrons or brightness at each pixel.

An image analysis software, ImageJ, was used to characterise some of the images of concrete specimens that were obtained from SEM and photography. For determination of the interfacial transition zone porosity, backscattered (BSE) images at 540x magnification captured from polished and coated concrete samples were analyzed. The cementitious region extending to 50 μm from the interface of aggregate particles was studied in order to locate the ITZ for each sample. The images were calibrated to enable quantification of parameters after which the thresholds were applied. The principle of pixel thresholding involves the computerised construction of a histogram based on the numbers and intensity values (shades of gray) of the pixels in the processed area where 0 intensity represents black and 255 represents white. This facilitated analysis of the outlined pores. Pixels with intensity values between 0 and 90 aided by visual examination were used to differentiate the detectable pores from other features in the image. Image analysis was also employed for the determination of the crack density and tortuosity of fracture due to corrosion, but these images were obtained from photography. Pixel thresholding was also done on the digitized photographs and this allowed for the segmentation of the image which helped to identify the voids in the concrete. The desired feature was placed in the foreground by assigning it an intensity value of 255 and all other features were assigned an intensity value of 0 to keep them in the background (Pan,

2002). Using the analyze particle tool from the menu, the volumes of the pores were obtained. An average of 10 measurements was used for each porosity value and the cracks from one fractured specimen were analyzed for the determination of the crack density of the corroded sample. In analyzing the tortuosity of the fracture, linear measurements were taken of the displaced distance and the tortuous path.

4.5.3. Mechanical Tests

4.5.3.1. COMPRESSIVE STRENGTH TEST

The procedure for conducting the compressive strength was carried out in accordance with the BS EN 12390-3. The test was carried out on saturated-surface dried specimens and the loading rate was approximately 0.6 MPa/s. The strength was obtained but the Dennison testing machine did not give the displacement and hence the modulus of elasticity was not computed.

4.5.3.2. FLEXURAL TENSILE TEST

Concrete prisms with dimensions 100 x 100 x 500 mm were used to determine the tensile strength of the concrete. The wet specimens were blotted with fabric and the testing surfaces were cleaned. The specimens were aligned on the loading frame and an initial loading not exceeding 20% of the anticipated ultimate load (estimated from trial test) was applied. The rate of loading was approximately 0.05 MPa/s.

4.5.3.3. ULTRASONIC PULSE TEST

A PUNDIT (portable ultrasonic non-destructive digital tester) instrument was used to determine the dynamic modulus of elasticity of concrete at the age of 28 days. The prisms

were placed with the longitudinal axis parallel to the working surface. Coupling cream was applied on the two transducers connected to the instrument and these were then held firmly against the two ends of each prism. The instrument was then set to obtain the transit pulse time and, hence, the velocity and modulus of elasticity.

4.5.4. Tests on Transport Properties

4.5.4.1. Porosity Test

This test was used to quantify the pores in the SCC samples. The level of penetrable pores in the hardened concrete was determined on 100 mm concrete cubes at the ages of 7 and 28 days just after removal from water tank. In order to obtain the saturated-surface dry mass (m_{ssd}) measurement, each specimen was patted with a dry chamois cloth and weighed. Subsequently, specimens of reference SCC and corrosion inhibiting SCC were oven-dried to constant mass at 100°C to remove the evaporable water. The samples were then allowed to cool to ambient temperature and then weighed (m_d). The measurement of absorbed water (n_p) is expressed as a percentage of the dry mass (Equation 4.5). As the absorbed water occupies the pores, it is used to quantify the volume of pores.

$$n_p(\%) = \frac{m_{ssd} - m_d}{m_d} \times 100 \qquad 4.5$$

4.5.4.2. Absorption

Three 100 mm concrete cubes from each mixture were oven dried at 100°C and then cooled. The peripheral sides of the inflow face of the specimen were sealed with paraffin after which the inflow face was immersed in water up to a depth of 5 mm (Gonen et al, 2007). Measurements of the mass of the specimens were taken before immersion in water and at 10, 20, 30, 60, 120 and 180 minutes after immersion. The quantity of absorbed water at each time interval was then computed and normalized over the exposed area. Equation 4.6 is used to

determine the coefficient of sorptivity which is depicted on a graph of absorption (I_Q) versus square root of time ($t^{0.5}$). It is suggested that changes in the microstructure resulting from leaching and/or advanced hydration can have an effect on the level of capillary absorption (Martys and Ferraris, 1997) but since the duration of this test is short this effect is neglected in the interpretation of the results from this test.

$$I_Q = S_\alpha t^{0.5} \qquad 4.6$$

Where

I_Q = the quantity of fluid absorbed per cross-sectional area of the inflow face of the specimen. The mass absorbed is in grams and the area is in square centimetre.

S_α = sorptivity with units of cm/min$^{0.5}$

t = time for the quantity of water to be absorbed in minutes

4.5.4.3. ELECTROMIGRATION

The non-steady state chloride electromigration test was done on 100 mm diameter x 50 mm thick specimens in accordance to NT Build 492 test method. A voltage of 60 V was applied to the electrochemical cell for a period of 6 hours.

4.5.4.4. ELECTRICAL RESISTIVITY

Concrete specimens with a diameter of 100 mm on the cross-sectional area (A) and a length (L) of 125 mm were tested following the procedure used by Polder (2001). To carry out the test, two copper plates that were attached to a T1653 multi-function tester were placed on the two ends of the water-saturated specimen. One sheet of water-saturated paper towel was placed between the concrete and each sheet to improve contact. A potential was applied to produce a current of 1 mA using 50 Hz AC (with sinusoidal wave) and the electrical resistance (Re) of the concrete was determined. The potential resistivity of the concrete (Γ) was computed using Equation 4.7

$$\Gamma = \frac{AR_e}{L} \qquad 4.7$$

4.5.5. Electrochemical Processes for Corrosion Tests

4.5.5.1. HALF CELL POTENTIAL

The half cell potential is a non-destructive test that determines the potential between a standard reference electrode and the embedded steel in reinforced concrete in order to predict the likelihood of corrosion initiation (Table 4.8). This test was included in the author's experimental programme to detect the onset of corrosion in the lollipop samples (Sections 4.4.2.3 - 5). The test was conducted in accordance with the ASTM C876 test method and the set up is illustrated in Figure 4.13. Instead of the copper-copper sulphate electrode (CSE) stipulated in the American test method, a saturated calomel electrode (SCE) was connected to the half cell circuit. The ASTM C876 interpretation of the voltmeter reading based on the SCE (x_p), is provided in Table 4.8.

The test provides instantaneous readings that immediately determine whether corrosion is in progress. That is, based on the magnitude of the potential reading, the probability of presence or absence of corrosion can be determined in accordance to Table 4.8. However the test does not quantify the rate of corrosion. Besides, there are instances when the reading can indicate that corrosion is initiated even though conditions in the local environment hinder corrosion. To overcome such an anomaly, potentiostat readings were taken when the half cell readings suggested that corrosion was initiated.

Table 4.8 Interpretation of potential readings based on SCE

Reading , x_p mV	**State of steel bar**
$x_p > -120$	90% Probability of no corrosion
$-270 \leq x_p \leq -120$	Uncertain
$x_p < -270$	90% probability of active corrosion

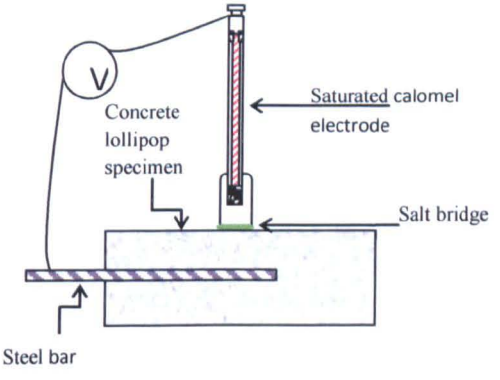

Figure 4.13 SCE half cell circuitry with sample and 10 MΩ impedance resistor-voltmeter (V)

4.5.5.2. IMPRESSED VOLTAGE

In order to determine the resistance to corrosion, the lollipop samples were exposed to an impressed voltage to accelerate corrosion. The working area of the embedded steel in each lollipop sample was 1.159×10^{-3} m^2. Three reinforced concrete specimens were made from each SCC mix. The impressed voltage was applied to samples in the experimental series that were designed to determine:

a. the potential for the depletion of the inhibitor through leaching in seawater or consumption in the chemical reaction when the concrete is under chloride attack and
b. the ability of the individual corroded reinforced sample to undergo self-restoration after their removal from the corrosive environment.

The lollipop specimens were subjected to an electrical field to accelerate corrosion of the reinforcing bars in order to produce cracks in the concrete in a short time. After trial tests, an electrochemical cell consisting of a 10% sodium chloride (NaCl) concentrated solution was made and connected to a 40V power supply to facilitate this process. Application of a high voltage in corrosion setup is not unique to this study. Other researchers (Kockal, 2008; Boğa and Topçu, 2012; and Güneyisi et al 2005) have used 10 - 30V DC in reinforced concrete durability studies to increase the reinforcement's response time to corrosion. The concentration of NaCl used in the solution for electrochemical activity in these studies ranged from 4 to 15%. The use of a high voltage introduces the potential for large rates of hydrogen production but, in fact, these researchers don't appear to have found this to be a problem. Whereas these previous researchers used a large steel area in the corrosion of the reinforced concrete in the respective studies, a small area of steel is used in this study, further reducing the possibility of hydrogen induced damage. Compared to the before mentioned studies, the smaller working area of steel will reduce the corrosion current for each level of current density and hence help to mitigate any emission of gas such as hydrogen.

A hollow perforated stainless steel cylinder serving as a cathode was placed in the solution. The 65 mm x 120 mm specimens were immersed in the electrolyte (and within the steel cylinder) and the anode and the cathode were connected to the respective positive and negative terminals of the DC power supply. A 10Ω resistor was also placed in series in the circuit (Figure 4.14).

The specimens were removed daily for the monitoring of surface cracking and corrosion current density (Section 4.5.5.3.) with a microscope and potentiostat/galvanostat respectively. As for the samples in the soaked/un-soaked test, there were three specimens and the corrosion

process for each specimen was terminated at 3, 4 and 6 days respectively after the commencement of the electrochemical process. The overall duration of the electrochemical process for each sample was therefore 6 days. Micro-structural examinations (Sections 4.5.2.1 - 4 and Sections 4.5.2.6 -7) were then carried out on some of the specimens at the end of the test.

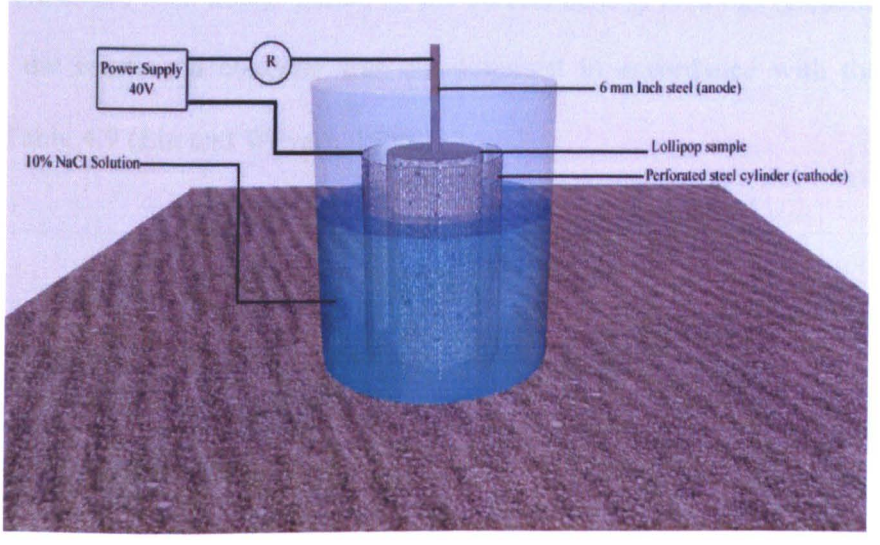

Figure 4.14 An electrochemical cell with resistor (R) and 40 volt set up to trigger corrosion in SCC samples

4.5.5.3. Corrosion Current Density

Measurement of corrosion current density was achieved with a linear polarisation resistance (LPR) via an ACM Gill 8 potentiostat/galvanostat instrument. A calomel electrode (+244 mV) was used as reference and a strip of steel sheet used as the auxiliary electrode. For the measurements, the reference, the auxiliary and working (steel rod) electrodes were connected to the potentiostat. Some steel rods had a working area of 5.935×10^{-4} m^2 while others had 1.159×10^{-3} m^2. The working areas were made small to maximise the effect of current on

corrosion. A scan rate of 0.1mV/s within a range of ±10 mV was used in the test. Similar settings were used by Al-Mehthel et al, 2009. The potentiostat was set to automatically compensate for the resistivity of the concrete samples. For each sample, a current/voltage test was done. This allowed the rest potential of the samples to be checked to determine that the rest potential was stable. A graphical display of the LPR test also showed a linear relationship between the potential and the current density during the test. Where it was detected that the rest potential was not stable, that sample was left for later testing, (in most instances, over 20 specimens were tested each time). Based on the current density readings (Equation 3.10), the corrosion in the reinforced concrete was characterised in accordance with the references provided in Table 4.9 (Liu and Weyers, 1998).

Table 4.9 Qualitative assessment of corrosion

Current density (mA/cm^2)	**State of corrosion**
< 0.0001	Passive
0.0001 – 0.0005	Low corrosion
0.0005 – 0.001	Moderate
> 0.001	High corrosion

4.6. CONCLUSION

As shown, efforts were made to select a combination of materials that would fulfil the requirements of the research. The concrete was designed to ensure that the possibility of harmful environmental effects was minimised. Additionally, the experimental programs consisted of test methods that produced the relevant data on the specific property under testing.

FRESH PROPERTIES

5.1. INTRODUCTION

Whereas in most traditional concrete the principal requirements of the fresh properties is adequate workability which is usually determined by the slump test, with SCC the emphasis is placed on the rheology of the material. It is important that this distinction is understood as workability is concerned with the ease of mixing, placing and compaction operations but rheology controls the ability of the material to flow uninhibited by objects to a desired location and to achieve a certain degree of compaction without other intervention. For example, if the slump spread of SCC is satisfactory, that by itself would not necessarily guarantee an acceptable rheological behaviour from the concrete. Therefore, the study of the rheology although applicable, is not an essential property of most types of traditional concrete but it is an integral aspect of SCC. Knowing the pivotal role of the rheology in the functionality of SCC, the study of the flow properties of the corrosion-inhibited SCC can be appreciated. The essence of this chapter is to determine if there is any modification, not only in workability but in the rheological related performance of SCC when corrosion inhibitor is incorporated in the mix. Since the setting of the cementitious material will impinge on the rheology, the setting time test is also included in the experimental programme described in this chapter.

5.2. POWDER PASTES

Powder pastes of different combination of the ordinary Portland cement (OPC), corrosion inhibitors, superplasticiser and the mineral admixtures (Section 4.3.1.1) used in the types of self-compacting concrete in this research were tested to identify the contributory effect of the corrosion inhibitors on the setting times of SCC. The setting times were established with a

water/powder ratio of 0.26 (for reason explained in Section 4.3.1.2) and with a penetration of 6 ± 3 mm from the base of the sample on a Vicat apparatus (Section 4.5.1.1). Two samples were used for each test and each end point is determined by two measurements in the same sample.

5.2.1. Setting times

Generally, in the testing of the powder pastes, it was noticed that the mixtures that did not contain any corrosion inhibitor or superplasticiser had a very sudden change in consistency when the initial setting point was approached. This resulted in a well defined setting point. Self-compacting concrete pastes with and without corrosion inhibitor on the other hand, showed a more gradual morphological transition. This seems to agree with earlier findings (Lee et al, 2004) that, when ultrasonic pulse velocity measurements were used to estimate setting time in cementitious materials, the development was gradual in high performance mortars and concretes, but abrupt in the normal concretes and mortars.

More specifically, the initial set of the CEM1 52.5R cement paste (1) at 20°C was 150 minutes. The initial setting times of the three fly ash SCC pastes, that is, FG, FM and FGC (Section 4.3.1.1), were significantly higher (Figure 5.1) than the pure cement paste. Fly ash is a pozzolanic material and it relies on the presence of an appreciable quantity of portlandite in the pore solution to trigger a reaction (Yang et al, 2011). It is also postulated that in the early stage of hydration of the paste, the fly ash acts as a nucleating site for crystal formation. These two phenomena serve to delay the reaction of fly ash (Neville, 2005 and Wade et al, 2010). Hence, marked setting retardation is seen with appreciable substitution (Colak, 2003). The direct effect of fly ash on the setting of cement can be seen by comparing the traditional fly ash paste (F) to the ordinary Portland cement paste (1).

The setting times for the silica fume SCC samples (SM and SG) are included in Figure 5.1. The carboxylic silica fume SCC (SM) paste also had higher setting times than the control SG paste. Other research has shown that silica fume, due to the micro-size particles, accelerates the early hydration times of cement (Cheng-yi and Feldman 1985) and this is confirmed by the setting times for the S paste shown in Figure 5.1. However, the combination of the multi-phase carboxylic inhibitor with the cement and silica fume resulted in an increase in the setting times of the OPC paste.

The superplasticising admixture that was incorporated in the fly ash SCC served to deflocculate the cement particles through steric repulsion and/or electrostatic action (Uchikawa et al, 1996). The superplasticising phase of the carboxylic admixture is thought to have carried out this function in a somewhat similar process. However, during the process, the superplasticiser also helped to delay the setting of the cement in the fly ash SCC mixes. This is illustrated in the setting times of the cement with the pure superplasticiser (G) which were markedly higher than the times for the pure cement paste (Figure 5.1). Nevertheless, the difference between the setting times of the reference SCC mixes FG and SG, and the corresponding inhibited SCC pastes (FM and FGC; and SM respectively) can be directly attributed to the inclusion of the corrosion inhibiting agents.

Corrosion inhibiting compounds have been known to influence the setting of cement but there is no general trend in their effect. Calcium nitrite based inhibitors usually expedite the setting process (Wombacher et al, 2004) but migrating corrosion inhibiting admixtures have been reported to have retarding actions on the cement hydration (De Schutter and Luo, 2004).

In the present study, the net effect of corrosion inhibitors on the initial setting times (shown qualitatively in Figure 5.2), of the three SCC concrete ranges from 19 to 104% with the carboxylic compound having the greatest effect in the fly ash mixes. The type of effect of all the admixtures is shown in Figure 5.2.

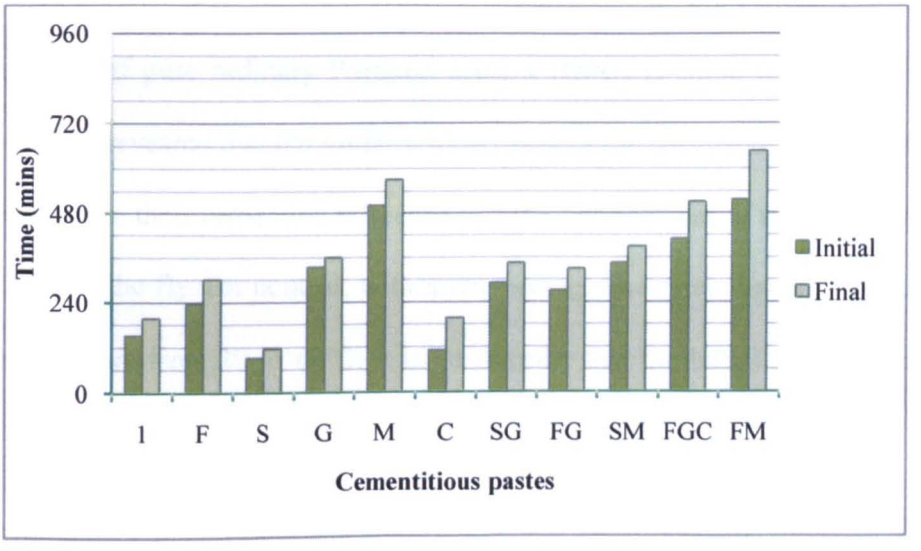

Figure 5.1 The change in setting times of cement in various powder mixes

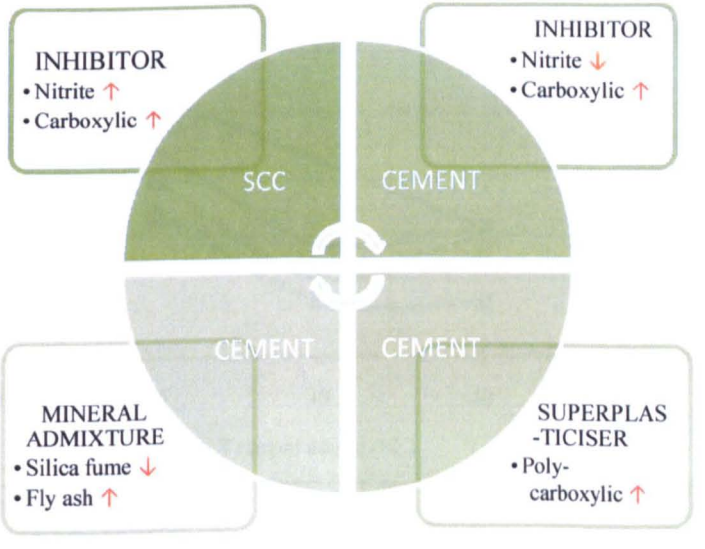

Figure 5.2 The influence of each admixture on the setting times of cement and SCC pastes

Figure 5.3 shows the change in setting times that occurred when the SCC pastes were subjected to higher mixing and curing temperatures. The general pattern was a decrease in the times as the temperature moved from 20 to 30°C with some of the samples (FG, FGC, SM and SG) experiencing an increase or marginal decrease in setting times as the temperature was further elevated to 40°C. This behaviour is consistent with the general pattern reported for the hydration of pure ordinary Portland cement (OPC) at these temperatures (Neville, 2005). The results revealed that the initial setting times of the corrosion-inhibited SCC pastes were all greater than their respective reference and the setting times of the FM paste deviated significantly from the fly ash control, with a decreasing, linear relationship between setting time and temperature from 20 to 40°C. It is noteworthy that the initial setting times at 40°C for all SCC pastes, with the exception of the SG sample, were very close.

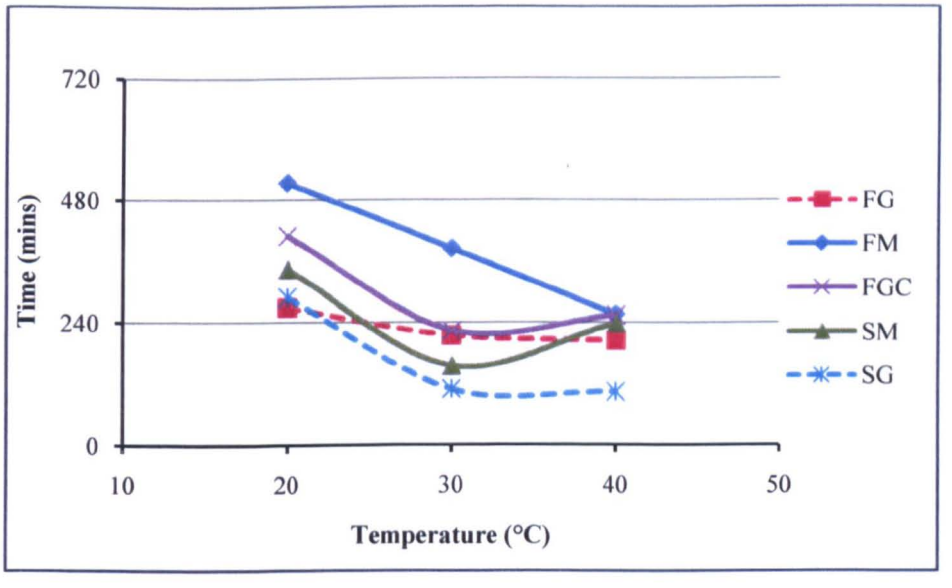

Figure 5.3 The effect of temperature variation on the initial setting times of SCC pastes

The study of the setting behaviour in the corrosion-inhibited SCC pastes with increase in inhibitor concentration is shown in Figure 5.4. Whereas there was little variability in the setting times of the nitrite-based paste (FGC) as the concentration changed from 0.3 to 1.0% (based on the powder content), the pastes incorporating carboxylic inhibitor (FM and SM) showed considerable increase in setting time as the dosage increased. The times for the final set are presented in Table 5.1. There is an established relationship between the initial ($\ddot{I}$) and final (S_{ft}) setting times (Neville, 2005) when the measurements are in minutes and it is provided in Equation 5.1. When this equation is used to estimate the setting times of the cementitious pastes under the various test conditions, the correlation coefficients for each is greater than 0.90, demonstrating that this relationship between initial and final setting time is valid for the cement pastes enriched with chemical admixtures.

$$S_{ft} = 90 + (1.2 \times \ddot{I}) \qquad 5.1$$

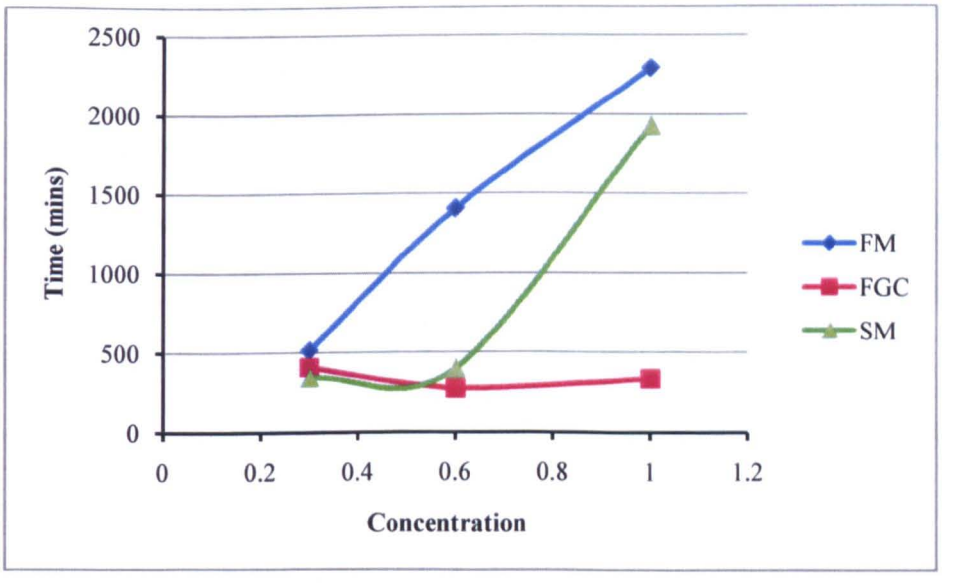

Figure 5.4 The effect of various concentrations of corrosion inhibitors on SCC pastes

Table 5.1 Final setting times of cementitious pastes

Types of pastes	Setting times (mins.)				
	Temperature			Concentration of corrosion inhibitor (%)	
	20°C	30°C	40°C	0.6	1.0
FG	330	300	255		
FM	645	495	315	1515	2460
FGC	510	285	315	300	405
SM	390	195	240	435	2070
SG	345	150	165		

5.2.2. Thermo-analytical Examination

In the hydration process, the introduction of water in cement initiates a reaction with the aluminates (C_3A and C_4AF) to produce calcium aluminate hydrates. Gypsum which is usually added to cement at a dosage of 3-5% is used to offset this reaction and participates in a reaction with these aluminates to form ettringite. The alite and belite, abbreviated as C_3S and C_2S, react to form calcium silicate hydrate (C-S-H) and in the process produce calcium hydroxide (CH).The production of calcium hydroxide is increased as hydration progresses. When a critical mass of calcium hydroxide, also known as portlandite, is made available the pozzolanic reaction will commence with the fly ash but the more chemically active mineral admixture - silica fume - is a little more spontaneous. Since in the very early stages the calcium hydroxide is not consumed in the pozzolanic reaction, this phenomenon underpins the theory for predicting the physiochemical development of the hydrating products in the cementitious materials.

Data acquired from the thermogravimetric analysis (TGA) programme (Section 4.5.2.3) are shown graphically with DTG (differential thermogravimetric) results versus temperature in Figure 5.5. Two sets of TGA tests were done on each sample, one set was used for analysis and the other was used to confirm the general behaviour of the material under test since it was done with a different TGA instrument. The points of interest are labelled 1, 2 and 3. The peaks at 1 and 2 indicate that calcium silicate hydrates, and ettringite (*Aft*) are decomposed in the temperature range of approximately 90 to 130°C (Paya et al, 2003). On the FG curve, peaks 1 and 2 are somewhat well developed with small overlap. Peak 1 is not distinguishable in the two inhibiting SCC pastes (FGC and FM) as there is significant overlap with peak 2. Calcium hydroxide was decomposed at temperature between 450 and 505°C as shown by peak 3 on the DTG graph (Loukili et al, 1999). The weight losses in the CH are given in Table 5.2.

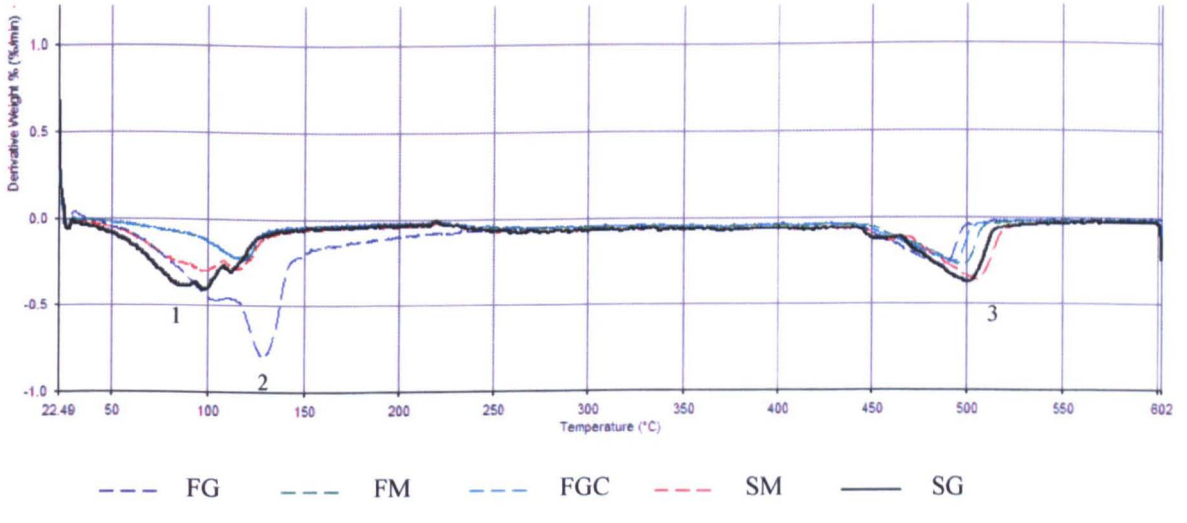

Figure 5.5 DTG curves showing decomposition of the hydration products of 12-hour old corrosion-inhibited and non-inhibited pastes

Table 5.2 Quantification of $Ca(OH)_2$ in SCC pastes

Cement Pastes	$Ca(OH)_2$	
	% loss	Peak temperature (°C)
FG	3.20	488
FM	3.04	494
FGC	3.09	496
SM	3.19	505
SG	3.33	501

Two methods that are generally used to determine the progress of hydration in concrete are a) the level of portlandite and b) the amount of bound water. When the level of portlandite is used to determine the degree of hydration in the cementitious materials it is seen that the three fly ash SCC curves almost completely overlap at the point of decomposition suggesting that the level of portlandite is approximately the same owing to the low generation of calcium hydroxide in the early stages. However, the values show that the calcium hydroxide is lower in the corrosion inhibited SCC than in the reference. Also, the more defined inflection points at peak 1 shows a more pronounced chemical activity in the growth of C-S-H in the FG control ash paste which is not seen in the corrosion-inhibited pastes (FGC and FM). The production of lower levels of C-S-H and ettringite in the initial hydration period suggests that

there is continued delay in the hydration of the corrosion-inhibited pastes at 12 hours. An observation of the two silica fume pastes DTG curves shows that both had higher levels of calcium hydroxide than the fly ash SCC pastes which, presumably is largely due to the higher cement content of the silica fume SCCs. However, between the silica fume based SCC pastes, the SM had less portlandite than the SG SCC paste at 12 hours, signifying that the hydration of the carboxylic silica fume paste was slightly delayed.

The development of the hydration process was monitored via XRD (Section 4.5.2.4) at 24 hours after production of the pastes. The relative quantity of calcium hydroxide in the different pastes is determined by the intensity of the peaks in Figure 5.6. The relative portion of calcium hydroxide is more distinct in this test. For example, it is seen that the calcium hydroxide peaks at 24 hours on the FG curve have a stronger intensity than those of the two fly ash corrosion inhibited pastes, indicating that the hydration is more advanced in the traditional SCC paste at 24 hours. It should also be mentioned that the peaks in FM paste are the weakest of these three pastes. Thus, the relative delay in hydration of the fly ash inhibiting pastes seen in the setting time and TGA tests is shown to have continued at 24 hours. Unlike fly ash that takes a long period to react, silica fume, because of its large specific surface area, reacts fairly early. At 24 hours, the fine particles of silica fume would have started significant pozzonlanic reaction and therefore its progress would be identified by reduction in the $Ca(OH)_2$. Based on this argument, it can be concluded that the SG sample at 24 hours is more advanced in its development than the SM sample.

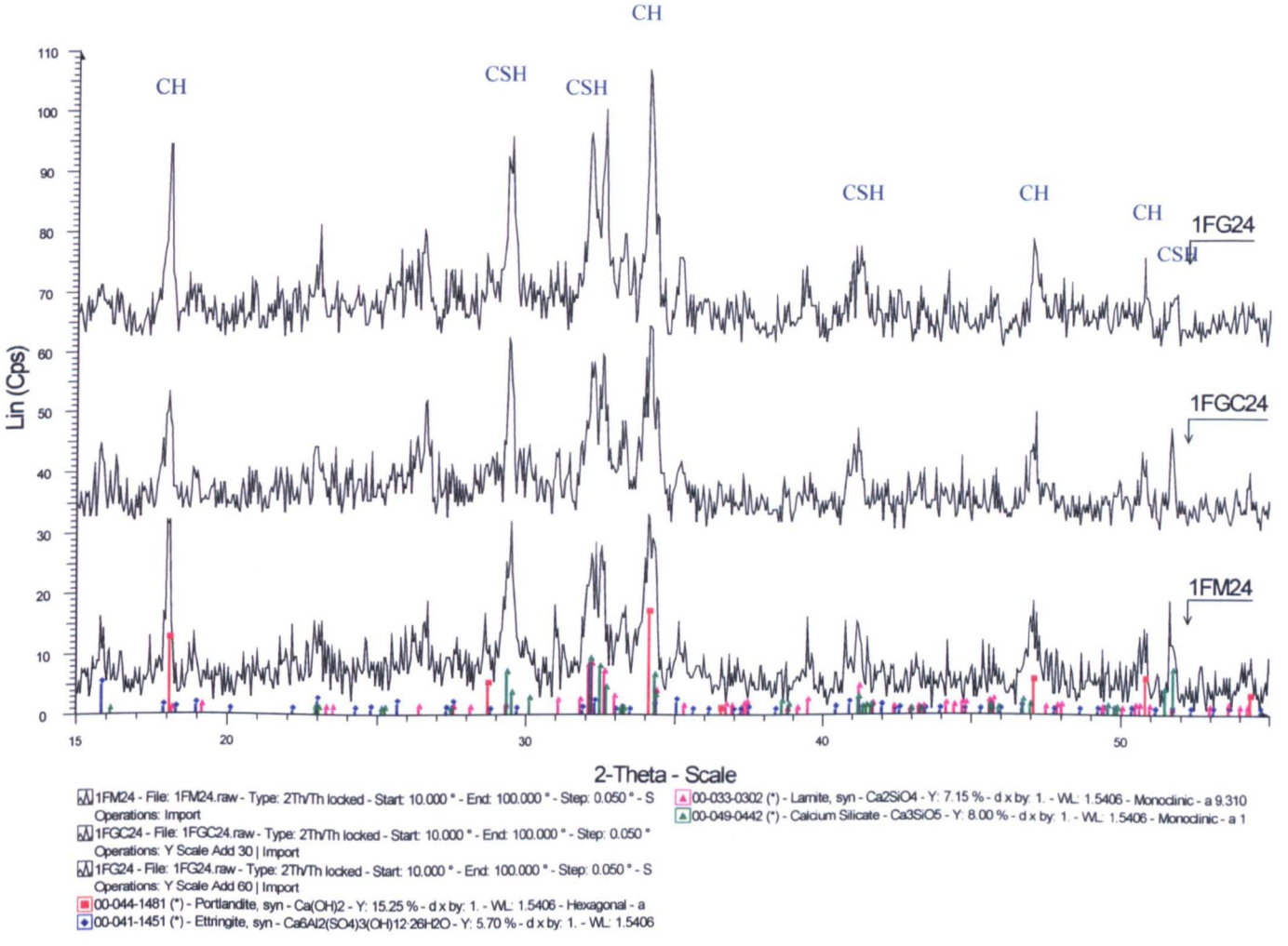

Figure 5.6 X ray diffractograms showing the approximate quantity of portlandite (CH) and calcium silicate hydrate (CSH) in each fly ash corrosion-inhibited SCC (with respect to the conventional fly ash SCC) at 24 hours

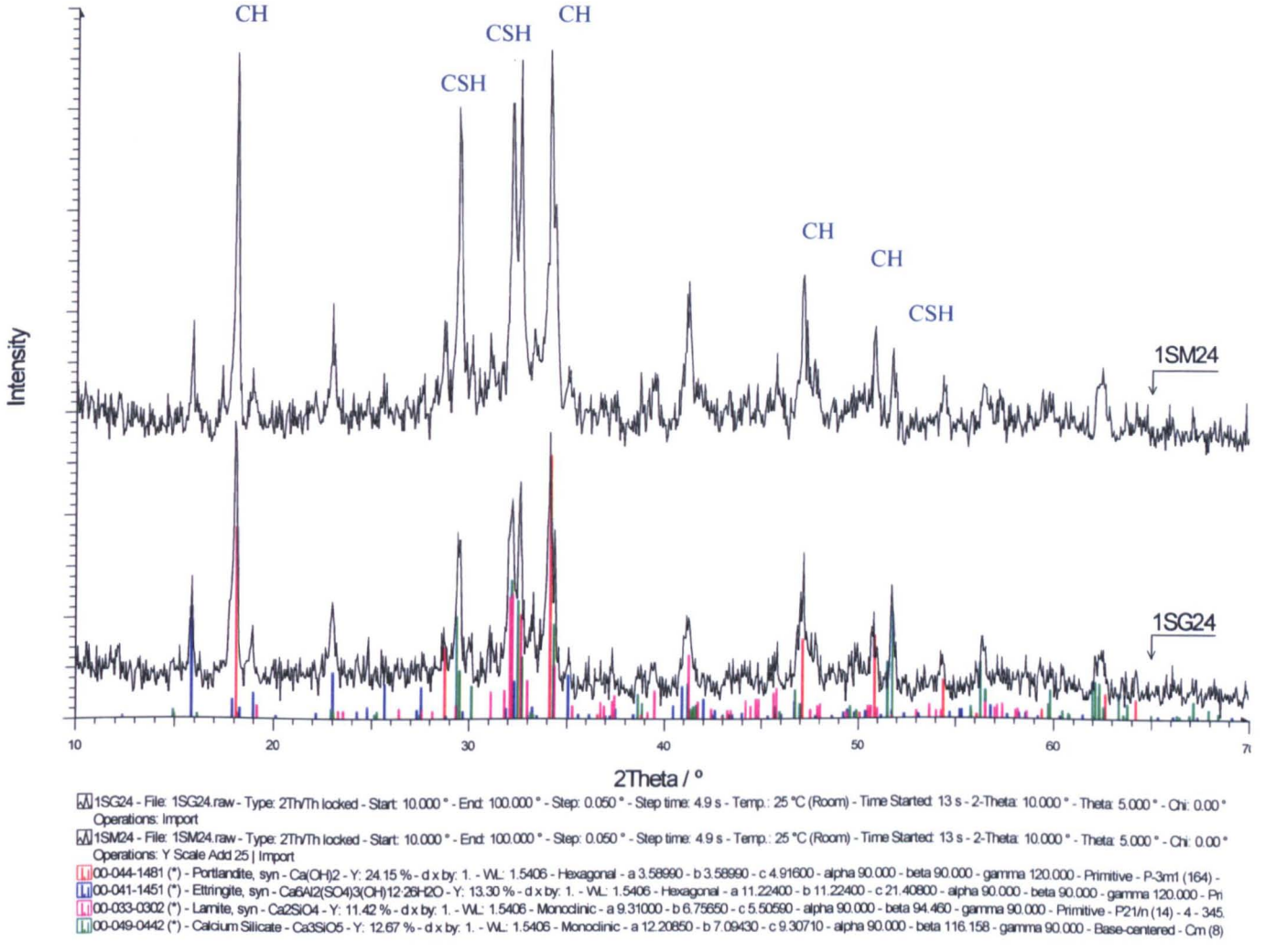

Figure 5.7 X ray diffractograms showing the approximate quantity of portlandite (CH) and calcium silicate hydrate (CSH) in silica fume corrosion-inhibited SCC (with respect to the conventional silica fume SCC) at 24 hours

5.3. CONCRETE

5.3.1. Rheology

Slump flow is an empirical test that gives a measure of the workability of concrete. However, the result of the test is predicated on the yield stress of the concrete. When the Abrams' cone is lifted, flow will take place if the stress created by the weight of the cone of concrete is greater than the yield stress in the concrete (Ferraris et al, 2001). The slump flow test was conducted on the 5 cementitious mixtures immediately after mixing and the results are displayed in Figure 5.8. The EFNARC (2005) lower and upper limits for SCC slump flow are 550 and 850 mm and therefore it is evident that all the control and inhibited cementitious mixes fall within these limits. The mixes were however proportioned to increase the probability of them satisfying the SCC requirements. The results of the slump flow, J-ring, V-funnel, segregation resistance and viscosity tests are each based on the average of two measurements.

An essential performance criterion of SCC is an efficient rheology to promote flow characteristics. Providing a continuous granulometry with particles of particular geometrical features will help to optimize the passing ability and filling ability of the concrete. As shown in Section 4.2.4, a well-graded combined aggregate with grading curve having exponential form was used. Additionally, aggregates with a high degree of roundness and smooth surface texture reduce inter-particle friction and hence help to maximize flow characteristics (Bogas et al, 2012 and Khaleel et al, 2011). The geometrically-related properties (Section 6.2) show that the relative compactness, smoothness, and roundness of the particles would have complemented the flow properties of each self-compacting concrete.

Further, samples of all the aggregates were tested in accordance with ASTM C40 to determine if there were organic compounds that could affect the setting of the concrete. The results from the colorimetric reference chart were between 1 and 2 for the aggregates, indicating that the levels of organics were negligible to low respectively. Thus the use of these aggregates was not expected to be deleterious to the setting of concrete and hence, from all indications, the aggregates used in this research should not have inhibited the rheological behaviour of any of the plastic concrete samples under study.

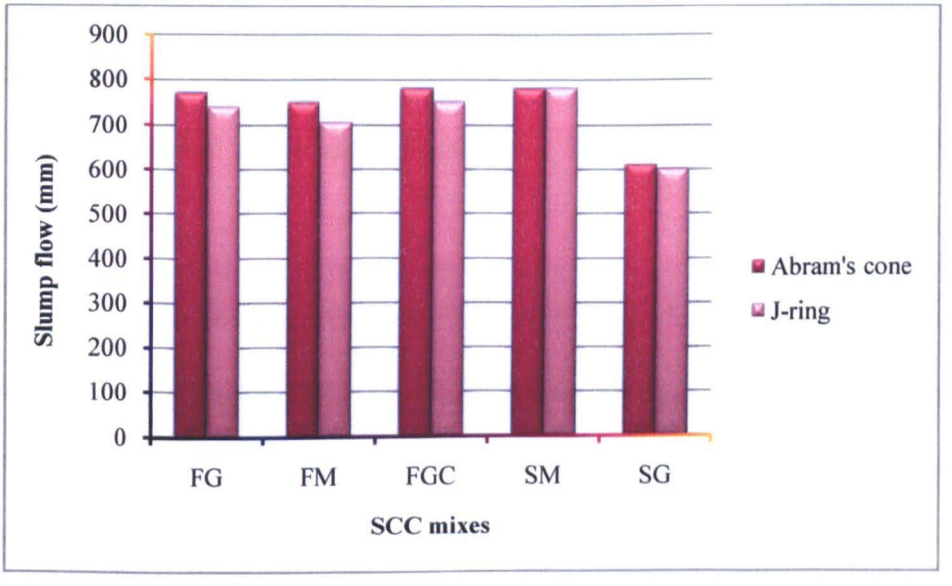

Figure 5.8 The effect of corrosion inhibitors on the slump flow of SCC

The reference fly ash SCC (FG) had a slump flow (Section 4.5.1.3) of 770 mm while the carboxylic (FM) and nitrite (FGC) counterparts had flow of 750 mm and 780 mm respectively (Figure 5.8). It is therefore seen that the inorganic nitrite inhibitor marginally increased the flow by 1.3% and the organic carboxylic inhibitor slightly reduced the flow by 2.6 %. The 22.3% increase in flow of the inhibited silica fume mix (SM) over the reference

SG mix is also attributed to the inclusion of the superplasticising corrosion inhibitor. The J-ring (Section 4.5.1.4.) was also used for the determination of this intrinsic property. As the J-ring tests creates obstacle in the flow path, the flow of all the mixes were lower than the respective flow in the normal slump flow but the order of magnitude of the slump values remained the same.

The record of the effects of corrosion inhibitors on the rheology of concrete is varied. In a study on traditional concrete with different types of corrosion inhibitors, it was shown that calcium nitrite based inhibitor increased the slump. On the other hand, when a migrating type of inhibitor was used it significantly increased the slump (De Schutter and Luo, 2004). However, there are limited studies on the rheological behaviour of corrosion-inhibiting SCC.

When the concentration of the corrosion inhibitor was increased to 2 times the basic dosage, it is shown in Figure 5.9 that the flow of the carboxylic inhibited fly ash mix (FM) was reduced while the flow in the carboxylic silica fume mix (SM) was increased. The texture of the fly ash concrete was also changed, giving the appearance that the concrete became more viscous. It is worth mentioning here that, with the appreciable addition of the carboxylic admixture, adjustment was made to the mixing water to ensure that the water/powder ratio was maintained at 0.32. The difference in the response of the flow properties of the silica fume and fly ash mixture to the increase in the concentration of carboxylic is interesting and while this difference cannot be explained it is clear that this multiphase organic compound exhibits different behavioural patterns in the different types of SCCs. A 100% increase in the concentration of the nitrite inhibitor decreased the slump of the concrete (FGC), indicating that this compound interferes with the physiochemical reaction between the molecules of the superplasticiser and the cement.

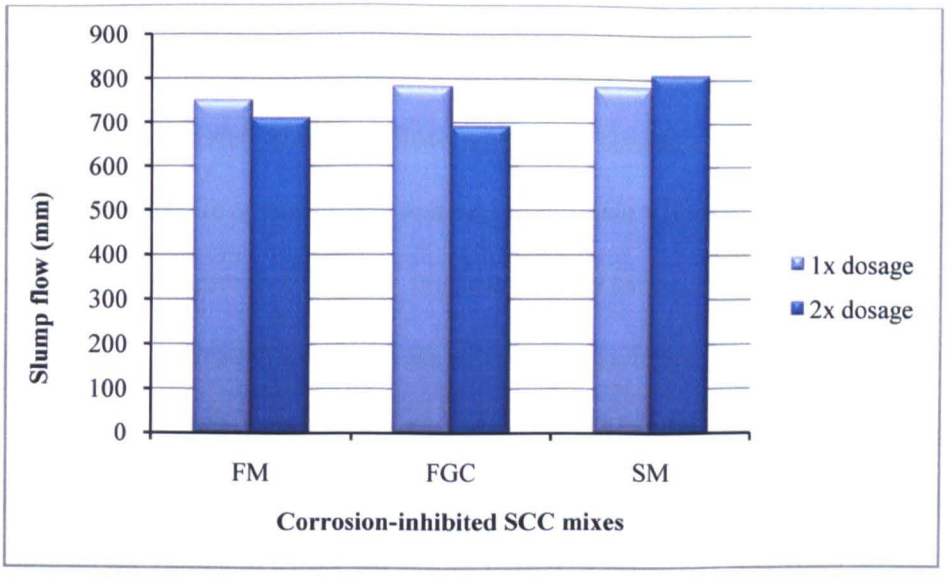

Figure 5.9 The change in slump flow of inhibited SCC as the concentration of corrosion inhibitor increases

The flow rate is a parametric measurement that is often reported with the slump flow. Although the flow rate is not a measure of viscosity, it is indicative of the retardation in flow of an aqueous material (Bonen, 2005). The slump flow rate (t_{500}) (Section 4.5.1.3) for all the corrosion-inhibited and reference SCCs are shown in Figure 5.10. The values range from 4.11 seconds for the nitrite fly ash SCC to 1.16 seconds for the carboxylic fly ash SCC. The flow rates were also determined with the V-funnel. This equipment has a greater capacity for concrete and a smaller outlet hence the flow times are higher. With the V-funnel, the FM mixture again had the fastest rate but the reference fly ash mix (FG) now had the slowest rate. The nitrite inhibiting SCC (FGC) however, had a very slow rate with this apparatus. Additionally, it is shown in both types of flow tests that the carboxylic inhibitor diminished the flow of the silica fume SCC.

In comparison to the FG control, flow rate for the FGC sample was slower and that of the carboxylic FM sample was faster. However, the flow rate of the carboxylic SM sample, as determined by Abram's cone was slower than the SG control. The V-funnel test (Section 4.5.1.5) was also used to determine the flow rate of the concrete samples as there is a strong correlation between the flow rate of this test and the plastic viscosity of concrete. The results from this apparatus (Figure 5.10) show that the incorporation of the respective nitrite and carboxylic inhibitors increased the flow rate of the SCC samples. The V-funnel test therefore indicates that the inhibitor reduced the viscosity of the traditional SCCs. In Figure 5.11, rheometry testing on the pastes of fly ash SCCs (Section 4.5.1.2) shows that the use of each inhibitor reduced the viscosity of the fly ash SCC pastes and hence this strongly suggests that the inhibitors had the same effect on the fly ash concrete.

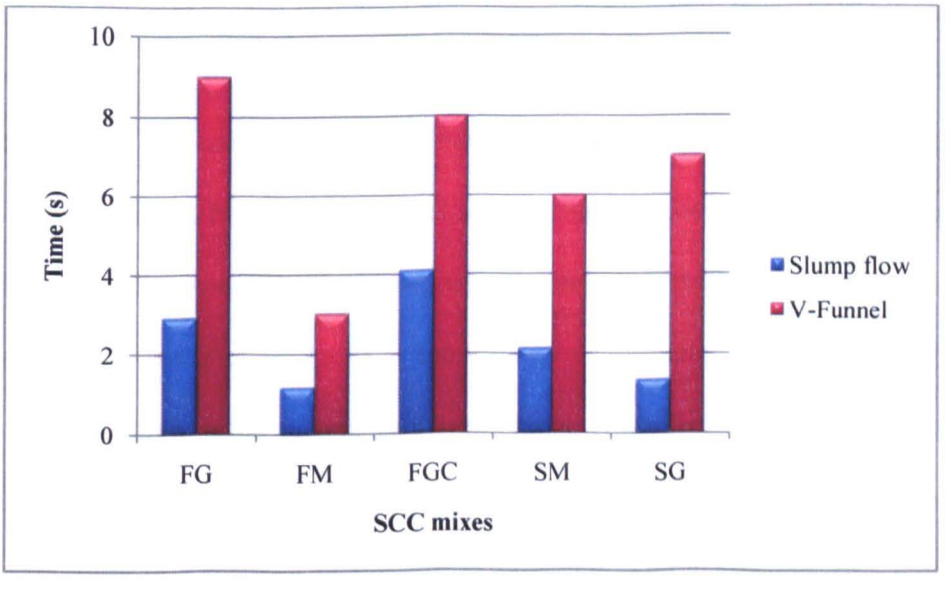

Figure 5.10 The effect of corrosion inhibitors on the flow rate of SCC

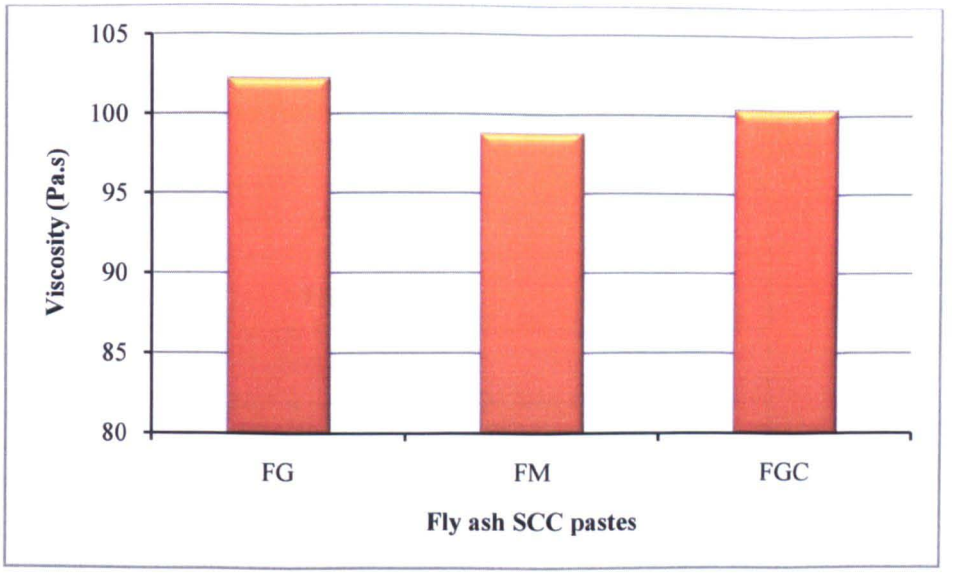

Figure 5.11 Rheology results showing the decrease in the viscosity of SCC pastes as corrosion inhibitor is introduced

One of the key features of self-compacting concrete is its ability to negotiate obstacles and confined spaces as it flows. This property is referred to as the passing ability and the degree of deformability of the concrete plays an important role in the quality of this property. The blocking step provides a measure of the risk to blocking. Values up to 20 mm are acceptable but measurements between 10 and 20 mm indicate that concrete has a moderate to high risk of blockage (De Schutter et al, 2008) in the vicinity of obstacles. It is evident in Table 5.3 that all mixtures show good resistance to blocking. However, the measurements for the corrosion-inhibited samples, FM and FGC, deviated from the reference FG measurement, showing that there is a reduced inclination to blocking. The evaluation also indicates that there is a less risk to blocking when the carboxylic inhibitor is incorporated in the silica fume SCC.

Table 5.3 Blocking step values for SCC samples

Mix	Blocking step
FG	5.0
FM	1.3
FGC	3.8
SM	5.0
SG	10.0

The sieve segregation test (Section 4.5.1.6.) was used to determine the static segregation of the concrete mixtures that were produced. Segregation indices that are less than 15% indicate that the concrete has good resistance to static segregation; and the segregation resistance increases as this index decreases (Khayat, 1998). Generally, the corrosion inhibitor decreased the resistance of the SCC to static segregation as determined by the test conditions (Figure 5.12).

In the determination of the slump loss with time, the slump flow and rate of each mix were determined at 5, 15, 30 and 60 minutes. Mixes that had slump less than 500 mm at the time of the test were not measured since the flow rate could not obtained. Approximately 12 l of concrete was used for each sample and the concrete was re-mixed for 10 seconds before repeating each slump flow test. It was felt that this would provide sufficient disturbance to appreciably remove the thixotropic effect in the concrete without significant damage to any setting that may have had occurred.

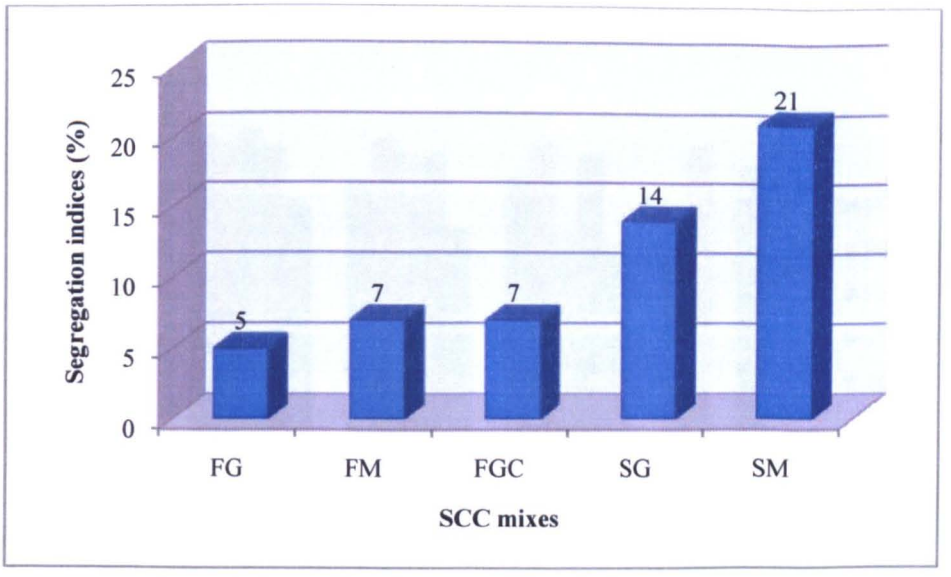

Figure 5.12 Sieve segregation indices of SCC mixes 15 minutes after mixing

Figure 5.13 gives a picture of the slump loss over a period of 60 minutes. It is seen that up to 30 minutes, the FG mix possessed slump flow that is acceptable for SCC but the SG reference mix was not able to attain a flow measurement over 500 mm. Compared to the traditional fly ash SCC, the nitrite SCC (FGC) had the higher slump loss rate, which resulted in failure to maintain acceptable flow characteristics at the 30-minute time frame. On the other hand, the two carboxylic-inhibited mixes (FM and SM) had the lowest slump loss rate and up to 60 minutes after mixing, demonstrated good deformability. From these results it can be inferred that the calcium nitrite inhibitor suppresses the workability over time but that the carboxylic inhibitor promotes good workability retention. The equations for predicting the slump flow (y_t) at specified time (x_n) up to 60 minutes after mixing are developed for each of the carboxylic SCC and the control fly ash samples (Figure 5.14). For two equations the points closely fit the straight line (FG and SM) but the coefficient of determination for the FM sample is less than 0.5.

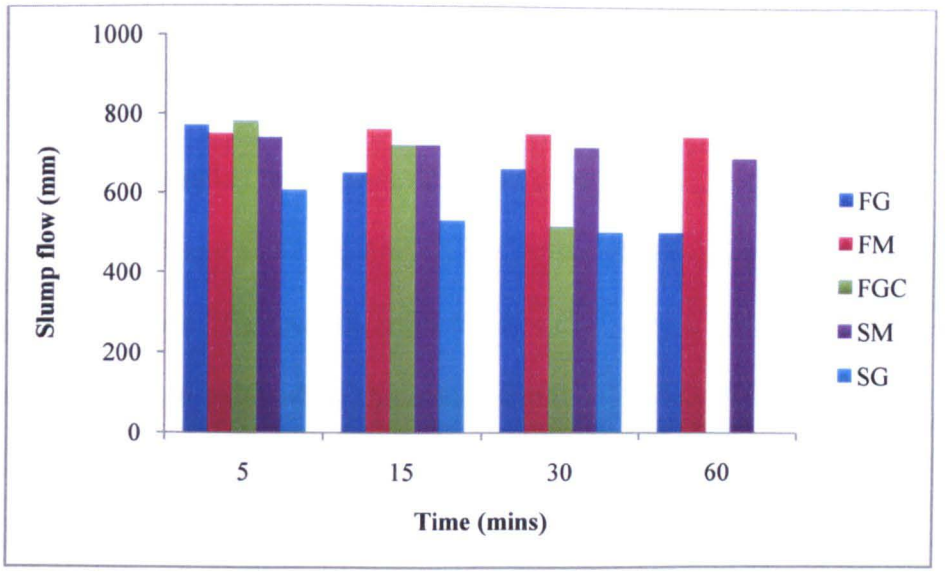

Figure 5.13 Depiction of the workability retention of SCC samples up to 60 minutes after mixing

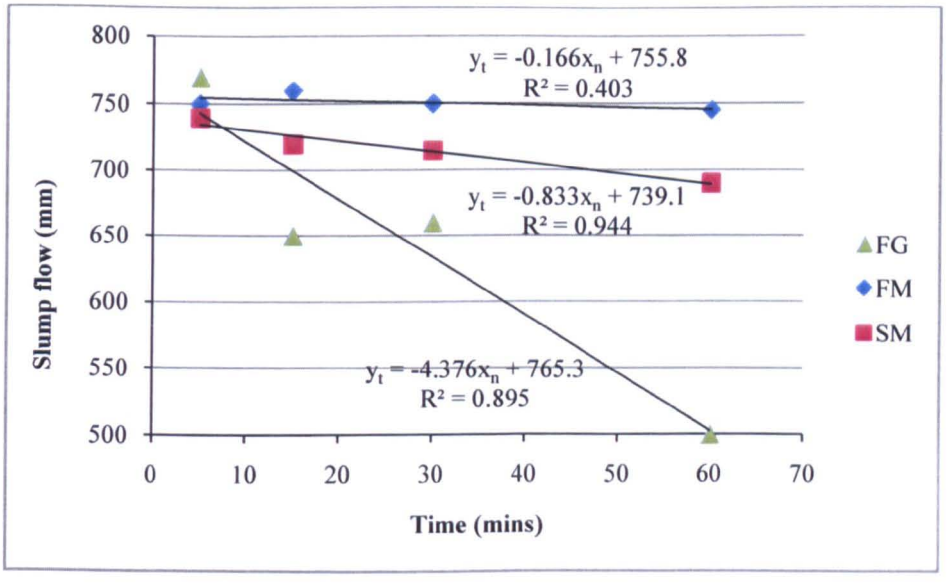

Figure 5.14 Linear relationships established between the flow of SCC and elapsed time since mixing

5.4. CONCLUSION

The series of tests performed on the plastic SCC pastes showed that the corrosion inhibitors affected the cementitious materials. It is seen that the use of the nitrite corrosion inhibitor in the fly ash control resulted in a marked increase in the setting times when the curing condition was set at 20 and 40°C respectively but there was little change in setting time when the curing condition was 30°C. Additionally, there was little variability in the setting times of the nitrite-based fly ash SCC when the concentration of this inhibitor was increased. The influence of the addition of the multi-phase carboxylic corrosion inhibitor on the fly ash and silica fume SCCs was also shown in the increased setting times of the samples at the curing temperatures at 20 and 30°C. Increase in the concentration of the carboxylic compound also produced significant increase in the setting times of the inhibited fly ash SCC. Although larger increases in the concentration of the carboxylic inhibitor in the inhibited silica fume SCC also significantly prolonged the setting times, low concentration increases resulted in slight increases to setting times.

Thermogravimetric and XRD tests done at the ages of 12 and 24 hours respectively confirmed the delay in the development of SCC pastes when the inhibiting compounds were introduced. However, it is noteworthy that the existing formula for estimating the final setting time of traditional concrete is found to be valid for both the conventional and inhibiting SCC pastes, not only at 20°C but also at temperatures up to 40°C.

The effect of the corrosion inhibitor was also manifested in the rheological performance of the concrete. The nitrite inhibitor reduced the yield stress in the fly ash SCC mix and hence

the slump flow increased although narrowly, after the incorporation of this inhibitor. The increase in the flow rate of the fly ash SCC after the incorporation of the nitrite inhibitor is attributed to the reducing effect of the nitrite on the viscosity of the concrete mixture. In the case of the other inhibitor, the addition of the carboxylic formulation to the fly ash concrete reduced the slump flow and increased the flow rate of this mixture. Since a decrease in the slump flow is largely the result of an increase in the yield stress of concrete, it is shown that the carboxylic inhibitor increased the yield stress in the fly ash concrete. Additionally, the increase in the flow rate of the fly ash SCC when the multi-phase inhibitor was added indicates that the carboxylic formulation reduced the viscosity of the fly ash SCC. On the other hand, the silica fume concrete experienced an increase in both the slump flow and the flow rate when the carboxylic inhibitor was added. This signifies that the use of the carboxylic inhibitor reduced the yield stress and the viscosity of the silica fume SCC. The difference in the effect of the carboxylic inhibitor on the two types of SCCs appears to depend on which of the phases of the multi-purpose organic inhibitor is dominating the functionalities in the concrete.

Improvements were seen in the workability of the two types of SCC incorporating the carboxylic formulation (FM and SM), where significant slump flow was retained up to 60 minutes, but the nitrite-based SCC (FGC), lost its slump and self-compactibility after 30 minutes. Equations with R^2 values between 0.4 and 0.9 were developed for predicting the workability retention of the carboxylic and control fly ash SCC samples. The effects of the nitrite and carboxylic inhibitors on some of the fresh properties of the fly ash and silica fume SCCs are summarised in Figure 5.15. The respective increase or decrease in the measurement of each parameter in Figure 5.15 is shown by an upward or downward arrow.

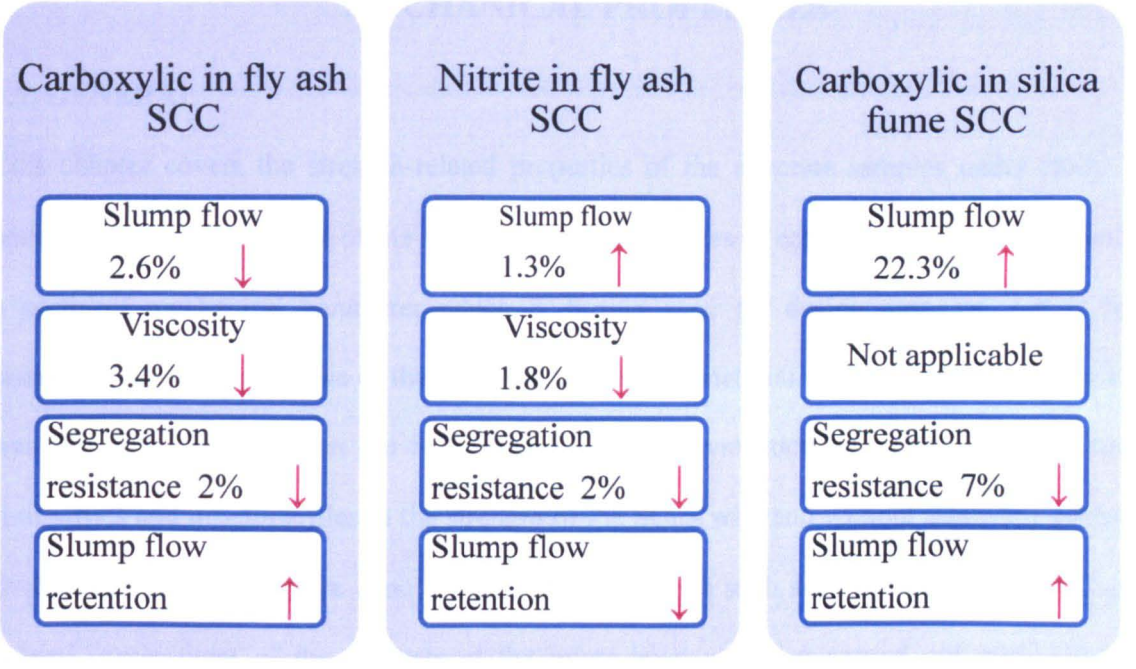

Figure 5.15 The effect of low concentration of nitrite and carboxylic inhibitors on the fly ash and silica fume SCCs as seen in the carboxylic FM and SM samples and in the nitrite FGC sample

MECHANICAL PROPERTIES

6.1. GENERAL

This chapter covers the strength-related properties of the concrete samples under study. The compressive strength is one of the most important properties of concrete as it not only quantifies a pertinent mechanical parameter which is further used for design purposes, but in many instances, it is also indicative of the overall quality of the material. The compressive strength test was therefore conducted on the SCC samples and an evaluation was done to determine the similarities and dissimilarities in the strength of the SCCs with and without corrosion inhibitors. Other mechanical tests were done to study the parameters such as tensile strength and fracture energy. Assessment of the concrete at the micro-level was also carried out with a view to understand the mechanism that contributed to peculiarities in the mechanical characteristics. In all the concrete specimens, the water/powder ratio and the powder content per cubic metre were kept constant.

6.2. CONCRETE AGGREGATE

One of the selection criteria of the aggregates for this research was to ensure that the geometrical configuration of the particles did not impede the flow properties of the concrete (Section 5.3.1.). Seven particles were assessed to determine the angularity, roundness and the surface roughness values. The roundness and angularity values (see Table 6.1) show that the aggregate particles were relatively well rounded. Images of the aggregate were captured and analysed with Image ProPlus software. The angularity refers to the relative sharpness of the edges and corners of an aggregate particle while roundness is somewhat the opposite, pointing to the amount of wear on

the corners and edges (Kuo and Freeman, 2000). The mathematical expressions for angularity and roundness are provided in Equations 6.1 and 6.2 respectively. Perimeter ellipse refers to a best fit ellipse circumscribing the particle while perimeter convex considers a polygon outlining the particle.

$$Angularity = \left(\frac{perimeter\ convex}{perimeter\ ellipse}\right)^2 \quad 6.1$$

$$Roundness = \frac{perimeter^{\,2}}{4\pi area} \quad 6.2$$

Values of angularity that are close to 1 show that the aggregate particle is somewhat elliptical in geometry, and as the value increases it signals greater angularity. Particle displaying a high degree of roundness as in spherical type will have roundness approximately equal to 1 and higher values suggest less roundness.

Aggregate particles possessing smooth surface texture also help to impart attributes that aid the flow ability of SCC (Khaleel et al, 2011). The surface roughness R_a, of a representative sample of gravel particles was quantified by a stylus profilometer to be 5.4. This property is a statistical value which gives the arithmetic mean of departure of a surface from a mean line (Vorburger and Raja, 1990). Compared to limestone that had a R_a value of 14.6, it can be concluded that the gravel particles were relatively smooth.

At the macro-level, the roundness and smoothness of the particles would have contributed to the mechanical properties of the concrete as the derived workability and compactibilty would help to achieve a denser concrete. However, at the micro-level, the mechanical interlock at the particles and paste interface would have limited the bond strength (Giaccio and Zerbino, 1998 and Donza, et al, 2002) and hence the strength of the concrete would not have been optimised with this type of aggregate. In tensile testing, concrete with a predominance of smooth and rounded aggregate will see more crack development taking place in this weaker zone at the aggregate and mortar interface (Giaccio and Zerbino, 1998) as was evident in some spots along the fracture place in some of these SCC samples (Figure 6.1). Therefore, where the strength of the concrete has to be optimised, it may be best to use sub-angular aggregates in SCC even though the workability will be compromised. On the other hand, as far as strength of the aggregate itself is concerned, the aggregate impact value, which was on average 12%, signifies that the strength of the aggregate was relatively high. With aggregates of this strength, cracks extending in the direction of aggregate will not easily create a path through the aggregate but will have to propagate in other directions which will result in a more tortuous fracture path (Giaccio and Zerbino, 1998) and hence, for this study, this aggregate property would have helped to mitigate the effect of the geometry on the mechanical performance of the SCCs.

Table 6.1 Characteristics of aggregate

Aggregate type	Angularity	Roundness	Surface roughness
Coarse Aggregate	1.12	1.25	5.4

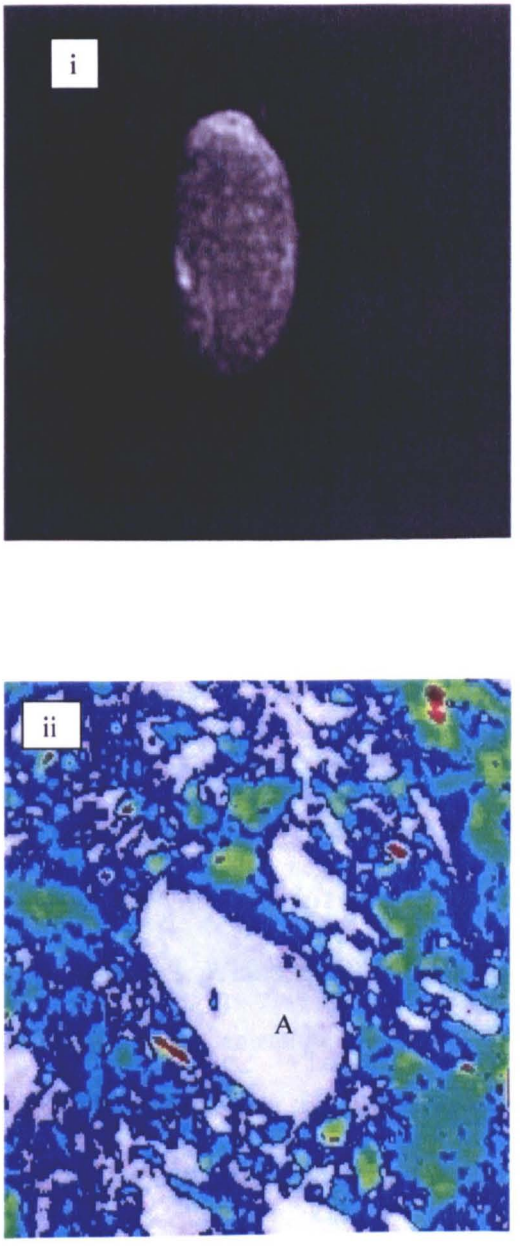

Figure 6.1 A fracture path passing through the ITZ in SCC sample; i) image of a relatively smooth aggregate particle from a fracture plane, ii) the smooth surface (A) left by this particle in the mortar.

6.3. STRENGTH

6.3.1. Results

All the specimens for compressive strength tests were performed on 100 mm concrete cubes with a water/powder ratio of 0.32 based on gravimetric measurements. A total of three measurements were used in the determination of compressive strength for each sample. When the sample made with the nitrite based corrosion inhibitor (FGC) is compared to the FG control, it is seen that the 28 day strength of the FGC sample was 35% higher (Figure 6.2). The relative density of the FGC sample was also higher than the relative density of the FG sample at 28 days. The relative density result was based on the average of three measurements. In order to examine the effect of the corrosion inhibitor on the overall development of strength in the concrete, the compressive strength of the sample was determined at vital points in the hydration process (Figure 6.3). At 7 days, the FGC sample had higher strength than that of the control and a much higher rate of development of strength up to 28 days. The subsequent rate of development of strength in the nitrite sample (FGC) however got lower and this resulted in a 90-day strength that was 2% lower than the FG sample at the same age. With reference to the SCC with the basic concentration of nitrite, it is shown that when the concentration of the nitrite inhibitor in the FGC sample was doubled, there was 19 and 30% reduction in the respective 28 and 90 day compressive strengths of the concrete (Figure 6.4) and an increase in the time for hardening of the concrete.

With regards to the carboxylic inhibiting SCC, the 28-day compressive strengths of the fly ash and silica fume SCC samples (FM and SM respectively) were less than those of the corresponding FG and SG control samples at the corresponding age.

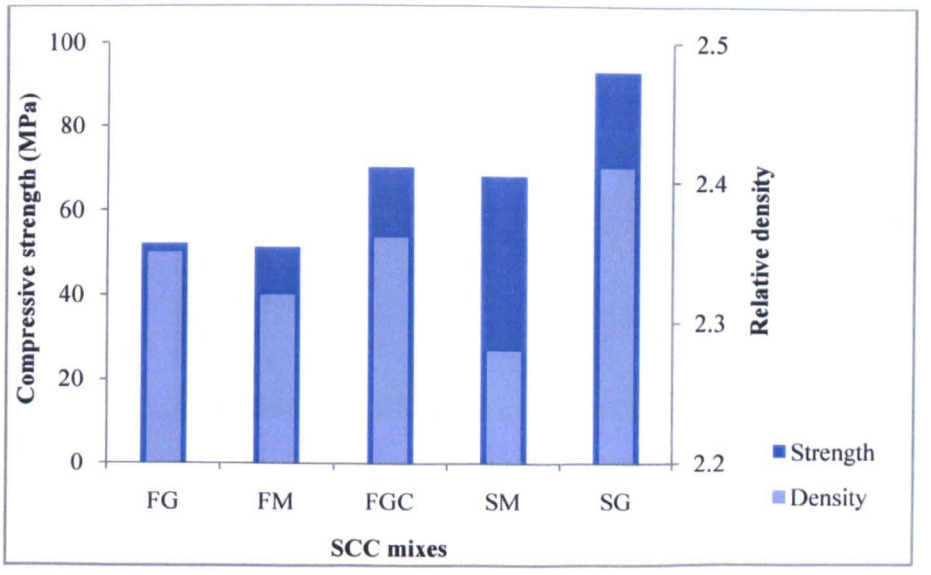

Figure 6.2 The relationship between the 28-day compressive strength and saturated surface-dry relative density of the SCC mixes

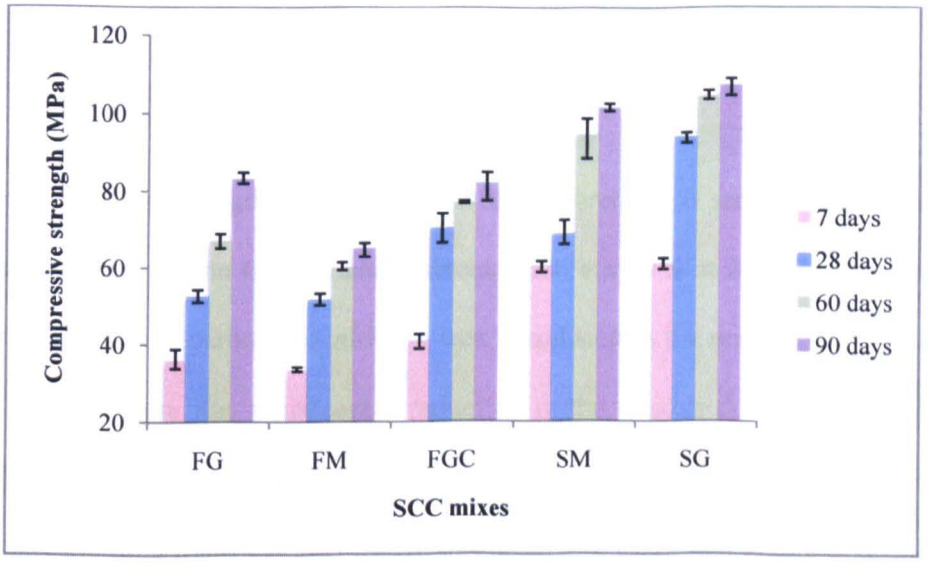

Figure 6.3 The effect of corrosion inhibitors on the development of strength in concrete between 7 and 90 days

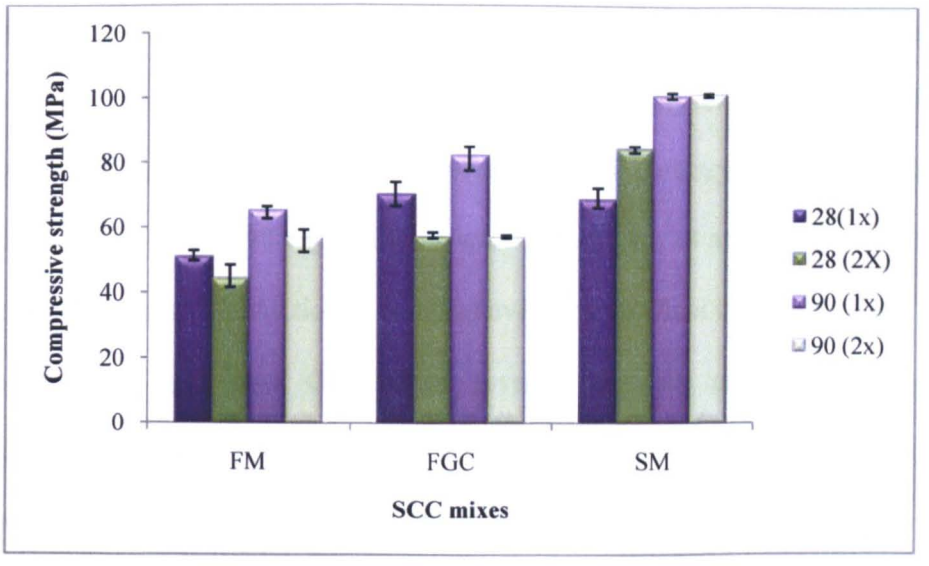

Figure 6.4 Comparison of strengths between SCC mixes with the basic (1x) and twice (2x) the concentration of corrosion inhibitor at ages 28 days and 90 days

While the difference in strength between the FM and reference FG samples was approximately (2%), the difference between the SM and reference SG was 37% at 28 days (Figure 6.2). It is also shown that when the carboxylic inhibitor was introduced in the respective fly ash and silica fume SCC samples there was a noticeable reduction in the relative density of each of the two samples (FM and SM). Charting of the development of compressive strength in the FM and SM samples at specific time frames is also shown in Figure 6.3. From this graph, it is observed that at 7 days, the compressive strength of the carboxylic fly ash SCC (FM) was 7% lower than that of the control FG sample, but at the 28th day the gap in the strengths reduced. However, after 28 days the rate of development of strength in the FM sample was considerably lower than that of

the FG sample. Similarly, the development of strength in the carboxylic silica fume sample was remarkably lower than that of the SG control except in the very early stages when the 7-day strengths were about the same. When the concentration of the carboxylic inhibitor was increased from 0.3 to 0.6%, the 28 and 90 day strengths were reduced by 14 and 12% respectively in the FM sample but there was no reduction in compressive strength when the SM samples were tested at these ages (see Figure 6.4). Observation revealed that the carboxylic compound also contributed to bleeding in the SCC samples, with the inhibiting fly ash samples, (FM), showing a greater susceptibility to bleeding than the inhibiting silica fume SCC (SM), and the propensity for bleeding in both samples increased as the concentration of the organic corrosion inhibitor increased. This phenomenon may be contrasted with one of the main features of fresh self-compacting concrete - its tendency to minimize bleed-water to the extent that the concrete often present some difficulty in the finishing operation. Additionally, the hardening of all the carboxylic samples was retarded but the degree of retardation was significantly higher in the fly ash samples, an effect that resulted in 24 hours and greater delay in the de-moulding of the samples.

The four point bending test was conducted on 100 x 100 x 500 mm concrete prisms at the age of 28 days in order to examine their behaviour under tensile loading. The result for each type of concrete is the average of four measurements and a typical load/deflection curve for each SCC specimen is shown in Figure 6.5. The fracture mechanism can be characterised by the energy required to initiate a crack, according to a constitutive law developed by Griffith (Carpinteri et al, 1997). Generally, the energy required to produce a fracture is consumed by the work to create

the fracture (surface energy, y_s) and the work expended in the plastic deformation y_p of the hardened concrete. The fracture energy (G_f), which is defined mathematically as the area under each curve (Carpinteri, 1997), was computed from the load/deflection curves (Roylance, 2001 and Mehta and Monteiro, 2006) up to the point of crack initiation (see Table 6.2). From the average results, it was found that the FGC sample attained higher deflection and slightly higher tensile strength than those of the reference FG sample, and this produced higher fracture energy in the nitrite SCC sample. On the other hand, when comparison is made with the respective control, the tensile strength of the carboxylic fly ash (FM) sample was 17.6% lower while that of the carboxylic silica fume (SM) was 41.8% higher. The relative order of magnitude of the fracture energy produced was consistent with that of the respective tensile strength in the respective samples. There are several power functions that are used to predict the tensile strength when the compressive strength of concrete is known but the correlation between the compressive and the flexural tensile strengths of these samples is not high enough to formulate an equation that will yield useful information. Usually, a high variability is associated with the results from this type of flexural tensile test (Ozyildirim and Carino, 2006) and hence a large representative set of samples is needed to accurately develop any mathematical relationship. However, it is also generally expected that the tensile strength (from splitting) is approximately 1/10 of the compressive strength of the concrete (Neville, 2006). When the tensile strengths are calculated from the compressive strength on this basis, with the exception of the silica fume control (SG), the values are found to be less than the values obtained from the 4 point bending test (Table 6.2).

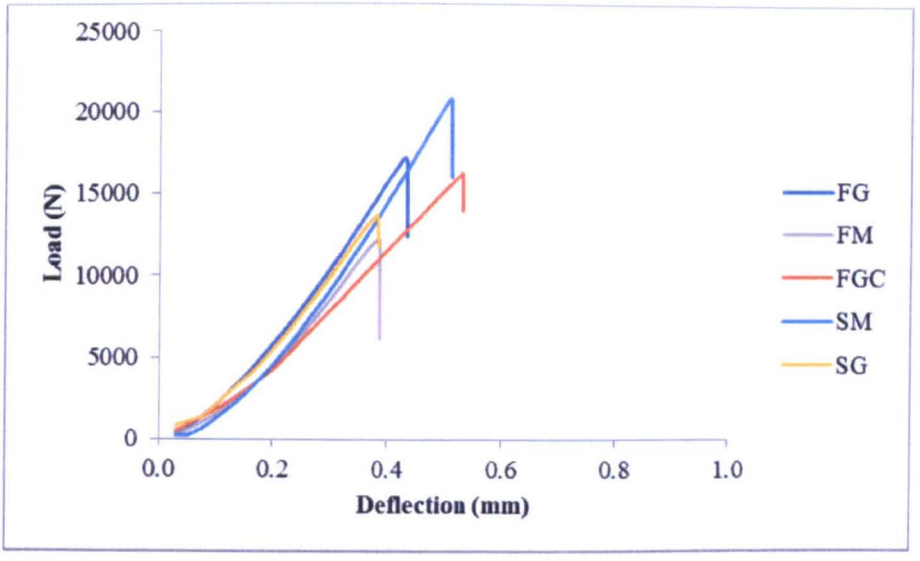

Figure 6.5 Typical load/deflection curves of SCCs

Table 6.2 The fracture energy associated with each SCC sample

SCC Samples	(G_f) N.mm	Tensile strength MPa	Calculated tensile strength MPa
FG	3716	10.2 ± 0.98	5.2
FM	2356	8.4 ± 0.34	5.1
FGC	4336	10.5 ± 0.45	7.0
SM	5345	12.2 ± 1.50	6.8
SG	2605	8.6 ± 0.44	9.3

6.3.2. Discussion

It is evident that the nitrite corrosion inhibitor affected the compressive and tensile strengths of the fly ash SCC samples. In the early and intermediate stages of hydration, the nitrite based inhibitor promoted higher development of compressive strength in the fly ash SCC (FGC) after its addition. This behaviour is typical of nitrite-bearing concrete (Al-Amoudi et al, 2003; Hansson et al, 1998) but the improvement of the rheological behaviour of the fly ash sample when the nitrite was added (Section 5.3.1) would have also contributed to the increase in strength. However, the use of this inorganic corrosion inhibitor also contributed to a 90-day compressive strength that was slightly less than that of the reference sample at 90 days. Explanation of the exact mechanism that is responsible for the promotion of strength in nitrite inhibiting concrete is hard to find, but since development in strength is largely attributed to the calcium silicate hydrates, it could mean that the use of the nitrite compound accelerated the production of C-S-H. The associated increase in the density of the concrete when the nitrite inhibitor is incorporated supports this theory. Results from the 28 day tensile strength test show that the introduction of the nitrite inhibitor in the fly ash SCC increased the tensile strength narrowly and in the process, with a higher displacement, the material is shown to have become slightly tougher and hence less brittle.

Generally, it is observed that the use of the carboxylic inhibitor resulted in a reduction of strength of varying degrees as is now explained. From comparison with the SG control, with differences of approximately 6 - 27% in compressive strengths at the various test points, it was observed that the use of the multi-phase carboxylic corrosion inhibitor noticeably reduced the

strength of the SM sample after the early age (7 days). Additionally, with the exception of the 28-day strength, the carboxylic inhibitor also significantly decreased the strength of the fly ash SCC (FM), resulting in approximately 7 - 21% reduction in compressive strength in relation to the SG control at the corresponding age. The effect on the early (7-day) strength of the fly ash SCC was also affected but much less. This multi-phase organic corrosion inhibitor is not a common concrete admixture, but the pure forms of organic corrosion inhibitors have been used in research and there are mixed views about the effects on the 28 day compressive strength of concrete. For example, there is research that shows that there is no difference in strength when inhibitor is incorporated in concrete (Wombacher et al, 2004), but there are others that state that there are increases (Al-Amoudi et al, 2003) and there are decreases in strength.

However, when this multi-phase corrosion inhibitor is used in the SCC samples (SM and FM), there was reduction in strength beyond that of the control that appears to be the result of a chemical modification in the structure of the SCC. This modification is also manifested in the inordinate delay in the setting times (see Section 5.2.1.) and in the observed retardation in hardening of the silica fume and fly ash SCCs (SM and FM), when the carboxylic compound was introduced. Since the water/cement was the same in the inhibited and reference SCCs, and there was no noticeable sign of bleeding in the control, it is evident that the delay in hardening contributed to bleeding and this phenomenon impacted the strength negatively. The phenomenon that caused the bleeding no doubt facilitated the kinetics that contributed to the high retention in workability in the FM and SM samples (Section 5.3.1). However, silica fume, because of its large surface, imbibes water and hence minimised the effect of bleeding. Since the FM SCC was

made from a high volume of fly ash powder, it was more sensitive to any reaction that resulted in retardation in the hydration process, which explains the greater degree of bleeding that was seen when higher concentration of carboxylic inhibitor was admixed in the FM SCC samples and hence the great reduction in strength. This difference in effect can also be seen in the 28-day tensile strengths of the fly ash and silica fume samples when the carboxylic inhibitor was added - the organic inhibitor contributed to a reduction of strength in the FM sample while it had no negative effect on the tensile strength of the SM SCC.

6.3.3. Significance

The advantage that is associated with the use of nitrite is that the high rate of development of strength up to 28 days will expedite the time for the removal of formwork and will facilitate early loading of the recipient concrete element. Beside, although the compressive strength used by engineering practitioners in concrete design is usually the characteristic strength at 28 days, strength developed at later age in the nitrite SCC (FGC) can be utilised to increase the economy of the design.

Any delay in the hardening process that extends the time for the removal of formwork from concrete is undesirable even if the delay contributes to increased workability retention. Usually, delays of the magnitude shown in some of the carboxylic fly ash and silica fume (FM and SM) SCCs will have negative time and cost implications on construction projects. Further, the resulting minimization of 60 and 90-day strengths in the fly ash (FM), and in particular, the silica

fume (SM) SCC when the carboxylic inhibitor is used, will be of concern to engineering practitioners, as this effect may lead to heavier load-bearing members. Concerning the manifestation of bleeding in the carboxylic samples: a little bleed-water is desired to facilitate finishing operations, but, as in the case of the FM samples, too much will lead to plastic shrinkage and latency which was observed in the fly ash samples with high carboxylic content and which can adversely affect the mechanical and durability-related performances and compromise the aesthetics of the concrete.

6.4. ULTRASONIC PULSE MEASUREMENT

Three rectangular prisms of dimensions 100 x 100 x 500 mm were prepared for ultrasonic evaluation of each SCC sample. The PUNDIT was set up with the transducers placed at the two ends of each specimen to transmit and receive ultrasonic pulses that are sent longitudinally through the concrete. The specimens were tested in the saturated surface-dry condition. The results for the transit time and velocity are presented in Figure 6.6 and those for the dynamic elastic modulii are posted in Figure 6.7.

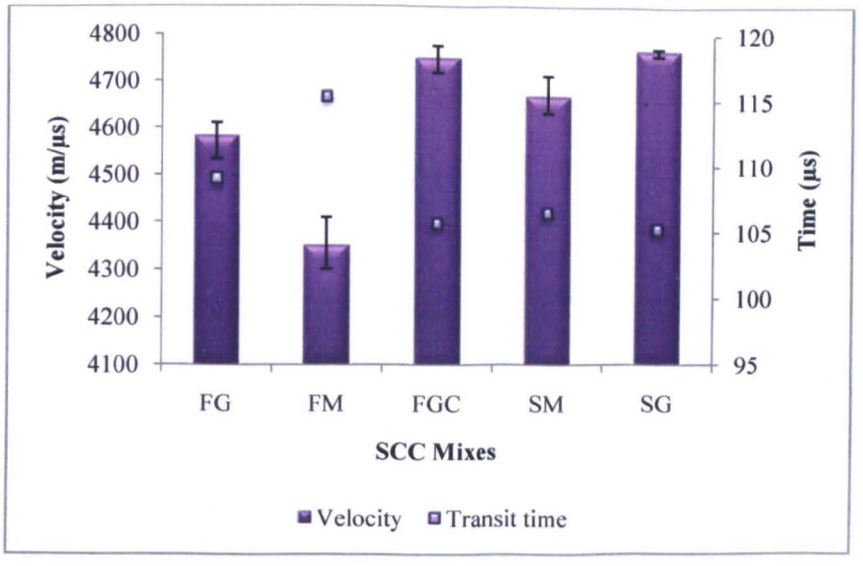

Figure 6.6 Reflection of the heterogeneity of the SCC specimens through ultrasonic measurements

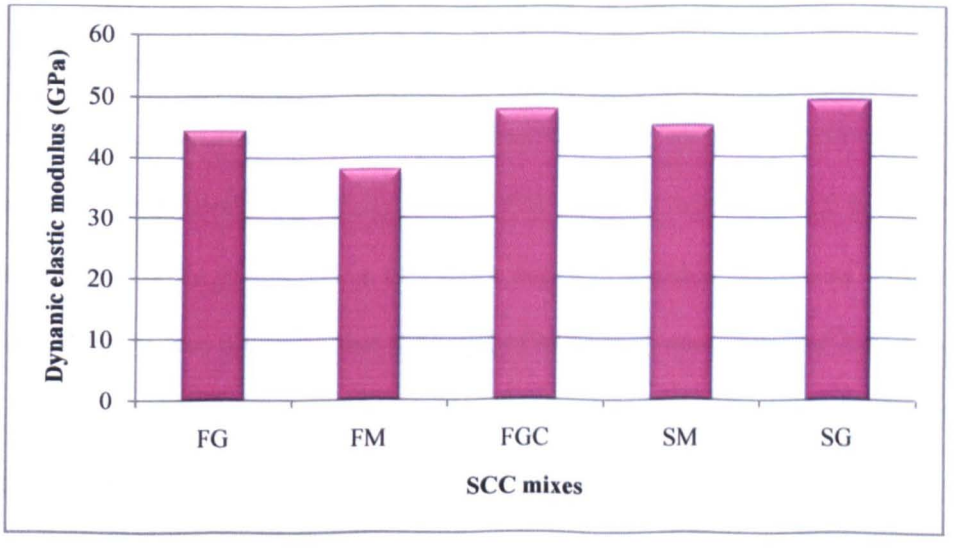

Figure 6.7 Comparison of the dynamic elastic modulii as computed from PUNDIT readings

The average time for the pulse to travel through each of the fly ash concrete samples is between 106 and 115 μs with the FM and FGC samples having the highest and lowest time respectively. Additionally, Figure 6.6 shows that the velocity (V) of the stress wave was the highest in the FGC sample and lowest in the FM sample. Computation of the velocity is carried out by Equations 6.3 and 6.4. The rate at which the pulse travels through the concrete is partly indicative of the level of heterogeneity. A higher velocity is found with more homogenous concrete (Malhotra, 2006). This suggests that the addition of the nitrite compound helped to increase the uniformity in the structure of the fly ash concrete (FGC) but the use of the carboxylic formulation contributed to a reduction in the homogeneity as seen in the FM sample. Figure 6.6 also shows that the addition of the carboxylic inhibitor to the silica fume (SM) concrete resulted in a structure that increased the time of transmission of the pulse and hence increased the velocity. This again shows that this inhibitor reduced the homogeneity of the concrete sample. Features in the concrete that contribute to heterogeneity are voids, cracks and moisture and since the difference in each series of concrete is in the paste, it can be inferred that the difference in homogeneity stems from the incorporation of the corrosion inhibitor. This shows that the higher level of porosity in the FM samples was detected by the ultrasonic equipment. Another point of interest is that there was a noticeable amount of shrinkage in the FM concrete. When it was observed that the level of shrinkage was such that it had a significant effect on the resistivity of the concrete, but time did not allow its inclusion in the testing programme. Therefore, shrinkage was not quantified, but, the phenomenon that is associated with shrinkage invariably results in cracking (Section 2.2.3) at the micro level and this will increase the heterogeneity and in no doubt have impact on the dynamic modulus.

$$V = \left(\frac{K-E_d}{\rho}\right)^{0.5} \quad 6.3$$

Where

$$K = \frac{(1-v)}{(1+v)(1-2v)} \quad 6.4$$

and

$\rho = density$ (from measurements)

v = Poisson's ratio

E_d = dynamic modulus of elasticity

Ultrasonic testing was also used to assess the dynamic modulus of elasticity of the different types of concrete. The measurements are largely predicated upon the elastic properties and mass of the material and hence the aggregate in concrete because its high stiffness can have a significant effect on the results (Lee et al, 2004). Since the same types of aggregates were used in the same proportion in all the SCC specimens, again the difference in the dynamic modulus will highlight the structural difference brought about by the incorporation of the corrosion inhibitors. With a noticeable reduction in the dynamic modulii of elasticity of the fly ash and silica fume SCC (FM and SM) samples when the carboxylic inhibitor was admixed in each type of SCC samples (Figure 6.7), it is shown that this type of organic inhibitor has a tendency to decrease the stiffness of concrete.

6.5. CONCLUSION

In summary, it is shown that the carboxylic corrosion inhibitor influenced the mechanical performance of the fly ash and silica fume concrete. In the fly ash and silica fume SCCs, the introduction of the carboxylic inhibitor had a profound reducing effect on the 60 and 90-day compressive strengths of fly ash (FM) SCC and on the 28 to 90-day compressive strengths of the silica fume (SM) SCC based on comparison made with the control at equivalent age (Sections 6.3.1-2). The relative densities of the carboxylic fly ash (FM) and silica fume (SM) samples also fell below those of the corresponding fly ash (FG) and silica fume (SG) controls by 1.3 and 5.4% respectively at 28 days. When the compressive strength of the SCC samples with high concentration are compared with the same sample made with low concentration of inhibitor, it was revealed that the high concentration of the carboxylic compound resulted in 14 and 12% strength reduction at 28 and 90-day respectively in the FM(2x) concrete but, compared to the SM sample with the basic concentration of inhibitor, the 28-day strength of the SM(2x) was 23% higher as the concentration was doubled. However, at 90 days, there was no noticeable difference in strength between the SM samples made with high and low contents of carboxylic inhibitor.

When the nitrite inhibitor was used in the fly ash SCC, it significantly increased the compressive strength of the FGC concrete at ages up to 60 days and at 90 days the strength fell slightly below the control sample (Sections 6.3.1 - 2). As the concentration of the nitrite inhibitor increased in the FGC sample, the 28 and 90-day compressive strengths of the FGC(2x) concrete were reduced by 19 and 30% respectively when reference is made to the basic FGC mix at the corresponding

age, indicating that at high concentration, the nitrite compound had an adverse effect on the SCC sample. Compared to the reference FG sample, the higher tensile strength and greater toughness value in the FGC sample signify that the nitrite inhibitor helped to optimise some of the properties of the fly ash SCC. The improvement is also evident from the ultrasonic signals that indicate that the incorporation of the nitrite inhibitor contributed to a more homogeneous fly ash SCC (FGC) with a higher elastic modulus at 28 days.

Using low concentration of carboxylic inhibitor in the fly ash SCC resulted in setting retardation, bleeding and shrinkage of the concrete. The flexural tensile strength test shows that, whereas the tensile property of carboxylic silica fume (SM) SCC was 41% higher than the SG control, the carboxylic fly ash (FM) mixture produced a concrete that was 17.6% inferior to the corresponding FG control. This means that the defects that occurred in the plastic state of the carboxylic FM SCC affected the physical structure of the concrete and this was confirmed by ultrasonic pulse in which the velocity of the transmitted waves was lowered by 233 m/μs as the test moved from the FG control to the carboxylic FM sample. The lower velocity is ascribed to a higher heterogeneity that resulted from the use of the carboxylic inhibitor. Despite the favourable tensile strength in the SM SCC, it was found that this inhibited silica fume SCC was also more heterogeneous than the SG control. However, the tensile strength of the FGC concrete was slightly higher (3%), the ductility increased and the concrete became more homogeneous when the nitrite inhibitor was used in this type of fly ash SCC.

It can therefore be concluded that the nitrite inhibitor will have no adverse effect on the short and medium term mechanical properties when used in low concentration in high volume fly ash SCC but it will marginally reduce the 90-day compressive strength of the FGC concrete (Section 6.3.1). Additionally, when used in high concentration, the nitrite compound can reduce the compressive strength of the FGC(2x) sample by over 19% of the basic FGC sample with 0.3% of carboxylic inhibitor. The incorporation of the carboxylic inhibitor in high volume fly ash SCC significantly reduced the quality of the FM concrete by decreasing the compressive and tensile strengths and by increasing the heterogeneity of the concrete. When added to the silica fume SCC, the carboxylic inhibitor had a mixed effect. The compressive strength and homogeneity of the silica fume SM concrete were reduced but the tensile strength was increased somewhat.

Results from the ultrasonic pulse measurements show that the incorporation of the carboxylic compound in the fly ash and silica fume (FM and SM) SCCs, resulted in a reduction of the propagation velocity of the shear waves, confirming that the heterogeneity of these mixes were increased. The associated dynamic modulii of elasticity of the FM and SM samples of concrete were also lower than those of the corresponding controls by approximately 14 and 8% respectively. The calcium nitrite, on the other hand, increased the velocity of the wave; indicating an improvement in the homogeneity and, thereby, an improvement in the dynamic elastic modulus when it was added to the fly ash SCC. The effects of the carboxylic and nitrite inhibitors (in the basic concentration - 1x, and high concentration - 2x) on the mechanical-related properties of the SCCs are summarised in Table 6.3.

Table 6.3 Effects of the corrosion inhibitors on the properties of SCCs at 28 days

	INHIBITOR					
	1x concentration			2x concentration		
	Carboxylic		Nitrite	Carboxylic		Nitrite
PROPERTIES	**Fly ash**	**Silica fume**	**Fly ash**	**Fly ash**	**Silica fume**	**Fly ash**
Compressive strength	Decreased	Decreased	Increased	Decreased	Increased	Decreased
Flexural strength	Decreased	Increased	Increased			
Heterogeneity	Increased	Increased	Decreased			
Bleeding	Noticeable	Slight	None	Significant	Noticeable	None
Delayed hardening	Noticeable	Slight	None	Significant	Noticeable	Slight

TRANSPORT PROPERTIES

7.1. GENERAL

The importance of transport properties stems from the fact that in many instances concrete has to co-exist with deleterious substances in its locality and the rate at which these substances penetrate the concrete will help to govern the extent of its service life. As the main objective of this research is concerned with the resistance of the corrosion inhibited samples to corrosion attack, this chapter covers the evaluation of the parameters that are related to the transport of water and chloride ions. Water plays a supportive role in many of the deteriorating process; either by participating in the reaction or acting as a channel for conveying harmful substances. In the case of chloride-induced corrosion, the rate of movement of the Cl^- ions is of great interest as chloride attack on concrete is one of the most aggressive forms of attack on concrete.

7.2. TRANSPORT PROCESSES

7.2.1. Results

Porosity can be defined as the measurement of the fraction of pores relative to the solid constituent of the concrete under specified condition of testing. The pores are theorized to be those of the evaporable water (Neville, 2005), which are the pores of interest as the contribution of the pores that contain non-evaporable water to the transport of fluids is infinitesimally small. The porosity measurements from tests (Section 4.5.4.1.) conducted on three specimens at ages 7

days and three specimens at 28 days for each SCC sample are shown in Figure 7.1. The ranges of porosity were 6.59 to 4.58% at 7 days and 5.52 to 4.01% at 28 days. At 7 days the nitrite SCC (FGC) sample attained a porosity value that was 30% lower than the FG control and at 28 days the porosity of the FGC sample was also lower than the FG sample but by 3%. In the case of the carboxylic samples, the FM SCC was approximately 10% lower and the SM SCC was 15% higher than the respective controls at 7 days. On the other hand, compared to the measurements of the respective FG and SG samples at 28 days, it is shown that with the carboxylic inhibitor in the FM and SM samples, the porosity increased by 27 and 18 %. All porosity measurements are displayed in Figure 7.1.

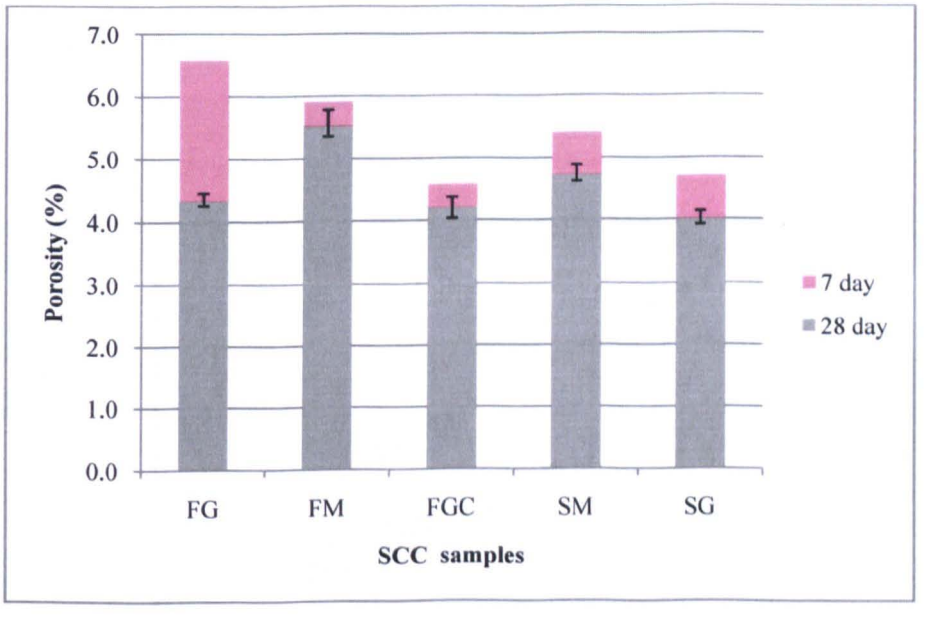

Figure 7.1 The relationship between the porosity at 7 and 28 days in SCC mixes

The absorption test (Section 4.5.4.2.) was conducted on the SCC samples to determine the movement of water under a moisture gradient. Testing was conducted on three specimens for each SCC at 7 and 28 days. The test was carried out over a two-hour period and readings were taken at designated times as shown in Figures 7.2 and 7.3. Amongst the fly ash samples the cumulative water uptakes at the age of 7 days were between 9.25 and 18.25 g and between 6.9 and 7.2 g at 28 days for the FG, FM and FGC samples. When the absorption measurements were taken at 7 days on the SM and SG samples, the results at the end of the two-hour test were 6.25 g and 10.7 g respectively; and the corresponding absorption values were 6.0 g and 6.8 g at 28 days. Linear regression was used to establish the relationship between the absorbed water in the concrete and the time of exposure to water. A linear relationship, with coefficient of determination greater than 0.9, was established. The sorptivity indices for the samples are provided in Table 7.1.

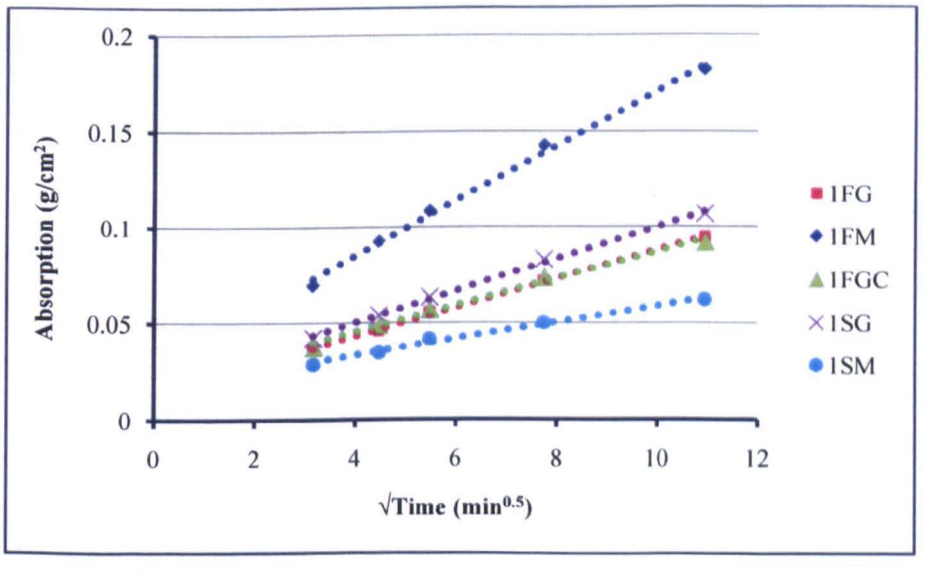

Figure 7.2 Degree of water absorbed over the square of time for SCC mixtures at 7 days

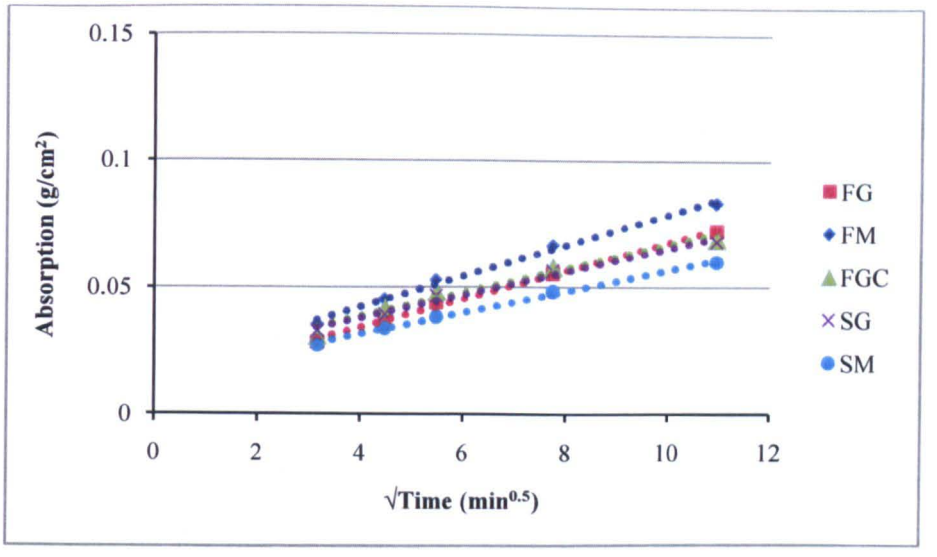

Figure 7.3 Degree of water absorbed over the square of time for SCC mixtures at 28 days

Table 7.1 Sorptivity indices for SCC samples

Samples	Sorptivity (cm/√min)	
	7- day	28 - day
FG	0.0075	0.0055
FM	0.00144	0.006
FGC	0.0069	0.0047
SM	0.0043	0.0042
SG	0.0083	0.0045

Mercury intrusion porosimetry (Section 4.5.2.1.) was used in the research to determine parameters related to the pore system of the mortar in the individual SCC samples. The computation of the porosity is based on the measurement of the mercury penetrated pores expressed as a fraction of the total volume of the sample (Galle, 2001). A semi-logarithmic display of pore diameter versus volume of pore intruded from MIP measurement is presented in Figure 7.4. In addition to the fact that the porosity test and the MIP examination used different types of permeates under different conditions, the porosity measurements of the individual SCC sample as assessed by the first of these tests, gives results that are usually lower than the porosity of the mortar that was measured by the MIP test from the same concrete. The results of the MIP tests are set out in Table 7.2 where it is shown that all the SCC samples underwent pore refinement, which is a typical feature of traditional SCC as, the pozzolanic activity from of powders such as fly and silica fume (Gesoğlu et al, 2009) helps to reduce the sizes of the pores. The reference point that is used for the occurrence of pore refinement is 0.1μm. With reference to the control FG and SG mortars, the respective porosity of the FM and SM mortars was 33 and 7.7% higher than the corresponding control at 28 days. The inclusion of the nitrite inhibitor in the traditional fly ash mortar, however, reduced the porosity of the FGC mortar by 8.3%.

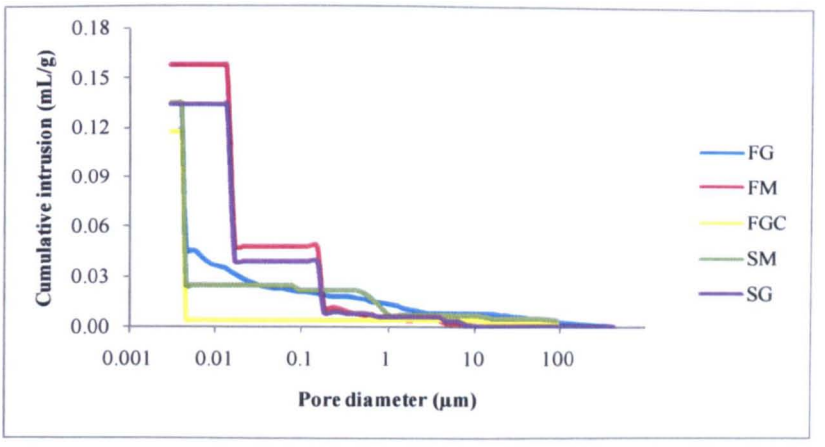

Figure 7.4 MIP measurements showing that a larger volume fraction of pores was less than 0.1μm in diameter

Table 7.2 Characterisation of pore structure of mortars at 28 day (via MIP)

SCC Mortars	Micro-pores %	Threshold value (μm)	Porosity %
FG	81	0.005	12
FM	70	0.02	16
FGC	98	0.004	11
SM	83	0.004	14
SG	71	0.02	13

Resistivity is a property that describes characteristics such as the degree of pore saturation, and the potential for chloride diffusion and corrosion initiation. For this test two samples, each with dimensions of 100 mm diameter and 125 mm in length were used. The electrical test applied a

voltage that delivered a current of 1 mA. The electrical resistivity measurements of the fully saturated SCCs at 28 days are shown in Table 7.3. Inspection of this table shows that the electrical resistivity of the FM SCC was 58% lower than the FG control at 28 days and that of the FGC SCC was 2% lower than the same fly ash control. Additionally, the electrical resistivity of the FGC and SM samples decreased by approximately 64% as the concentration of the nitrite and carboxylic inhibitor in the respective sample increased by 100%.

Another type of resistivity test that was performed on the concrete specimen is the non-steady state electrical migration (D_{nssm}) test. The test was carried out on 100 mm diameter x 50 mm thick specimens to ascertain the capacity for the migration of chloride ions under an electrical field. The average measurements from three specimens were used for the D_{nssm} reading of each sample. All the readings for the rapid migration tests are reported in Table 7.3. Whereas the chloride electromigration coefficient of the FM sample was 400% higher, the chloride migration coefficient of the FGC sample was 55% lower than that of the FG control. Comparatively, the SM SCC had a chloride migration coefficient that was approximately 12% higher than the SG control's. It was further shown that the D_{nssm} values of the FGC and SM samples increased by 40 and 84% above that of the respective FG and SG samples as the concentration of inhibitor increased by 100%.

Table 7.3 Electrical resistivity and electromigration measurements of SCCs

SCC samples	Electrical resistivity (Ωm)	D_{nssm} x 10^{-12} (m^2/s)
FG	954 ±17	2.2 ±0.2
FM	397 ±34	11.2 ±0.6
FGC	936 ±14	1.0 ±0.3
SM	1008 ±20	1.9 ±0.4
SG	882 ±15	1.7 ±0.5
FGC(2x)	330 ±48	1.4
SM(2x)	367 ±27	3.5

7.2.2. Discussion

Figure 7.1 shows that the level of porosity in each SCC sample is reduced as the age moved from 7 days to 28 days, confirming that with adequate curing, the porosity of concrete is reduced as hydration is advanced (Hall and Yau, 1987). The nitrite FGC SCC, however, attained a significantly lower degree of porosity than the FG control at 7 days, but at 28 days the difference in porosity was reduced as shown in Section 7.2.1. Basically, the development of porosity in the FGC sample shows that the nitrite compound is responsible for the relatively low percentage of porosity in the FGC sample, as the water/cement ratio and the basic ingredients in this sample and the control sample were the same. The nitrite compound accelerated the hydration process and produced more C-S-H in the FGC sample than that which was developed in the FG control. Therefore, although the FG and FGC samples were at the same age, the stage of hydration was

not the same, that is, the FGC sample was more mature. Typically, at the very advanced stages of hydration, the incremental growth in C-S-H is reduced (Section 2.2.2) and hence the reduction in porosity is decreased gradually. This provides the reason for the low reduction in porosity of the FGC sample as the sample aged from 7 to 28 days (Figure 7.1); compared to the movement in the porosity of the fly ash (FG) sample over the same period. Structural development of this nature means that the resistance to ingress of fluids is more likely to be greater in the nitrite FGC concrete than in the fly ash control. As surmised, the sorptivity index of the FGC sample was lower than that of the fly ash (FM) control, which confirms that the capacity for absorption was lower in the nitrite SCC specimen.

Although the percentage porosity of the carboxylic FM sample was lower than that of the FG control at 7 days, the FM sample had a higher porosity than the control at 28 days (Section 7.2.1). The SM SCC also possessed a higher porosity than that of the SG control at 7 and 28 days. It is worth mentioning that this type of porosity test is not an absolute measurement of porosity as water can only access the penetrable pores and therefore results from this test cannot be used to give fine details of the hydration process but it can give an indication of the general developmental process. It is observed that, while the percent reduction of porosity was over 30% in the FG control, the reduction of porosity in the carboxylic FM sample was approximately 7% as the concrete samples moved from 7 days to 28 days. During this period, if hydration was not accelerated, the rate of development of the carboxylic FM sample should have been be close to that of the control sample and, by extension, the porosity reading of the FM sample would have been closer to the FG control. Comparing the two silica fume samples, the carboxylic SM specimen experienced approximately 13% reduction in porosity from 7 to 28 days while the SG

control underwent approximately 15% reduction in porosity over the same period. At 28 days, porosity of the SM sample was also appreciably higher than the reference SG sample (Section 7.2.1). From these observations, it can be said conclusively that, compared to the traditional SCCs, the carboxylic inhibitor contributed to an overall higher level of porosity and an apparent lower rate of development in the FM and SM samples.

The sorptivity indices in the SM sample at 7 and 28 days were lower than those in the SG sample at 7 and 28 days respectively. On the contrary, the 7-day and 28-day sorptivity indices for the FM samples were higher than the indices of the FG control at the respective 7 and 28 days. In some instances the correlation between the porosity and absorption values for concrete for each sample is high. In this study, whereas the correlation coefficient between these parameters in the control samples is fairly high, it is approximately 0.7 in the inhibited SCC, of which the main contribution to the variance is from the carboxylic samples. This suggests that in addition to the volume of pores, other factors such as the size of pores, inter connectivity of pores and the tortuosity of the transport path may have had a more influencing role in the absorption of water in the carboxylic samples.

The MIP results show that, when comparison is made with the mortar of the FG sample, the FGC mortar had a smaller void content (Section 7.2.1), which is consistent with the trend of the porosity measurements in the two samples and the test further shows that the nitrite inhibitor was better able to reduce porosity and cracking that could develop in the ITZ between the mortar and aggregate. The FGC sample also attained a higher level of pore refinement and the threshold

diameter of the pores was also smaller in the nitrite SCC samples. The threshold diameter quantifies the pore size at which further mercury intrusion is limited and the pore refinement shows that a large quantity of the pores is less than 0.1 μm. These pore parameter values indicate that the diameter of the pores in the bulk mortar of the FGC sample was smaller than that which was obtained in the traditional FG SCC and this improvement helped to mitigate the transport processes in the nitrite sample.

The characterization of the pore structure of the FM mortar by MIP shows that it had an appreciably higher volume of pores (Section 7.2.1) and a lower degree of pore refinement than the mortar of the FG mortar. Besides, the measurements indicate that the FM mortar consisted of a large volume of voids, of which the majority were large in diameter. This is confirmed by the large threshold diameter of the pores. This configuration supports a high network of connectivity between pores, a condition that is ideal for the transport of fluids. This condition explains the relatively high uptake of water in the absorption test.

On the other hand, the porosity of the SM mortar was just marginally higher than that of the SG control, but there was a higher degree of pore refinement. In addition to this, the lower threshold diameter of pores in the SM mortar reveals that, although it has a slightly higher porosity than the SG control sample (Section 7.2.1), the pores in the carboxylic silica fume mortar are more discreet and hence it will attenuate the flow of injurious substances through transport processes such as absorption. At this point, it should be reiterated that samples that were prepared for the MIP test were taken from the bulk of the mortar and the presence of cracks would have been

limited since the samples were small and the fragments would have originated from fracture along pre-existing cracks when such cracks occur. Therefore, it is shown distinctly that most of the volume of pores above that of the control SG sample in the porosity test on the sample, did not reside in the SM mortar as capillary pores but reside in the SM sample as cracks or voids in the interfacial transition zone between the mortar and the aggregates.

The test results that have been discussed so far had focused on the physical properties of the concrete. The electrical resistivity of the concrete considers not only the geometry of the pore system but the chemical composition of the concrete also. At 28 days under saturated surface-dry condition, the resistivity of the FGC sample was lower, although slightly, than the resistivity of the fly ash control. This result cannot be fully explained since it is already shown that the volume and size of the pores in the FGC sample is lower than those of the FG sample, and it is expected that the essence of the inhibitor is to increase the resistivity of the concrete. However, this is a different test that takes other variables into consideration. Contrastingly, when the diffusion test was conducted on the FGC concrete it showed specifically that the nitrite fly ash sample was better able to limit the flow of chloride ions through the pore solution than the FG sample. Since the diffusion test takes into consideration the physical and chemical binding of the chloride ions, it reliably shows that the nitrite inhibitor will help to improve the resistance of the fly ash SCC to chloride-induced corrosion.

The results from the diffusion test on the carboxylic fly ash and silica fume SCC's are somewhat supportive of the results from the resistivity test. The addition of the carboxylic compound made

the fly ash (FM) SCC less electrically resistant and more vulnerable to the diffusion of chloride ions but made the silica fume SCC more resistant to the flow of electrical current under water saturated condition while maintaining almost the same level of chloride diffusion. This improvement occurred in the SM sample despite the higher level of porosity (relative to the traditional silica fume SCC) mainly because the pores in the bulk of the SM SCC were more discreet, making the transport path longer and more tortuous.

Additionally, data from the electrical resistivity and migration tests show that, when the concentration of the nitrite and carboxylic inhibitors in the respective fly ash and silica fume concrete increased, the transmission of electrical current and chloride ions in these two types of concrete samples increased. It is therefore deduced that with higher inhibitor concentration, the transport path became more accessible and the durability of the inhibited samples reduced.

7.3. RELATIONSHIPS AND CORRELATION

Permeability is a mode of transport that shows strong correlation with porosity and it can be defined as the ingress of substances into a material under a pressure gradient. As it is a relevant transport property in concrete, it is desirable to determine this parameter. Darcy's Law shows the permeability k can be computed from the formula in Equation 7.1. The terms v_l and μ_0 are the respective apparent velocity and viscosity of the fluids and $\frac{\delta p}{\delta l}$ represents the differential pressure over the path length in consideration.

$$v_1 = \frac{k}{\mu_0} \cdot \frac{\delta p}{\delta l} \qquad 7.1$$

Carman Kozeny formula, with the use of Darcy's Law gives the relationship between intrinsic permeability, porosity and specific surface as shown in Equation 7.2. The original model for the determination of the permeability was based on straight capillary channels and so a tortuosity term (φ) was introduced to compensate for tortuous paths in materials and h_0 is a form factor that helps to characterize the pore space. The tortuosity term is defined as the ratio between the length of the tortuous path and the length of a straight line between the start and the end points of this path but it can be ascertained from Equation 7.3 where the density (ρ) of the concrete can be measured and the total specific volume (V_t) can be obtained from MIP. As the cross sectional area of the capillary channel varies, the radius will change accordingly (see Figure 7.4). Therefore the median radius (r_c) will be used in this formula to obtain intrinsic permeability of the concrete. The median radius occurs at the point where approximately half of the pore volume is intruded with mercury (Ramachandran and Beaudoin, 2001). The porosity measurements Ψ, determined by water immersion and S_v values which were calculated in accordance with Equation 7.4, were used for the computation of intrinsic permeability.

$$k = \frac{1}{h_0 \varphi} \frac{\psi^3}{S_v(1-\psi^2)} \qquad 7.2$$

where

$$\varphi = 2.23 - 1.13\rho V_t \qquad 7.3$$

$$S_v = S_{vp}\left(\frac{\psi}{1-\psi}\right) \qquad 7.4$$

and where the specific surface per unit area S_{vp} is defined as:

$$S_{vp} = \frac{2}{r_c}$$

Application of this formula yields values as shown in Table 7.4.

Table 7.4 Permeability coefficients

Samples	Intrinsic permeability x 10^{-11} (m^2)
FG	0.78
FM	12.7
FGC	0.76
SM	0.97
SG	6.06

7.4. CONCLUSION

From the tests designed to determine the transport properties it was shown that, the nitrite inhibitor made the traditional fly ash SCC less penetrable and hence the ingress of liquids and ions such as Cl^- was reduced in the FGC SCC. This was the result of a 3% reduction in porosity of the concrete and a 20% higher pore refinement in the matrix when basic content of nitrite

inhibitor was introduced in the fly ash concrete. This type of improvement that is imparted by the nitrate inhibitor will help to increase the sustainability of the fly ash SCC.

There is not much affinity between the carboxylic inhibitor and the high volume fly ash SCC. Compared to the FG control, the propensity of the FM SCC to imbibe water through absorption was increased as a result of the incorporation of the organic inhibitor. The coefficient of chloride electromigration in the FM sample was also 400% higher, and the electrical resistivity was 58% lower than those of the control Additionally, when the parameters of the concrete was used in calculation, it was shown that the intrinsic permeability of the FM concrete was 16 times that of the FG control. This decline in transport properties will make the concrete more susceptible to deterioration through processes such as chlorine induced corrosion and therefore this type of concrete will not be very durable.

The introduction of the carboxylic compound in the silica fume concrete produced mixed results. The organic inhibitor, when added, increased the resistance of the silica fume concrete, (SM), to water absorption and the electrical resistivity was increased by 2% when the concrete was saturated with pure water. This was achieved despite the 18% increase in porosity brought about by the incorporation of the carboxylic inhibitor in the silica fume concrete and the improvement is ascribed to the greater degree of pore refinement and higher level of discreet pores that were imparted in the silica fume mortar. It was shown that the silica fume SM SCC experienced a higher porosity through cracks and/or voids that formed in the ITZ between the aggregate and

the mortar when the organic inhibitor is used and this helped to increase the electromigration of chloride ions in the concrete by 12% beyond that of the SG control.

CORROSION– FORMS AND MICRO-STRUCTURAL EXPLANATIONS

8.1. INTRODUCTION

An important aspect of this research is the investigation of the performance of the corrosion-inhibited SCC samples to determine if extra level of corrosion protection can be achieved by the addition of corrosion inhibitor. The provision of high corrosion-resistant concrete will provide a solution to chloride attack in aggressive chloride-laden environment. This will help with the sustainability of reinforced concrete infrastructures and contribute to the reduction of harmful environmental effects that are associated with the production of cement. This chapter focuses on the inhibiting capacity of SCCs admixed with corrosion inhibitor by examining the corrosion resistance of these types of SCCs under conditions that will affect the performance of the individual inhibited-SCC sample. The performance of the inhibited will be made with reference to traditional SCCs with inhibitor. The causes and the effects of the corrosion process in the different types of inhibited-SCCs will also be investigated to gain an understanding of the factors that aid the corrosion process and the concrete's properties that are affected by the electrochemical process.

Two types of conditions were used to test the corrosion-inhibited concrete samples. In one series of tests, the samples were contaminated with 1% NaCl to evaluate the magnitude of the defence to chloride-induced corrosion in the corrosion-inhibited SCC samples. In this series of tests the chloride load was reduced to 0.1% in one instance and in another instance the concentration of the corrosion inhibitor was increased by 100% to determine the efficiency of

the inhibited SCCs in abating corrosion at small and large chloride loads. The samples admixed with NaCl were exposed to cyclic wetting and drying to accelerate corrosion. The other condition employed the method of impressed voltage to accelerate the corrosion of the lollipop samples that were made free of entrained chloride. These samples were made primarily to determine

a. the inhibiting power of the mix formulations in an environment that was designed to promote leaching/consumption of the inhibitor
b. the level of healing that can be achieved with corrosion-inhibited SCC samples.

8.2. CORROSION

Figure 8.1 shows that none of the corrosion-inhibited SCC samples or the control specimens in the wetting and drying experimental series experienced corrosion within the 36-week period of the experiment. The analysis for corrosion initiation was based on corrosion potential (E_{corr}) results determined by half cell-potential readings with SCE (+244 mV) where the reference point used for 90% probability of no occurrence of corrosion is -120mV and higher according to ASTM C876 and Myrdal (2007). Each E_{corr} value is the average of three measurements. At the very beginning of the experiment the corrosion potential readings of a few of the samples were between -120 and -270 mV (see Section 4.5.5.1), which showed a slight uncertainty as to whether corrosion was initiated. However, the E_{corr} readings for these samples became more positive as the passivity increased and showed that, like the rest of the samples, there was no inclination to corrosion initiation.

The current density (i_{corr}) was computed for all the samples using the Stern and Geary equation (Equation 8.1), after obtaining the polarization resistance (R_p) with the aid of the ACM potentiostat/galvanostat instrument. The value used herein for the constant B is 26 (Yu et al, 2012). Again, three specimens were tested for each SCC sample. It is shown from Figure 8.2 that the current density (i_{corr}) of the nitrite sample with 1% NaCl (FGC) was substantially less than that of the control FG with 1% NaCl at the early stage and it remained lower for the entire duration of the test. The actual corrosion reading on the FGC sample was close to $1x10^{-4}$ mA/cm^2 after 28 days of wetting and drying, but as the time elapsed, its current density reduced at a higher rate than the current density of the control. When the sodium chloride concentration was reduced from 1.0 to 0.1% (FGC(0.1)), the current density on the embedded steel was noticeably reduced at all inspection points and when the corrosion inhibitor in the nitrite sample was increased by 100% (FGC(2x)), while maintaining the NaCl concentration at 1%, the current density was essentially the same as the FGC sample (with 1% NaCl) in the early stages but increased as the specimen aged.

$$i_{corr} = \frac{B}{R_p} \qquad 8.1$$

The measurements of the corrosion density attained in the reinforced carboxylic fly ash SCC specimens are depicted in Figure 8.3. The fly ash sample with 1% NaCl (FM) had a corrosion current density of approximately 5 x 10^{-4} mA/cm^2 at 28 days and the reading declined by slightly less than one order of magnitude over the 36-week period of the test.

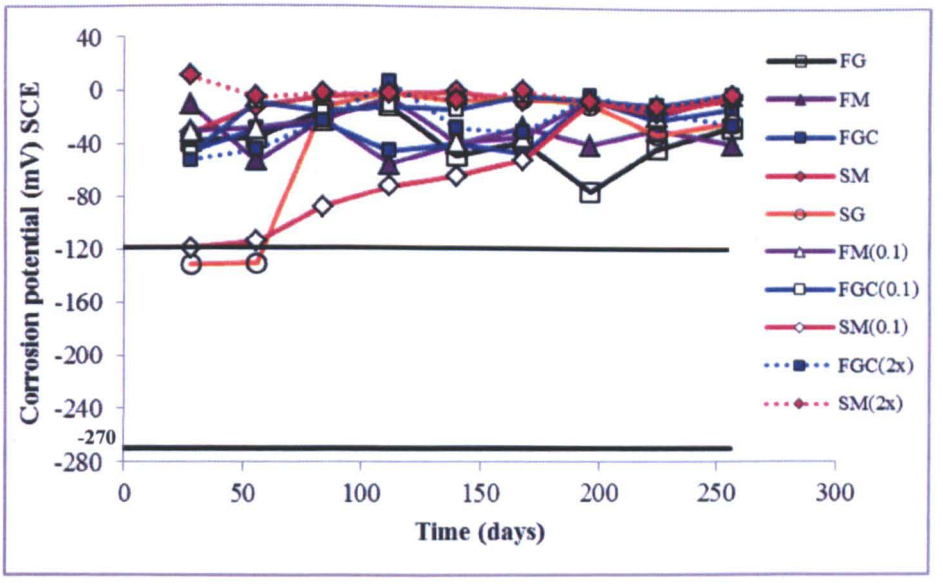

Figure 8.1 This graph shows E_{corr} measurement development with time

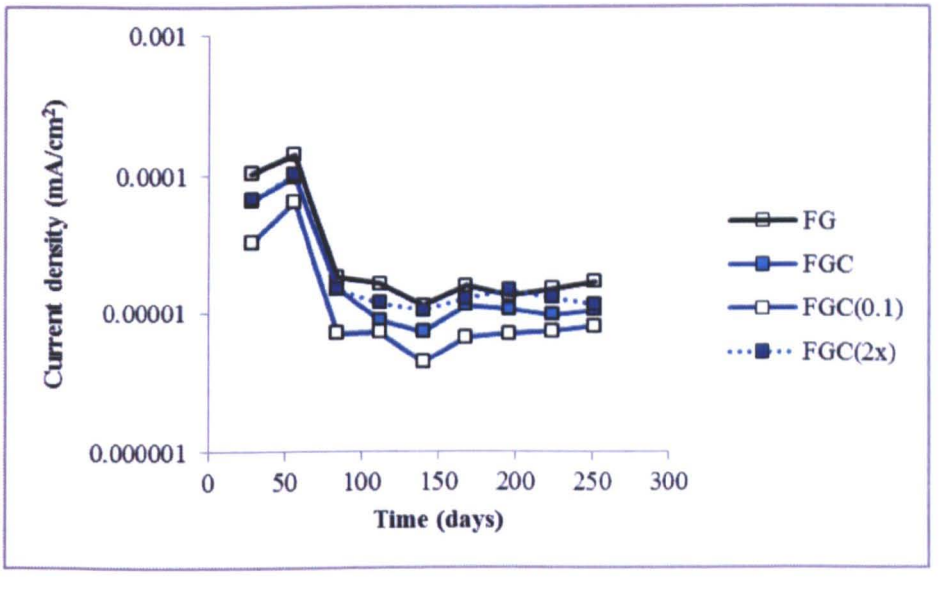

Figure 8.2 Graph showing the relative corrosion resistance of the different types of FGC and the control SCC samples during the period of cyclic wetting and drying

All readings of current density of this sample were higher than that of the FG control with 1% NaCl which was monitored at the same times. The current density readings also declined by almost one order of magnitude at each inspection point when the concentration of the sodium chloride in the carboxylic fly ash sample was reduced from 1.0 to 0.1% (FM(0.1)). Samples of the fly ash SCC made with 1% NaCl and a 100% increase in carboxylic concentration (FM(2x)) were discarded as the samples did not solidify completely and hence lacked the requisite strength for handling. The carboxylic silica fume sample that was contaminated with 1% NaCl however performed better in resisting corrosion when comparison is made with the SG reference containing the same level of sodium chloride. All current density readings for the silica fume sample with 1% NaCl (SM) were less than 1.0×10^{-4} mA/cm^2 which is the point for the initiation of corrosion (Yu et al, 2012), as shown in Figure 8.4. When the concentration of NaCl was reduced from 1.0 to 0.1% in the carboxylic silica fume SCC (that is SM(0.1)), the corrosion density was reduced slightly. Increasing the concentration of carboxylic compound in the silica fume SCC by 100% (SM2x) resulted in a noticeable reduction in corrosion density initially but the difference in current density became negligible with time and eventually the current density of the SM(2x) was higher than the SM at the 36th week. The evolution of corrosion in the sample shows that in the early stages, the concentration of chloride ions at the steel surface is higher than the passivity layer can adequately resist. However, after 56 days the protection film on the steel is strengthened substantially and the corrosion current is reduced. This is the general trend in all the samples in this series of test (see Figures 8.2 and 8.3) which indicates that it took at least 84 days for the steel to fully develop its oxide layer.

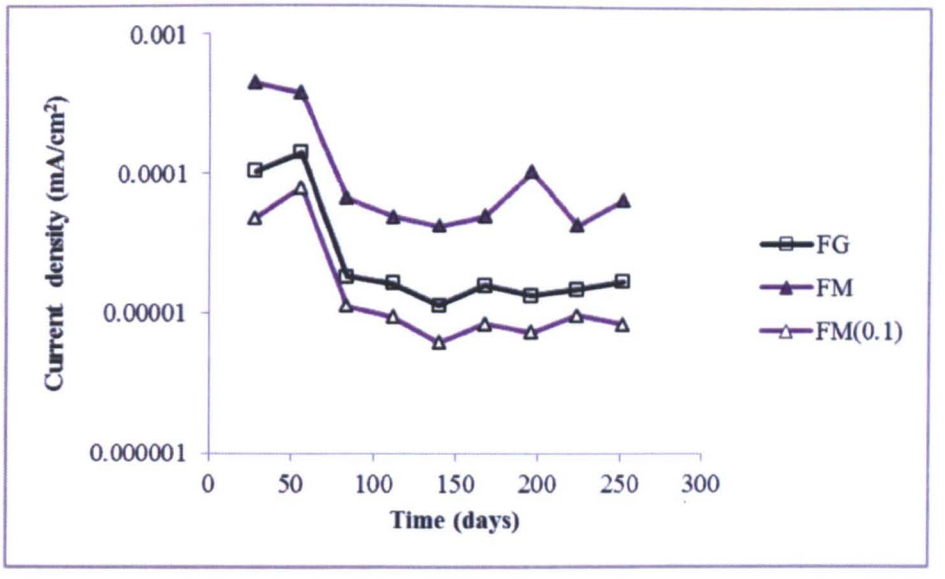

Figure 8.3 Graph showing the relative corrosion resistance of the different types of FM and the control SCC samples during the period of cyclic wetting and drying

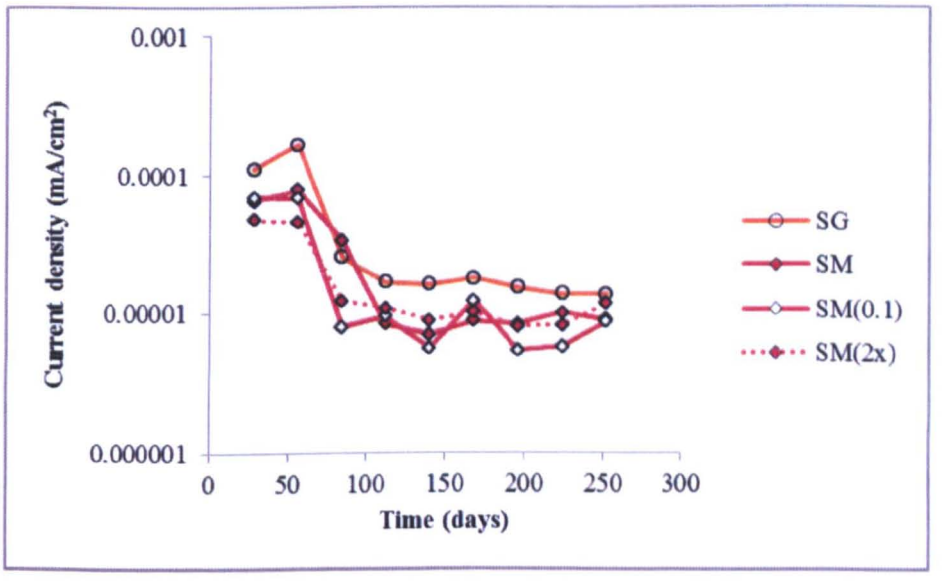

Figure 8.4 Graph showing the relative corrosion resistance of the different types of SM and the control SCC samples during the period of cyclic wetting and drying

The i_{corr} results, after six days of accelerated test to check the reduction of the inhibitor in inhibited-samples from the saline solution are shown in Figure 8.5 alongside the results of moist-cured replicates subjected to the same test. Additionally, Figure 8.6 shows the results of the leaching test when the inhibitor content was increased by 100% and the results from parallel test on the replica un-soaked samples. Samples that experienced large levels of corrosion and had large cracks were removed from the electrochemical cell before the 6th day. The comparison between the results of the soaked and un-soaked samples shows the susceptibility of the inhibited samples to leaching and/or consumption of the inhibitor. With the exception of the soaked and un-soaked SM(2x) samples, when the comparison is made, the soaked inhibited SCC samples showed a higher level of current density than the un-soaked replicates. On the other hand, the comparison between the controls shows that the corrosion density of the soaked samples were lower than or approximately equivalent to the un-soaked samples (FG and SG samples in Figure 8.5), indicating that the early exposure to the chloride solution had negligible effect on the propensity to corrosion. Interestingly, all the corrosion results were higher when the content of the respective corrosion inhibitor was increased.

The steel bars from the un-soaked samples were examined after the six days of exposure to the impressed voltage to determine the nature of corrosion that occurred on the steel bars. When the steel rods embedded in the fly ash samples were tested with the Surpak profilometer (see Figure 8.7 for typical profiles), it was observed that the steel rod in the FGC sample had a Ra value of 0.41μm (shown in Table 8.1) demonstrating that it had a smoother surface than the FG control. The Ra value of the SM sample was also lower than the SG control. The measurements of the deepest penetrations and the pitting factors were also

determined and placed in Table 8.1. The pitting factor gives as an indication of the nature of the corrosion and is determined according to Equations 8.2 – 8.4 and 3.7.

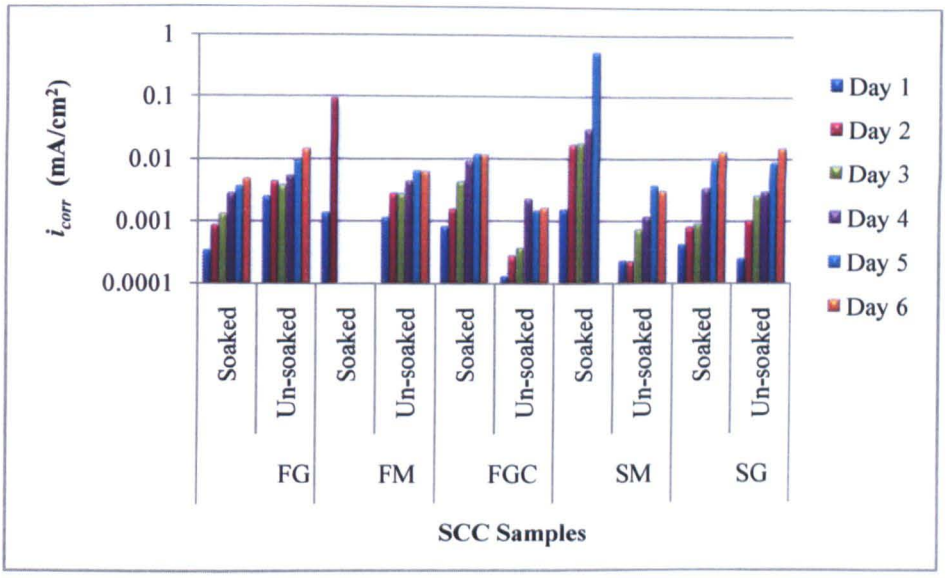

Figure 8.5 Comparison of the i_{corr} values of saline soaked and un-soaked SCC specimens with the basic concentration of the respective corrosion inhibitor

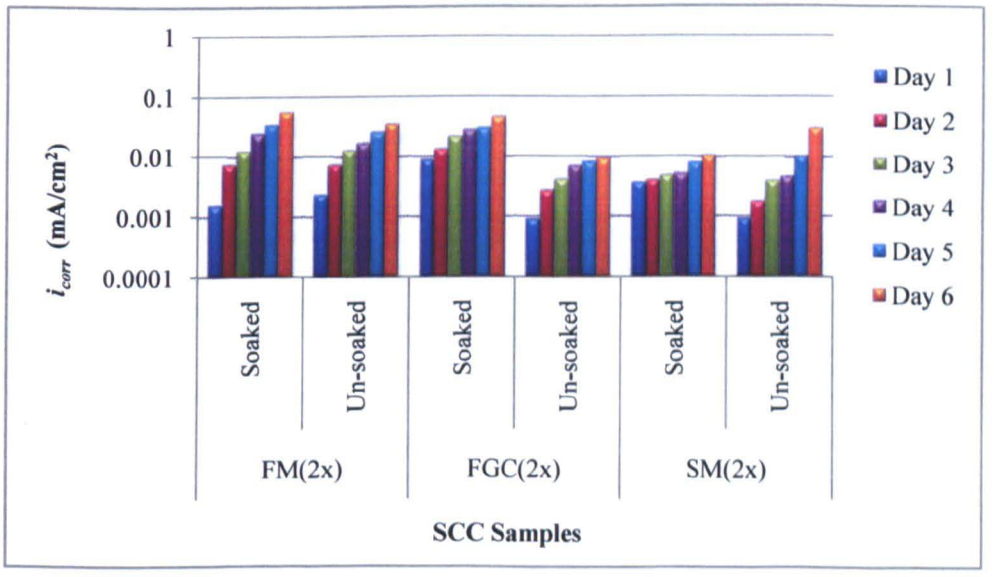

Figure 8.6 Comparison of the i_{corr} values of saline soaked and un-soaked SCC specimens with twice the concentration of the respective inhibitor used in the basic SCC formulation

$$Pitting\ factor = \frac{deepest\ penetration\ (p_s)}{average\ metal\ corrosion\ (d_{mc})} \quad 8.2$$

Where

$$d_{mc} = \frac{mass\ of\ metal\ lost\ (m)}{area\ of\ corroded\ steel\ (A_{cs}) x\ steel\ density\ \rho_{st}} \quad 8.3$$

and

$$m = \frac{Ztl_{corr}}{nF} \quad 3.7$$

Therefore the average corrosion along the steel is given by:

$$d_{mc} = \frac{Ztl_{corr}}{nF A_{cs} \rho_{st}} \quad 8.4$$

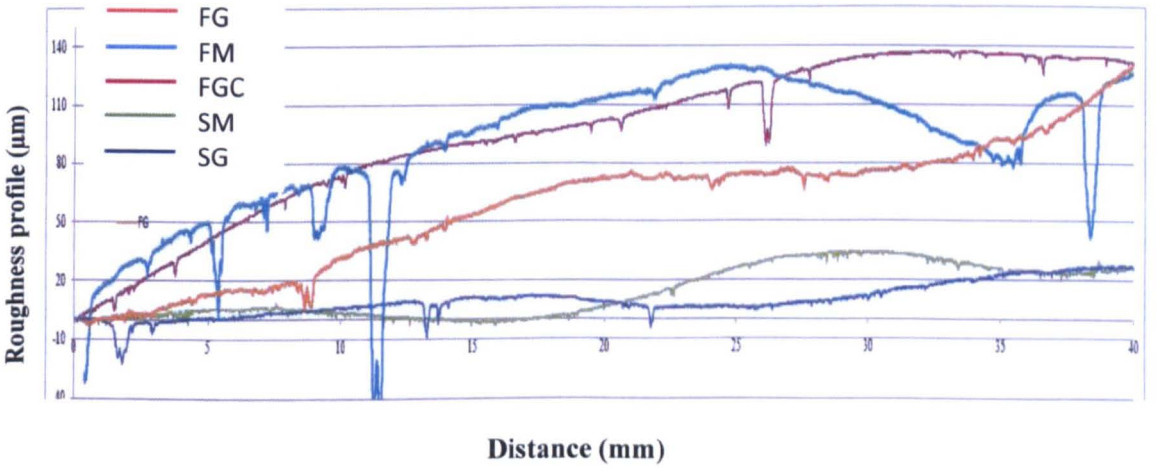

Figure 8.7 Longitudinal profile of the surface of corroded steel rods after cleaning

Table 8.1 Characteristics of steel bar from SCC lollipop samples

Sample	Deepest penetration µm	Widest pit mm	Pitting factor	Ra µm	Strength reduction (%)
FG	22.6	0.416	96	0.44	17
FM	38	1.45	609	> 0.45	20
FGC	3.8	0.212	161	0.41	11
SM	6.9	0.084	141	0.31	21
SG	5.9	0.276	25	0.36	21

As the pitting factor approaches 1, the corrosion can be characterised as uniform (Uhlig and Revie, 1985), and the probability of significant reduction of the diameter (D_s) of the steel is reduced; a situation that is more favourable for the mechanical integrity of the reinforced concrete. Pitting is developed when the Cl^- ions breakdown the passivity layer and start attacking the steel in isolated spots (Valcarce and Vazquez, 2008). The reductions in the tensile strength of the steel rods after corrosion are shown in Table 8.1.

The propensity of corrosion healing in the SCC samples is presented in Figure 8.8 where the broken lines show the time the samples were in the cell under the electrochemical process and the solid markers on the lines show the time that surface cracking was detected on the

samples. Observations of the cracking that occurred in the healing test of concrete showed that the fracture caused by the flakes of rust was positioned primarily parallel to the direction of the steel bar - the source from which the voluminous corrosion products originated. However, there were also transverse cracks branching from the main crack. The cracking patterns of the samples are shown on the crack maps in Figure 8.9. The cracks relegated the degree of resistivity and accounts for the sharp increases in the corrosion current density where it occurred in the concrete samples. In the case of the nitrite sample (FGC), there was a noticeable reduction of 42% in current density immediately after the 24-hour in which the sample was removed from the cell but, the percentage reduction was 58% in the control FG sample. The differences in the corrosion density of the respective FM and SM before and after removal were approximately 5.4 and 4.8% in the positive and negative directions respectively, suggesting that, for practical purposes, no healing occurred.

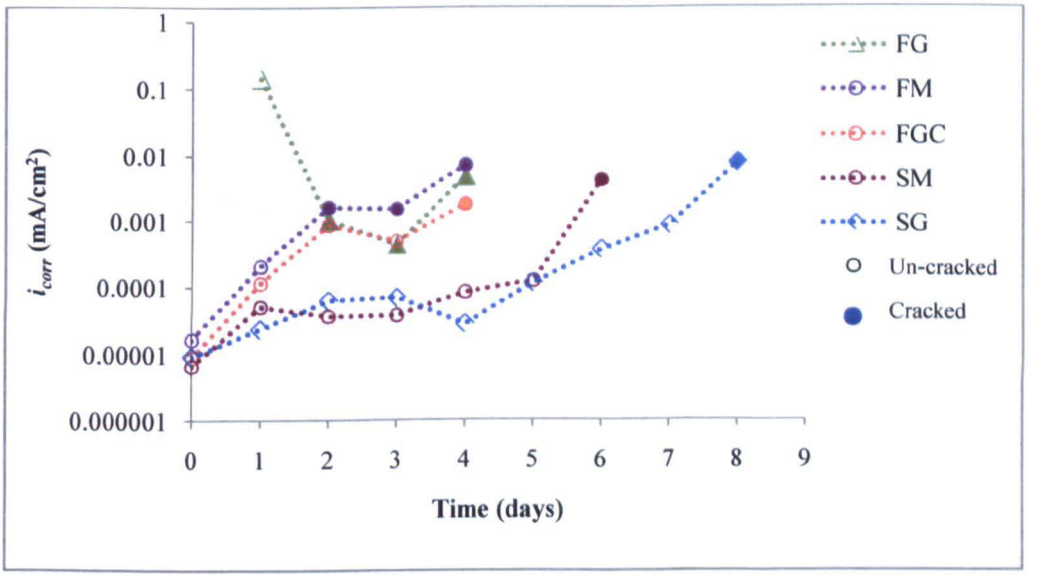

Figure 8.8 The display of the tendency for healing and surface cracking in reinforced SCC samples after 1 day (2^{nd} – 3^{rd} day) removal from the corrosive cell

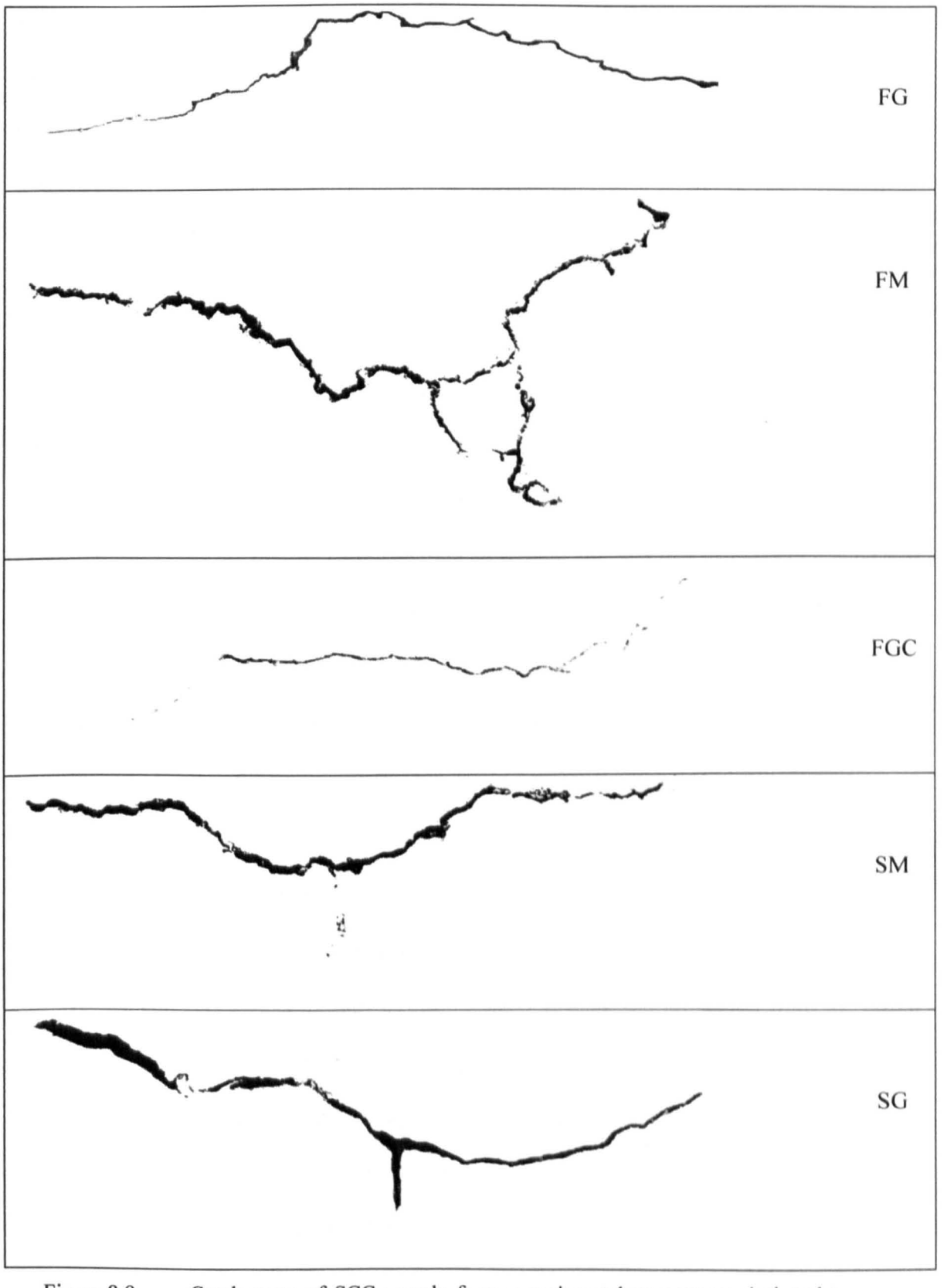

Figure 8.9 Crack maps of SCC sample from experimental programme designed to detect healing of the corroded steel rods

8.3. CAUSES OF CORROSION

It is seen that the performance of the corrosion-inhibited concrete samples varied and this is due to the distinct feature of each individual sample. In this research, the level of resistance to corrosion in the samples is based mainly on the resisting capacity of the corrosion inhibitor and the penetrability of the concrete as will be explained.

In the cyclic wetting and drying test, it is shown that the FG control with 1% NaCl, had a current density that was approximately 1.6 times that of the nitrite sample (FGC) with the same level of sodium chloride - demonstrating that the FGC sample displayed a better performance in resisting corrosion (Figure 8.10), and the resistance of the FGC SCC to corrosion improved by 24% when the content of sodium chloride was lowered to a level that was closer to the lowest maximum permissible limit for concrete (Section 4.2.6.1). These attributes can be partly ascribed to the nitrite corrosion inhibitor. The calcium nitrite-type formulation is an anodic inhibitor whose NO_2^- ions are chemically favoured over the Cl^- ions to react with the dissolved ferrous ions. It is the products of this reaction that coats the steel and enhances the existing passivity layer, making it more resistant to corrosion (Saricimen et al, 2002). This high degree of protection continued to work after the corrosive environment was removed and this resulted in a reduction in the acidity in the anodic zone that partially restored the embedded steel as seen in Figure 8.8. The chemical protection from the nitrite will remain effective in abating corrosion initiation as long as the NO_2^-/Cl^- ratio at the steel/concrete interface exceeds an approximate value of 0.6 but it is shown that the effectiveness of the corrosion inhibitor can reduced when the host concrete is placed in saturated chloride environment which lowers its inhibiting power.

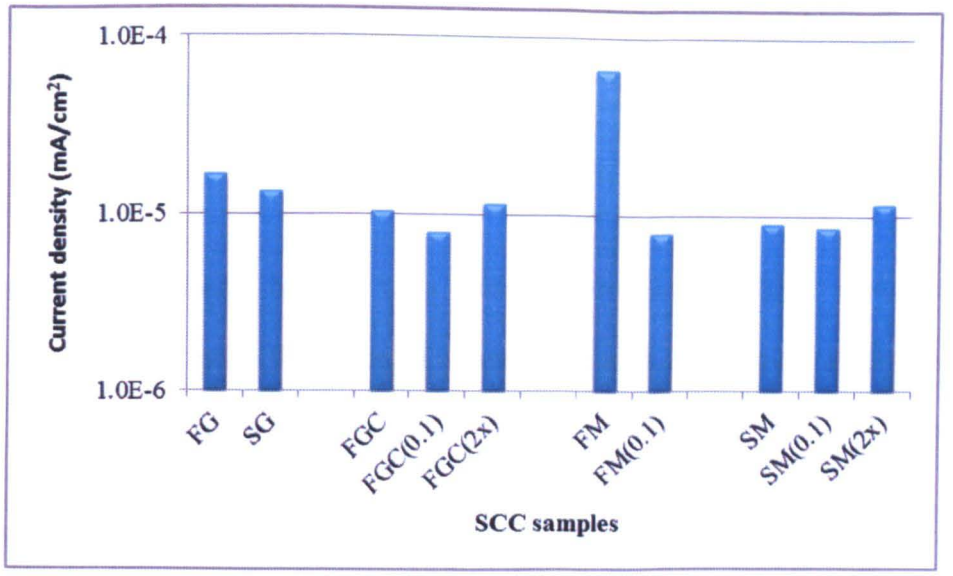

Figure 8.10 The resistance of corrosion-inhibited and non-inhibited SCC samples with 1% NaCl and the basic concentration of corrosion inhibitor. Comparison is made with SCC samples that have NaCl level reduced to 0.1% (0.1) and those with concentration of corrosion inhibitor doubled (2x)

The penetrability of the concrete is also pertinent in the mechanism that attenuates corrosions through chloride contamination. The rate at which the Cl^- accumulates at the steel interface is dependent on the quality of the transport properties of the concrete. From the MIP test it was shown that the mortar of the FGC sample underwent a high level of pore refinement and the ITZ appeared less porous than the control and hence, this produced a denser sample than the control (see Section 7.2). This kind of densification will manifest itself in a high level of resistivity and this is confirmed by the chloride electromigration coefficient (D_{nssm}) and the porosity result determined by the water submersion of the samples at 28 days (Section 7.2). These characteristics certainly helped to significantly reduce the diffusion of the admixed chloride ions in the nitrite SCC and helped to keep the current density low. The increase of the concentration of the nitrite inhibitor in the FGC sample however, modified the structure of the concrete, making it more porous as indicated by the electromigration diffusion

coefficient (see Section 7.2) and this limited the improvement that could have been obtained in the mitigation of corrosion in the FGC(2x) sample.

The carboxylic formulation belongs to a class of corrosion inhibitor which deploys a mechanism that results in the formation of a monomolecular layer on the steel which serves to shield the cathodic and the anodic sites (Vedalakshmi et al, 2009; and Soylev and Richardson, 2006) and this method of mitigating corrosion just seems to halt further corrosion but not to reverse any existing damage done to the steel, as seen in the FM and SM samples, after the temporary removal of the corrosive conditions from the locality. Additionally, the result of corrosion test on saline soaked samples shows that there is a strong possibility that the inhibiting phase of the carboxylic compound in the FM and SM SCC can be reduced and make the concrete more vulnerable to chloride attack.

In relation to the performance of the SM and FM samples in the cyclic wetting and drying environment, it is evident that the mechanism associated with the carboxylic inhibitor helped to minimize the current density in the SM sample with 1% NaCl as the current density of the SG control with the same level of sodium chloride was 1.5 times that of the SM SCC. The carboxylic inhibitor however, was less effective in mitigating corrosion in the fly ash SCC as the FM sample with 1% NaCl sustained current density that was approximately 3.8 times that of the FG control with 1% NaCl. This therefore points to the other main feature that influenced the corrosion resistance of the concrete samples which is now discussed.

The transport properties largely govern the rate at which deleterious substances such as chloride ions advances through the concrete. From Section 7.2, the results of the porosity, electromigration and the resistivity tests, the FM sample had a higher level of penetrability than the FG SCC sample and this resulted in a faster accumulation of chloride ions at the steel surface, rendering the inhibitor less effective in delaying the initiation of corrosion. The result of the transport property tests on the carboxylic silica fume SCC is less definitive as, depending on the transport process under consideration, the SM sample can give a higher or lower performance than the SG sample. However the diffusivity of the SM sample was slightly higher than the SG control but the carboxylic compound was able to suppress the current density and produce a concrete that was more resistant to corrosion than the non-inhibited control sample. Therefore, from the analysis of corrosion and transport parameters of these two carboxylic samples, it is apparent that the inhibitor caused a physical disturbance in the samples that increased the diffusivity to Cl^-. Whereas the physical disturbance was low in the SM sample, it was so high in the FM sample that it dominated the kinetics that is associated with the inhibitor and which would have normally controlled the electrochemical reactions.

8.4. EFFECTS OF CORROSION

The primary reason given for the cracking of the reinforced concrete is the stress created by the corrosion products which are more voluminous than the parent metal. The dissolved iron firstly fills the space between the concrete and steel and nearby interstices and the stress builds up as this space is used up. The process of cracking was however slightly different in the SCC samples. The fly ash control produced hidden longitudinal cracks when the resulting stress exceeded the tensile strength of the concrete. The crack increased the ingress of chloride ions in the locality which, by extension, increased the electrochemical activity and

the flow of ferrous ions in the same general direction where the crack commenced. The crack therefore widened and propagated towards the surface of the concrete in two days. Observations of three specimens and their images were made for each SCC sample.

There was similarity in the evolution of the cracks in the FGC and FG samples as the nitrite sample developed cracks longitudinally that gradually widened and lengthened as the flow of the Cl^- became more accessible. The propagation of the crack was therefore in the same direction where the crack developed and hence the tortuosity of the crack was close to that of the control FG sample (Table 8.2). When compared to the FG sample, it however took a longer time for the crack to propagate to the surface of the FGC sample and the crack density was noticeably lower. Quantification of the tortuosity was determined via image analysis (Section 4.5.2.7) of the cracks of one specimen for each SCC sample.

Cracking of the FM sample showed a more meandering pattern than the pattern in the control FG sample, and there were a couple of cracks branching from the main crack (Figure 8.9). The manner of cracking in the FM sample is attributed to the highly porous structure (Figure 7.1), when the carboxylic inhibitor is added to the fly ash SCC. This structure facilitated a multi-directional migration of the chlorine ions inwards and of ferrous ions outwards. The scattered corroded areas on the steel bars confirm this manner of corrosion. It also appears as if the upper portion of the FM lollipop sample was more porous than the lower portion as the crack did not extend to the base of the sample. Usually when bleeding occurs, the water/cement ratio of the lower section of the concrete is reduced and this increases the strength in this region. As bleeding takes place the porosity of the concrete is also increased from the base upwards. These factors mitigated the electrochemical activity and the stress in

the base of the concrete and hence early cracking was prevented in this region. At two days the meandering pattern of the crack in the FM sample contributed to a fracture that was more tortuous than the fracture that occurred in the FG sample. The crack density in the FM sample was also appreciably higher than that of the control (see Table 8.2).

It took a longer time for cracking to appear in the silica fume samples than in the fly ash samples as the rate of corrosion was slower. As the diffusivity of the SG sample was lower than the diffusivity of the carboxylic SM sample, it took a longer time for crack propagation to occur in the SG sample. Compared to the fly ash samples, when the fracture extended to the surfaces of the two silica fume samples, the cracks appeared less gradually and the cracks were larger, which showed a fracture that is typical of brittle materials. There were also manifestations of transverse cracking in the silica fume samples. The crack however occurred where the tape on the steel ended but the presence of this type of crack is ascribed to the great pressure that developed in the lower portion on the lollipop sample. Linear regression fitting shows that there is a relationship between the tortuosity and the porosity of the specimens as shown in Figure 8.11. The correlation coefficient also shows that it is fairly probable that the crack density from corrosion fracture will increase when the tensile strength of the SCC is increased.

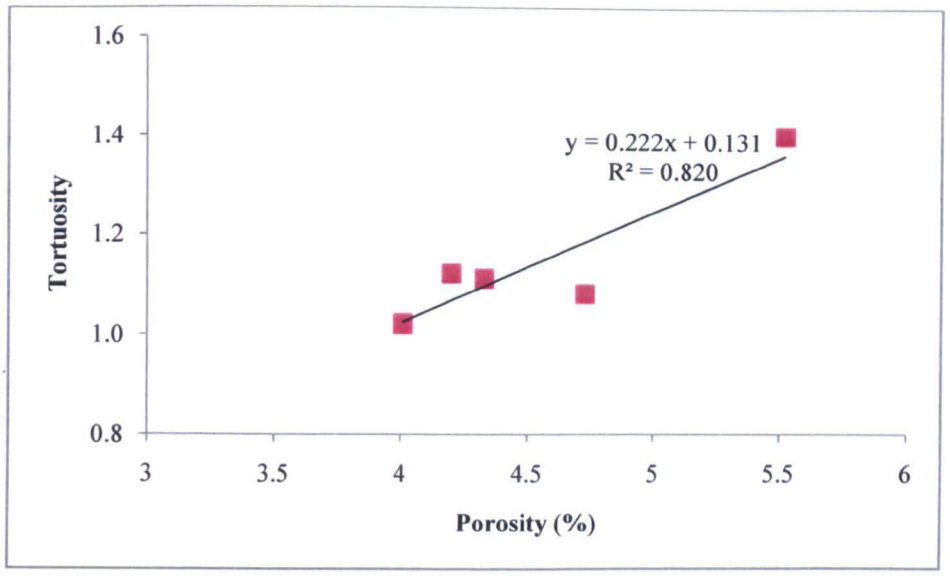

Figure 8.11 The tortuosity of the cracks from corrosion is proportional to porosity of the concrete

Table 8.2 Crack parameters of SCC samples

Sample label	Total Crack length cm	Crack density mm^{-1}	Tortuosity of crack
FG	11.02	2.92	1.11
FM	20.41	6.36	1.40
FGC	11.2	1.64	1.15
SM	29.9	7.19	1.08
SG	39.8	19.46	1.02

In this research it was found that at a low level of corrosion, the troughs are narrow and the number and width of the trough increased as the degree of corrosion increases. It was also found that the troughs were aligned to the cracks in the concrete. The cross section immediately below the taped section on each steel bar was reduced in the samples. Researchers have ascribed this to crevice corrosion but it appears to be highly linked to the differential stress between the corroding and non-corroding areas that is concentrated at that section of the simulated reinforced concrete.

The longitudinal profile of the steel rods that were removed from the inhibited replicates (un-soaked samples), showed that the FGC and SM SCCs were able to reduce the relative roughness of the recipient rods when comparison is made with the respective FG and SG samples but the carboxylic FM SCC was not effective in maintaining a roughness equivalent or lower than that of the FG control. There is really no correlation between the R_a values and the pitting factors. Generally the inhibited samples showed a higher proclivity for pitting than the non-inhibited samples based on the definition of pitting factor (Equation 8.2). Therefore, it is seen that the FGC sample which had a relatively shallow pit and a thin corrosion layer produced a high pitting factor. However, this high pitting factor did not have any adverse effect on the tensile strength of the reinforcing bar as the FGC rod had a higher mechanical integrity than the control after the 6-day period. This is understandable as the pitting factor did not give a good indication of the reduction in cross-sectional area of the steel after corrosion (see Table 8.1). In fact, from all the readings, it is shown that with a coefficient of correlation (R) greater than 0.6, there is a stronger correlation between the roughness value and the tensile strength than between the pitting factor and the strength and this suggests that although a high importance is attached to the pitting factor, the *Ra* value is more useful in

predicting the strength of the corroded bar when the current density falls below 0.015 mA/cm^2.

8.5. MICROSTRUCTURAL EXAMINATION

The microscopic examination of the structure of the SCC samples provided a good insight of the pore structure in relation to the other features of the respective concrete. It is shown in the micrograph that the interfacial transition zone (ITZ) of the samples varies. A quantification of the porosity in the interface between the aggregate particles and the bulk mortar via image analysis (Section 4.5.2.7), shows that, when comparison is made with the FG control, the porosity of the ITZ in the FGC SCC was 4% smaller than that of the FG control (Table 8.3). It is already shown that the large volume of powder in the typical SCC does not only contribute to pore refinement but also helps to improve packing density around the large aggregate particles and hence reduces the impact of 'wall effect'. The improvement in the nitrite fly ash SCC is derived from the overall higher rheological performance which produced a greater compactibility in the concrete. It is therefore seen that, compared to the FG control, the nitrite fly ash sample had low porosity in the mortar and in the ITZ and this accounts for the low penetrability indicated by the various transport indices and the high level of homogeneity as deduced from the PUNDIT velocity.

The individual porosity in the ITZs of the FM and SM samples is however larger than that of the ITZ of the respective controls (Table 8.3). The porosity of the ITZ in the FM was 26% larger than that of the fly ash control. The examination also showed that the porosity of the ITZ in the SM sample was approximately 7% larger than the ITZ porosity of the SG sample. This situation prevented the carboxylic samples from achieving the optimum effectiveness in

abating corrosion. Since the rheology of the FM and SM samples was acceptable, this would have contributed to good compactibility of the respective SCC mixes but, the adverse effect of bleeding is manifested in the large ITZ and this helps to explain the higher heterogeneity that was shown in the carboxylic FM and SM SCCs when reference is made with the respective FG and SG controls.

Table 8.3 Average porosity of the ITZ between aggregate and mortar

Sample	Porosity (%)
FG	9.18
FM	11.60
FGC	8.79
SM	8.63
SG	8.02

As the concentration of the respective corrosion inhibitors increased in the SCC samples, the porosity of the ITZ increased and there was a more pronounced manifestation of cracking in the concrete. In most cases the cracks emanated from the aggregate interface and extend in the mortar but in other cases the cracks are suspended in the mortar (see Figure 8.12). These cracks could be the result of plastic settlement that occurred as a result of the movement of the water to the surface and settlement of the rest of the constituents in the concrete during hardening. However, it is believed that the rapid removal of water also brought about shrinkage in the concrete and this resulted in shrinkage cracks, especially around the aggregates that were more dimensionally stable.

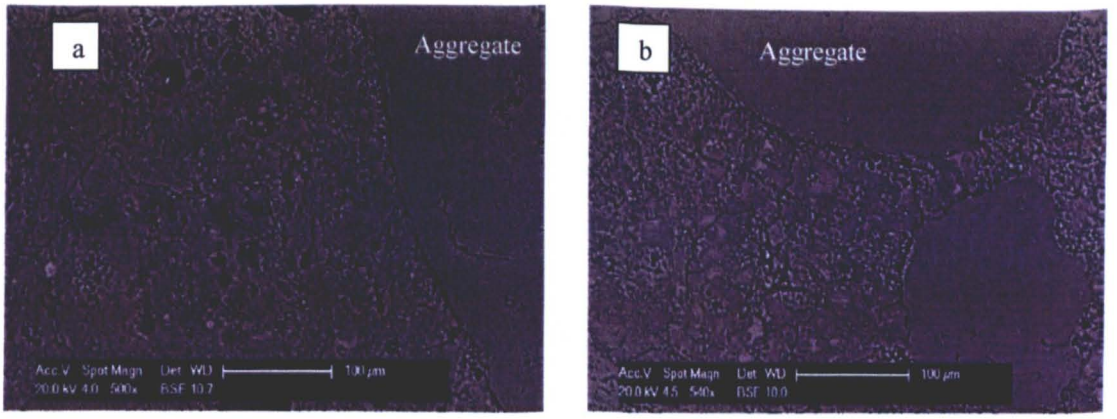

Figure 8.12 Micro-cracks shown in FGC (a) and SM (b) samples with high concentration of corrosion inhibitor

A peculiar phenomenon was observed in the SCC samples. Firstly, there was the pronounced presence of calcium aluminate hydrate (CAH) in the various specimens. The ettringite formation occurred earlier in the control samples but was noticeably delayed in the samples containing inhibitor as seen in the TGA of the cement paste (Section 5.2.2). This contributed to a more complete reaction and significantly lower levels of ettringite in the control samples within the first 28 days (Figure 8.13) but there was still a significant amount of ettringite at 28 days in the samples containing inhibitor as indicated in XRD analysis (Fernandez-Carrasco and Vazques, 2009) shown in Figures 8.14 to 8.16 and in the micrographs in Figures 8.17 and 8.18. Interestingly however, the ettringite formed around the larger types of cementitious particles and provided various degree of coverage mainly to the fly ash particles (Figures 8.19 and 8.20). The subsequent production of monosulphoaluminate seems to reside around the particles if the reaction of the latter is delayed as seen in 10-month SM sample from the cyclic wetting and drying corrosion test in Figure 8.21.

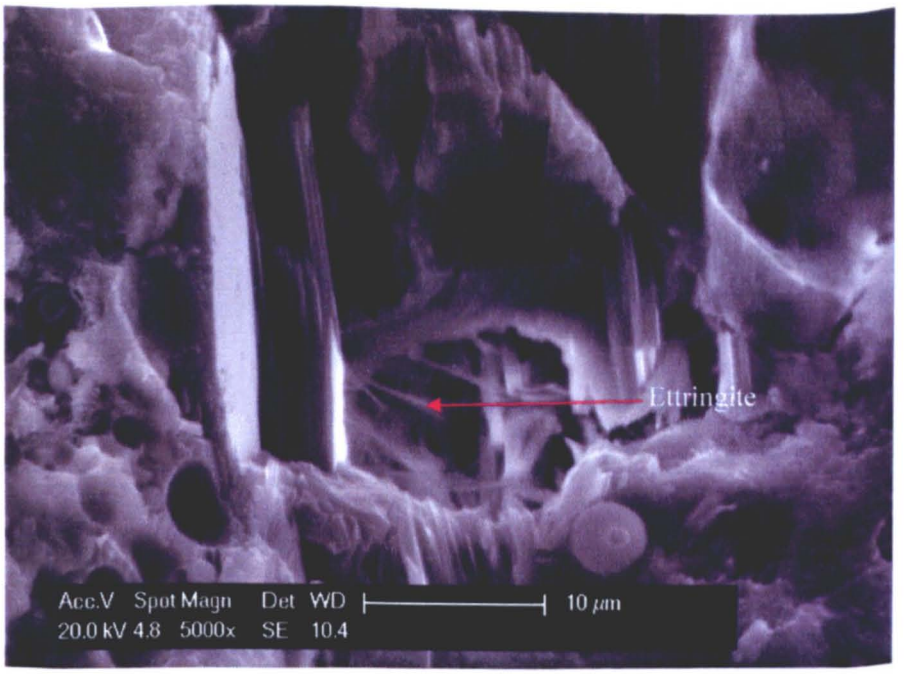

Figure 8.13 Relatively low level of ettringite formation in corroded fly ash SCC control at 28 days

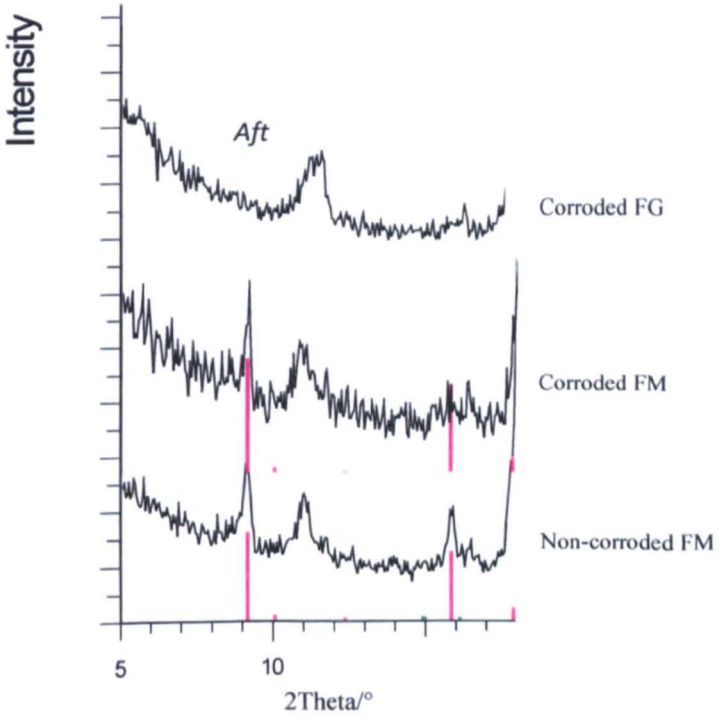

Figure 8.14 The X Ray diffractograms showing the FM sample before and after 3-day corrosion having more ettringite (*Aft*) than the control FG

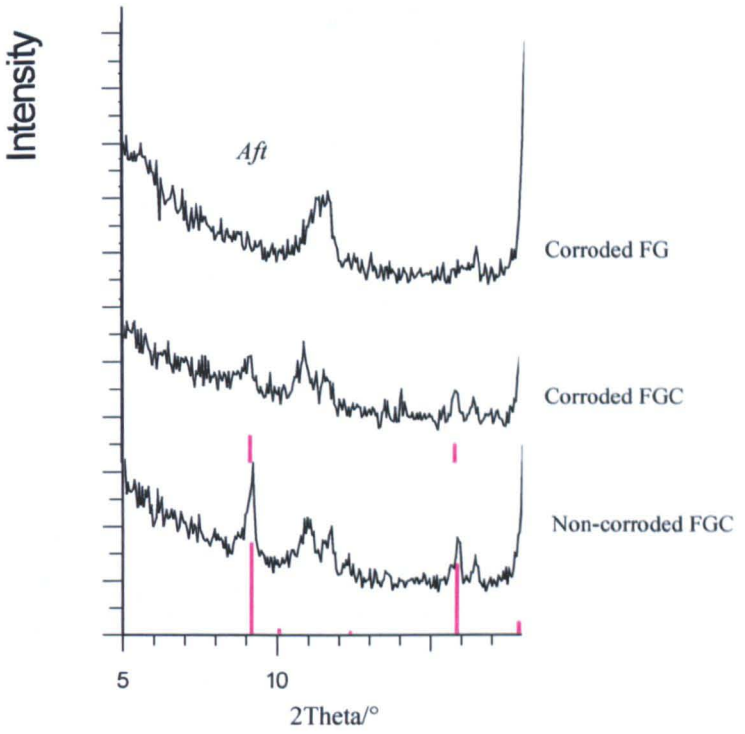

Figure 8.15 The X Ray diffractograms showing the FGC samples before and after 3-day corrosion having more ettringite (*Aft*) than the control FG

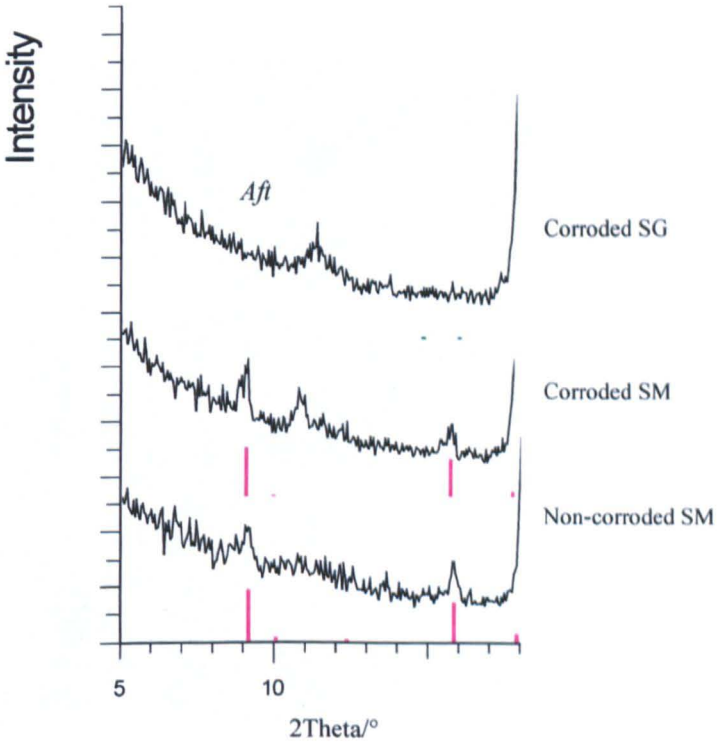

Figure 8. 16 The X Ray diffractograms showing the SM sample before and after 3-day corrosion having more ettringite (*Aft*) than the control SG

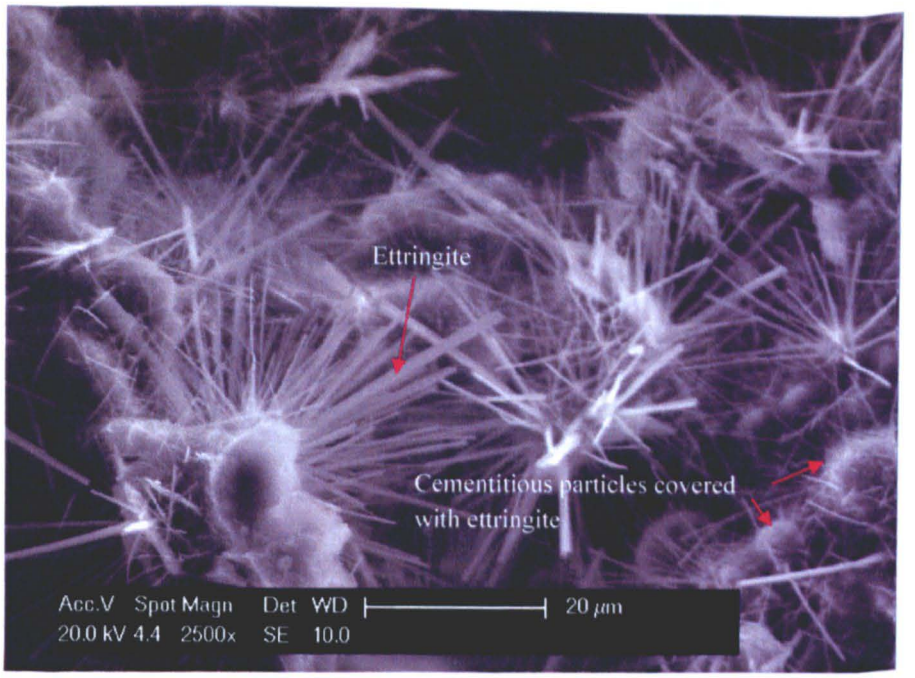

Figure 8.17 The presence of appreciably high level of ettringite in carboxylic fly ash SCC at 28 days

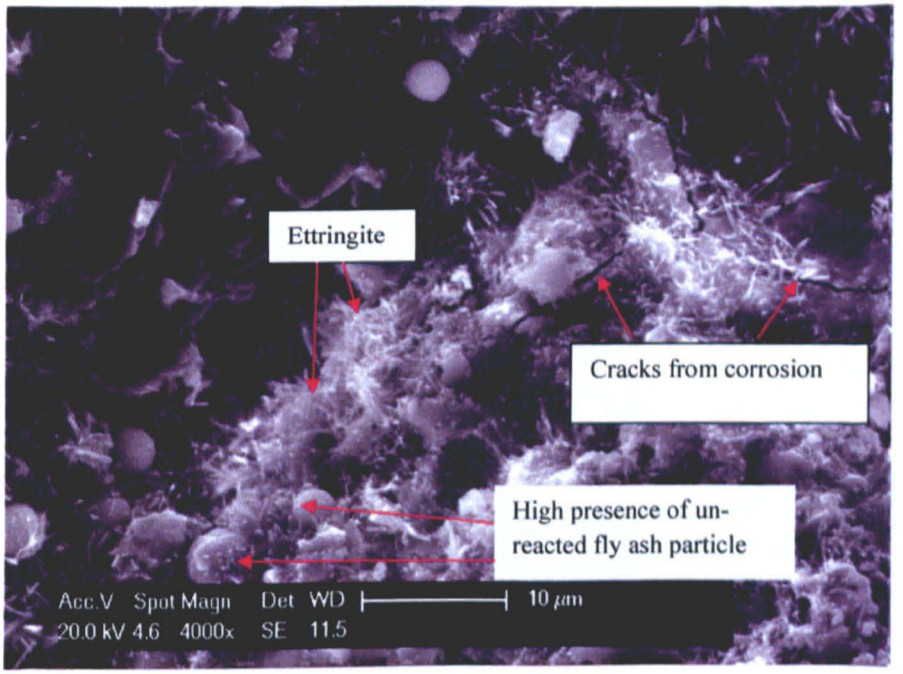

Figure 8.18 Ettringite surrounding the fly ash particles in FM sample subject to 6 days of accelerated corrosion

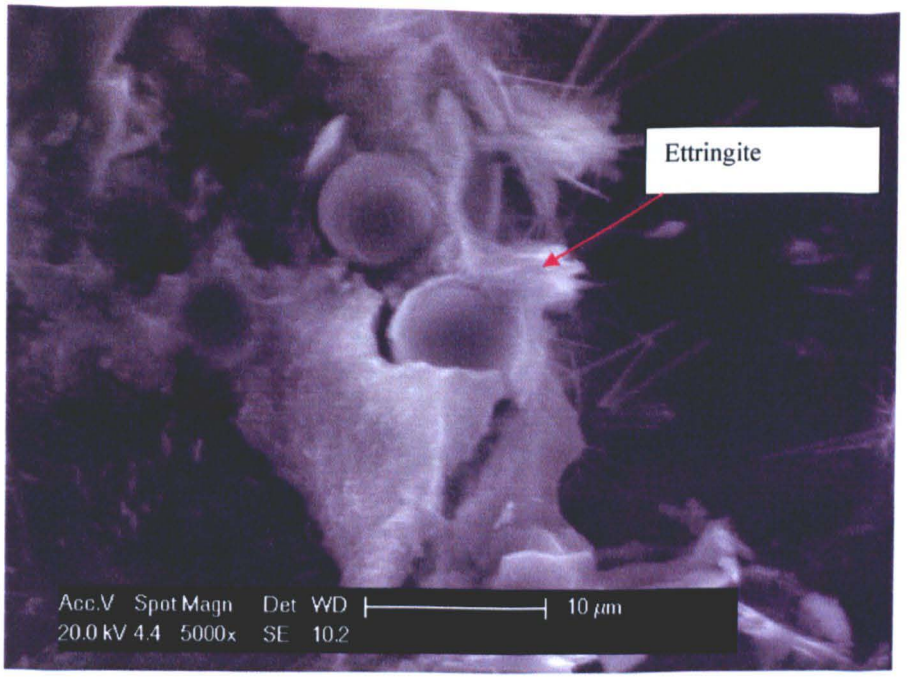

Figure 8.19 A micrograph showing cement particles surrounded by ettringite

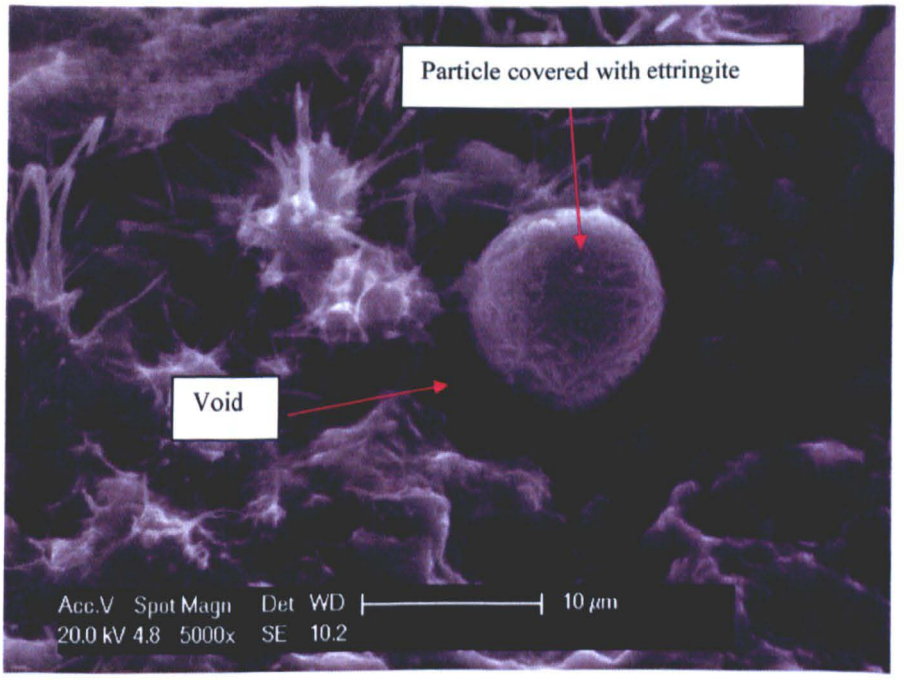

Figure 8.20 A fly ash particle covered with ettringite

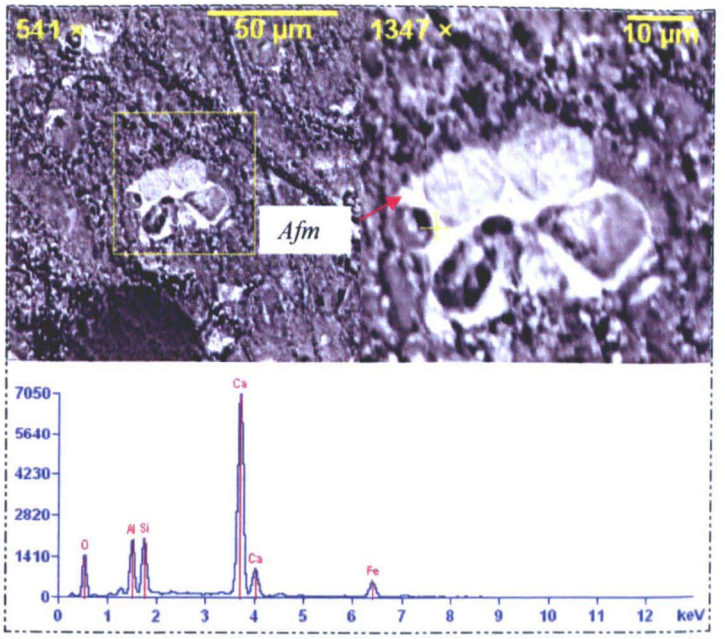

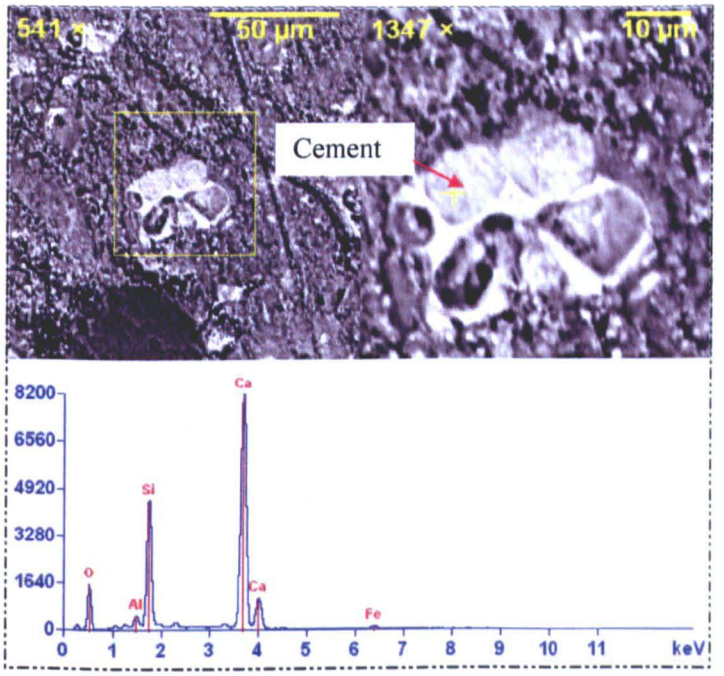

Figure 8. 21 BSE images of un-hydrated cement particle surrounded by monosulphoaluminate (*Afm*) both indentified by EDX plots as shown beneath images

Generally, ettringite (*Aft*) formation is reported to be at its highest level in the first 24 hours after mixing of the concrete. The C_3A and C_4AF in the cement react with the SO_4^{2-} from the clinker and $CaSO_4$ to form *Aft* but as the anions are consumed the remaining aluminate compounds react with the existing ettringite to form monosulphoaluminate (Lagerblad and Utkin, 1994). It is reported that the ettringite formed in the early stages are deposited at the cement particle along with the other C-S-H products. In more recent research it is reported that the superplasticiser is adsorbed on the ettringite (Kadri, et al, 2009) and suppresses stiffening, hence prolonging workability beyond what would have been achieved in the traditional concrete. These events explain the development in the conventional control SCC samples in this research. However, the incorporation of the inhibitors has further adjusted the kinetics associated with the early hydration process but the extent of such retardation depends on the constituents of the concrete. With the FGC sample, the nitrite promotes the growth of ettringite and accelerates the hydration process and this minimized the extended retardation. Additionally, the SM sample with the highly reactive particles and the great affinity to water reduced the effect of retardation. The FM samples however, with nothing to chemically stabilize the hydration and with the heavy reliance on the production of portlandite to advance the pozzolanic reaction of the high volume of fly ash, experienced further retardation as a result of the late growth of the CAH that covered the fly ash particles and severely affected the development of the concrete. It should however be pointed out that when the concentration of the inhibitor was increased in each inhibited SCC sample, the counteracting effects from the FGC and SM SCCs were less effective in preventing the delaying mechanics and all three inhibited samples showed some amount of retardation.

8.6. STATISTICAL ANALYSIS

The cyclic wetting and drying test was carried out for 9 months and in this time corrosion was not initiated in any of the SCC samples. In order to determine the time required for the initiation of corrosion, a statistical analysis of the current density in these samples over the duration of the test was conducted. Seven samples of concrete were successfully used in the corrosion experimental programme namely, FG, FM, FGC, SM, SG, FGC2x and SM2x. All these samples were contaminated with 1.0% NaCl but only the FM, FGC and SM samples were also contaminated with 0.1% NaCl. The variables that may impact chloride-induced corrosion were identified and the correlation of each variable and the corrosion current density was determined to confirm the relevance of each parameter to the corrosion process. It was concluded that the following were, substantially, independent variables were significant to the development of the corrosion current density (i_{corr}). The S_{cc} term takes into consideration the contribution of the interaction of the chemical admixtures and the mineral admixture.

- Sodium Chloride concentration % (C_{co})
- Electromigration values x 10^{12}, m^2/s (D_{nssm})
- Time, days (t_d)
- Set of SCC samples FG, FM etc. (S_{cc})

Statistical software R (Dalgaard, 2008) was used to evaluate the data with a view to establishing a model that will help to predict the corrosion current densities of the samples at different ages. Multi-variate regression modelling was performed on the response variable (i_{corr}), and the independent variables. The residuals were used to evaluate the validity of the model, which was established mainly using the quantile-quantile normal plot and the plot of the residuals about zero. An analysis of the variables (ANOVA) was also performed on the

result of each trial to determine the significance of each term in the model. The observed significance, often referred to as the *P value*, establishes the relevance of each term (Schaeffer and McClave, 1990). In fact, this value is the probability that the variable is accepted by chance. The Equation 8.5 was thereby formulated from the model and it shows the relationship between the current density and the relevant variables. The coefficient and significance of each term in Equation 8.5 are shown in Tables 8.4 and 8.5 respectively.

$$\ln i_{corr} = k_1 + k_2 D_{nssm} + k_3 t_d + k_4 t_d^2 + k_5 D_{nssm} \log C_{co} + k_6 D_{nssm}^2 + k_7 \log C_{co} + k_8 S_{cc} \qquad 8.5$$

Table 8.4 Values of coefficients of terms used in Equation 8.5

Coefficients	Values	Substitute term for S_{cc}	Values of k_8 for S_{cc} substitutes
k_1	-7.91	FG	0.457
k_2	-3.35×10^{-2}	FM	4.402
k_3	-4.09×10^{-2}	FGC	-0.125
k_4	1.11×10^{-4}	SM	-0.179
k_5	0.14	SG	0.30
k_6	-2.127×10^{-2}		
k_7	-7.49×10^{-2}		

The S_{cc} term is a dummy variable, of numeric value 1. It is included to indicate that the coefficient k_8 must be selected on the basis of the particular SCC sample (that is FG, FM, FGC, SM or SG) under consideration. The coefficient for each sample type is given in Table 8.4. Therefore, when the sample FG is being considered, the $k_8 S_{cc}$ term is expressed as 0.457x1.

Based on Equation 8.5, the estimated times for the initiation of corrosion of the SCC samples from the cyclic wetting and drying test are shown in Table 8.6. The similarity of the predicted times for the samples in each NaCl group is expected but the difference in initiation times between each sample with high and low chloride concentration appears too narrow (for example, FGC with 0.1 and 1.0 NaCl). These predictions could be checked with result from an alternative statistical analysis, but this was not possible within the timescale of the project. Therefore this is left as a suggestion for future work.

Table 8.5 Significance of terms used in statistical analysis

Term	Significance
t_d	2.2×10^{-16}
t_d^2	2.2×10^{-6}
D_{nssm}	1.85×10^{-10}
$log_{10}(C_{co})$	3.36×10^{-8}
D_{nssm}^2	4.6×10^{-2}
S_{cc}	4.435×10^{-5}
$D_{nssm} \times log(C_{co})$	3.47×10^{-7}

Table 8.6 Estimated time of corrosion initiation

Samples	Predicted time of corrosion initiation (days)	
	0.1% NaCl	1 % NaCl
FG	334	327
FM	337	286
FGC	342	341
SM	350	345
SG	334	330

8.7. CONCLUSION

The nitrite fly ash and carboxylic silica fume samples (FGC and SM), with high chloride content were better able to suppress corrosion than the respective FG and SG controls, but the carboxylic FM sample with the same high chloride content experienced higher level of corrosion than the corresponding FG control (Figure 8.10). The current densities in all the inhibited SCC samples (FM, FGC and SM), were, however reduced to approximately the same level when the concentration of the respective inhibitor remained the same but the chloride load was reduced to a lower level – a load that is more likely to occur in less than moderate chloride attack (Section 4.2.6.1). Interestingly, when the quantity of the respective inhibitor was doubled in the inhibited SCCs and the chloride load kept constant, the

corrosion-inhibiting capacity of all the samples was reduced. This is because the additional inhibitor caused an increase in pore and cracks which increased connectivity in the pore system and this allowed the chloride to migrate to the steel surface more easily. In the case of the carboxylic FM SCC, the increase in the concentration of the inhibitor significantly delayed the hardening of the samples.

The SCC samples containing inhibitor (FM, FGC and SM), experienced delay in growth of ettringite. The late growth of the *Aft* and the resulting *Afm* that formed around the cementitious particles, particularly around the fly ash particles, reduced the production of portlandite in the concrete. This combined phenomenon retarded the setting of the inhibited concrete and reduced the rate of the pozzolanic activity. The effect of this phenomenon on the nitrite FGC and on the carboxylic SM samples was somewhat negated. That is, the nitrite-based SCC counteracted the adverse effect with its accelerating characteristics and the silica fume SCC with the highly reactive fine particles and greater affinity for water. The effect on the carboxylic sample with high content of fly ash (FM), was however pronounced as there was no ameliorating effect from any of its constituents. The increase in the concentration of the respective inhibitor increased the kinetics related to retardation and this resulted in a delay in development of hydration for all three inhibited samples, with the effect being more pronounced in the carboxylic FM sample.

When the inhibited FM, FGC and SM samples were tested to determine the sustainability of the inhibiting capacity in a saturated chloride solution, it was revealed that, compared to the replicates that were kept in an un-soaked condition, the corrosion resistance of each of the saline-soaked inhibited samples was lower (Figure 8.5). However, when the non-inhibiting

(FG and SG) samples in the same two conditions were compared, the levels of corrosion of the saline-soaked samples were the same as or less than the un-soaked replicates. This strongly suggests that the inhibiting capacity of the corrosion inhibiting samples will be reduced over time when subjected to saturated saline conditions.

Analysis of corrosion data from impressed voltage shows that the carboxylic FM and SM lollipops will prevent the progression of corrosion, but will not reverse the electrochemical process when the corrosive environment is removed. The nitrite FGC reinforced concrete however displayed the ability to appreciably restore the embedded corroded steel upon the removal of the chloride-laden environment. The difference in the healing capacity is that, while the carboxylic inhibitor is adsorbed on the surface of the steel to provide a protective film, the NO_2^- ions not only react with the ferrous ions to produce products that strengthens the oxide layer but also reduces the acidity in micro-environ and hence continually repair any damage to the surface of the steel and this provides a self-healing mechanism in the nitrite-based fly ash concrete.

Analytical test done on the corroded steel sample after cleaning shows that the steel rods from the nitrite-based FGC and the carboxylic SM samples were smoother than the respective control sample, which show that the corrosion inhibitor is able to minimize the tendency for pitting and influence the corrosion pattern so that optimal mechanical properties are maintained in these samples. The strong relation between the roughness valve and the strength suggests that, like the pitting factor, the roughness value is a good indicator of the mechanical integrity of the reinforcement on the concrete.

Typically, with the exception of the FGC sample, the self-compacting concrete with the highest theoretical strength took the longest time for the evolution of crack, cracked at the highest current density and the appearance of crack in this sample was more sudden than the others. These samples therefore experienced more cracking and hence the crack densities were higher. The nitrite fly ash and the carboxylic silica fume samples had crack densities lower than the respective SCC control but the carboxylic fly ash sample had crack density higher than the fly ash control SCC.

Therefore, from the analysis of results in this chapter it is shown that:

- the use of the carboxylic corrosion inhibitor altered the kinetics associated with hydration and delayed the setting of the SM SCC, but more profoundly retarded the FM SCC with high fly ash content.
- the inhibiting phases of the carboxylic and nitrite inhibitors are likely to become depleted when placed in saturated chloride environments and increase the vulnerably of the reinforced SCC to corrosion when there is an aggressive chloride attack. Whereas the nitrite FGC SCC possess self-healing characteristics, the carboxylic reinforced SCC that is under corrosion will not gain any restoration of the steel after removal from the corrosive environment.
- The use of high concentration of corrosion inhibitor in silica fume and fly ash SCCs formulated with similarity herein, will not increase the corrosion resistance of the concrete.

Knowing the effect of the mixtures in SCC, the mechanism that controlled the effect and the process of the mechanism gives a better understanding of the inhibited self-compacting concrete.

CONCLUSION AND RECOMMENDATIONS

9.1. INTRODUCTION

This chapter summarises the findings while showing the associations and relationships of the effects and parameters that have been identified by the study. The recommendations for further research on the subject matter under study are also presented.

9.2. CONCLUSION

9.2.1. Effect of Inhibitors on Plastic Behaviour of Mixes

Comparison of the inhibited-SCCs and the corresponding traditional SCCs shows that, generally the inhibitors contributed to a slightly lower segregation resistance (Figure 5.12) in the SCCs with the corrosion inhibitor. Therefore, the inhibited-SCC samples (FM, FGC and SM) experienced slightly higher segregation than the corresponding FG and SG controls. The use of two inhibitors in the silica fume and fly ash concretes also reduced the viscosity of the traditional SCCs as shown by the V-funnel test (Figure 5.10). Rheometry test also showed that the viscosities of the FM and FGC pastes were reduced by 2-3% when comparison is made with the paste of the FG control (Figure 5.11). This reduction in the viscosity is a contributory factor to the higher tendency for segregation of the inhibited-SCCs. Further, the reduction in the viscosity means that the flow rate of the SCCs will be increased when the inhibitors are used. The effect of the inhibitor on the flow spread of the traditional SCCs varied (Figure 5.8), which means that the inhibitor may increase or reduce the yield stress in traditional SCCs. This effect was evident in the nitrite FGC and carboxylic SM mixes where

the slump flow results were higher than that of the FG control; and in the carboxylic FM sample that had a lower slump flow than the FG control.

The use of the carboxylic corrosion inhibitor in the fly ash and silica fume SCCs helped to retain the consistency of the FM and SM SCCs up to 60 minutes after mixing (Figure 5.13). This extension to the workability is the result of the significant retardation in the setting of the pastes of these two SCCs when the carboxylic inhibitor was used (Figure 5.1) as explained in Section 9.2.2.

9.2.2. Effect of Inhibitors on the setting of Mixes

When the carboxylic inhibitor was added to the silica fume and fly ash SCCs it delayed the hardening process of the respective SM and FM SCCs. It was also seen that the initial setting times of the powder pastes of these two SCCs were delayed by 19 and 91% respectively after the addition of the carboxylic inhibitor (Figure 5.1). The delays resulting from the carboxylic were more pronounced in the fly ash cementitious mixtures than in the silica fume counterparts. The incorporation of the nitrite inhibitor in the fly ash SCC paste retarded the initial setting time of the fly ash powder paste by 52% (Figure 5.1), but when the nitrite compound was added to the traditional fly ash SCC the delay in hydration was minimised and therefore, at the time of de-moulding the samples, there was no noticeable sign of delay in the hardening of the fly ash SCC that was incorporated with the nitrite inhibitor.

It was found that, the established relation between the initial and final setting times of ordinary Portland cement paste of traditional concrete is valid for the powder pastes of traditional and inhibited-SCCs (Equation 5.1).

The use of the carboxylic inhibitor in the fly ash SCCs caused bleeding (in the FM sample), which was the result of settlement in the concrete. However, the rheology tests showed that the inhibited FM sample was relatively stable in the plastic state. Therefore, the settlement was not initiated by the physical process of sedimentation but appeared to be caused by the kinetics that govern the hydration process. This is a concern as it contributes to significant segregation which cannot be detected at the production stage.

The carboxylic SM sample also showed sign of bleeding but to a lesser extent when compared to the FM sample. Because the silica fume particles have higher specific surface than the fly ash particles, more water is used to wet the surfaces of particles in the SM and therefore less free water was available in the mix. Compared to the fly ash particles, the silica fume particles are smaller and, hence, better able to remain suspended in a liquid medium. These attributes better helped to maintain stability in the SM mix and, hence, compared to the FM counterpart, it displayed a higher capacity to reduce the effects of bleeding.

9.2.3. Effect of Inhibitors on Hardened Properties of Mixes

As seen in the MIP (Figure 7.4) and porosity evaluation (Figure 7.1), adding the nitrite inhibitor to the fly ash SCC reduced the porosity in the mortar and in the interfacial transition zones (ITZs) and generally reduced the heterogeneity of the nitrite FGC concrete. The

PUNDIT test (Figure 6.6) was used to establish the relative level of homogeneity that was attained in the SCC samples. The 3% reduction in the porosity of the nitrite FGC sample over the FG SCC would contribute to an increase in the bond strength between the mortar and the aggregate of the former; hence, the nitrite fly ash SCC was able to sustain a higher compressive stress before the commencement of failure in the interfacial transition zones. Compared to the traditional FG control, a higher compressive stress was also required in the FGC sample for the development of fracture as the relative density of the nitrite SCC was higher (Figure 6.2). Up to 60 days, these features account for the higher strength that was attained in the nitrite FGC sample relative to the fly ash control.

A factor that contributed to the reduction in the mechanical properties of the carboxylic FM and SM samples is the higher level of porosity (Figure 7.1), which was manifested in larger volume of voids in the ITZs and in mortar (Table 7.2) of these carboxylic SCCs. The respective porosity of the FM and SM samples were 27 and 18% larger than that of the corresponding FG and SG controls. These features served to reduce the bond strength between the aggregate and the mortar and increased the heterogeneity of the two traditional SCCs after the incorporation of the carboxylic inhibitor. Analysis of the compressive strength and ITZ porosity in the carboxylic FM and SM SCCs shows that, the higher porosity in the ITZs of the carboxylic-inhibited SCCs presumably also contributed to reduction in bond strength in the FM and SM samples and this reduction initiated compression failure at lower stresses in the carboxylic SCC samples. In addition, the tensile strength of the fly ash SCC was reduced after the addition of the organic inhibitor (see the carboxylic FM sample and FG control in Table 6.2). It therefore shows that the tensile strength that was needed to resist lateral movement resulting from compression loading was lower in the carboxylic FM SCC than in the FG control. These are some of the reasons for the differences in the compressive

strengths of the carboxylic FM and SM samples and the respective FG and SG controls. However, it should also be pointed out that after 28 days, the slower rate of C-S-H production (Figure 8.14) in the FM sample (relative to the fly ash control) also contributed to a reduction in the strength of the carboxylic fly ash SCC.

9.2.4. Effect of Inhibitor on Corrosion and Durability Indicators

When the carboxylic inhibitor was mixed with a high volume of fly ash in the SCC sample, the interactions of the constituents altered the kinetics of the hydration process and the pozzolanic reaction as seen in the TGA result on the FM powder paste (Figure 5.5) and from XRD analysis on the FM concrete and powder paste (Figures 8.14 and 5.6). MIP and image analyses showed that this occurrence affected the physical micro-structure of the FM sample as the porosity in the mortar and in the ITZ (Tables 7.2 and 8.3) were respectively 33 and 26% higher than the porosity of the same properties of the control FG SCC. The increase in the porosity of the FM sample therefore made the resistivity of the carboxylic fly ash SCC lower than that of the traditional fly ash control as shown by the sorptivity, chloride diffusivity and electrical resistivity indices (Tables 7.1 and 7.3).

The interactions between the carboxylic inhibitor and the ingredients in the silica fume SCC also altered the kinetics of the hydration process and the pozzolanic reaction as shown in TGA results on the SM powder paste (Figure 5.5) and from XRD analysis on SM concrete and powder paste (Figures 8.16 and 5.7). However, as explained in Section 9.2.5, the extent of the effect was not as significant in the carboxylic SM as in the carboxylic FM sample. Therefore, from MIP analysis (Figure 7.4), it is shown that the use of the carboxylic in the silica fume SCC brought about a 7.7% increase in the porosity of the SM mortar and an almost similar increase in the porosity of the ITZ between the aggregates and the mortar in

the SM sample (Sections 7.2.1 and 8.5) . However, the sizes of the pores in the SM mortar were generally smaller than those of the SG control and apparently more disconnected. This effect therefore helped to produce mixed result in the transport properties of the SM sample. Consequently, it was seen that the use of the carboxylic inhibitor in the silica fume SCC contributed to increases of different magnitudes in the electrical resistivity and chloride diffusivity indices (Table 7.3) and to a decrease in the sorptivity index (Table 7.1).

As with the carboxylic-inhibited SCCs, the addition of the nitrite corrosion inhibitor to the fly ash SCC altered the kinetics of the hydration and pozzolanic processes but the modification did not have much adverse effect on the transport properties of the FGC SCC. The overall porosity of the fly ash SCC was reduced by 30% and the sizes of the pores became finer when the nitrite inhibitor was added and, therefore, the sorptivity and chloride diffusivity indices of the FGC sample were reduced but the electricity resistivity index was also reduced.

The current densities of the specimens used in the wetting and drying corrosion experiment were all less than 0.0001 mA/cm^2 at the end of the experiment. This showed that corrosion was not initiated in the samples. In order to predict the time of chloride initiation in the SCC samples (Table 8.3), a statistical model was developed as shown in Equation 8.5. Generally, it is shown from the wetting and drying corrosion test that the formulation of the SCC with mineral admixture and corrosion inhibitor may or may not improve the corrosion resistance of SCC.

The carboxylic inhibitor did not increase the corrosion resistance of the fly ash SCC in high chloride concentration (Figures 8.3 and 8.10) as the use of the inhibitor resulted in a decline in the resistivity of the fly ash concrete and caused the FM sample to initiate corrosion 12.5% earlier than the time it took to initiate corrosion in the FG control when exposed to 1% NaCl. However, from statistical modelling, it is shown that the addition of the carboxylic inhibitor to fly ash SCC will improve the corrosion resistance of the concrete to low chloride concentration (Table 8.6) but the carboxylic FM sample will not delay the time of the initiation of corrosion by more than 1%. The inclusion of the carboxylic compound in the reinforced fly ash SCC removed the self-healing capacity of the corroded steel in the FM concrete but prevented the progression of corrosion (Figure 8.8). On the other hand, the addition of the carboxylic compound to the silica fume SCC increased the corrosion resistance of the concrete to high (Figures 8.4) and low levels of chloride concentration. This caused the carboxylic SM sample to reduce the time of the initiation of corrosion in the FG control by slightly over 4.5% when attacked by 0.1 and 1.0% NaCl (Table 8.6). It was seen that the chloride diffusivity of the SM sample was higher than that of the traditional silica fume SCC but when the carboxylic compound was used in the latter, the corrosion resistance was increased. Whereas the traditional silica fume SCC assisted in the self-restoration of corroded steel reinforcement, when the carboxylic inhibitor was included in this silica fume concrete there no support for the self-restoration of the corroded steel embedded in the SM concrete. Instead, the SM SCC only halted the progression of corrosion.

When the traditional fly ash SCC was incorporated with the nitrite inhibitor, the corrosion resistance in high and low chloride concentrations increased. This is due to the low chloride diffusivity and the corrosion protection offered by the fly ash SCC after the addition of the

nitrite inhibitor (FGC). Additionally, like the control FG SCC, the nitrite FGC sample supported self-restoration to the embedded steel reinforcement.

It was shown that the corrosion resistance of the three carboxylic and nitrite inhibited-SCCs can be reduced after prolonged exposure to an aqueous saline environment. Presumably, the concentration of the corrosion inhibitor was reduced due to i) consumption of the inhibiting molecules in the corrosion process and/or ii) leaching of the inhibitor to the saline solution.

9.2.5. Micro-scale Explanation for Mix Characteristics

Thermogravimetric analysis at 12 hours showed that, compared to the traditional SCC pastes, chemical activity in the three inhibited-SCC pastes was slow (Figure 5.5). This was determined by the relative amount of ettringite formation in the samples. TGA was also used to determine the progress of hydration in the SCCs by computing the amount of $Ca(OH)_2$ formed in the paste of each SCC samples at 12 hours (Table 5.2). It was shown that the hydration of the inhibited FM, FGC and SM samples was slower than the hydration of the respective control FG and SG SCCs. At 24 hours, XRD evaluation (Figures 5.6 and 5.7) of the SCCs showed that the delay in the hydration of the pastes of the inhibited fly ash SCCs continued. These tests showed that relative to the hydration of the respective control SCC, the inhibited-SCC pastes experienced delay in the hydration process.

It was seen that at 28 days and 90 days there was a greater presence of ettringite in the inhibited-SCC than in the traditional SCC. X-ray diffraction analysis (Figures 8.14 – 8.16) and scanning electron microscopy (Figures 8.17 - 8.20) were used for the examination of the micro-structural features. The late growth of the *Aft*, and consequently the *Afm*, (Figure 8.21)

formed around the cementitious particles and contributed to varying degree of coverage to the particles, in particular the fly ash particles. This occurrence reduced the rate of production of portlandite and further obstructed the pozzolanic activity of the fly ash SCC. The accelerating characteristics of the nitrite inhibitor and the highly reactive silica fume particles reduced the impact of the modification in the kinetics; hence, the nitrite FGC sample did not suffer much retardation and the carboxylic SM SCC did not experience any appreciable delay. However, at a higher concentration of inhibitor, the phenomenon that contributed to a delay in the hydration process was evident in all the inhibited-SCC samples.

Micro-scale measurement via MIP showed that the nitrite inhibitor reduced the sizes of the pores in the fly ash SCC mortar, and this contributed to a higher level of pore refinement in the FGC mortar. The porosity of the fly ash mortar was also reduced after the addition of the nitrite inhibitor. The carboxylic compound, when used, reduced the sizes of the pores in the silica fume mortar, but the volume of pores in SM mortar was higher than that of the SG mortar. Using the carboxylic compound in the fly ash SCC increased the volume of pores and increased the sizes of the pores in the FM mortar. The pore system of the fly ash SCC was therefore made coarser with the use of the carboxylic compound.

After the 6 days of testing, the steel bars of the un-soaked SCC specimens used in the impressed voltage tests were analysed by a stylus profilometer to obtain the roughness value and the pitting factor of the surfaces of the corroded bars. The strength reductions of the steel bars were also determined after the corrosion tests. It was shown that the strength reductions in the carboxylic silica fume (SM) and the control silica fume (SG) SCCs were 21%. With strength reductions of 11 and 20% respectively, it is shown that the strength of the FGC and FM SCCs after 6 days of corrosion were correspondingly lower and higher than the

traditional FG SCC. The FG control suffered 17% strength reduction after corrosion over the same period. The reductions in the tensile strengths of the steel bars are largely due to the respective reductions in the cross-sectional area of the steel bars. The roughness values are shown to give better indications of the reductions in cross sectional areas of the steel bars than the pitting factor. This higher correlation between the strength reduction values and the roughness values than with the values of the former parameter and the pitting factors shows that, at low levels of corrosion, the roughness value can be used to give a better indication of the strength reduction of the concrete.

After the corrosion test that was designed to detect healing was completed, the cracked samples were analysed with image analysis software. The use of the carboxylic and nitrite inhibitors in the respective silica fume and fly ash SCCs reduced the crack densities in the traditional SCCs as seen in the SM and FGC samples in Table 8.2. On the other, the carboxylic fly ash (FM) concrete had a greater crack density than the control FG sample. When the corrosion inhibitors were used in the respective control SCCs, the tortuosity of the cracks increased in all cases. It was shown that, while the tortuosity of the cracks in the corroded reinforced SCC samples was proportional to the porosity of the specimens, the crack density of the SCC samples was proportional to the tensile strength of the specimens (Section 8.4).

9.3. RECOMMENDATIONS

The following recommendations for further study will help in gaining a more complete understanding of the behaviour of self-compacting concrete with inhibitors.

- The leaching and consumption of the inhibitor in SCC in aggressive chloride environment needs to be studied in order to quantify the depletion of the inhibiting phase of the chemical compound.
- A study of the propensity for alkali-silica reaction in corrosion inhibited SCC will help to establish any limitation on the use of the chemical admixtures and the type of aggregates.
- A study of the effect of corrosion inhibitor on the electrostatic attraction between the cement particles and the superplasticiser molecules.
- An investigation of the effect of fly ash replacement levels with respect to a range of different concentrations of inhibitor on SCC in order to establish the range of the proportions of the admixtures that are compatible for making carboxylic fly ash.
- Comparative analysis of the predicted times for corrosion initiation in the samples using the programme R (used herein) and another statistical tool.

REFERENCES

Al-Amoudi, O. S. B., Maslehuddin, M., Lashari, A. N. and Almusallam, A. A. (2003) *Effectiveness of corrosion inhibitors in contaminated concrete.* Cement and Concrete Composites 25 (4), 439 – 449.

Alarcon-Ruiz, L., Platret, G., Massieu, E. and Ehrlacher, A. (2005) *The use of thermal analysis in assessing the effect of temperature on cement paste.* Cement and Concrete Research, 35, 609 – 613.

Al-Mehthel, M., Al-Dulaijan, S., AL-Idi, S. H., Shameem, M., Ali, M. R. and Maslehuddin (2009) *Performance of generic and proprietary corrosion inhibitors in chloride-contained silica fume cement concrete.* Construction and Building Materials, 23 (5), 1768 – 1774.

Alonso, C. and Andrade, C. (2002) *Corrosion rates of concretes made with different binders and exposed for 10 years in natural sea water.* In: Andrade, C. and Kropp, J. (eds). Proceedings of the 3rd International RILEM Workshop on Testing and Modelling the Chloride Ingress into Concrete (Pro 38), Madrid. Cachan, France: RILEM Publications, pp. 77 – 91.

Alonso, C., Andrade, C., Castellote, M. and Castro, P. (2000) *Chloride threshold values to depassivate reinforcing bars embedded in standardized OPC mortar.* Cement and Concrete Research 30 (7), 1047 - 1055.

ASTM C 40 (1999) *Standard Test Method for organic impurities in fine aggregates for concrete.* Book of standards volume 04.02. ASTM International, West Conshohocken, PA

ASTM C 876 (1991) *Standard Test Method for Half-Cell Potentials of uncoated steel in concrete.* Book of Standards Volume 03.02. ASTM International, West Conshohocken, PA.

ASTM C 1202 (2002) *Standard test method for electrical indication of concrete's ability to resist chloride ion penetration.* Book of Standards Volume 04.02. ASTM International, West Conshohocken, PA

Audenaert, K., Boel, V. and De Schutter, G. (2005) *Chloride penetration in self compacting concrete by cyclic immersion.* In: Yu, Z., Shi, C., Khayat, K. L. and Xie, Y. (eds). Proceedings of the 1st International Symposium on Design, Performance and Use of Self-Compacting Concrete (Pro 42), China. Cachan, France: RILEM Publications, pp. 355 – 362.

Audenaert, K. and De Schutter, G. (2003) *Chloride penetration in self-compacting concrete.* In: Wallevik, O. and Nielsson, (eds). Proceedings of the 3rd International RILEM Symposium on Self-Compacting Concrete (Pro 33), Reykjavik. Cachan, France: RILEM Publications, pp. 818 – 825.

Bassuoni, M. and Nehdi, M. L. (2009) *Durability of self-compacting concrete to sulphate attack under combined cyclic environments and flexural loading.* Cement and Concrete Research, 39, 206 – 226.

Berke, N. S. and Hicks, M. C. (2004) *Predicting long-term durability of steel reinforced concrete with calcium nitrite corrosion inhibitor.* Cement and Concrete Composites 26 (3), 191 - 198.

Bertolini, L., Elsener, B., Pedeferri, P. and Polder, R. (2004) *Corrosion of steel in concrete: prevention, diagnosis, repair.* Weinheim: Wiley-VCH, 392.

Boğa, A. R. and Topçu, I. B. (2012) *Influence of fly ash on corrosion resistance and chloride ion permeability of concrete.* Construction and Building Materials 31, 258 - 264.

Bogas, J., Gomes, A., Pereira, M. (2012) *Self-compacting lightweight concrete produced with expanded clay aggregate.* Construction and Building Materials 35, 1013-1022.

Bonen, D. and Shah, S. P. (2005) *Fresh and hardened properties of self-compacting concrete.* Progress in Structural Engineering and Materials 7 (1), 14 – 26.

Broomfield, J. P. (2007) *Corrosion of Steel in Concrete: Understanding, Investigation and Repair,* (2nd ed). London: Taylor and Francis, 277.

Brouwers, H. J. H. and Radix, H. J. (2005) *Self-compacting concrete:the role of the particle size distribution.* In: Yu, Z., Shi, C., Khayat, K. L. and Xie, Y. (eds). Proceedings of the 1st International Symposium on Design, Performance and Use of Self-Compacting Concrete (Pro 42), China. Cachan, France: RILEM Publications, pp. 109 - 118.

BS EN 196-3 (2005) *Methods of testing cement – Part 3: Determination of setting times and soundness.* London: British Standards Publication.

BS EN 197-1 (2000) *Cement – Part 1: Composition, Specifications and Conformity Criteria for Common Cements.* London: British Standards Publication.

BS EN 206-1 (2000) Concrete Part 1:*Specification, performance, production and conformity.* London: British Standards Publication.

BS EN 812-2 (1995) *Testing aggregates – Part 2: Methods of determination of density.* London: British Standards Publication

BS EN 12350-8 (2010) *Testing fresh concrete – Part 8: Self-compacting concrete - Slump-flow test.* London: British Standards Publication.

BS EN 12390-3 (2009) *Testing hardened concrete – Part 3: Compressive strength of test specimens.* London: British Standards Publication

Byfors, J. (1999) *SCC is an important step towards industrialization of the building industry.* In: Skarendahl, Å. and Petersson, Ö. (eds). Proceedings of the 1st International RILEM Symposium on Self-Compacting Concrete (Pro 7), Stockholm. Cachan, France: RILEM Publications, pp. 15 – 21.

Carpinteri, A., Chiaia, B. and Nemati, K. M. (1997) *Complex fracture energy dissipation in concrete under difficult loading conditions.* Mechanics of Materials 26, 93 -108.

Cheng-yi, H. and Feldman, R. F. (1985) *Hydration reactions in portland cement-silica fume blends.* Cement and Concrete and Research, 15 (4), 585-592.

Colak, A. (2003) *Characteristics of pastes from a Portland cement containing different amounts of natural pozzolan.* Cement and Concrete Research, 33, 585 – 593.

Dalgaard, P., (2008) *Introductory statistics with R,* 2nd ed. London: Springer, 363.

Day, K. W. (1999) *Concrete mix design, quality control, and specification* 2nd ed. London: E and FN Spon, 391.

De Schutter, G., Bartos, P. J. M., Domone, P. and Gibbs, J. (2008) *Self-compacting concrete.* Dunbeath : Whittles, 296.

De Schutter, G. and Luo, L. (2004) *Effect of corrosion inhibiting admixture on concrete properties.* Construction and Building Materials 18 (7) 483-489.

Diamond, S. (2000) *Mercury porosimetry – an appropriate method for the measurement of pore size distributions in cement based materials.* Cement and Concrete Research, 30, 1517 – 1525.

Donza, H., Cabrera, O. and Irassar, E. F. (2002) *High-strength concrete with different aggregate.* Cement and Concrete Research, 32, 1755 - 1761.

Dotto, J. M. R., Abreu, A. G. D., Molin, D. C. C. D. and Müller, I. L. (2004) *Influence of silica fume addition on concretes physical properties and on corrosion behaviour of reinforcement bars.* Cement and Concrete Composites, 26, 31 - 39.

EFNARC (2005) *The European guidelines for self-compacting concrete – Specification, production and use.* (Online) Available at: http://www.europeanconcrete.eu/index.php?option=com_docman&task=doc_details&gid=1&Itemid=5 (Accessed March 3, 2009)

Elsener, B. (with support from a Task Group of Working Party 11 on Corrosion of reinforcement in concrete) (2001) *Corrosion inhibitors for steel in concrete - State of the art report*: (EFC 35). Maney Publishing.

Elsener, B., Büchler, M. and Böhni, H. (1998) *Corrosion inhibitors for steel in concrete.* In: Mietz, J., Elsener, B. and Polder, R. (eds). Proceedings of *EUROCORR '97* - Corrosion of Reinforcement in Concrete – Monitoring, Prevention and Rehabilitation (EFC 25), Norway. Maney Publishing, pp. 54 – 69.

Emborg, M. (1999) *Rheology tests for self-compacting concrete - How useful are they for the design of concrete mix for full-scale production?* In: Skarendahl, Å. and Petersson, Ö. (eds). Proceedings of the 1st International RILEM Symposium on Self-Compacting Concrete (Pro 7), Stockholm. Cachan, France: RILEM Publications, pp. 95 – 105.

Fernández-Carrasco, L. and Vázquez, E. (2009) *Reactions of fly ash with calcium aluminate cement and calcium sulphate.* Fuel 88 (9), 1533 – 1538.

Ferraris, C. (2005) *Concrete Rheology: What is it and why do we need it?* In: Yu, Z., Shi, C., Khayat, K. L. and Xie, Y. (eds). Proceedings of the 1st International Symposium on Design, Performance and Use of Self-Compacting Concrete (Pro 42), China. Cachan, France: RILEM Publications, pp. 229 – 236.

Ferraris, C. F., Obla, K. H. and Hill, R. (2001) *The influence of mineral admixtures on the rheology of cement paste and concrete.* Cement and concrete research, 31, 245 – 255.

Fib (2000) *Structural concrete, 2nd ed.* Switzerland: International Federation for Structural Concrete Vol. 1, 235.

Galle, C. (2001) *Effect of drying on the cement-based materials pore structure as identified by mercury porosimetry, acomparative study between oven-, vacuum-, and freeze-drying.* Cement and concrete research, 31, 1467 – 1477.

Gesoğlu, M., Güneyisi, E. And Ozbay, E. (2009) *Properties of self-compacting concretes made with binary, ternary and quaternary cementitious blends of fly ash, blastfurnace slag and silica fume.* Construction and Building Materials, 23 (5), 1847 – 1854.

Giaccio, G. and Zerbino, R. (1998) *Failure mechanism of concrete: combined effects of coarse aggregates and strength level.* Advanced Cement Based Materials, 7(2), 41-48.

Gibbs, J. C. and Zhu, W. (1999) *Strength of hardened self-compacting concrete.* In: Skarendahl, Å. and Petersson, Ö. (eds). Proceedings of the 1st International RILEM Symposium on Self-Compacting Concrete (Pro 7), Stockholm. Cachan, France: RILEM Publications, pp. 199 - 209.

Gonen, T. and Yazicioglu, S. (2007) *The influence of mineral admixtures on the short and long-term performance of concrete.* Building and Environment, 42, 3080 – 3085.

González, J. A., Ramirez, E. and Bautista A. (1998) *Protection of steel embedded in chloride-containing concrete by means of inhibitors.* Cement and Concrete and Research, 28 (4), 577 – 589.

Gram, H. E. and Piiparinen, P. (1999) *Properties of SCC – Especially early age and long term shrinkage and salt resistance.* In: Skarendahl, Å. and Petersson, Ö. (eds). Proceedings of the 1st International RILEM Symposium on Self-Compacting Concrete (Pro 7), Stockholm. Cachan, France: RILEM Publications, pp. 211 – 220.

Graves, R. E. (2006) *Grading, shape and surface texture.* In: Lamond, J. and Pielert, J. (eds.) Significance of tests and properties of concrete and concrete-making materials, ASTM STP 169D. ASTM International, West Conshohocken, PA., pp 314-336.

Gunasekaran, K., Annadurai, R. and Kumar, P. S. (2013) *Study on the reinforced lightweight coconut shell concrete beam behaviour under flexure.* Materials and Design, 46, 157 – 167.

Güneyisi, E., Gesoğlu, M., Ozturan, T. and Ozbay, E. (2009) *Estimation of chloride permeability of concretes by empirical modelling: Considering effects of cement type, curing condition and age.* Journal of Construction and Building Materials, 23 (1), 469 - 481.

Güneyisi, E., Özturan, T. and Gesoğlu, M. (2005) *A study on reinforcement corrosion and related properties of plain and blended cement concretes under different curing conditions.* Cement and Concrete Composites 27, 449 - 461.

Hall C. and Yau M. H. (1987) *Water movement in porous buildings materials LX. The water absorption and sorptivity of concretes.* Building and Environment II 22(1) pp. 7-82.

Hansson, C. M., Mammoliti, L. and Hope, B. B. (1998) *Concrete Inhibitors in concrete – Part 1: The principles.* Cement and Concrete Research, 28 (12), 1775 – 1781.

Hassan, A. A. A., Hossain, K. M. A. and Lachemi, M. (2009) *Corrosion resistance of self-compacting concrete in full-scale reinforced beams.* Cement and Concrete Composites 31 (1), 29 - 38.

Hewlett, P. (ed) (1998) *Lea's chemistry of cement and concrete. (4th ed).* London: Arnold, 1052

Holton, I. (2004) *Self-compacting concrete.* Watford: BRE Centre for Construction, 8.

ISO 8044 (1999) *Corrosion of metals and alloys – Basic terms and definitions*

Jackson, N. and Dhir, R. K. (eds) (1996) *Civil engineering materials.* London: Macmillan, 534.

Jones, D. A. (1996) *Principles and prevention of corrosion.* (2nd ed). New Jersey: Prentice-Hall, 572.

Kadri, E. H., Aggoun, S. and De Schutter, G. (2009) *Interaction between C_3A, silica fume and naphthalene sulphonate superplasticiser in high performance concrete.* Construction and Building Materials, 23 (10), 3124 - 3128.

Kanellopoulos, A., Petrou, M. F. and Loannou, L. (2012) *Durability performance of self-compacting concrete.* Construction and Building Materials 37, 320 - 325.

Khaleel, O. R., Al-Mishhadani, S. A. And Razak, H. A. (2011) *The effect of coarse aggregate on fresh and hardened properties of self-compacting concrete (SCC).* Procedia Engineering. 14, 805-813.

Khayat, K. (1998) *Viscosity – enhancing admixtures for cement-based materials – An overview.* Cement and Concrete Composites 20, 171-188

Kockal, N. U. (2008) *Effects of lightweight fly ash aggregate properties on the performance of lightweight concretes.* PhD Thesis. Bogazici University, Turkey.

Kosmatka, S. H., Kerkhoff, B. and Panarese, W. (2008) *Design and control of concrete mixtures.* New Jersey: Portland Cement Association, 358.

Kumar, R. and Bhattacharjee, B. (2003) *Porosity, pore size distribution and in situ strength of concrete.* Cement and Concrete Research, 33, 155 - 164.

Kuo, C.Y. and Freeman, R.B. (2000) *Imaging indices for quantification of shape, angularity and surface texture of aggregates.* Transportation Research Records, 1721(7) 57-65.

Lachemi, M., Hossain, K. M. A., Lambros, V., Nkinamubanzi, P. and Bouzoubaa, N. (2004) *Performance of new viscosity modifying admixtures in enhancing the rheological properties of cement paste.* Cement and Concrete Research, 43, 185 - 193.

Lee, H. K., Lee, K. M., Kim, Y. H., Yim, H. and Bae, D. B. (2004) *Ultrasonic in-situ monitoring of setting process of high performance concrete.* Cement and Concrete Research, 34, 631 – 640.

Leemann, A., Münich, B., Gasser, P. and Holzer, L. (2006) *Influence of compaction on the interfacial transition zone and the permeability of concrete.* Cement and Concrete Research 36 (8), 1425 – 1433.

Liu, M. (2010) *Self-compacting concrete with different levels of fuel ash.* Construction and Building Materials, 24, 1245 – 1252.

Liu, T. and Weyers, R. W. (1998) *Modeling the dynamic corrosion process in chloride contaminated concrete structures.* Cement and Concrete Research 28, 365 – 379.

Lothenbach, B. and Winnefeld, F. (2006) *Thermodynamic modelling of the hydration of Portland cement.* Cement and Concrete Research 36, 209 – 226.

Loukili, A. K., Kkelidji, A. and Richard, P. (1999) *Hydration kinetics, change of relative humidity, and autogenous shrinkage of ultra-high strength concrete.* Cement and Concrete Research, 29 (4), 577 – 584.

Maaddawy, T., E. and Soudki, K. (2007) *A model for the prediction of time from corrosion initiation to corrosion cracking.* Cement and Concrete Composites, 29, 168-175.

Maage, M., Helland, St. and Carlsen, J. E. (1994) *Chloride penetration in high performance concrete exposed to marine environment.* In: Sommer, H. (ed). Proceedings of the RILEM International Workshop Proposed by RILEM 3C Coordinating Committee for Concrete Technology organized and hosted by the Austrian Cement Research Institute, Vienna. Cachan, France: RILEM Publications, pp. 195 – 203.

Malhotra, M. (2006) *Nondestructive tests.* In: Lamond, J. and Pielert, J. (eds.) Significance of tests and properties of concrete and concrete-making materials, ASTM STP 169D. ASTM International, West Conshohocken, PA., pp 314-336.

Martys, N. S. and Ferraris, C. F. (1997) *Capillary transport in mortars and concrete.* Cement and Concrete Research, 27, (5), 747 – 760.

McGovern, M. ed. (2002) *Going with the flow.* Concrete Technology Today 23 (2), 1 – 8.

Mehta, P. K. and Monteiro, P. J. M. (2006) *Concrete, microstructure, properties and materials*, 3rd ed. London: McGraw-Hill, 659.

Mohammed, T. U. and Hamada, H. (2003) *Relationship between free chloride and total chloride contents in concrete.* Cement and Concrete Research, 33 (9), 1487 - 1490.

Montemor, M. F., Simões, A. M. P. and Salta, M. M. (2000) *Effect of fly ash on concrete reinforcement corrosion studied by EIS.* Cement and Concrete Composites, 22, 175 - 185.

Müller, H. S., and Rubner, K. (1994) *High-strength concrete – microstructural characteristics and related durability aspects.* In: Sommer, H. (ed). Proceedings of the RILEM International Workshop Proposed by RILEM 3C Coordinating Committee for Concrete Technology organized and Hosted by the Austrian Cement Research Institute, Vienna. Cachan, France: RILEM Publications, pp. 23 – 37.

Myrdal, R. (2007) *The electrochemistry and characteristics of embeddable reference electrodes for concrete (EFC 43).* Cambridge: Woodhead Publishing Company, pp 11.

Neville, A. M. (2006) *Concrete: Neville's insights and issue.* London: Thomas Telford, 289.

Neville, A. M. (2005) *Properties of concrete. 4th and final ed.* Essex: Pearson Education Limited, 844.

Ngala, V. T., Page, C. L. and Page, M. M. (2002) *Corrosion inhibitor systems for remedial treatment of reinforced concrete. Part 1: calcium nitrite.* Corrosion Science 44 (9), 2073 – 2087.

NT Build 492 *Chloride migration coefficient for non-steady state migration experiments* Concrete, Mortar and Cement-based Repairs Materials. Nordic council of ministers.

Okamura, K. and Ouchi, M. (2003a) *Application of self-compacting concrete in Japan.* In: Wallevik, O. and Nielsson, I. (eds). Proceedings of the 3rd International RILEM Symposium on Self-Compacting Concrete (Pro 33), Reykjavik. Cachan, France: RILEM Publications, pp. 3 – 5.

Okamura, K. and Ouchi, M. (2003b) Self-*compacting concrete.* Journal of Advanced Concrete Technology 1 (1), 5 – 15.

Okamura, K. and Ouchi, M. (1999) Self-*compacting concrete. Development, present and future.* In: Skarendahl, Å., Petersson, Ö. (eds). Proceedings of the 1st International RILEM Symposium on Self-Compacting Concrete (Pro 7), Stockholm. Cachan, France: RILEM Publications, pp. 3- 14.

Ouchi, M. (2005) *Self-compactability of fresh concrete.* In: Yu, Z., Shi, C., Khayat, K. L. and Xie, Y. (eds). Proceedings of the 1st International Symposium on Design, Performance and Use of Self-Compacting Concrete (Pro 42), China. Cachan, France: RILEM Publications, pp. 65 – 73.

Ouchi, M. and Edamatsu, Y. (1999) *A simple evaluation method for interaction between coarse aggregate and mortar particles in self-compacting concrete.* In: Skarendahl, Å., Petersson, Ö. (eds.) Proceedings of the 1st International RILEM Symposium on Self-Compacting Concrete (Pro 7), Stockholm. Cachan, France: RILEM Publications, pp. 121 – 130.

Ozyildirim, C. and Carino, N. J. (2006) *Concrete strength testing.* In: Lamond, J. and Pielert, J. (eds.) Significance of tests and properties of concrete and concrete-making materials, ASTM STP 169D. ASTM International, West Conshohocken, PA., pp. 120-140.

Page, C. L., Short, N. R., and Tarras, E. L. (1981) *Diffusion of chloride ions in hardened cement pastes.* Cement and Concrete Research, 11(3), 395 – 406.

Pan, T. (2002) *Fine aggregate characterization using digital image analysis.* MSc. Thesis. Louisiana State University and Agricultural and Mechanical College, USA.

Paya, J., Monzo, J., Borrachero, M. V. and Velazquez, S. (2003) *Evaluation of the pozzolanic activity of the fluid catalytic cracking catalyst residue (FC3R). Thermogravimetric analysis studies on FC3R-Portland cement pastes.* Cement and Concrete Research, 33(4), 603 – 609.

Persson, B. (2003) *Sulphate resistance of self-compacting concrete.* Cement and Concrete Research, 33, 1933 – 1938.

Petersson, O., Gibbs, J. and Bartos, P. (2003) *Testing – SCC: A European project.* In: Wallevik, O. and Nielsson, I (eds). Proceedings of the 3rd International RILEM Symposium on Self-Compacting Concrete (Pro 33), Reykjavik. Cachan, France: RILEM Publications, pp. 299 – 304.

Pillai, R. G. and Trejo, D. (2005) *Surface condition effects on critical chloride threshold of steel reinforcement.* American Concrete Institute

Polder, R. (2001) *Rilem TC 154-EMC: Electrochemical techniques for measuring metallic corrosion.* Material and Structures, 33, 603 – 611.

Pomeroy, C. D. (1994) *Random thoughts on the durability of high performance concrete.* In: Sommer, H. (ed). Proceedings of the RILEM International Workshop Proposed by RILEM 3C Coordinating Committee for Concrete Technology organized and Hosted by the Austrian Cement Research Institute, Vienna. Cachan, France: RILEM Publications, pp. 3 - 13.

Pop, I., De Schutter, G., Desnerck, P. and Onet, T. (2013) *Bond between powder type self-compacting concrete and steel reinforcement*. Construction and Building Materials 41, 824 – 833.

Poppe, A. M. and De Schutter, G. (2005b) *Cement hydration in the presence of high filler contents.* Cement and Concrete Research 35 (12), 2290 – 2299.

Ramachandran, V. S. and Beaudoin, J. J. (2001) *Handbook of analytical techniques in concrete science and technology.* New York: Noyes Publication, 964.

Rixom, R. and Mailvaganam, N. (1999) *Chemical admixtures for concrete.* 3rd ed. London: E and FN Spon Ltd., 437.

Roylance, D. (2001) *Stress-strain curves.* (Online) Available at: http://ocw.mit.edu/courses/materials-science-and-engineering/3-11-mechanics-of-materials-fall-1999/modules/ss.pdf [Accessed on November, 2011].

Saak, A. W., Jennings, H. M. and Shah, S. P. (2001) *The influence of slip stress and viscoelastic measurements of cement paste.* Cement and Concrete Research, 31, 205 – 212.

Saghafifar, H. (2011) *Microstructural stability of a nickel-based alloy overlay on a 2.25Cr1Mo steel substrate.* PhD Thesis. University of University, UK.

Saricimen, H., Mohammad, M., Quddus, A., Shameem, M. and Barry, M. S. (2002) *Effectiveness of concrete inhibitors in retarding rebar corrosion.* Cement and Concrete Composites, 24 (1), 89 - 100.

Schaeffer, R. L. and McClave J. T. (1990) *Probability and statistics for engineers, 3rd ed.* Boston: PWS-Kent Publishing Company, 696.

Shah, V. N. And Hookham, C. J. (1998) *Long-term aging of light water reactor concrete contaminants.* Nuclear Engineering Design 185(1), 51 – 81.

Skarendahl, Å. (2005) *Changing concrete construction through use of self-compacting concrete.* In: Yu, Z., Shi, C., Khayat, K. L. and Xie, Y. (eds). Proceedings of the 1st International Symposium on Design, Performance and Use of Self-Compacting Concrete (Pro 42), China. Cachan, France: RILEM Publications, pp. 17 – 24.

Skarendahl, Å. (2003) *The present – the future.* In: Wallevik, O. and Nielsson, I. (eds). Proceedings of the 3rd International RILEM Symposium on Self-Compacting Concrete (Pro 33), Reykjavik. Cachan, France: RILEM Publications, pp. 6 – 14.

Skarendahl, A and Billberg, P. (2006) *Casting of self-compacting concrete – Final report.* Rilem Technical Committee 188 – CSC. France: RILEM Publications, 26.

Söylev, T. A. and Richardson, M. G. (2008) *Corrosion inhibitors for steel in concrete: State of the art report.* Construction and Building Materials 22 (4), 609 – 622.

Tang, L. and Nilsson, L. (1992) *Chloride diffusivity in high strength concrete at different ages.* Nordic Concrete Research Publication 11(1), 162 – 170.

Tattersall, G. H. and Banfill, P. F. G. (1983) *The rheology of fresh concrete.* London: Pitman Advanced Publishing Program, 356.

Taylor, H. F. W. (1997) *Cement chemistry.* 2nd ed. London: Thomas Telford, 459.

The Concrete Society (2005) *Self-compacting concrete - A review.* Technical report No.62. Camberly: Concrete Society, 80.

The Concrete Society (2008) *Permeability testing of site concrete - A review of methods and experience.* Technical report no.31. Camberly: Concrete Society, 80.

Turcry, P. and Loukili, A. (2003) A *study of plastic shrinkage of self-compacting concrete.* In: Wallevik, O. and Nielsson, I. (eds). Proceedings of the 3rd International RILEM Symposium on Self-Compacting Concrete (Pro 33), Reykjavik. Cachan, France: RILEM Publications, pp. 576 – 585.

Uchikawa, H., Hanehara, S. and Sawaki, D. (1996) *The role of steric repulsive force in the dispersion of cement particles in fresh paste prepared with organic admixture.* Cement and Concrete Research 27 (1), 37 – 50.

Uhlig, H. H. and Revie, R. W. (1985) *Corrosion and corrosion control – An introduction to corrosion science and engineering.* 3rd ed. New York: John Wiley and Sons, 441.

Vachon, M. (2002) *ASTM puts self-consoildating concrete to the test.* ASTM Standardization News. (Online) Available at: http://www.astm.org/SNEWS/JULY_2002/vachon_jul02.html [Accessed on May 15, 2009].

Valcarce, M. B. and Vazquez, M. (2008) *Carbon steel passivity examined in alkaline solutions: the effect of chloride and nitrite ions.* Electrochimica Acta, 53 (15), 5007 – 5015.

Vedalakshmi, R., Rajagopal, K. and Palaniswamy, N. (2009) *Determination of migration efficiency of amino alcohol based migration corrosion inhibitor through concrete.* Corrosion Engineering, Science and Technology, 44 (1), 20 – 31.

Vennesland, Ø., Raupach, M. and Andrade, C. (2007) *Recommendation of Rilem TC154-EMC: "Electrochemical technigues for measuring corrosion in concrete2 – measurements with embedded probes.* Materials and Structures , 40 (8), 745 – 758.

Vorburger, T. V. and Raja, J. (1990) *Surface finish metrology tutorial, NISTIR 89-4088.* National Institute of Standards and Technology, Massachusetts, pp. 159.

Wade, S. A., Nixon, J. M., Schindler, A. K., Barnes, R. W. (2010) *Effect of temperature on the setting behaviour of concrete.* Journal of Materials in Civil Engineering 22 (3), 214 – 222.

Wallevik, O. H. (2003) *Rheology – A scientific approach to develop self-compacting concrete.* In: Wallevik, O. and Nielsson, I. (eds). Proceedings of the 3rd International RILEM Symposium on Self-Compacting Concrete (Pro 33), Reykjavik. Cachan, France: RILEM Publications, pp. 23 – 31.

Winnefeld, F., Becker, S., Pakusch, J. and Gotz, T. (2007) *Effects of the molecular architecture of comb-shaped superplasticizers on the performance in cementitious systems.* Cement and Concrete Composites, 29, 251-262.

Wombacher, F., Maeder, U. and Marazzani, B. (2004) *Aminoalcohol based mixed corrosion inhibitors.* Cement and Concrete Composites 26, 209-216.

Yang, H., Fang, K. and Tu, S. (2011) *Pozzolanic reaction of supplementary cementitious materials and its effects on the strength of mass concrete.* Advanced Materials Research 168-179, 505 – 511.

Yu, H., Chiang, K. & Yang, L. (2012) *Threshold chloride level and characteristics of reinforcement corrosion initiation in simulated concrete pore solutions.* Construction and Building Materials 26, 723-729

Yuan, Q., Shi, C., De Schutter, G., Audenaert, K. and Deng, D. (2009) *Chloride binding of cement-based materials subjected to external chloride environment – A review.* Journal of Construction and Building Materials, 23 (2), 1 - 13.

Zhang, Y. M., Sun, W. and Yan, H. D. (2000) *Hydration of high-volume fly cement paste.* Cement and Concrete Composite, 22, 445 - 452.

Zhu, W. and Bartos, P. J. M. (2005) *Microstructure and properties of interfacial transition zone in SCC.* In: Yu, Z., Shi, C., Khayat, K. L. and Xie, Y. (eds). Proceedings of the 1st International Symposium on Design, Performance and Use of Self-Compacting Concrete (Pro 42), China. Cachan, France: RILEM Publications, pp. 319 – 327.

Zhu, W. and Bartos, P. J. M. (2003) *Permeation properties of self-compacting concrete.* Cement and Concrete Research, 33 (6), 921 – 926.